RIVER SEEPAGE INVESTIGATION

HYDRAULIC LABORATORY
UNIVERSITY OF CALIFORNIA, BERKELEY

WATER RESOURCES CENTER
CONTRIBUTION NO. 20

RIVER SEEPAGE INVESTIGATION

by

David K. Todd

and

Jacob Bear

Water Resources Center
Contribution No. 20

Hydraulic Laboratory
University of California, Berkeley

September 1, 1959

TABLE OF CONTENTS

LIST OF FIGURES

LIST OF FIGURES (cont.)

LIST OF TABLES

I. Introduction

A. The Problem in California

Seepage from rivers and natural channels is a serious problem in the Sacramento Valley of California. Impairment of land use occurs along the Sacramento, Feather, Yuba, and Bear Rivers as a result of intermittent periods of high ground water or ponded surface water. When channel levels exceed the adjacent ground surface elevation, water moves through and under the confining levels into adjacent lands. If drainage facilities are inadequate, the soil becomes saturated and water often ponds on the surface. The water damages orchards and perennial and annual crops, and prevents working of land, resulting in delays in or prevention of normal planting of annual crops.

A survey of seepage along the Sacramento River by the U. S. Bureau of Reclamation led to the following statement (9):*

"The survey indicates that the influence of high winter and spring stages of the Sacramento River diminishes rapidly and is not noticeable beyond 1.5 miles of the river and normally is negligible at 0.5 of a mile. The degree to which the river contributes water to the underground varies greatly from place to place along the river depending upon the geology of the area and on the extent to which river stages are above or below the level of the adjoining land. In those areas that have sand strata connecting to the river, the river makes large and rapid contributions to the ground water as the river stage rises. In other areas, where the river channel is in heavy clay, the river contributes water to the ground very slowly during periods of high river

---

*Numbers in parentheses refer to references at the end of the report.

stage and does not create groundwater problems unless the river stages are maintained at high levels for a month or longer."

Extensive seepage damage occurred in Sacramento Valley in the winters of 1937-38, 1940-41, 1941-42, 1951-52. Surveys of economic losses by seepage during the period 1937-1953 show an average of 18,000 acres affected annually. The average annual loss (at 1953 prices) amounted to $1,834,000, or $102 per acre affected (21).

Most investigations of the problem have been concerned with the field conditions involved, including areas affected, periods and durations of flooding, and economic losses sustained. Little has been done to study the physical picture of the flow of water from the stream channel through subsurface strata to the adjacent ground surface. It is the purpose, therefore, of this investigation to analyze the hydraulics of seepage flows for conditions similar to those existing in Sacramento Valley.

B. Approach to the Problem

The natural conditions governing seepage from a stream channel into adjacent lands include geology and soils, topography, ground water, rainfall and runoff, and channel stage. The range of conditions for each of these variables, together with their possible combinations, makes it apparent that not all situations for reaches in the Sacramento Valley could be studied. Instead, key variables were selected for study so that results could be generalized. Modifications can then be made to apply the results to particular situations.

This study is a laboratory investigation of seepage flow nets for steady flows. Boundary conditions were selected to correspond to a variety of field conditions. Data were obtained from an electric

analogy model constructed for this purpose. Results have been presented in graphical form to facilitate interpretation and application to similar situations found in the field.

C. Previous Contributions

Surveys of seepage conditions in Sacramento Valley are summarized in reports by the Joint Committee on Water Problems of the California Legislature (9) and by Plumb and others (21). The latter report also contains a critical review of methods for controlling seepage. Illustrations of the complex geology of alluvial deposits in the Valley are contained in the report by Plumb and others (21) and by McClure and others (17). Discussion of seepage conditions at particular locations can be found in works by Kabakov (10), Scott and Luthin (23), and Todd (28).

The engineering literature contains many references to seepage through earth dams, under masonry dams, from canals, and to relief wells. Significant contributions toward analytic solutions have been made by Lane (11), Bennett (2), Middlebrooks and Jervis (18), Barron (1), Shea and Whitsett (25), and Hammad (5). Discussion of various field conditions of seepage can be found in papers by Mansur and Kaufman (16) and Esmiol (4). Hydraulic models have often served as a valuable tool to supplement analytic approaches (29, pp. 307-325). Applications of the electric analogy model to seepage problems have been made by Harza(6), Selim (24), and Johnson (8). Turnbull and Mansur (30) employed a sand model, while Todd (28) investigated an unsteady case with a Hele-Shaw model.

The electrolytic type of electric analogy model designed for tests in this study is well known. Discussions of the model design and its application to seepage studies date from the work of Pavlovsky (20), and

include Lane, Campbell, and Price (12), Vreedenburgh and Stevens (32), Stevens (27), Reltov (22), and Luthra and Ram (13). A recent summary of the theory of the analogy has been prepared by Malavard (15).

The subsurface conditions in which seepage occurs in Sacramento Valley necessitated study of flow through layered anisotropic soils. Fundamental contributions to the mechanics of this phenomenon have been made by Casagrande (3), Maasland (14), Vreedenburgh (31), and Stevens (26).

D. Acknowledgments

This report covers one portion of a continuing research program in ground water hydrology sponsored by the Water Resources Center of the University of California. This investigation was conducted in the Hydraulic Laboratory of the College of Engineering at Berkeley.

Information on field seepage conditions was supplied by the California Department of Water Resources and the United States Geological Survey. Mr. G. E. Wilson and Mr. G. S. Sivanna assisted in the laboratory work, while Dr. G. de Josselin de Jong furnished advice on the theoretical computations.

II. Seepage Cross-Section

A. Topography

Reaches along the Sacramento River can be classified into three principal types:

(1) Reaches where the adjacent ground surface is higher than the highest water surface in the river. In these reaches water flowing underground from the river will not reach ground surface. The water table, whether free or controlled by drains, is always below ground surface; hence seepage is not a problem.

(2) Reaches where the adjacent ground surface is below the river stage. A continuous seepage flow exists in this situation with the rate of water movement at any location being governed by the difference in elevation between the river stage and the water table in lands adjoining the river. The water table may vary in elevation depending upon the subsurface flow rates, may be controlled near one level by subsurface drains, or may rise to the ground surface and appear as ponded water during periods of excessive seepage. (In this connection it should be noted that water ponded in fields back of levees may result also from excessive rainfall and inadequate surface drainage facilities).

(3) Reaches where the adjacent ground surface is below the river stage only a portion of the time. Seepage becomes a seasonal problem here because high stages are invariably associated with winter and spring floods and associated upstream releases from dams.

In the upper reaches of the river, above Hamilton City (see Fig. 1), ground surface slopes generally from the foothills on either side of the valley toward the river. The river slope decreases in the vicinity

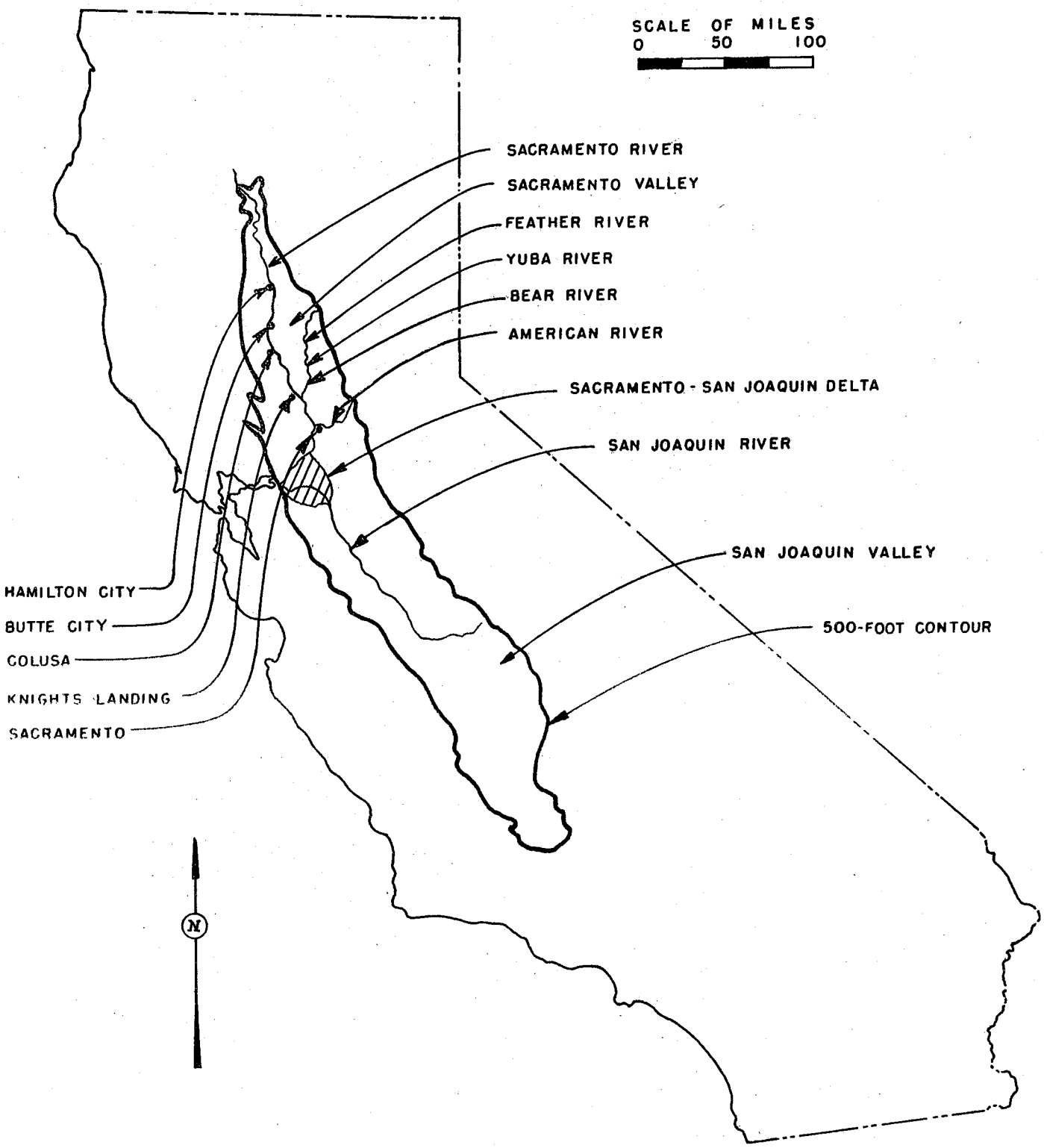

FIG. 1 MAP OF CALIFORNIA SHOWING SACRAMENTO VALLEY

of Butte City resulting in the formation of natural levee deposits from overflows. These have created a ridge within which the river flows and with land sloping away from the river on both sides. Low areas parallel the river on both sides, inclduing Colusa Trough and Yolo Basin on the west side and Butte Basin and Sutter Basin on the east side, and extend southward to the Delta. A break in slope usually occurs about one-fourth mile from the river, formed by the edge of the heavier material deposited by the rivers on the natural levees (21).

The Sacramento River merges with the San Joaquin River in the Sacramento-San Joaquin Delta and thereafter flows into San Francisco Bay. The Delta constitutes an area of nearly 400,000 acres of irrigated agricultural land interlaced by more than 600 miles of tidal channels which surround more than 50 islands. Most of the islands contain deposits of peat at the surface. Intensive agricultural development of the land, combined with drainage to lower the water table, has resulted in loss of peat from the surface. Oxidation and wind erosion are major contributing factors. The destruction of peat has produced an average lowering of the ground surface of about 3 inches per year; consequently, many islands are saucer-like depressions 10-15 feet below sea level and surrounded by levees.

Seepage constitutes a problem in Sacramento Valley, therefore, along the Sacramento River south of Hamilton City, along the lower reaches of the Feather, Yuba, and Bear Rivers, and throughout the Sacramento-San Joaquin Delta.

B. Geology and Soils

Seepage in Sacramento Valley occurs almost entirely in Recent and Pleistocene alluvial deposits adjacent to and underlying the major

rivers. These deposits may be classified (21) as follows:

(1) Deposits that are moderately to highly permeable and most likely to contain and transmit river seepage:

(a) Natural levee deposits

(b) Younger and older point bar deposits

(2) Deposits that are relatively impermeable and not likely to transmit seepage, or to transmit it at a very slow rate:

(a) Fine-grained river basin deposits

(b) Abandoned channel fillings

Each deposit is briefly discussed in the following paragraphs.

Natural levee deposits and the medium to fine-textured deep permeable soils developed on these deposits appear to have a greater influence on river seepage than any other geologic unit. These deposits are located on both sides of the Sacramento and Feather Rivers in the Valley at elevations above the flood plain. During high river stages the coarser-grained portion of the natural levee is submerged so that water travels through the levees from the river to lower-lying adjacent land. Outer margins of the natural levees are usually finer grained. If no impermeable barrier restricts the horizontal movement of seepage water, it appears at ground surface and spreads out over low-lying impermeable river basin deposits.

Point bar deposits have an appreciable influence on river seepage. These deposits, and the coarse to medium-textured soils developed on them, are located mainly between present river channels and the artificial levees. They are most extensively developed in the upper and central reaches of Sacramento River from Hamilton City south to Colusa. During

high river stages point bar deposits are in direct hydraulic contact with the river; hence seepage can extend under and outside of the artificial levees if no adjacent deposits restrict flow.

Relatively impermeable river basin deposits and the impermeable soils developed on them are not effective for seepage transmission. These deposits occur in topographically low areas adjacent to natural levees along the central and lower reaches of Sacramento River. They tend to act as seepage barriers rather than seepage conduits.

Abandoned channel fillings are located on both sides of Sacramento River and are closely associated with point bar deposits between Hamilton City and Knights Landing. These fillings are generally long, narrow depressions formed by compaction of clay deposits. Although these areas often contain standing water which has seeped from rivers through adjacent deposits, channel fillings are not likely to serve as conduits for transmission of seepage.

In order to obtain estimates of seepage through representative cross-sections, it was necessary to determine relative permeabilities. Extensive field measurement of permeability would lead to average values for each type of deposit, but considerable scatter could be anticipated around each mean. Because only relative permeabilities were needed for the present purpose, rough estimates of permeabilities were made from representative grain size distributions of the deposits from data by Plumb and others (21). Permeabilities were determined by the relation

$$K = 7100\ d_{20}^{2.27}$$

where K is the standard coefficient of permeability (gal/day/ft^2)

and d_{20} is the 20 per cent finer grain size (mm). Results are shown in Table I. Relative values of K are those in relation to the lowest permeability, that of abandoned channel fillings. Assumed relative values of K are grouped by order of magnitude. These values were then divided by ten for convenience to obtain relative permeabilities for the deposits in the model. Note that the permeabilities of abandoned channel fillings and river basin deposits were assumed negligible in relation to the other deposits.

Table I - Estimates of Relative Permeabilities for Fine-Grained Alluvial Deposits

Geologic Deposit	d_{20}, mm	K, gpd/ft^2	Relative K	Assumed relative K	Relative K for model
Older point bar	0.032	2.8	1200	500	50
Younger point bar	0.020	1.0	420		
Natural levee	0.0045	3.4×10^{-2}	14	10	1
Natural levee (outer fringe)	0.003	1.3×10^{-2}	5		
River basin deposit	0.0022	6.5×10^{-3}	3	1	0
Abandoned channel fillings	0.0014	2.4×10^{-3}	1		

C. Representative Geologic Sections

An investigation of well logs near Sacramento River and of geologic sections plotted by Plumb and others (21) showed a wide diversity of layered alluvial deposits. Fig. 2 shows an actual section; the irregularities, based on the limited data available, are typical. This variety, combined with inadequate field data, precluded any possibility pf determining seepage through actual geologic sections. Instead, a number of hypothetical sections were constructed for model tests which are representative of seepage conditions in Sacramento Valley.

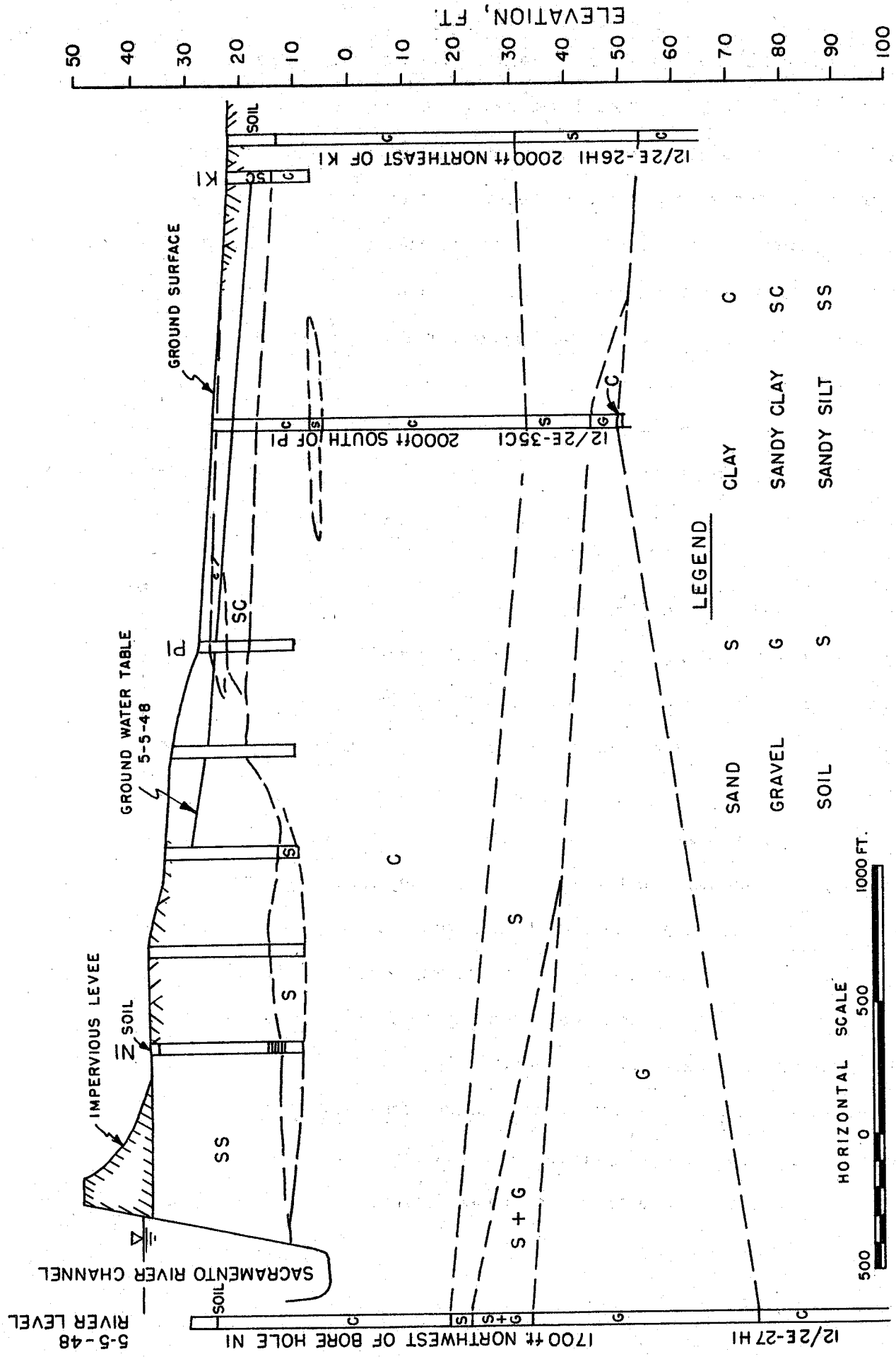

FIG. 2 GEOLOGICAL CROSS-SECTION OF EAST RIVER FARMS LINE

Almost all seepage occurs in the zone above the highest more or less continuous clay layer. This layer may occur anywhere from near ground surface to depths approaching 100 feet. It acts as a lower impermeable boundary for the seepage flow pattern. In the permeable zone various layers of deposits can be found. Based on the geologic deposits discussed in the previous section, layers could be reduced to ones having relative permeabilities of 50, 1, and 0. These layers are essentially horizontal, but may vary in thickness and in their relative vertical positions. As most seepage occurs within a mile of the river, the model was limited to a maximum distance of 3,000 feet inland from the levee. A maximum depth of 100 feet below the water table was also selected. If symmetry is assumed about the center of the river, a section on only one side of the river need be investigated.

Other assumptions made for the model investigation were that the river channel is rectangular with a depth of 25 feet (a few cases of other depths were also studied) and a width of 600 feet. Levees were assumed to be situated adjoining the river channel, to be impermeable, and to have a base width of 100 feet at the elevation of the inland water table. An impermeable levee, of course, implies that all seepage passes under the levee. Depending upon the mode of construction and materials employed, levee seepage may or may not be a significant item. In any event, seepage tnrough a levee may be considered as occurring independently of that under a levee.

A final variable necessary to consider in evaluating seepage is that of the anisotropy of permeable zones. Most alluvial strata are deposited horizontally with a pronounced tendency for a greater uniformity

in grain size and depositional structure horizontally than vertically. Commonly this results in a condition of anisotropic permeability where the horizontal permeability may greatly exceed that of the vertical. Ratios of vertical to horizontal permeability of 1, 0.1, and 0.01 were selected to give a range of representative conditions.

D. Water Table

The position of the water table relative to river stage and to ground surface determines relative seepage rates and how soon seepage may appear at ground surface. Seepage to a deep water table from a short duration flood stage may not affect surface conditions, whereas the same situation at a location with a high water table may have a marked surface effect.

Water table slopes along Sacramento River are generally toward the river. Exceptions occur in Butte Basin, south of Sacramento, and in the Delta; here slopes are away from the river even during periods of low flow. Depths to water table vary widely depending on location, season, river stage, and subsurface drainage facilities. Extremes range from about 20 to zero feet below ground surface. It is known (28; 29, pp. 163-165) that with a rise and fall of river stage, a corresponding fluctuation occurs in the adjoining water table. The magnitude decreases with distance from the river and the time of the maximum height lags with distance inland.

In most of the irrigated agricultural land in Sacramento Valley the water table is controlled to within narrow limits by subsurface drainage facilities. The level is commonly maintained at 3 to 4 feet below ground surface. For steady flow conditions studied in the electric analogy model, the water table was assumed stationary. This

might represent levels controlled either by subsurface drains or by ponding at ground surface. Both horizontal and sloping water tables were investigated.

E. River Fluctuations

With upstream regulation Sacramento River in the Valley area is not subject to large fluctuations in stage. In the central portion of the Valley dam releases and flood flows raise river stages in winter and spring for periods of from a few days to a few weeks at a time. The number of such periods and the magnitudes of the rises are, of course, governed by seasonal rainfall and snowmelt conditions. South of Sacramento and in the Delta, the river is subject to tidal action. The short tidal period (approximating 12 hours) is too small to have an appreciable effect on seepage; hence only the mean elevation above sea level need be considered.

Field (9) and laboratory (28) investigations have confirmed that seepage from flood flows is proportional to a duration-height factor; hence the nonsteady factors need no further consideration. This study was limited to the steady case with emphasis on the distribution of seepage inland from the river. Factors of river stage magnitude and duration are variables necessary in applying these results to obtain quantitative seepage for a given situation and location.

F. Cross-Section Assumed for Model Analysis

Previous sections have reviewed field conditions governing seepage in Sacramento Valley and have indicated assumptions necessary to obtain representative model data. The general cross-section to be studied is shown in Fig. 3 together with symbols identifying the constants and variables involved.

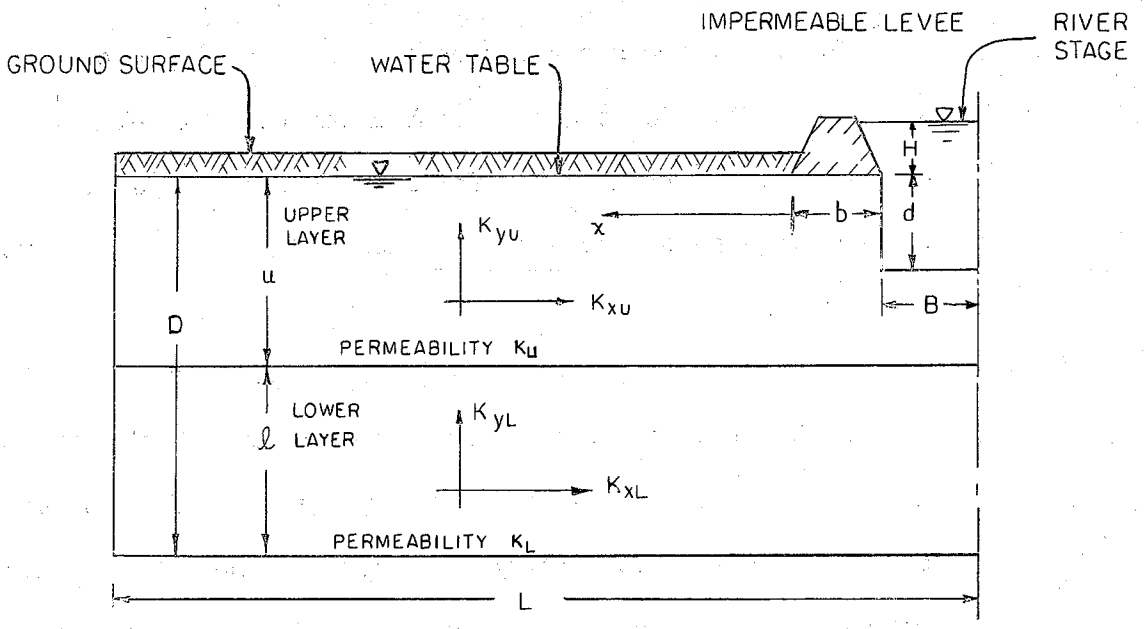

Legend

Item	Symbol	Range of Values
Channel depth	d	0 - 100 ft.
Permeable zone depth	D	100 ft. (constant)
Thickness of upper layer	u	10 - 100 ft.
Thickness of lower layer	l	0 - 90 ft.
Length of cross-section from centerline of river	L	1000 - 3300 ft.
River stage above levee base	H	(None assigned)
Channel half-width	B	100 - 300 ft.
Levee base width	b	100 ft. (constant)
Distance landward from toe of levee	x	600 - 2900 ft.
Permeability of upper layer	K_U	(None assigned)
Permeability of lower layer	K_L	(None assigned)
Anisotropy of upper layer	K_{yU}/K_{xU}	1:1 - 1:100
Anisotropy of lower layer	K_{yL}/K_{xL}	1:1 - 1:100
Ratio of permeabilities of the two layers	K_U/K_L	1:50; 50:1

Figure 3 - Definition Sketch of Cross-Section Assumed for Model Analysis

The total cross-section depth D and the levee base width b were held constant. The channel depth d and the channel half-width B were constant for all but a few model tests. Significant variables are the thicknesses of the upper and lower layers, u and l, respectively. These are related by

$$D = u + l = 100 \text{ ft.}$$

The length of cross-section L was varied as required to obtain a practical vertical scale to define the seepage flow pattern of each model test. The river stage H determines the rate of subsurface flow, but has no effect on the distribution of seepage; therefore, no values were assigned. Similarly, the permeabilities of the layers, K_U and K_L, were unassigned, but their relative values expressed by their ratio K_U/K_L form a key variable of the investigation. The anisotropies of the individual layers are expressed by the ratio of their respective directional permeabilities, K_{yU}/K_{xU} and K_{yL}/K_{xL}. Ratios were varied from 1 to 0.01.

Based on the variables defined in Fig. 3 and on a study of field conditions in seepage areas of Sacramento Valley, a series of model tests were outlined covering various combinations of the significant variables. Table II lists 56 tests, identified by number, together with values assigned for each parameter. The policy followed in selecting these tests was to adopt cross-sections typical of the area of interest. Test results, supplemented by field data on river stage and permeability, should enable quantitative estimates of seepage amount and distribution to be made for a large variety of field conditions. Furthermore, modification of test results, as described later, extends the applicability of results to many other conditions similar to those in the test series.

Table II - List of Model Tests

(All dimensions refer to field conditions)

Test No.	Length of cross-section L, ft.	Thickness of upper layer (u), ft.	Thickness of lower layer (l), ft.	Permeability ratio K_U/K_L	Anisotropy K_{yU}/K_{xU}	Anisotropy K_{yL}/K_{xL}	Channel depth d, ft.
1*	1000	100	0	-	1:1	-	25
2	1500	100	0	-	1:10	-	25
3	3000	100	0	-	1:100	-	25
4	1000	10	90	1:50	1:10	1:1	25
5	1000	10	90	1:50	1:10	1:10	25
6	1000	10	90	50:1	1:10	1:1	25
7	1000	10	90	50:1	1:100	1:1	25
8	1000	10	90	50:1	1:10	1:10	25
9	1500	10	90	50:1	1:100	1:10	25
10	1000	25	75	1:50	1:1	1:1	25
11	1000	25	75	1:50	1:1	1:10	25
12	1000	25	75	1:50	1:10	1:1	25
13	1000	25	75	1:50	1:10	1:10	25
14	1000	25	75	50:1	1:1	1:1	25
15	1000	25	75	50:1	1:10	1:1	25
16	1000	25	75	50:1	1:100	1:1	25
17	1000	25	75	50:1	1:1	1:10	25
18	1000	25	75	50:1	1:10	1:10	25
19	1500	25	75	50:1	1:100	1:10	25
20	1000	50	50	1:50	1:1	1:1	25
21	1000	50	50	1:50	1:1	1:10	25
22	1500	50	50	1:50	1:1	1:100	25
23	1000	50	50	1:50	1:10	1:1	25
24	1000	50	50	1:50	1:10	1:10	25
25	2000	50	50	1:50	1:10	1:100	25
26	1000	50	50	50:1	1:1	1:1	25
27	1000	50	50	50:1	1:10	1:1	25
28	1500	50	50	50:1	1:100	1:1	25
29	1000	50	50	50:1	1:1	1:10	25

Table II (cont.)

Test No.	Length of cross-section L, ft.	Thickness of upper layer (u), ft.	Thickness of lower layer (l), ft.	Permeability ratio K_U/K_L	Anistropy K_{yU}/K_{xU}	Anistropy K_{yL}/K_{xL}	Channel depth d, ft.
30	1000	50	50	50:1	1:10	1:10	25
31	2000	50	50	50:1	1:100	1:10	25
32	1000	75	25	1:50	1:1	1:1	25
33	1000	75	25	1:50	1:1	1:10	25
34	1000	75	25	1:50	1:1	1:100	25
35	1000	75	25	1:50	1:10	1:1	25
36	1000	75	25	1:50	1:10	1:10	25
37	1500	75	25	1:50	1:10	1:100	25
38	1000	75	25	50:1	1:1	1:1	25
39	1000	75	25	50:1	1:10	1:1	25
40	1000	75	25	50:1	1:1	1:10	25
41	1000	75	25	50:1	1:10	1:10	25
42	2000	75	25	50:1	1:100	1:10	25
43	3000	100	0	-	1:100	-	50
44	3000	100	0	-	1:100	-	50
45	3000	100	0	-	1:100	-	50
46	1500	100	0	-	1:10	-	50
47	3000	75	25	1:50	1:100	1:100	50
48	3000	75	25	50:1	1:100	1:100	50
49	3000	25	75	1:50	1:100	1:100	50
50	3000	25	75	50:1	1:100	1:100	50
51	3000	100	0	-	1:100	-	0
52	1500	100	0	-	1:10	-	0
53	3300	100	0	-	1:100	-	100
54	1800	100	0	-	1:10	-	100
55*	1500	100	0	-	1:10	-	25
56*	1500	100	0	-	1:10	-	25

B = 300 ft. for Tests 1-54, 100 ft. for Test 55, and 200 ft. for Test 56.

III. Electric Analogy

A. Theory

The electric analogy is a well-known device for studying the field of flow of fluid through porous media (8, 12, 19, 24). The analogy is based on the similarity between the differential equations which describe the flow of fluid through porous media, and those which govern the flow of electric current through conducting materials (15).

Ohm's law for the flow of electricity through a conducting material can be written

$$\vec{I} = -\sigma \text{ grad } V \qquad (1)$$

where

$\vec{I}$ = vector of electric current per unit area

σ = conductivity of the conducting material

V = electric potential

Similarly, Darcy's law for the laminar flow of fluid through porous media can be written

$$\vec{q} = -K \text{ grad } \varphi \qquad (2)$$

$\vec{q}$ = discharge rate per unit area

K = permeability

φ = potential (or head) of the liquid; $\varphi = z + \frac{p}{\gamma}$

p = pressure

z = elevation

γ = specific weight of fluid

For steady flow in a region with no sources or sinks, the electric potential V satisfies the differential equation

$$\text{div } \vec{I} = \text{div } (-\sigma \text{ grad } V) = 0 \qquad (3)$$

which reduces to the Laplace equation

$$\nabla^2 V = \frac{\partial^2 V}{\partial x^2} + \frac{\partial^2 V}{\partial y^2} + \frac{\partial^2 V}{\partial z^2} = 0 \qquad (4)$$

for an isotropic conducting material. Similar considerations of continuity for the steady flow of an incompressible liquid through a homogeneous and isotropic porous medium lead to the equation

$$\text{div } \vec{q} = \text{div } (-K \text{ grad } \varphi) = 0 \qquad (5)$$

or

$$\nabla^2 \varphi = \frac{\partial^2 \varphi}{\partial x^2} + \frac{\partial^2 \varphi}{\partial y^2} + \frac{\partial^2 \varphi}{\partial z^2} = 0 \qquad (6)$$

Comparison of Eqns. (1) and (2) and Eqns. (4) and (6) leads to the conclusion that any steady incompressible fluid flow problem having a potential φ (x, y, z) may be investigated by an electrical model with the following analogies:

Fluid flow through porous media	Flow of electricity
Porous media	Conducting media
φ = fluid potential	V = electric potential
$\vec{q}$ = specific fluid discharge	$\vec{I}$ = electric current per unit area
K = permeability	σ = electric conductivity
Darcy's law and Laplace's equation	Ohm's law and Laplace's equation

Thus, an unknown function φ (x, y, z) in a specified domain with given boundary conditions can be defined by an electric potential V (x, y, z) of a conducting material model having the same geometric shape and satisfying analogous boundary conditions. Measurements of the electric potential V in the model provide a numerical solution for φ (x, y, z) which satisfies Eqn. (6) and the given boundary conditions.

The electric analogy can be used for studying three-dimensional as well as two-dimensional fields of flow. The present work is concerned only with the two-dimensional case of flow in the vertical (x, y) plane.

Here the Lapacian operator in Eqns. (4) and (6) reduces to

$$\nabla^2 = \frac{\partial^2}{\partial x^2} + \frac{\partial^2}{\partial y^2} \tag{8}$$

The imitation of a nonhomogeneous domain with a conductivity which varies from point to point in the three-dimensional case can only be accomplished if the variations take the form of large homogeneous sub-domains which can be imitated by the use of different conducting materials. In the case of a two-dimensional field it is possible to represent variable permeability by varying the thickness of the conducting material in the model. The electric potential must not vary with the thickness coordinate. This restriction has to be considered when the permeability changes by a large amount abruptly along a line. Here, varying the thickness of the conducting material in the model is not possible because the abrupt change of thickness by a large factor causes the electric potential to vary along the thickness coordinate. To circumvent this difficulty different conducting materials, or different electrolyte concentrations of the same depth, can be installed in the model.

For two-dimensional cases where variations in the thickness of the conducting material are permissible, Eqn. (1) can be written in the form

$$\vec{I}' = -\sigma\, h\,(x,y)\ \text{grad}\ V \tag{9}$$

where

$\vec{I}'$ = electric current per unit width

$h\,(x, y)$ = thickness of conducting material

σ = electric conductivity

If σ is constant, then

$$\text{div}\ \vec{I}' = 0 = -\sigma\ \text{div}\ (h\ \text{grad}\ V) \tag{10}$$

and

$$\frac{\partial}{\partial x}\left(h\,\frac{\partial V}{\partial x}\right) + \frac{\partial}{\partial y}\left(h\,\frac{\partial V}{\partial y}\right) = 0 \qquad (11)$$

In addition to the analogy between φ and V, a second analogy exists between the fluid stream function ψ and the electric current function W. The current element dW represents the current intensity dI across an arc dS, so that

$$dW = -\sigma h\left(\frac{\partial V}{\partial x}\,\varepsilon + \frac{\partial V}{\partial y}\,\theta\right) dS \qquad (12)$$

where ε and θ are the direction cosines of the normal to dS (see Fig. 4) defined by $\varepsilon = -\frac{dy}{ds}$ and $\theta = \frac{dx}{ds}$. Eqn. (12) becomes

$$dW = -\sigma h\left(\frac{\partial V}{\partial y}\,dx - \frac{\partial V}{\partial x}\,dy\right) \qquad (13)$$

but also by definition

$$dW = \frac{\partial W}{\partial x}\,dx + \frac{\partial W}{\partial y}\,dy \qquad (14)$$

Comparing terms gives the relations between the functions V and W,

$$\frac{\partial V}{\partial x} = \frac{1}{\sigma h}\,\frac{\partial W}{\partial y} \qquad (15)$$

and

$$\frac{\partial V}{\partial y} = -\frac{1}{\sigma h}\,\frac{\partial W}{\partial x} \qquad (16)$$

Taking the derivative of Eqn. (15) with respect to y and of Eqn. (16) with respect to x and subtracting yields

$$\frac{\partial}{\partial x}\left(\frac{1}{h}\,\frac{\partial W}{\partial x}\right) + \frac{\partial}{\partial y}\left(\frac{1}{h}\,\frac{\partial W}{\partial y}\right) = 0 \qquad (17)$$

Eqns. (11) and (17) have the same form, and from them it can be seen that both V and W satisfy the Laplace equation when h is constant.

Similar equations can be obtained for the functions φ and ψ.

If the permeability of a porous medium is variable, then

$$\operatorname{div}(-K \operatorname{grad} \varphi) = -\frac{\partial}{\partial x}\left(K\,\frac{\partial \varphi}{\partial x}\right) - \frac{\partial}{\partial y}\left(K\,\frac{\partial \varphi}{\partial y}\right) = 0 \qquad (18)$$

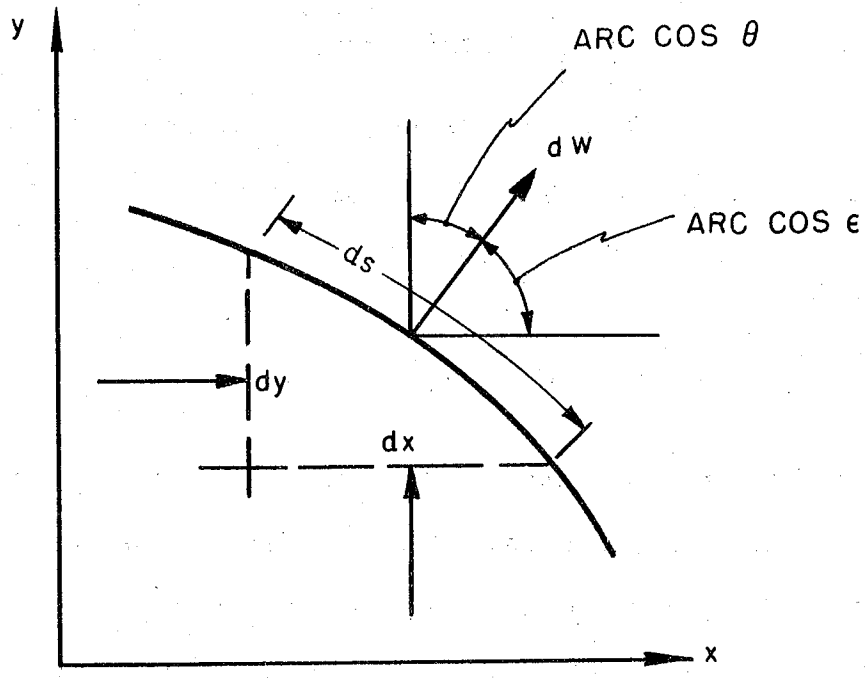

FIG. 4 DEFINITION SKETCH OF d W

and

$$d\psi = \frac{\partial \psi}{\partial x} dx + \frac{\partial \psi}{\partial y} dy = -K \frac{\partial \varphi}{\partial y} dx + K \frac{\partial \varphi}{\partial x} dy \quad (19)$$

Values of φ and ψ are related by

$$\frac{\partial \varphi}{\partial x} = \frac{1}{K} \frac{\partial \psi}{\partial y} \quad (20)$$

and

$$\frac{\partial \varphi}{\partial y} = -\frac{1}{K} \frac{\partial \psi}{\partial x} \quad (21)$$

If K is constant, both φ and ψ satisfy the Laplace equation.

There are, therefore, two types of analogy, which can be stated as

$$\text{Type I:} \quad \varphi = mV; \quad \psi = nW; \quad h = \frac{mK}{n\sigma} \quad (22)$$

and

$$\text{Type II:} \quad \varphi = m'W; \quad \psi = -n'V; \quad h = \frac{n'}{m' \sigma K} \quad (23)$$

where m, n, m' and n' are constants depending upon the system of units employed.

From the experimental standpoint, it is simpler to measure and plot the electric potential V (x, y) than the stream function W (x, y). Plotting the electric equipotentials V (x, y) = constant gives in the Type I analogy the equipotential lines φ = constant; and for the Type II analogy, the steamlines ψ = constant. These lines form an orthogonal network in homogeneous media.

Eqn. (6) (or Eqn. (18) for the nonhomogeneous case) is not sufficient in itself to determine the unknown function φ. Supplementary conditions, usually in the form of boundary conditions, must be added. If these boundary conditions can be satisfied by the electric analogy model, the flow pattern can be ascertained.

Usual boundary conditions fall into one of three categories:

(a) The function φ (x, y) is given on the boundary (the Dirichlet condition).

(b) The normal derivative $\partial \varphi / \partial n$, representing the velocity per-

pendicular to the boundary, is given on the boundary (the Neumann condition).

(c) Both φ and $\partial \varphi / \partial n$ in the form of

$$\varphi + a \frac{\partial \varphi}{\partial n} = b \qquad (24)$$

are given on the boundary (the Fourier, or mixed, condition).

The most common boundary conditions are those in the first two categories. They are particularly simple to reproduce in an electric analogy model when they reduce to the form $\varphi (x, y) = \text{constant}$ or $\frac{\partial \varphi}{\partial n} = 0$. In the case of $\varphi (x, y) = \text{constant}$, the boundary is made of an electrode raised to the corresponding potential $V = \text{constant}$. If $\frac{\partial \varphi}{\partial n} = 0$, corresponding to an impervious boundary in the prototype, an insulating boundary is installed in the model so that no electric current crosses the boundary.

When φ or $\partial \varphi / \partial n$ vary along the boundary, the analog representation of these boundary conditions is somewhat more complicated. The boundary of the model for these cases is usually covered by a large number of small electrodes which are insulated from each other. In the case of Dirichlet conditions, each electrode is raised to a potential V corresponding to the potential φ at the midpoint of that electrode. Thus, the continuous distribution of φ is replaced by a stepwise distribution. In the case of Neumann conditions, each of these electrodes is set to allow a certain current I to flow. The value of I is given by

$$I = - \sigma S \left(\frac{\partial V}{\partial n} \right)_s \qquad (25)$$

where S is the length of the electrode and $\left(\frac{\partial V}{\partial n} \right)_s$ is the average $\frac{\partial V}{\partial n}$ over the length of the electrode.

B. Scales

The main aim of the present work was to map the flow net, composed of equipotential curves φ = constant and streamlines ψ = constant. In order to simplify construction of the model, it was decided to compute rates of flow from the flow net rather than measure electric currents and convert these to rates of flow. Scales for discharge are described in Appendix I.

The two-dimensional flow fields to be studied are nonisotropic and nonhomogeneous. In general, they consist of two layers with different permeabilities. Each layer is nonisotropic; thus the permeabilities K_x, K_y, and K_z in the three coordinate directions x, y, and z, respectively, are different.

Let φ_0 and φ_1 be the lowest and highest potentials in an analogy of Type I. A potential difference $V_1 - V_0$ furnished by an electric current source in the model corresponds to the difference $\varphi_1 - \varphi_0$. It is convenient to express potentials as percentages by installing a potential divider of 100 divisions; the potential difference between terminals $V_1 - V_0 = 100$. From Eqn. (22)

$$\varphi = mV$$

$$\varphi_1 - \varphi_0 = m(V_1 - V_0) = 100\, m$$

and

$$m = \frac{\varphi_1 - \varphi}{100} = \frac{\varphi}{V}$$

Therefore,

$$\varphi = \frac{\varphi_1 - \varphi_0}{100} V \tag{26}$$

or letting $\varphi_0 = 0$,

$$\varphi = \frac{\varphi_1}{100} V \tag{27}$$

Let q_x, q_y, q_z and K_x, K_y, K_z be, respectively, the specific discharges and the permeabilities in the coordinate directions of a homogeneous anisotropic media. From Eqn. (2)

$$q_x = - K_x \frac{\partial \varphi}{\partial x}; \quad q_y = - K_y \frac{\partial \varphi}{\partial y}; \quad q_z = - K_z \frac{\partial \varphi}{\partial z} \tag{28}$$

and, by the continuity equation (Eqn. 5),

$$\text{div } \vec{q} = \frac{\partial q_x}{\partial x} + \frac{\partial q_y}{\partial y} + \frac{\partial q_z}{\partial z} \tag{29}$$

or

$$K_x \frac{\partial^2 \varphi}{\partial x^2} + K_y \frac{\partial^2 \varphi}{\partial y^2} + K_z \frac{\partial^2 \varphi}{\partial z^2} = 0 \tag{30}$$

In an electric analogy model it is convenient to work with isotropic media. It will, therefore, be shown first that an anisotropic system can be made equivalent to an isotropic system by scale distortion.

To facilitate the following discussion, the subscript e will refer to the equivalent system, the subscript p to the prototype, and the subscript r' to the ratio between the two. For prototype conditions Eqn. (27) becomes

$$K_{xp} \frac{\partial^2 \varphi_p}{\partial x^2_p} + K_{yp} \frac{\partial^2 \varphi_p}{\partial y^2_p} + K_{zp} \frac{\partial^2 \varphi_p}{\partial z^2_p} = 0 \tag{31}$$

For the isotropic equivalent system, Eqn. (30) can be written

$$K_e \frac{\partial^2 \varphi_e}{\partial x^2_e} + K_e \frac{\partial^2 \varphi_e}{\partial y^2_e} + K_e \frac{\partial^2 \varphi_e}{\partial z^2_e} = 0 \tag{32}$$

Considering only the two-dimensional case, let

$$x_{r'} = \frac{x_e}{x_p}; \quad y_{r'} = \frac{y_e}{y_p}; \quad \varphi_{r'} = \frac{\varphi_e}{\varphi_p}; \quad K_{xr'} = \frac{K_e}{K_{xp}}; \quad K_{yr'} = \frac{K_e}{K_{yp}} \tag{33}$$

Inserting these values in Eqn. (32) gives

$$\frac{K_{xr'} \varphi_{r'}}{x^2_{r'}} K_{xp} \cdot \frac{\partial^2 \varphi_p}{\partial x^2_p} + \frac{K_{yr'} \varphi_{r'}}{y^2_{r'}} K_{yp} \cdot \frac{\partial^2 \varphi_p}{\partial y^2_p} = 0 \tag{34}$$

By comparing Eqn. (34) with Eqn. (31), the design conditions for the

equivalent system

$$\frac{K_{xr'}\ \varphi_{r'}}{x_{r'}^2} = \frac{K_{yr'}\ \varphi_{r'}}{y_{r'}^2} = a \tag{35}$$

$$\frac{K_{xr'}}{K_{yr'}} \cdot \frac{K_{yp}}{K_{xp}} = \frac{x_{r'}^2}{y_{r'}^2} \tag{36}$$

are obtained. Here $x_{r'}$ and $y_{r'}$ are the horizontal and vertical length scales of the equivalent isotropic system, and a is a constant.

Eqn. (36) shows that an anisotropic system is equivalent to an isotropic system with distorted scales. The equivalent permeability K_e can be determined by considering the flow through an arc with co-ordinate projections Δx_p and Δy_p in an anisotropic flow field. Let the equivalent transformed projections be Δx_e and Δy_e in the isotropic field with the equivalent permeability K_e. The total flow through the given section must be the same in both systems when $\varphi_e = \varphi_p = \varphi$; hence

$$\Delta y_p\ K_{xp}\ \frac{d\varphi}{dx_p} + \Delta x_p\ K_{yp}\ \frac{d\varphi}{d_{yp}} = K_e \left(\Delta y_e \frac{d\varphi}{dx_e} + \Delta x_e \frac{d\varphi}{dy_e} \right) \tag{37}$$

Rewriting Eqn. (36) in the form

$$\frac{\Delta y_e}{\Delta x_e} = \left(\frac{K_{xp}}{K_{yp}}\right)^{\frac{1}{2}} \cdot \frac{\Delta y_p}{\Delta x_p}$$

and inserting into Eqn. (37) yields

$$K_{xp} \frac{\Delta y_p}{\Delta x_p} + K_{yp} \frac{\Delta x_p}{\Delta y_p} = K_e \left(\frac{\Delta y_e}{\Delta x_e} + \frac{\Delta x_e}{\Delta y_e} \right)$$

$$= K_e \left[\frac{\Delta y_p}{\Delta x_p} \left(\frac{K_{xp}}{K_{yp}}\right)^{\frac{1}{2}} + \frac{\Delta x_p}{\Delta y_p} \left(\frac{K_{yp}}{K_{xp}}\right)^{\frac{1}{2}} \right]$$

Multiplying by $\Delta x_p\ \Delta y_p$,

$$K_{xp}\ \Delta y_p^2 + K_{yp}\ \Delta x_p^2 = K_e \left(\frac{K_{xp}}{K_{yp}}\right)^{\frac{1}{2}} \Delta y_p^2 + K_e \left(\frac{K_{yp}}{K_{xp}}\right)^{\frac{1}{2}} \Delta x_p^2$$

$$(K_{xp} \Delta y_p^2 + K_{yp} \Delta x_p^2) \left(1 - \frac{K_e}{\sqrt{K_{xp} K_{yp}}}\right) = 0$$

and finally,

$$K_e = \sqrt{K_{xp} K_{yp}} \tag{38}$$

Similar considerations for a three-dimensional case lead to

$$K_e = \sqrt{K_{xp} K_{yp} K_{zp}/K_o} \tag{39}$$

where K_o is an arbitrary constant having the dimensions of permeability ($L T^{-1}$).

The next step is to transform the isotropic equivalent system into the isotropic model. Let subscript m denote model values and subscript r denote model-prototype ratio. The equivalent permeability is related to that of the model by

$$K_e = C K_m$$

where C defines a scale factor to be selected in designing the model. For an electric analogy K_m is replaced by the conductivity σ, while $\varphi_m = \frac{\varphi_1}{100}$ V.

The model dimensions are obtained from the equivalent system through a scale reduction by a factor μ. Hence:

$$x_m = \mu x_e \; ; \; y_m = \mu y_e ; \; x_{r'} = \frac{x_m}{x_p} \cdot \frac{1}{\mu} = \frac{x_r}{\mu}$$

$$y_{r'} = \frac{y_m}{y_p} \frac{1}{\mu} = \frac{y_r}{\mu}$$

$$K_e = CK_m ; \; K_{xr'} = \frac{K_e}{K_{xp}} = \frac{K_m}{K_{xp}} = CK_{xr}$$

$$K_{yr'} = \frac{K_e}{K_{yp}} = C \frac{K_m}{K_{yp}} = C K_{yr}$$

$$\varphi_r = \varphi_{r'}$$

Inserting these values in Eqns. (35) and (36) yields

$$\frac{K_{xr} \varphi_r}{x_r^2} = \frac{K_{yr} \varphi_r}{y_r^2} = a \tag{40}$$

and

$$\frac{K_{xr}}{K_{yr}} = \frac{K_{yp}}{K_{xp}} = \frac{x_r^2}{y_r^2} \tag{41}$$

Replacing a by $\frac{K_{xm}\varphi_r}{K_o}$, where K_o is an arbitrary constant having the dimensions of permeability ($L\,T^{-1}$), one obtains

$$x_m = \left(\frac{K_o}{K_{xp}}\right)^{\frac{1}{2}} x_p \qquad y_m = \left(\frac{K_o}{K_{yp}}\right)^{\frac{1}{2}} y_p \tag{42}$$

Eqn. (42) indicates that the two steps described above, that is, from an anisotropic prototype to an equivalent isotropic prototype and from an equivalent isotropic prototype to an isotropic model, can be carried out in one step. It shows that the anisotropy in permeability is equivalent to modifying the coordinates of a point in the flow field. By shrinking or expanding the coordinates of an anisotropic prototype according to these equations, an equivalent isotropic system is obtained.

In a three-dimensional case it can be shown that if the square root of each directional permeability is plotted in its corresponding direction at a point of an anisotropic medium, an ellipsoid, designated the ellipsoid of direction (14), is formed.

If K_n is the permeability in direction n making angles θ_x, θ_y, and θ_z with the coordinate axes, then

$$\frac{1}{K_n} = \frac{\cos^2\theta_x}{K_x} + \frac{\cos^2\theta_y}{K_y} + \frac{\cos^2\theta_z}{K_z} \tag{43}$$

and the equation of the ellipsoid is

$$\frac{x^2}{K_x} + \frac{y^2}{K_y} + \frac{z^2}{K_z} = 1 \tag{44}$$

For the two-dimensional case, the ellipsoid reduces to the ellipse shown in Fig. 5, for which

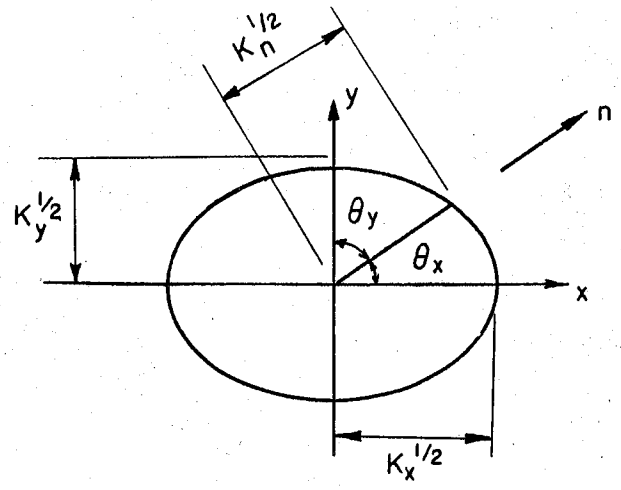

FIG. 5 ELLIPSE OF DIRECTIONAL PERMEABILITIES FOR TWO DIMENSIONAL FLOW

$$\frac{1}{K_n} = \frac{\cos^2 \theta_x}{K_x} + \frac{\cos^2 \theta_y}{K_y} \tag{45}$$

and

$$\frac{x^2}{K_x} + \frac{y^2}{K_y} = 1 \tag{46}$$

In an isotropic medium equipotentials and streamlines form an orthogonal network. For a nonisotropic medium, the equipotentials are conjugate to the streamlines with regard to the ellipse (14). In general, therefore, the potential gradient and the streamlines do not have the same direction.

In the two-dimensional case, let α be the angle between the flow direction and the x-axis and β be the angle between the normal to the equipotential line and the x-axis (Fig. 6). Then

$$q_x = q \cos \alpha = - K_x \frac{\partial \varphi}{\partial x} = - K_x \left(\frac{\partial \varphi}{\partial n} \right) \cos \beta$$

$$q_y = q \sin \alpha = - K_y \frac{\partial \varphi}{\partial y} = - K_y \left(\frac{\partial \varphi}{\partial n} \right) \sin \beta$$

from which it follows that

$$\frac{\tan \alpha}{\tan \beta} = \frac{K_y}{K_x} \tag{47}$$

This equation gives the relation between the direction of the steamlines and equipotentials in a two-dimensional anisotropic system and the ratio of permeabilities in the principal directions of anisotropy.

In addition to being anisotropic, the investigated cross-sections are also nonhomogeneous due to the two layers of different permeability. Fig. 7 shows the case of flow at the boundary of two homogeneous isotropic layers with permeabilities K_1 and K_2. Continuity requires that the flow between the two streamlines be the same in both regions. Therefore,

$$K_1 \frac{\Delta h}{A'B} A A' = K_2 \frac{\Delta h}{A B'} B B'$$

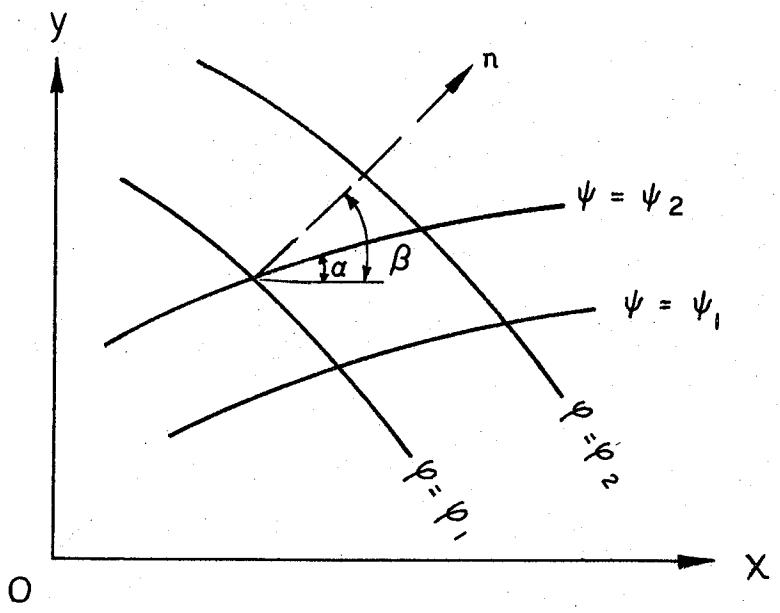

FIG. 6 STREAMLINES AND EQUIPOTENTIAL LINES IN AN ANISOTROPIC SYSTEM

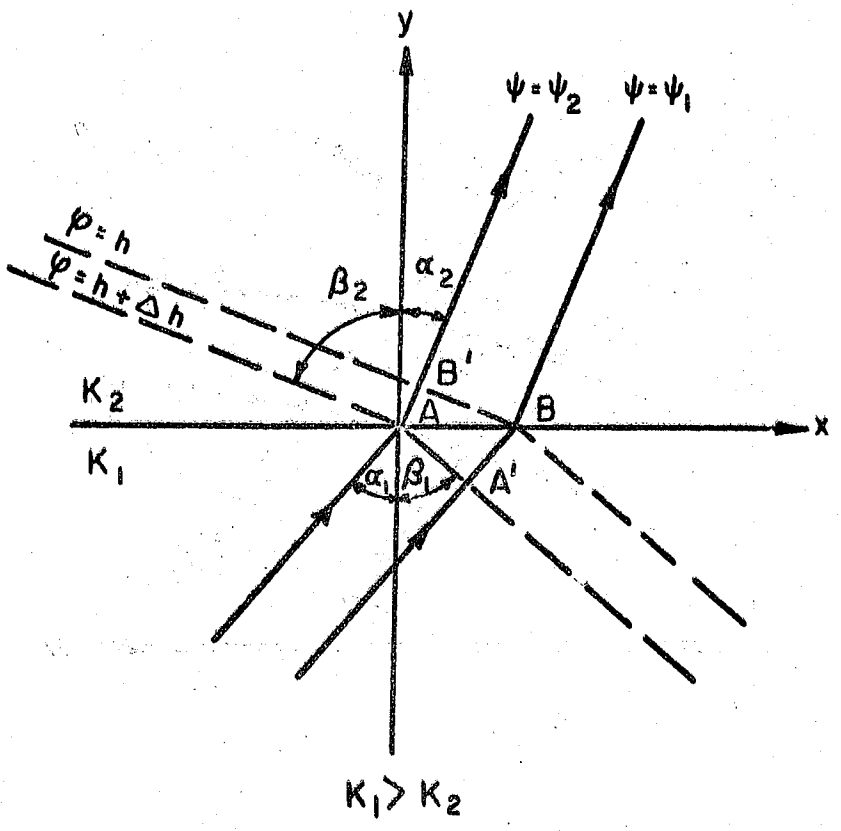

FIG. 7 REFRACTION AT THE BOUNDARY BETWEEN TWO HOMOGENEOUS ISOTROPIC LAYERS

and

$$K_1 \cot \alpha_1 = K_2 \cot \alpha_2$$

or

$$\frac{\tan \alpha_1}{\tan \alpha_2} = \frac{K_1}{K_2} \tag{48}$$

From

$$\alpha_2 + \beta_2 = \alpha_1 + \beta_1 = 90^\circ$$

it follows that

$$\frac{\cot \beta_1}{\cot \beta_2} = \frac{K_1}{K_2} \tag{49}$$

Eqns. (48) and (49) define the refraction of streamlines and equipotential lines, respectively, at a permeability boundary.

When anisotropy is introduced into the layers, the relation given by Eqn. (38) aids in defining the refraction. For two anisotropic layers with permeabilities K_{x1}, K_{y1}, K_{x2}, and K_{y2}, the refraction formula for the transformed system will be

$$\frac{\tan \alpha_1}{\tan \alpha_2} = \frac{\tan \beta_2}{\tan \beta_1} = \left(\frac{K_{x1} K_{y1}}{K_{x2} K_{y2}}\right)^{\frac{1}{2}} \tag{50}$$

Selection of model scales is governed not only by the conversion of anisotropic layers to fictitious isotropic ones, but also by the need to make the individual layers have coincident adjoining boundaries. Consider the example of Fig. 8.

The anisotropy for the lower region is defined by the ellipse O_L with semi-axes $(K_{L1})^{\frac{1}{2}}$ and $(K_{L2})^{\frac{1}{2}}$. The anisotropy for the upper region is defined by the ellipse O_U with semi-axes $(K_{U1})^{\frac{1}{2}}$ and $(K_{U2})^{\frac{1}{2}}$. Let the principal directions of O_U make a 45° angle with the coordinate direction and let those of O_L coincide with the original coordinate directions.

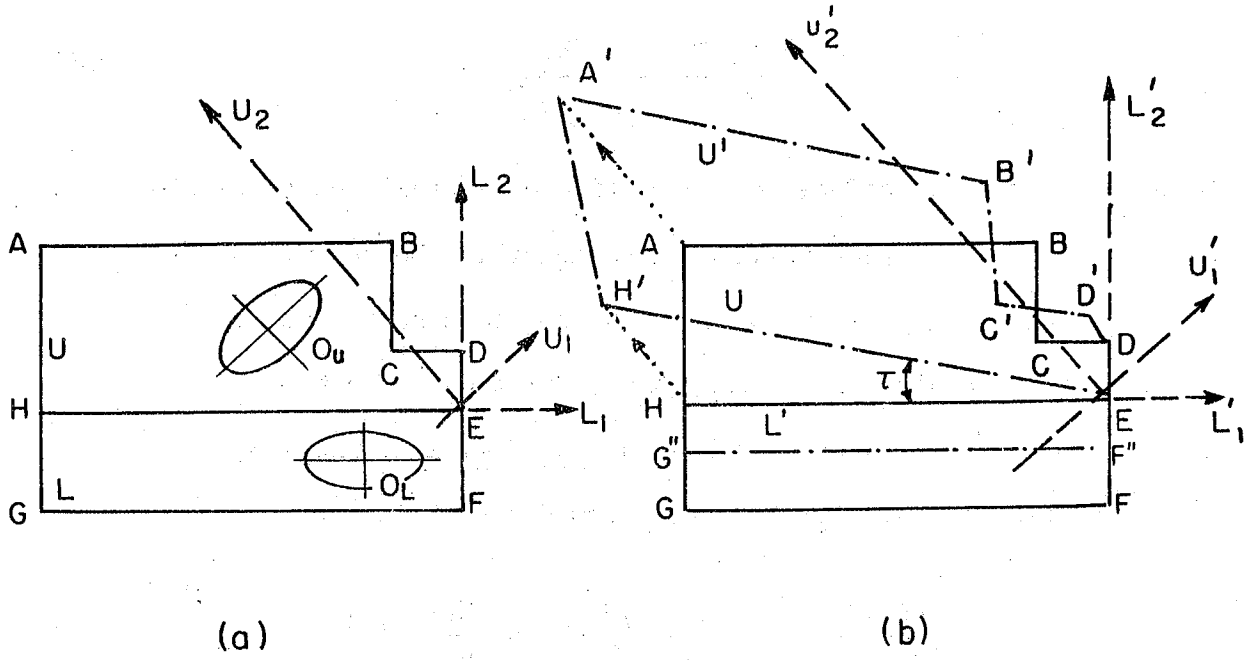

FIG 8 TRANSFORMATION OF AN ANISOTROPIC TWO-LAYER SYSTEM (a) INTO A FICTITIOUS ISOTROPIC TWO-LAYER SYSTEM (b)

In the upper region let E be a fixed point and transform the U_1U_2 plane into a $U_1'U_2'$ plane, according to Eqn. (42) by

$$U_1' = \left(\frac{K_{oU}}{K_{U1}}\right)^{\frac{1}{2}} U_1 \quad ; \quad U_2' = \left(\frac{K_{oU}}{K_{U2}}\right)^{\frac{1}{2}} U_2 \tag{51}$$

By letting $K_{oU} = K_{U1}$, the transformation shifts points only in the U_2 direction. As a result the region ABCDEH is transformed into A'B'C'D'EH' such that every ordinate U_2 becomes

$$U_2' = \left(\frac{K_{U1}}{K_{U2}}\right)^{\frac{1}{2}} U_2 \tag{52}$$

Similarly, for region L, the transformations

$$L_1' = \left(\frac{K_{oL}}{K_{L1}}\right)^{\frac{1}{2}} L_1 \quad ; \quad L_2' = \left(\frac{K_{oL}}{K_{L2}}\right)^{\frac{1}{2}} L_2 \tag{53}$$

are applied. If E is kept fixed again and $K_{oL} = K_{L1}$, then $L_1' = L'$ and the region EFGH is transformed into EF"G"H such that for every ordinate L_2

$$I_2' = \left(\frac{K_{L1}}{K_{L2}}\right)^{\frac{1}{2}} L_2 \tag{54}$$

It can be seen in Fig. 8 that the two transformed regions do not coincide along the common boundary EH. To connect this line, EH' is first rotated through an angle τ, then all dimensions of one region are multiplied by a factor such that the common boundary will have the same length in both regions. This could also be accomplished by selecting K_{oL} such that

$$EH' = \left(\frac{K_{oL}}{K_{L1}}\right)^{\frac{1}{2}} EH \tag{55}$$

The connected transformed isotropic regions now have equivalent permeabilities

$$K_U = (K_{U1}\, K_{U2})^{\frac{1}{2}} \tag{56}$$

and

$$K_L = (K_{L1}\, K_{L2})^{\frac{1}{2}} \tag{57}$$

The flow net can now be determined with aid of an electric analogy, and the results transformed back to the original anisotropic regions.

When the boundary between the two regions is an arbitrary curve, the boundary lines of the transformed regions cannot be made to coincide with one another. However, common points on the boundary can be identified in each transformed region. In an electric model, each transformed region is reproduced separately and the common boundary is composed of many small separate electrodes. If electrodes of corresponding points are connected by conductors having negligible resistance, the flow fields in the two regions can be determined simultaneously.

In the present work the boundary between the two regions is always horizontal and the principal directions of the hydraulic conductivities are horizontal and vertical.

From Eqn. (38)

$$x_{rU}^2 = \frac{K_{oU}}{K_{xU}} \quad ; \quad x_{rL}^2 = \frac{K_{oL}}{K_{xL}}$$

$$y_{rU}^2 = \frac{K_{oU}}{K_{yU}} \quad ; \quad y_{rL}^2 = \frac{K_{oL}}{K_{yL}}$$

hence

$$\frac{x_{rU}^2}{y_{rU}^2} = \frac{K_{yU}}{K_{xU}} \quad ; \quad \frac{x_{rL}^2}{y_{rL}^2} = \frac{K_{yL}}{K_{xL}} \tag{58}$$

By selecting

$$x_{rL} = x_{rU} = x_r \tag{59}$$

the common boundary of each section coincides after transformation. Eqns. (58) and (59) provide the basis for establishing the model

scales and dimensions. An illustrative example of a typical cross-section follows.

Example:

Figure 9a shows the prototype cross-section for Test 4 (see Table II). Given the length of the model to be 5 ft., then the length of 1000 ft. in the prototype establishes

$$x_r = \frac{5}{1000} = \frac{1}{200}$$

From Eqn. (41)

$$y_{rU}^2 = x_r^2 \frac{K_{xU}}{K_{yU}}$$

$$y_{rU} = x_r \left(\frac{K_{xU}}{K_{yU}}\right)^{\frac{1}{2}} = \frac{1}{200}\left(\frac{10}{1}\right)^{\frac{1}{2}} = \frac{1}{63.4}$$

and similarly,

$$y_{rL} = x_r \left(\frac{K_{xL}}{K_{yL}}\right)^{\frac{1}{2}} = \frac{1}{200}\left(\frac{1}{1}\right)^{\frac{1}{2}} = \frac{1}{200}$$

Figure 9b shows the dimensions of the resulting model constructed for Test 4.

The model scales and dimensions selected to carry out the tests listed in Table II are shown in Table III. In all tests $L_m = 5$ ft.

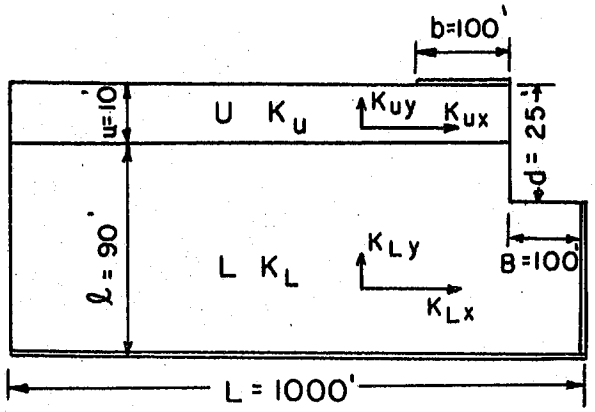

(a) PROTOTYPE

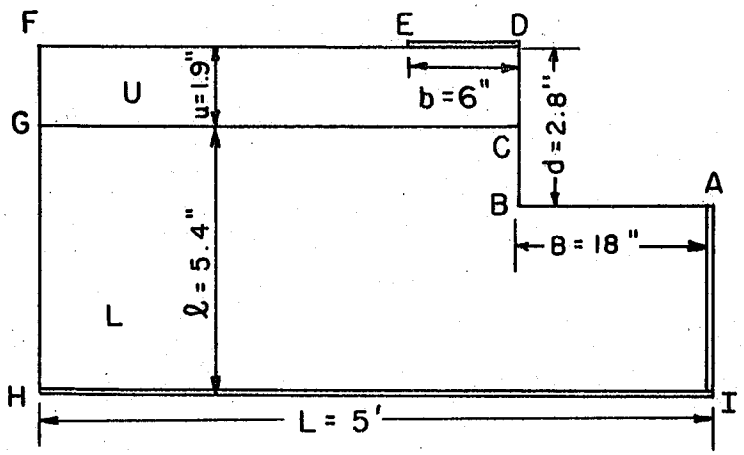

(b) MODEL

FIG. 9 PROTOTYPE AND MODEL DIMENSIONS FOR TEST 4 CROSS-SECTION

Table III - Model Scales and Dimensions

Test Number	X_r	Y_{rU}	Y_{rL}	u_m in.	l_m in.	d_m in.	D_m in.	b_m in.	B_m in.
1	1:200	1:200	-	6.00	0	1.50	6.00	6.00	18.00
2	1:300	1:948	-	12.65	0	3.16	12.65	4.00	12.00
3	1:600	1:60	-	20.00	0	5.00	20.00	2.00	6.00
4	1:200	1:63.4	1:200	1.90	5.40	2.80	7.30	6.00	18.00
5	1:200	1:63.4	1:63.4	1.90	17.05	4.73	18.95	6.00	18.00
6	1:200	1:63.4	1:200	1.90	5.40	2.80	7.30	6.00	18.00
7	1:200	1:20	1:200	6.00	5.40	6.90	11.40	6.00	18.00
8	1:200	1:63.4	1:63.4	1.90	17.05	4.73	18.95	6.00	18.00
9	1:300	1:30	1:94.8	4.00	11.40	5.90	15.40	4.00	12.00
10	1:200	1:200	1:200	1.50	4.50	1.50	6.00	6.00	18.00
11	1:200	1:200	1:63.4	1.50	14.20	1.50	15.70	6.00	18.00
12	1:200	1:63.4	1:200	4.73	4.50	4.73	9.23	6.00	18.00
13	1:200	1:63.4	1:63.4	4.73	14.20	4.73	18.93	6.00	18.00
14	1:200	1:200	1:200	1.50	4.50	1.50	6.00	6.00	18.00
15	1:200	1:63.4	1:200	4.73	4.50	4.73	9.23	6.00	18.00
16	1:200	1:20	1:200	15.00	4.50	15.00	19.50	6.00	18.00
17	1:200	1:200	1:63.4	1.50	14.20	1.50	15.70	6.00	18.00
18	1:200	1:63.4	1:63.4	4.73	14.20	4.73	18.93	6.00	18.00
19	1:300	1:30	1:94.8	10.00	9.50	10.00	19.50	4.00	12.00
20	1:200	1:200	1:200	3.00	3.00	1.50	6.00	6.00	18.00
21	1:200	1:200	1:63.4	3.00	9.50	1.50	12.50	6.00	18.00
22	1:300	1:300	1:30	2.00	20.00	1.00	22.00	4.00	12.00
23	1:200	1:63.4	1:200	9.50	3.00	4.73	12.50	6.00	18.00
24	1:200	1:63.4	1:63.4	9.50	9.50	4.73	19.00	6.00	18.00
25	1:400	1:127	1:40	4.75	15.00	2.38	19.75	3.00	9.00
26	1:200	1:200	1:200	3.00	3.00	1.50	6.00	6.00	18.00
27	1:200	1:63.4	1:200	9.50	3.00	4.73	12.50	6.00	18.00
28	1:300	1:30	1:300	20.00	2.00	10.00	22.00	4.00	12.00
29	1:200	1:200	1:63.4	3.00	9.50	1.50	12.50	6.00	18.00
30	1:200	1:63.4	1:63.4	9.50	9.50	4.73	19.00	6.00	18.00

Table III (cont.)

Test Number	X_r	Y_{rU}	Y_{rL}	u_m in.	l_m in.	d_m in.	D_m in.	b_m in.	B_m in.
31	1:400	1:40	1:127	15.00	4.75	7.50	19.75	3.00	9.00
32	1:200	1:200	1:200	4.50	1.50	1.50	6.00	6.00	18.00
33	1:200	1:200	1:63.4	4.50	4.75	1.50	9.25	6.00	18.00
34	1:200	1:200	1:20	4.50	15.00	1.50	19.50	6.00	18.00
35	1:200	1:63.4	1:200	14.20	1.50	4.73	15.70	6.00	18.00
36	1:200	1:63.4	1:63.4	14.20	4.73	4.73	18.93	6.00	18.00
37	1:300	1:94.8	1:30	9.50	10.00	3.20	19.50	4.00	12.00
38	1:200	1:200	1:200	4.50	1.50	1.50	6.00	6.00	18.00
39	1:200	1:63.4	1:200	14.20	1.50	4.73	15.70	6.00	18.00
40	1:200	1:200	1:63.4	4.50	4.75	1.50	9.25	6.00	18.00
41	1:200	1:63.4	1:63.4	14.20	4.73	4.73	18.93	6.00	18.00
42	1:400	1:40	1:127	22.50	2.37	11.20	24.87	3.00	9.00
43	1:600	1:60	-	20.00	-	10.00	20.00	2.00	6.00
44	1:600	1:60	-	20.00	-	10.00	20.00	2.00	6.00
45	1:600	1:60	-	20.00	-	10.00	20.00	2.00	6.00
46	1:300	1:94.8	-	12.64	-	6.32	12.64	4.00	12.00
47	1:600	1:60	1:60	15.00	5.00	10.00	20.00	2.00	6.00
48	1:600	1:60	1:60	15.00	5.00	10.00	20.00	2.00	6.00
49	1:600	1:60	1:60	5.00	15.00	10.00	20.00	2.00	6.00
50	1:600	1:60	1:60	5.00	15.00	10.00	20.00	2.00	6.00
51	1:600	1:60	-	20.0	-	0	20.00	2.00	6.00
52	1:300	1:94.8	-	12.65	-	0	12.65	4.00	12.00
53	1:600	1:60	-	20.0	-	20.00	20.00	2.00	(6.00)
54	1:300	1:94.8	-	12.65	-	12.65	12.65	4.00	(12.00)
55	1:300	1:94.8	-	12.65	-	3.16	12.65	4.00	4.00
56	1:300	1:94.8	-	12.65	-	3.16	12.65	4.00	8.00

C. Description of the Model

The electric analogy model for this study consisted of several components, including the electrolytic tank, the electrical circuit, the conducting medium, the analogy boundaries, and the drawing table. A sketch of the assembly is shown in Fig. 10; two photographic views are given by Fig. 11. Individual model components are discussed in the following subsections.

(1) Electrolytic Tank

As the conducting medium was an electrolyte, a large shallow tank was constructed to hold the liquid. The tank was made of $\frac{1}{2}$-inch Lucite plates with dimensions of 25 inches by 60 inches and a depth of 3 inches. The bottom was plane and was levelled to insure a uniform depth of electrolyte.

In all tests the maximum length of the tank was utilized. It was found that making a test of the largest possible size in the model minimized inaccuracies and boundary errors.

(2) Electrical Circuit

The electric circuit for the model is shown in Fig. 12. A 60-cycle alternating current was connected to the electrolytic tank. The voltage was reduced by a transformer from 110 volts to 12.6 volts to avoid dangerous voltages and heating of the electrolyte. The potential divider is a 2000 ohm precision Helipot which can accurately divide the voltage into 1,000 subdivisions.

Visual identification of the potential at the probe position in the tank was obtained with a cathode ray oscilloscope (RCA Model 158, 5 inch) connected to the probe and the Helipot. The amplitude of the sinusoidal wave on the oscilloscope screen decreased as the probe approached a preset potential; when the wave was reduced to a horizontal

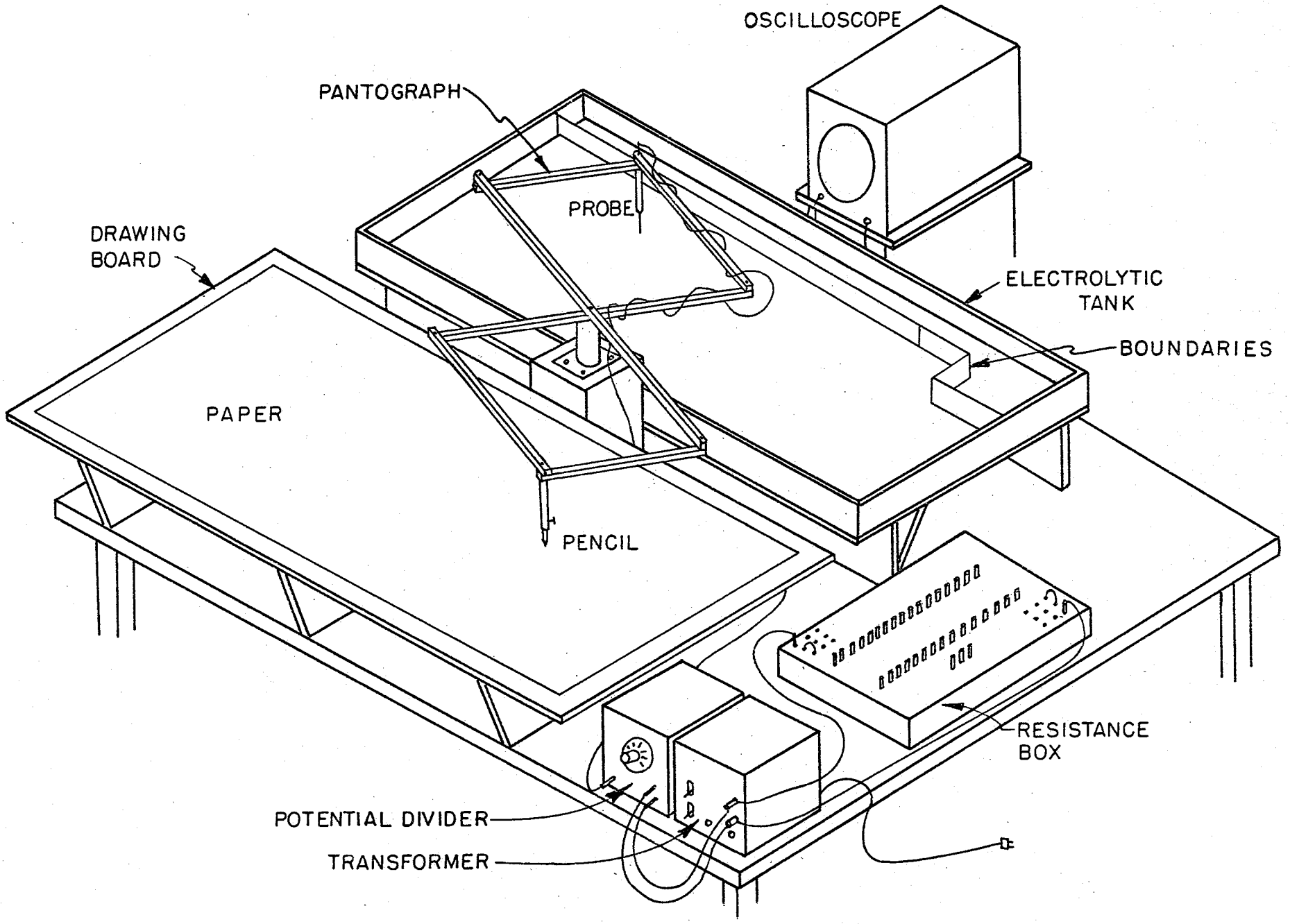

FIG.10 SCHEMATIC VIEW OF THE ELECTRIC ANALOGY MODEL

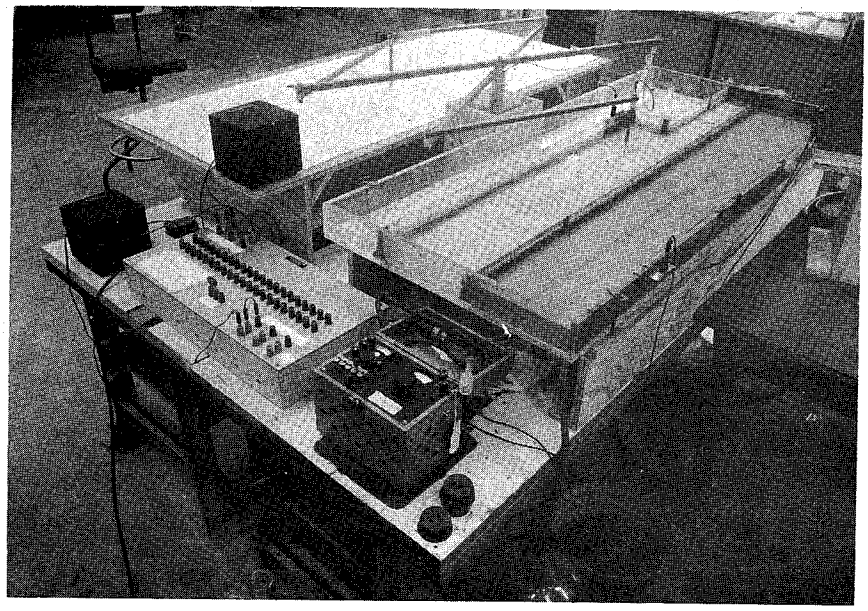

(a)

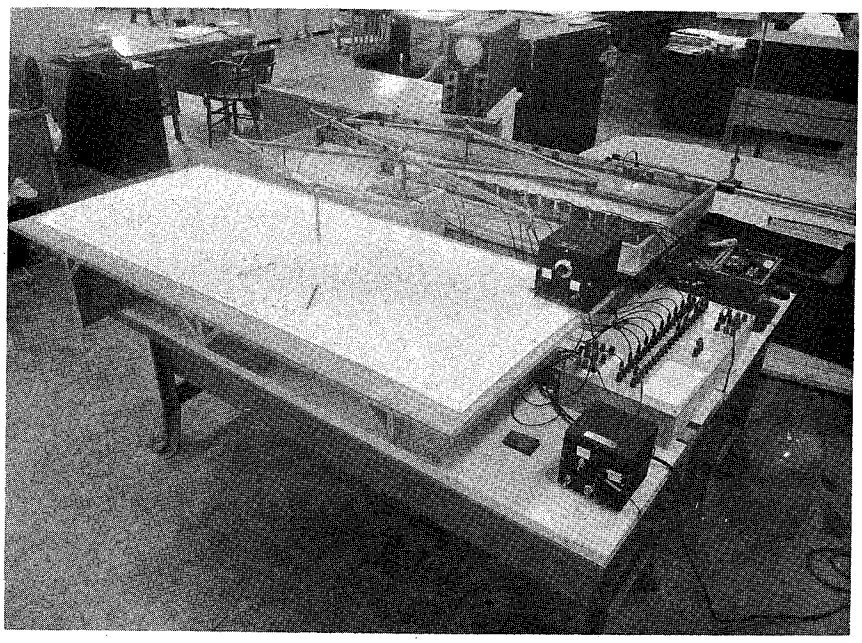

(b)

FIG.11 TWO VIEWS OF THE ELECTRIC ANALOGY MODEL

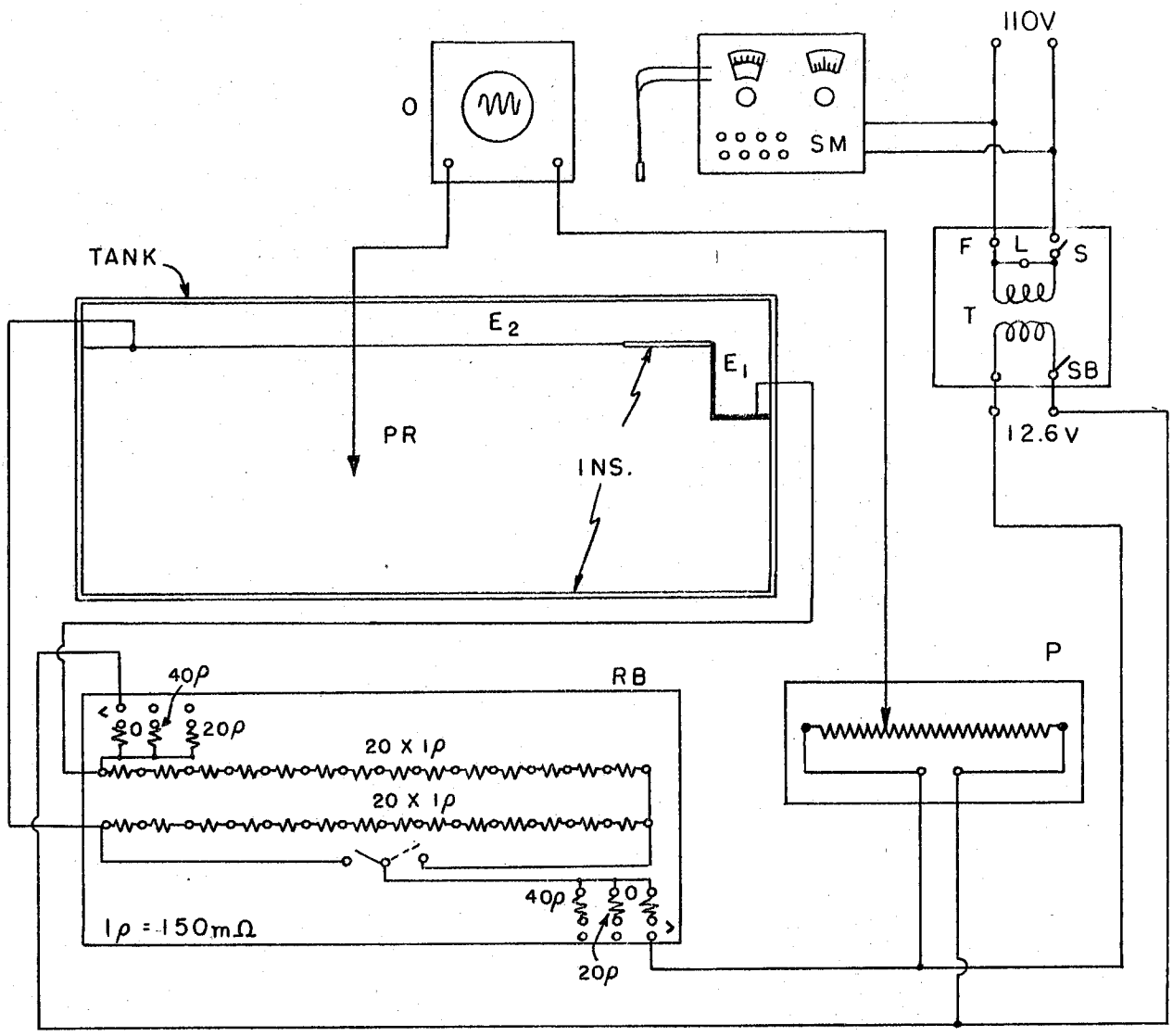

LEGEND

T TRANSFORMER
SM SALINITY METER
SB STANDBY SWITCH
F FUSE
L LAMP
S SWITCH
P POTENTIAL DIVIDER
RB RESISTANCE BOX
INS. INSULATING BOUNDARY
E_1 E_2 ELECTRODES
PR PROBE
O OSCILLOSCOPE

FIG. 12 ELECTRIC CIRCUIT FOR THE ELECTRIC ANALOGY MODEL

line, the probe was on the desired potential. In this position there was no potential difference between the probe and the potentiometer; hence no current flowed through the oscilloscope.

The resistance box provided a means for establishing a wide variety of fixed potentials on electrodes in the tank. Most tests required only the limiting potentials of 0 and 100 per cent; but to represent sloping water tables, intermediate potentials with specified differences were necessary. The box contained 40 precision resistors of 150 milliohms each, connected in series. A plug can be connected to the end of each resistance so that potential differences of 2.5 per cent can be obtained. Larger resistances, which can be added at either or both ends of the series, increase the possible combinations of potential ranges and differences. Table IV lists the possibilities.

Table IV - Combinations of Resistances Possible in the Resistance Box

Resistance added at the beginning	Resistance in the main series	Resistance added at the end	Number of outlets	Range (per cent)	Potential increment (per cent)
0	40p*	0	40	0-100	2.5
0	20p	0	20	0-100	5
20p	20p	0	20	50-100	2.5
0	20p	20p	20	0-50	2.5
0	40p	40p	40	0-50	1.25
40p	40p	0	40	50-100	1.25
20p	40p	20p	40	25-75	1.25
40p	40p	20p	40	40-80	1
40p	40p	40p	40	33.3-66.7	0.83

*1p = 150 milliohms

In order to avoid further adjustments when intermediate potentials were being connected to the electrodes in the tank, resistances in the resistance

box were made relatively small as compared to the resistance of the electrolyte in the tank. In this way only very small amounts of current were consumed at the intermediate points on the main line. The deviation by variable current from a linear distribution of potentials along the line was negligible.

(3) Conducting Medium

A weak electrolyte was selected as the conducting medium for these tests. Various concentrations of a copper sulfate solution as well as tap water were employed. Liquid conductors are advantageous when a large number of tests with different boundaries are to be studied. Solutions could be poured into the model readily, and after each test could be drained into storage containers. Also, where a permeability ratio in two layers of 50:1 was under investigation, this difference was obtained by selecting solutions with a corresponding conductivity ratio. Tap water with a resistivity of about 2,000 ohms/cm and a copper sulfate solution with a resistivity of about 40 ohms/cm met the requirements. Conductivities (reciprocals of resistivities) were checked with a conductivity bridge before each test and adjustments were made as necessary. Fig. 13 shows the relation between concentration and conductivity of $CuSo_4$. Liquid depths over the entire cross-section were kept equal to about 2 inches.

With alternating current, copper electrodes, and a copper salt in the tank, no problems of polarization were encountered at the electrode surfaces.

(4) Analogy Boundaries

Three kinds of boundaries were required in the model: permeable and impermeable outer boundaries, and inner boundaries between layers of different permeability. The construction of each is described below.

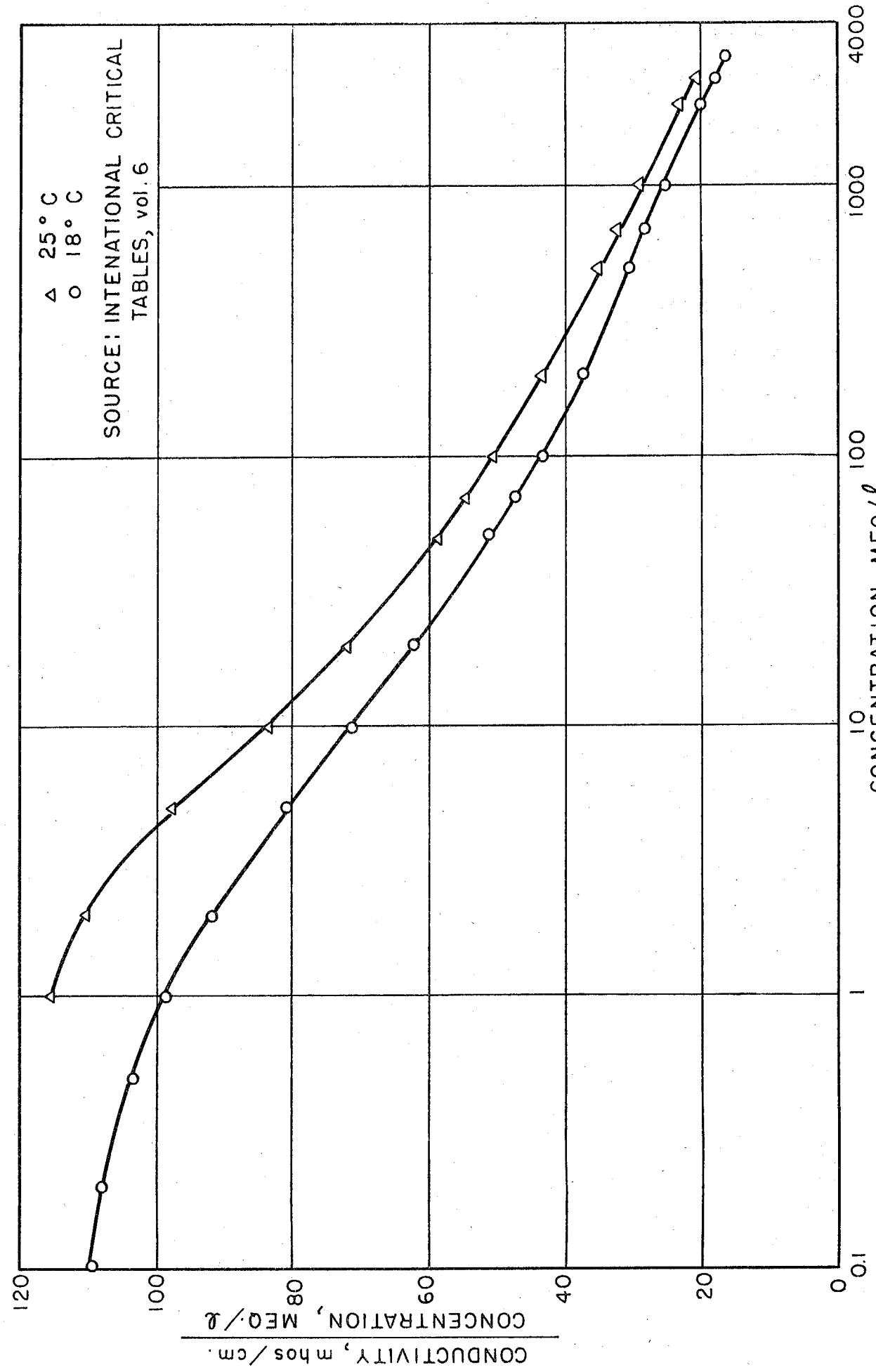

FIG. 13 ELECTRICAL CONDUCTIVITY OF COPPER SULPHATE

Permeable boundaries were made of strips of No. 21 copper 3 inches wide. These were bent to fit the configuration of the boundary and carried a given potential by means of a connection with the resistance box. The strips were held in place at the top by small copper clamps and at the bottom by modeling clay. For boundaries representing sloping water tables, a variable potential was required. Because the pressure is constant (atmospheric) on a water table, the potential is everywhere in proportion to the elevation. Therefore, such a boundary was reproduced by a series of closely spaced copper electrodes (see Fig. 11b), each connected to its corresponding potential in the resistance box. The potentials along the boundary were expressed in percentages of the total head difference between the channel water level and the lowest water table elevation.

Impermeable boundaries were nonconducting strips of Lucite, 3 inches wide by 1/16-inch thick. These were held in place at the bottom by modeling clay. Where an impermeable boundary coincided with an edge of the tank, the Lucite wall of the tank served as the boundary.

The inner boundaries between layers had to provide a waterproof seal between the two liquids, had to conduct electricity freely across it, but each point on a boundary had to maintain a unique potential value. The boundary was constructed by modifying a procedure first suggested by Vreedenburgh and Stevens (27, 32). Lucite strips, 3 inches wide by 1/16-inch thick, were notched and perforated at 3/16-inch intervals. A short length of 1 mm diameter copper wire was inserted in each hole and bent so that the ends crossed in the notch above. Fig. 14 shows a photograph of a short section of the boundary. The boundary was held in place by modeling clay at the bottom. Thus, the Lucite and clay furnished the waterproof boundary, and the individual copper loops pro-

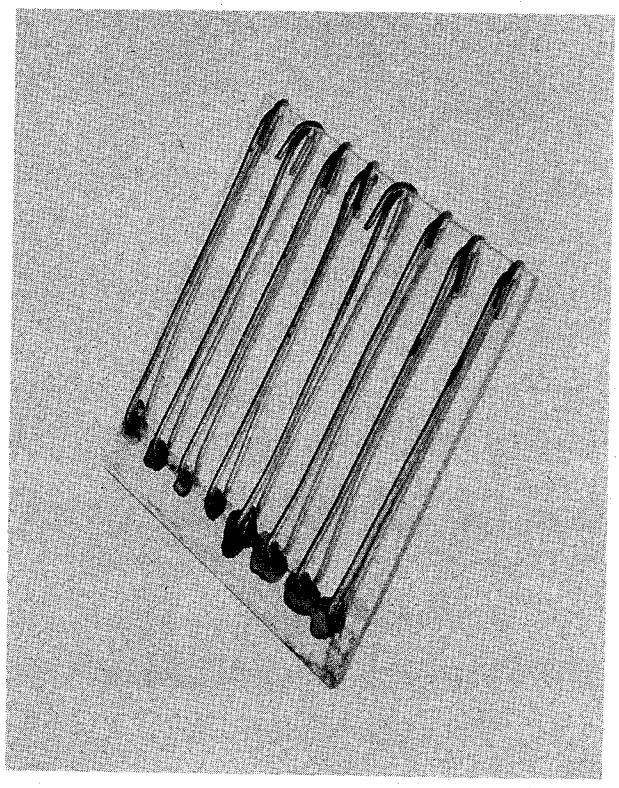

FIG. 14 PHOTOGRAPH SHOWING A SECTION OF AN INNER BOUNDARY BETWEEN LAYERS OF DIFFERENT PERMEABILITY IN THE MODEL

vided for the passage of current through but not along the boundary.

Outer boundaries were interchanged during each test. As described previously, electrodes on permeable boundaries enabled equipotential lines of electricity and flow to be sketched. Placing electrodes on impermeable boundaries allowed streamlines to be located. Variable potential boundaries could be interchanged only after computing the redistribution of potentials along such boundaries.

(5) Drawing Table

The drawing table can be seen in Figs. 10 and 11. A pantograph held the electrical probe at one end and a pencil at the other end. Movement of the probe was recorded on a drawing paper at a 1:1 scale. Whenever a point on a desired equipotential line was located by a zero indication on the oscilloscope, the pencil was depressed to leave a mark on the drawing paper. By connecting points of the same equipotential, each equipotential line was obtained. Sketching time for one set of lines of a cross-section amounted to about 30 minutes.

D. Flow Net

(1) General

As already mentioned, the solution of a two-dimensional seepage problem in an isotropic homogeneous region requires finding the potential function $\varphi(x, y)$ and the stream function $\psi(x, y)$ which are related to each other by the conditions

$$\frac{\partial \varphi}{\partial x} = \frac{1}{K} \frac{\partial \psi}{\partial y}$$

$$\frac{\partial \varphi}{\partial y} = -\frac{1}{K} \frac{\partial \psi}{\partial x}$$

and which satisfy the Laplace equations

$$\nabla^2 \varphi = 0 \quad \text{and} \quad \nabla^2 \psi = 0$$

The curves $\varphi(x,y)$ = constant and $\psi(x,y)$ = constant form two orthogonal families of curves which together form the flow net. Each two neighboring streamlines form a flow channel, in which the amount of flow is equal to the difference between the two ψ values of the corresponding streamlines. Usually a flow net is constructed with an integer number of flow channels, each transmitting the same amount of flow. Similarly, the number of equipotential lines is chosen such that the drop of head between adjacent ones will be the same throughout.

If H = total loss of head,

N_e = number of equipotential drops ΔH, and

N_s = number of stream channels with a flow rate ΔQ in each,

then by Darcy's law

$$\Delta Q = K \frac{\Delta H}{b} \; a \cdot 1$$

$$\frac{Q}{N_s} = K \frac{H}{N_e} \frac{a}{b}$$

or

$$\frac{a}{b} = \frac{Q}{KH} \frac{N_e}{N_s} \tag{60}$$

The quantities a and b are spacings defined in Fig. 15. The ratio $\frac{a}{b}$ remains constant throughout any homogeneous isotropic region. Sometimes N_s and N_e are chosen such that a = b. The flow net for these cases is composed of "squares" and the total flow per unit length of channel is given by

$$Q = KH \frac{N_s}{N_e} \tag{61}$$

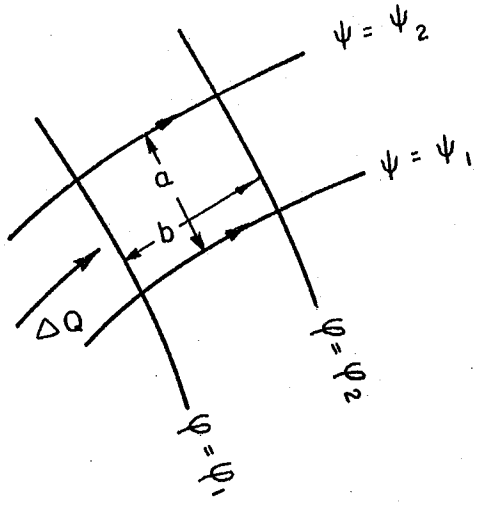

FIG. 15 DEFINITION SKETCH OF AN ELEMENTAL RECTANGLE IN A FLOW NET

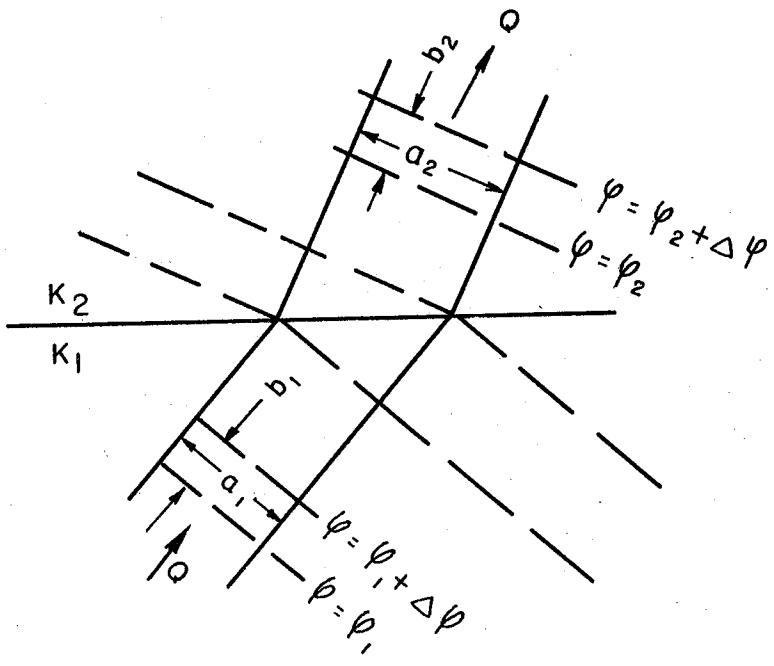

FIG. 16 MODIFICATION IN a AND b IN CROSSING A BOUNDARY OF PERMEABILITY

For reasons of simplicity it was decided to draw the flow nets for the present work with $N_e = N_s = 20$. This gave a potential drop between two equipotential lines equal to 5 per cent of the total available head H, and a flow in each flow channel equal to 5 per cent of the total flow from the river. The total flow was given by

$$Q = KH \frac{a}{b} \tag{62}$$

and an average of $\frac{a}{b}$ from several measured "squares" was found sufficient to insure a reliable flow value.

When two layers are present, the ratio $\frac{a}{b}$ is different in each zone. From Fig. 16

$$Q = K_1 a_1 \frac{\Delta \varphi}{b_1} = K_2 a_2 \frac{\Delta \varphi}{b_2}$$

hence

$$\frac{a_1}{b_1} = \frac{K_2}{K_1} \frac{a_2}{b_2} \tag{63}$$

The refraction on the boundary is given by Eqns. (48) and (49).

(2) Equipotential Lines

The Type I analogy was used for drawing equipotential lines. The river bank and bed (ABCD in Fig. 9b) were connected to the 100 per cent electric potential, and the ground water level and the end of the model (EFGH in Fig. 9b) were connected to the 0 per cent electric potential. The impervious base of the levee (ED), the impervious bottom (HI), and the right edge of the model which is a line of symmetry (IA) were made of non-conductive Lucite. From a theoretical standpoint the line FH should have been infinitely distant from the channel, but the error introduced by assuming it to be about 1000-2000 feet from the channel is negligible. For these boundaries and a given K_U/K_L ratio, the equipotentials were drawn.

(3) Streamlines

The Type 2 analogy was used for drawing the streamlines. Boundaries for the equipotential lines were reversed. At the same time the conductivities of the two layers have to be interchanged. This follows from comparing Eqn. (49) with Eqn. (48). The streamlines have to satisfy Eqn. (48), but when they are measured as equipotentials they satisfy Eqn. (49). When K_1 and K_2 are interchanged, the boundary condition given by Eqn. (48) is satisfied.

When more than two layers are present, Eqns. (48) and (49) must be satisfied for the streamlines and for the equipotentials on each boundary, respectively. Let K_1, K_2, K_3 . . . denote the permeabilities of the layers 1, 2, 3, . . . and K_{10}, K_{20}, K_{30}, . . . denote the permeabilities of the same layers when boundaries are interchanged in order to obtain the streamlines. Then because

$$\frac{K_{10}}{K_{20}} = \frac{K_2}{K_1}, \frac{K_{20}}{K_{20}} = \frac{K_2}{K_2}, \frac{K_{30}}{K_{20}} = \frac{K_2}{K_3}, \text{ etc.}$$

it follows that

$$K_{10} : K_{20} : K_{30} : \ldots = \frac{1}{K_1} : \frac{1}{K_2} : \frac{1}{K_3} : \ldots \qquad (64)$$

The flow net drawn directly from the isotropic model is an orthogonal one. The prototype itself is anisotropic; therefore, the actual flow net is not orthogonal. When the drawing is reduced by distorted scales, that is, the horizontal reduction differs from the vertical, the resulting drawing is also a nonorthogonal flow net (see Plates 1-56).

(4) Sloping Water Table

Almost all tests, listed in Table II, have an upper boundary formed by a fixed horizontal water table, the elevation of which was taken as the datum level ($\varphi = 0$). This approximated conditions existing in

fields adjacent to a river where surface drains control the water table. In this way the problem of investigating flow having an unknown phreatic surface was avoided. Such cases can only be studied by trial and error.

However, in some field cases of interest the controlled steady water table is not horizontal, but slopes away from the river with a gradient of from about 1:500 to 1:1500. Tests 43 and 44 were performed with sloping water tables to study these situations. The lowest point of the water table (at a distance of 3000 ft. from the center of the river) was taken as the datum level ($\varphi = 0$). A slope of 1:500 was assumed for the water table, so that the drop equaled $\frac{2600}{500} = 5.2$ ft. In Test 43 it was assumed that this drop represents 30 per cent of the total available head of H ft. or $H = \frac{5.2}{0.3} = 17.35$ ft. In Test 44 it was assumed that the drop of 5.2 ft. represents 60 per cent of the total available head; hence $H = \frac{5.2}{0.6} = 8.68$ ft. Both tests involved a homogeneous anisotropic aquifer with $K_{yp}/K_{xp} = 1:100$. All the prototype dimensions are shown on Fig. 17; other scales and data are given in Tables II and III.

The equipotential lines for Tests 43 and 44 were drawn by the electrical analogy, while the streamlines were drawn by constructing an orthogonal family of curves to the equipotential lines according to the rules of graphical flow net construction (3).

Drawing the streamlines by exchanging boundaries and liquids—as was done in the cases with a horizontal water table—is not possible because the sloping water table is neither a streamline nor an equipotential line. It can, however, be done in an approximate way without resorting to trial and error. The procedure is described in Appendix II.

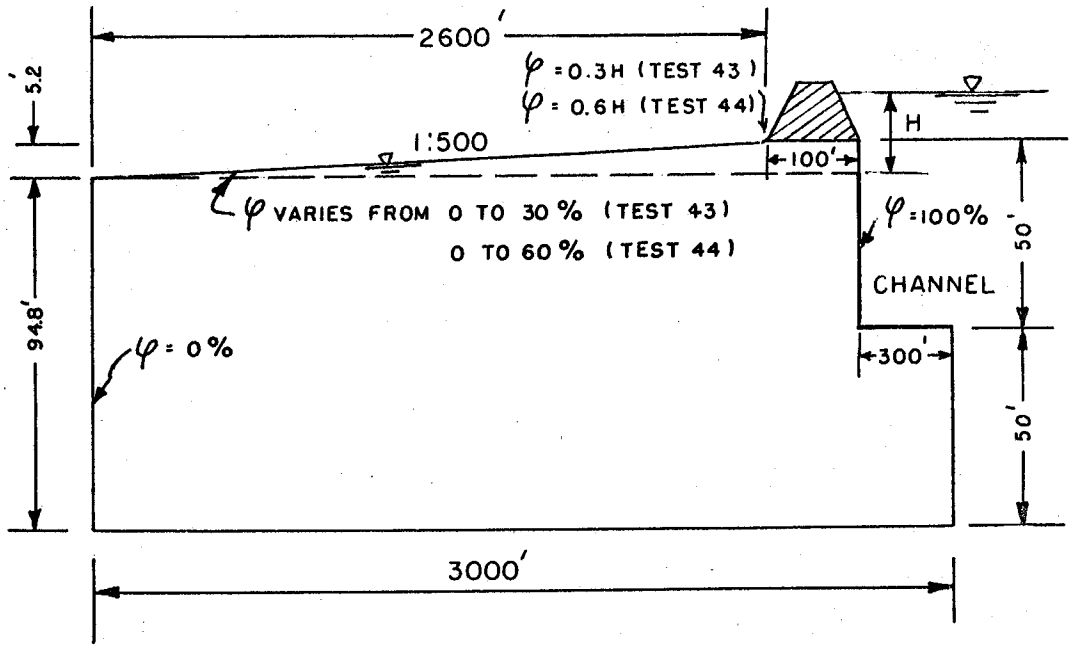

FIG. 17 CROSS SECTION WITH SLOPING WATER TABLE

E. Errors and Limitations

The following limitations of an electric analogy model should be mentioned.

(1) Only steady flows can be investigated.

(2) Flow lines cannot be directly obtained for the more complicated cross-sections, such as those with a sloping water table.

(3) Experiments involving an unknown water table can be investigated only by trial and error.

(4) A sloping water table, which means a continuous drop of potentials in the prototype, can be represented only by a step-like change of potentials in the model where each step represents the average potential in the vicinity.

(5) In some cases, because of the anisotropy ratio, one layer in the model might become too narrow (less than one inch) or it might become wider than the model tray. Such tests cannot be investigated without changing the tray size.

(6) When the boundary between adjacent layers differs from a horizontal line, the transformed boundaries in the model become more complicated and require special construction.

(7) The copper-wound plastic strips representing permeability boundaries in the model introduce errors in the potential distribution near these boundaries. The copper wires act as a line of sinks on one side and as a line of sources on the other side (Fig. 18). It can be shown that the errors depend upon the spacing between the wires and the wire diameter. The effect diminishes rapidly with distance from the boundary, the error being negligible at distances greater than approximately the spacing between the wires.

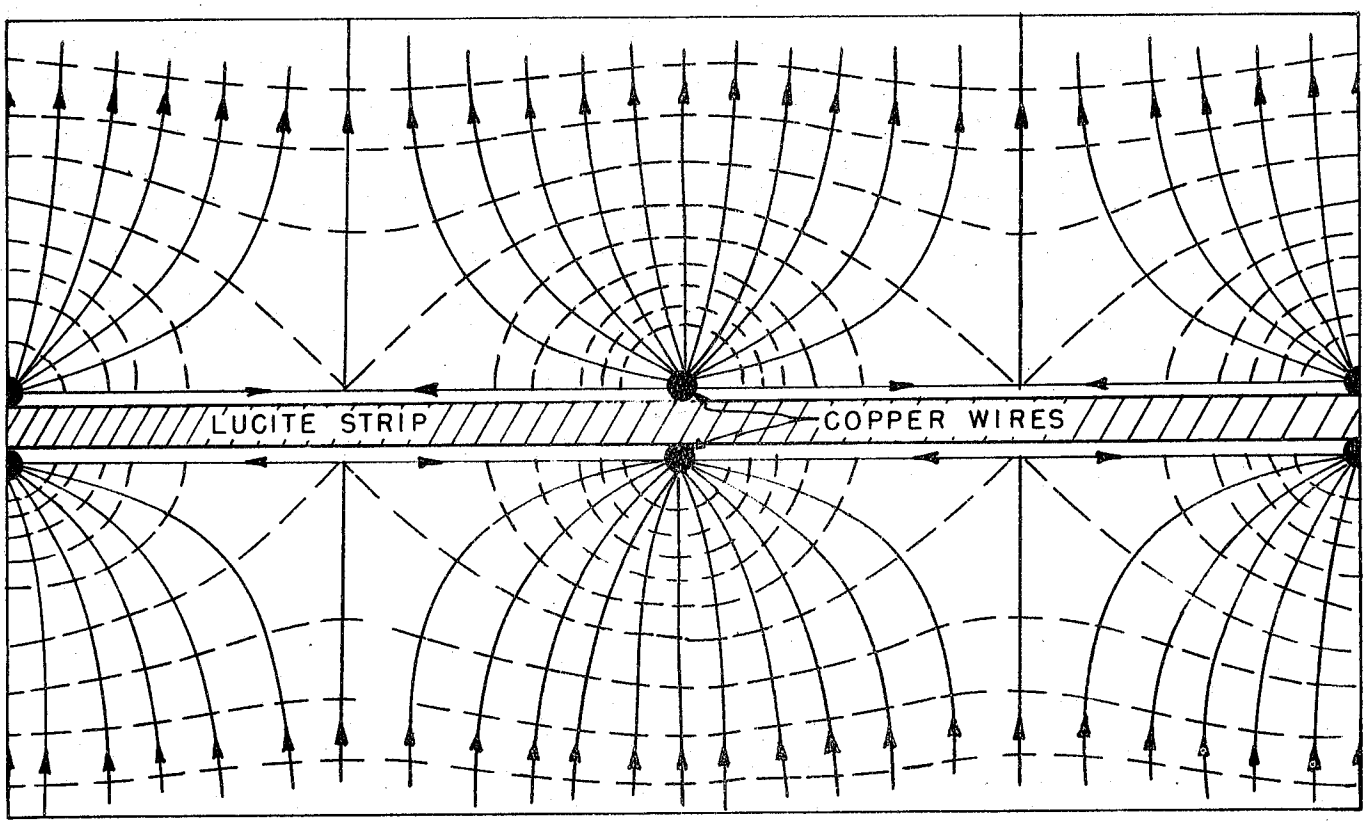

FIG. 18 DETAIL OF THE MODEL INNER BOUNDARY SHOWING MODIFICATION OF STREAMLINES AND EQUIPOTENTIAL LINES

In general, with proper instrumentation, any degree of accuracy can be obtained in an electrolytic model. As the present work is concerned with ground water flow, basic data such as boundaries, permeabilities, and anisotropy ratios are only approximately known. Therefore, a high degree of accuracy was not required in the idealized model cross-sections. Results are estimated to be accurate to within ± 5 per cent.

IV. RESULTS

A. Presentation of Results

In Tables II and III the various prototype conditions studied in the model, together with the model scales and dimensions, were listed. Results of the model tests are summarized in Plates 1-56 and in Tables V and VI. Plate and test numbers are identical. The plates show the flow net for each of the 56 cross-sections. Solid lines are streamlines and dashed lines are equipotential lines. It should be noted that the distortion of scales in reduction of flow nets to plate size results in nonorthogonal flow nets.

Data in Table V summarizes the seepage quantities and distribution for each test. The total seepage factor values were obtained from measured values of $\frac{a}{b}$ in the upper layer, and from Eqn. (62),

$$\frac{Q}{K_U H} = \frac{a}{b} \tag{65}$$

Therefore, the total seepage from one side of the channel for a given cross-section is obtained by multiplying the factor by appropriate values of K_U and H. The percentage of bank seepage gives the fraction of total seepage from the channel that emerges through the vertical side of depth d (Fig. 3). The remaining columns in Table V indicate the distribution of seepage occurring at ground surface as a function of the distance inland from the levee. Thus, in Test 1, 97 per cent of the channel seepage appears at ground surface within the first 250 feet inland from the levee. Blank values indicate values that could not be determined because of limitations of model size.

Table VI lists scales that enable dimensions in Plates 1-56 to be converted to prototype conditions. The columns headed X'_{rU}, Y'_{rU},

and Y'_{rL} give the ratio of the plate length to the prototype distance for the corresponding dimensions. Note that primed values are used to distinguish them from model-prototype scales. No column is necessary for X'_{rL} because $X'_{rU} = X'_{rL}$. The right column of Table VI contains values of α, a dimensionless scaling factor that enables the test data to be extended to other anisotropies of the upper and lower layers. The factor is related to the permeabilities and scales by

$$Y'_{rU} = \alpha X'_{rU} \sqrt{\frac{K_{xUp}}{K_{yUp}}} \tag{66}$$

and

$$Y'_{rL} = \alpha X'_{rL} \sqrt{\frac{K_{xLp}}{K_{yLp}}} \tag{67}$$

An example showing application of the scaling factor appears in a subsequent section.

Table V - Seepage Quantities from Model Tests

Test	Total seepage factor Q/K_UH	Percentage of bank seepage	Percentage of total seepage occurring up to a distance of X ft. from levee			
			X = 250	X = 500	X = 750	X = 1000
1	0.64	50	97	99.5	-	-
2	1.08	60	85	96.5	99	99
3	1.88	73	70	82	89	92.5
4	9.16	41	39	51	-	-
5	21.20	40	17	23.5	-	-
6	0.29	98	99	-	-	-
7	0.68	99	98	99	-	-
8	0.42	97	99	99.5	99.5	99.5
9	0.69	98.8	97.5	97.5	-	-
10	8.45	35	50	65	-	-
11	17.90	10	23	34	-	-
12	8.70	6	25	35	-	-
13	16.20	4	11	13	-	-
14	0.29	90	99	-	-	-
15	0.66	97	99	-	-	-
16	1.17	98	87	97.5	-	-
17	0.34	90	99	-	-	-
18	0.59	97	99	99.5	-	-
19	1.14	99	84	98	99.5	99.5
20	4.60*	10	40	61	-	-
21	6.50	10	20	28	-	-
22	5.35	7	14	21.5	27	31
23	2.85	28	33	42	-	-
24	3.50	20	16.5	19.	-	-
25	3.05	20	18.	22.	25	27
26	0.36	60	99.	99.	-	-
27	0.88	70	93.	98.	-	-
28	1.46	80	75.	90.	95.5	97
29	0.40	55	97.	99.5	-	-
30	0.86	70	91.	99	-	-

* Result questionable.

Table V (cont.)

Test	Total seepage factor $Q/K_U H$	Percentage of bank seepage	Percentage of total seepage occurring up to a distance of X ft. from levee			
			X = 250	X = 500	X = 750	X = 1000
31	1.47	80	75	89	95.5	99
32	2.20	15	50	64	-	-
33	3.50	15	26.5	32.5	-	-
34	3.70	10	12.5	16.5	-	-
35	1.87	37	44.	50.5	-	-
36	2.20	30	27.5	32.5	-	-
37	2.45	30	27.5	31.5	33.5	36
38	0.50	55	99	99	-	-
39	1.03	60	88	96	-	-
40	0.48	60	99	99	-	-
41	0.96	60	88	96	-	-
42	1.71	82	67	84	90	93.5
43	1.55	84	62	73	82	86
44	0.91	79	45	58	64	68
45	2.16	85	63	77	85	90
46	1.22	75	83	96	98	99
47	2.7	64	36	45	51	52
48	1.75	87	64	80	88	92
49	16.1	60	9	13	17	20
50	1.14	99.5	84	96	98	99
51	1.06	0	72	83	90	93
52	0.90	0	84	95	95	95
53	2.03	100	59	74	83	89
54	1.30	100	83	97.5	97.5	97.5
55	1.10	55	87	97.5	97.5	97.5
56	1.15	55	85	98	98	98

Table VI - Scales for Converting Flow Nets of Plates to Prototype Conditions

Test	Scale from plate to prototype			Scale from plate to any prototype
	X'_{rU}	Y'_{rU}	Y'_{rL}	α
1	1:1200	1:240	-	5.00
2	1:1800	1:240	-	2.36
3	1:3600	1:240	-	1.50
4	1:1200	1:92.5	1:292	4.11
5	1:1200	1:240	1:240	1.58
6	1:1200	1:92.5	1:292	4.11
7	1:1200	1:46	1:460	2.61
8	1:1200	1:240	1:240	1.58
9	1:1800	1:925	1:292	1.95
10	1:1200	1:240	1:240	5.00
11	1:1200	1:636	1:202	1.89
12	1:1200	1:117	1:370	3.24
13	1:1200	1:240	1:240	1.58
14	1:1200	1:240	1:240	5.00
15	1:1200	1:117	1:370	3.24
16	1:1200	1:78	1:780	1.54
17	1:1200	1:628	1:199	1.91
18	1:1200	1:240	1:240	1.58
19	1:1800	1:117	1:369	1.54
20	1:1200	1:240	1:240	5.00
21	1:1200	1:500	1:158	2.40
22	1:1800	1:1320	1:132	1.36
23	1:1200	1:158	1:500	2.40
24	1:1200	1:240	1:240	1.58
25	1:2400	1:500	1:158	1.52
26	1:1200	1:240	1:240	5.00
27	1:1200	1:158	1:500	2.40
28	1:1800	1:132	1:1320	1.36
29	1:1200	1:500	1:158	2.40

Table VI (cont.)

Test	Scale from plate to prototype			Scale from plate to any prototype
	X'_{rU}	Y'_{rU}	Y'_{rL}	α
30	1:1200	1:240	1:240	1.58
31	1:2400	1:158	1:500	1.52
32	1:1200	1:240	1:240	5.00
33	1:1200	1:368	1:117	3.26
34	1:1200	1:780	1:78	1.54
35	1:1200	1:199	1:628	1.91
36	1:1200	1:231	1:231	1.64
37	1:1800	1:368	1:117	1.54
38	1:1200	1:240	1:240	5.00
39	1:1200	1:199	1:628	1.91
40	1:1200	1:368	1:117	3.26
41	1:1200	1:240	1:240	1.58
42	1:2400	1:202	1:642	1.19
43	1:3600	1:240	-	1.50
44	1:3600	1:240	-	1.50
45	1:3600	1:240	-	1.50
46	1:1800	1:240	-	2.37
47	1:3600	1:240	1:240	1.50
48	1:3600	1:240	1:240	1.50
49	1:3600	1:240	1:240	1.50
50	1:3600	1:240	1:240	1.50
51	1:3600	1:240	-	1.50
52	1:1800	1:237	-	2.40
53	1:3600	1:240	-	1.50
54	1:1800	1:237	-	2.40
55	1:1800	1:237	-	2.40
56	1:1800	1:237	-	2.40

B. Analysis of Results

The seepage flow nets for the cross-sections studied depend upon the following variables:

(1) Channel depth

(2) Channel width

(3) Levee base width

(4) Anisotropy

(5) Arrangement and thickness of layers

(6) Water table slope

From the test results an effort was made to determine the effect of each of these factors on the seepage. Analyses are discussed individually in the following subsections.

(1) Effect of channel depth

An indication of the effect of channel depth can be obtained by comparing Tests 52, 2, 46, and 54 with Tests 51, 3, 46 and 53, respectively. Discharges as $Q/K_U H$ are plotted for these tests against the depth ratio d/D in Fig. 19. In general, the discharge increases with depth, the rate of rise being dependent upon the anisotropy ratio. For an increase in depth ratio of 0.25 to 1.00, the seepage increases 8 per cent for an anisotropy ratio of 1:100. This may be compared to an increase of approximately 45 per cent for an increase of depth ratio from 0 to 0.25. For an anisotropy ratio of 1:10 the increase in discharge is 5 per cent for an increase in depth ratio from 0.25 to 1.00 and the same for an increase in depth ratio from 0 to 0.25.

Analytic evaluations of channel depths d = 0 and d = D are discussed in Appendix III.

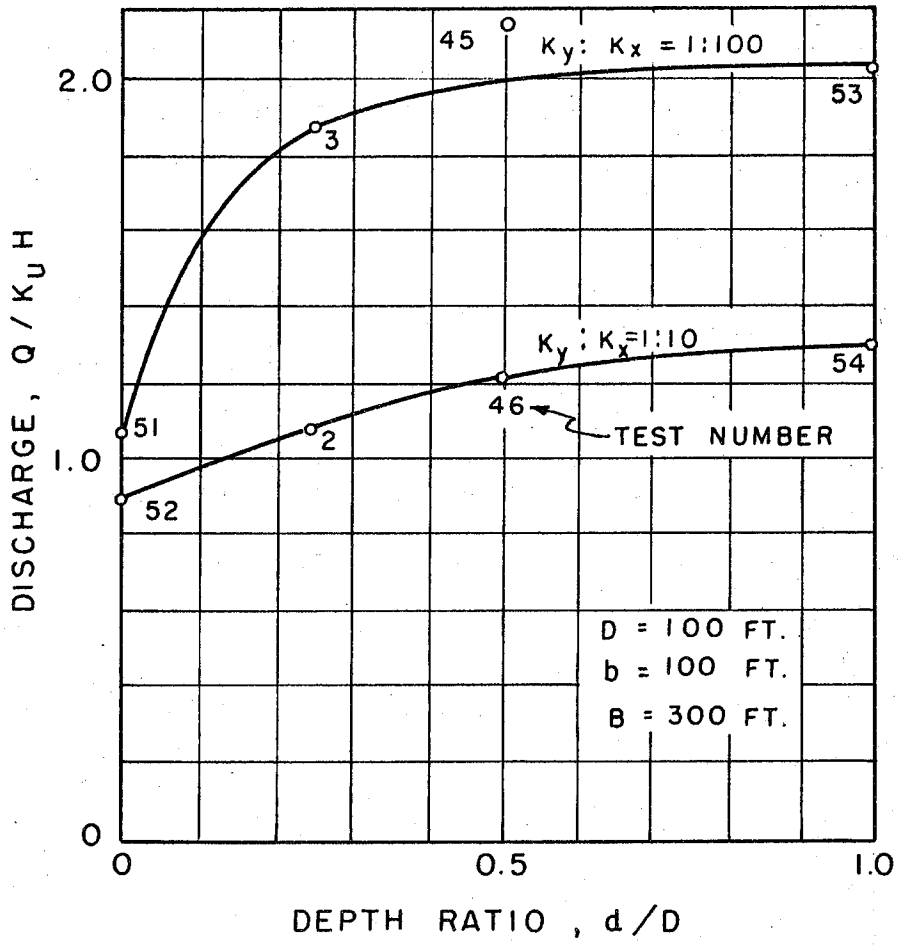

FIG. 19 EFFECT OF CHANNEL DEPTH

(2) Effect of channel width

Most of the tests were performed with the half channel width equal to 300 ft., so that a direct observation as to this effect for the various anisotropy ratios and thicknesses of layers cannot be made. However, it can be seen that a relatively small portion of the total seepage takes place through the channel bottom in all cases where the upper layer is a pervious one not extending appreciably below the channel bottom. Tests 6-9, 14-19, and 26-31 indicate this trend. The variations within each of these groups are due to variations in the anisotropy ratio. Tests 14, 15, 16 and 27-28, among others, show that seepage decreases through the bottom of the channel with a decreasing anisotropy ratio in the upper pervious layer.

In those tests where the bottom of the upper pervious layer extends to well below the channel, the percentage of seepage through the bottom increases up to approximately 50 per cent. The exact percentage depends in each case upon the geometry of the cross-section and the anisotropy ratio. When the upper layer is semipervious, most of the seepage takes place through the bottom (Tests 10-13, 20-25, and 33-37) unless the thickness of this layer is smaller than the depth of the channel (Tests 4 and 5).

The small effect of channel width for the homogeneous anisotropic case can be demonstrated by comparing Tests 2, 55, and 56, having bottom widths of 300, 200, and 100 ft., respectively. The resulting seepage discharges were $Q/K_UH = 1.08$, 1.10, and 1.15, respectively. Similarly, small differences were obtained in the analytic treatment of a zero depth channel, described in Appendix III. Here for a homogeneous isotropic section with $b/D = 1$, $Q/KH = 1.335$, 1.325, and 1.265 for $B = 300$, 200, and 100, respectively (see Fig. III-j).

(3) Effect of Levee Base Width

Because all tests were performed with a levee base width of 100 ft., no conclusions can be drawn as to the effect of this factor. However, for the theoretical case of a channel with zero depth, described in Appendix III, the effect of levee base width was determined (see Fig. III-j). For a given B/D ratio, the discharge decreases with increasing levee base width b/D. This trend is believed to be generally true also for the investigated cross-sections.

(4) Effect of anisotropy

Fig. 20 shows discharge as a function of the anisotropy ratio of the more permeable layer. In general, the seepage rate increases as the anisotropy ratio becomes smaller, that is, as the horizontal permeability becomes increasingly greater than the vertical. This relation holds both for the homogeneous cases (Curve I) and for two layer cases (Curves II, III, and IV).

It is apparent from the flow nets that the flow in the semipervious layer, when it occurs as an upper layer, is mainly vertical so that its anisotropy ratio is unimportant (see, for example, Plates 5, 10, 12, 13, 20, 21, 24, 25, 32, 33, 34, 36). Also, whenever the semipervious layer lies below the pervious one, the flow transmitted through it is very small so that the effect of its anisotropy is again negligible.

The distribution of seepage through the side of the channel depends upon the anisotropy ratio. For both the homogeneous and the layered cases with the more permeable layer on top, the seepage through the banks increases as the anisotropy ratio decreases. When the less permeable layer is on top the seepage through the banks increases with an increase in the anisotropy ratio. These

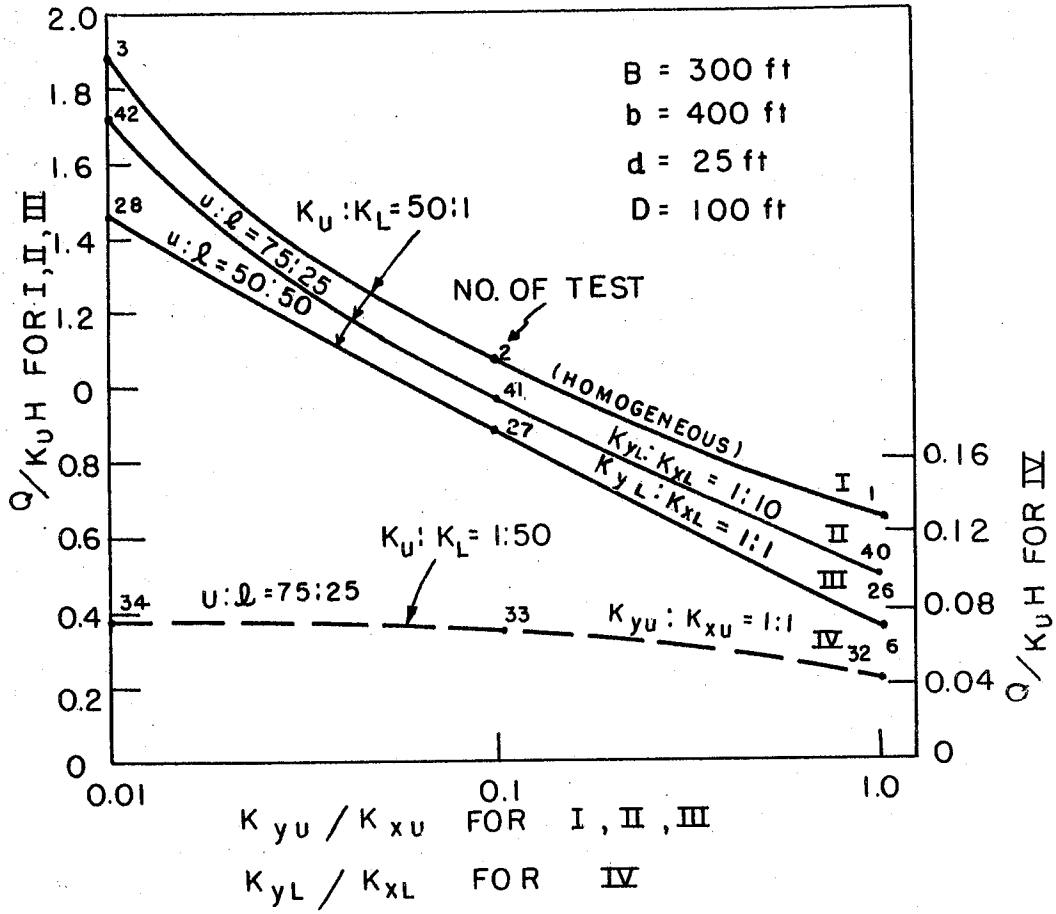

FIG. 20 EFFECT OF ANISOTROPY ON TOTAL SEEPAGE DISCHARGE

trends are shown on Fig. 21. In some cases the effect is negligible.

The distribution of seepage with landward distance from the levee is shown in Fig. 22 for three tests with homogeneous cross-sections and for three tests with isotropic semipervious layers on top. These results verify that seepage is distributed further inland as the anisotropy ratio decreases. Similar effects for an upper more permeable layer can be observed by noting results of Tests 14-19 and 26-31 in Table V.

(5) Effect of Arrangement and Thickness of Layers

In comparing the effect of the position of the relatively permeable layer to that of the relatively impermeable layer, certain observations can be noted. Data from selected pairs of tests, summarized in Table VII, illustrate this effect. In all pairs (except the first), the discharge is greater when the more permeable layer is on top. Also, a greater concentration of seepage appears near the levee, as indicated by the right column of Table VII.

The effect of the relative thicknesses of the two layers is shown in Fig. 23 for selected tests. These show, for different anisotropies, that the discharge decreases as the thickness of an upper permeable layer decreases (Fig. 23a) but the converse is true if the the upper layer is the relatively impermeable one (Fig. 23b).

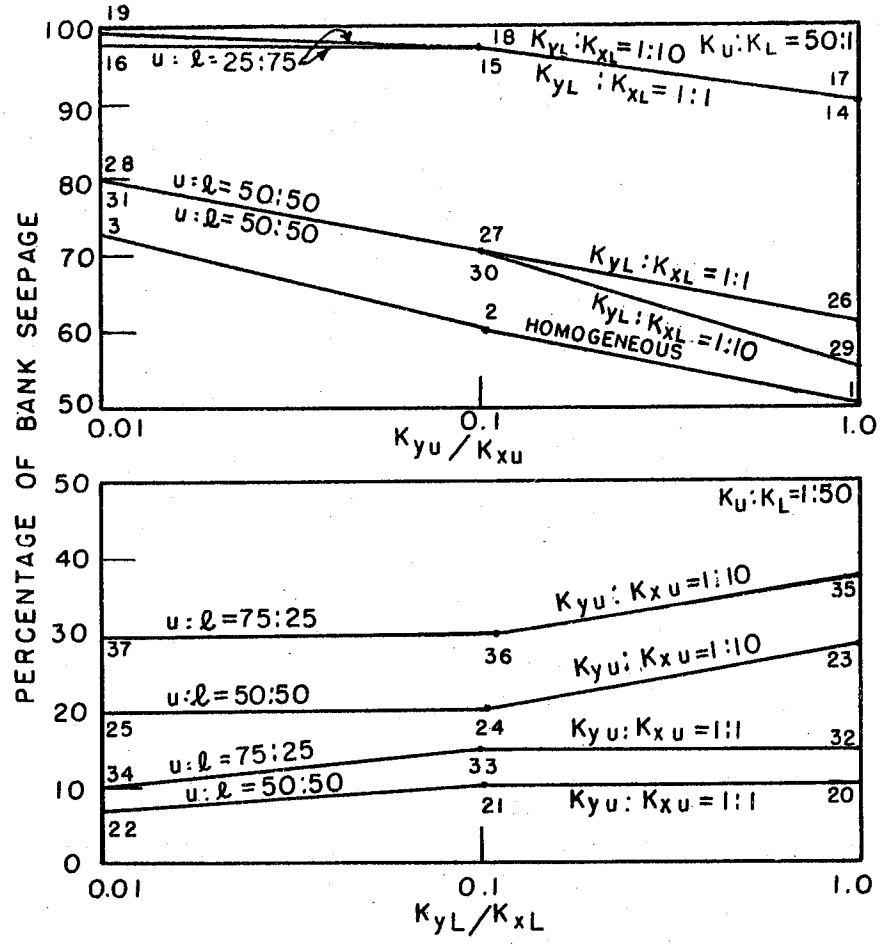

FIG. 21 EFFECT OF ANISOTROPY ON BANK SEEPAGE

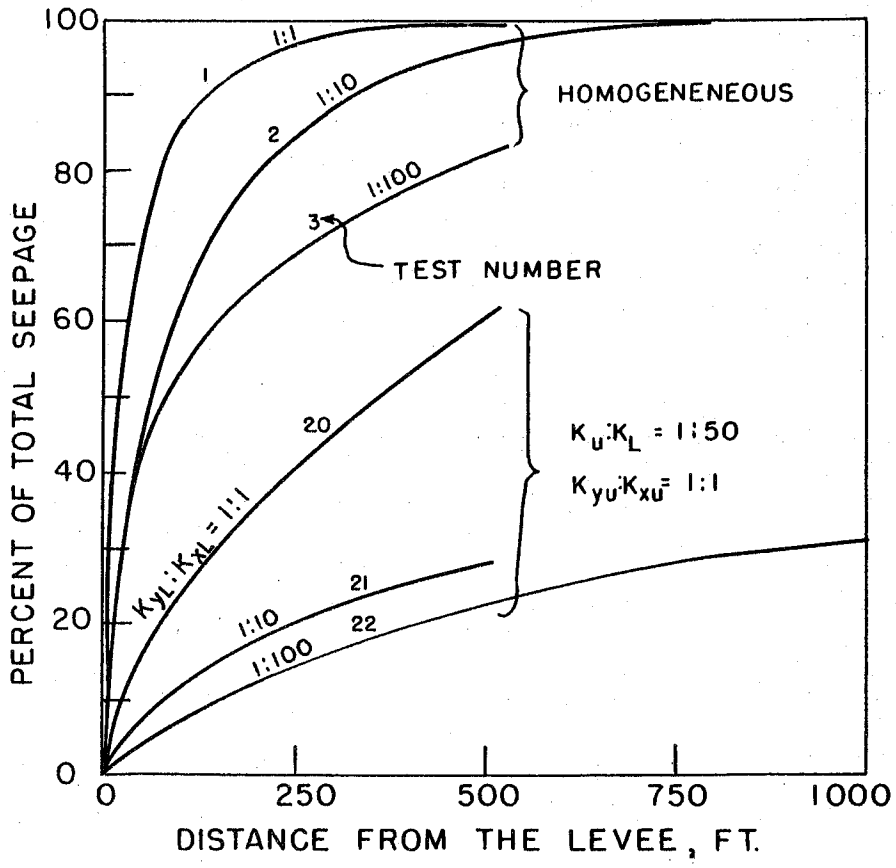

FIG. 22 EFFECT OF ANISOTROPY ON SEEPAGE DISTRIBUTION

Table VII - Test Results Showing Effect of Position of Layers on Seepage

Test	$\frac{U}{L}$	$\frac{K_U}{K_L}$	$\frac{K_{yU}}{K_{xU}}$	$\frac{K_{yL}}{K_{xL}}$	$\frac{Q}{K_U H}$	$\frac{Q}{KH}$ *	Percent of total seepage at X = 250 ft.
5	$\frac{10}{90}$	1:50	1:10	1:10	21.2	0.42	17
8		50:1			0.42	0.42	99
10	$\frac{25}{75}$	1:50	1:1	1:1	8.45	0.17	50
14		50:1			0.29	0.29	99
13	$\frac{25}{75}$	1:50	1:10	1:10	16.20	0.32	11
18		50:1			0.59	0.59	99
20	$\frac{50}{50}$	1:50	1:1	1:1	4.60	0.09	40
26		50:1			0.36	0.36	99
27	$\frac{50}{50}$	1:50	1:10	1:10	3.50	0.07	16.5
30		50:1			0.86	0.86	91
32	$\frac{75}{25}$	1:50	1:1	1:1	2.20	0.04	50
38		50:1			0.50	0.50	99
47	$\frac{75}{25}$	1:50	1:100	1:100	2.7	0.05	36
48		50:1			1.75	1.75	64

* In this column K is the permeability of the more permeable layer.

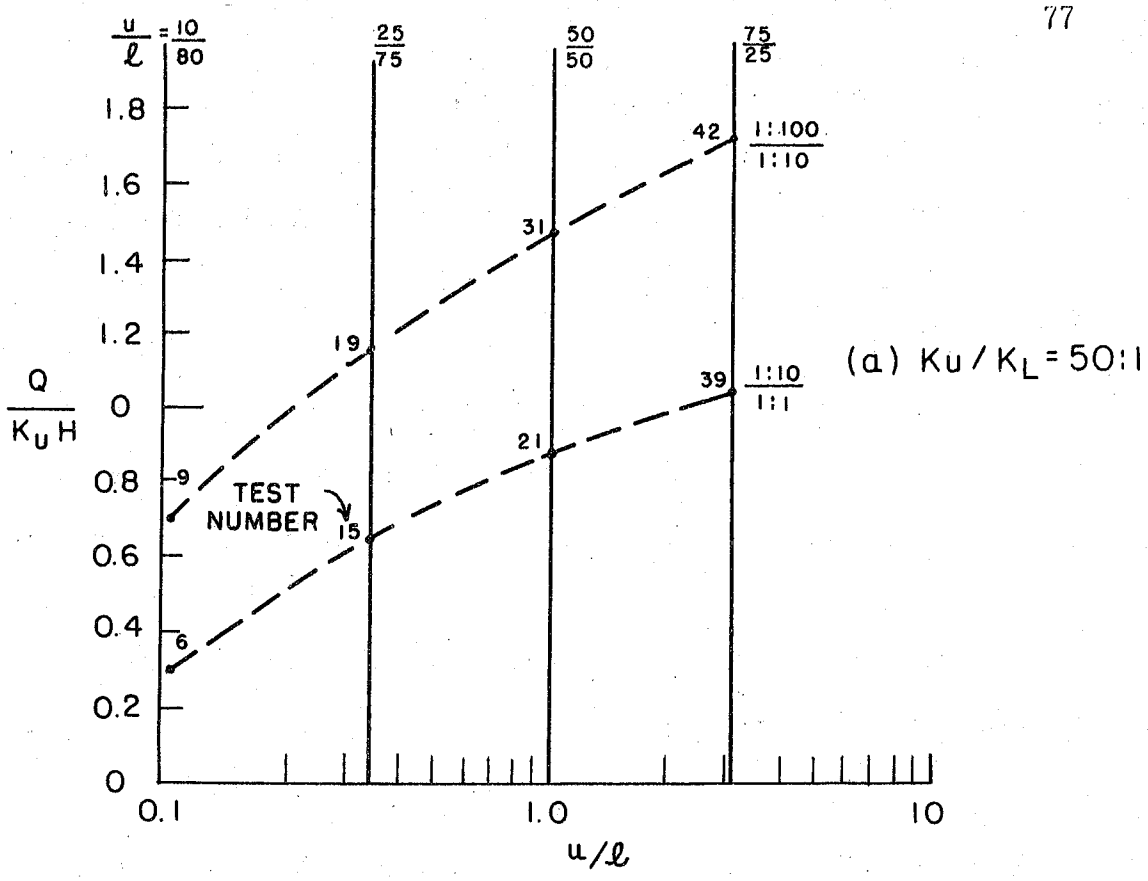

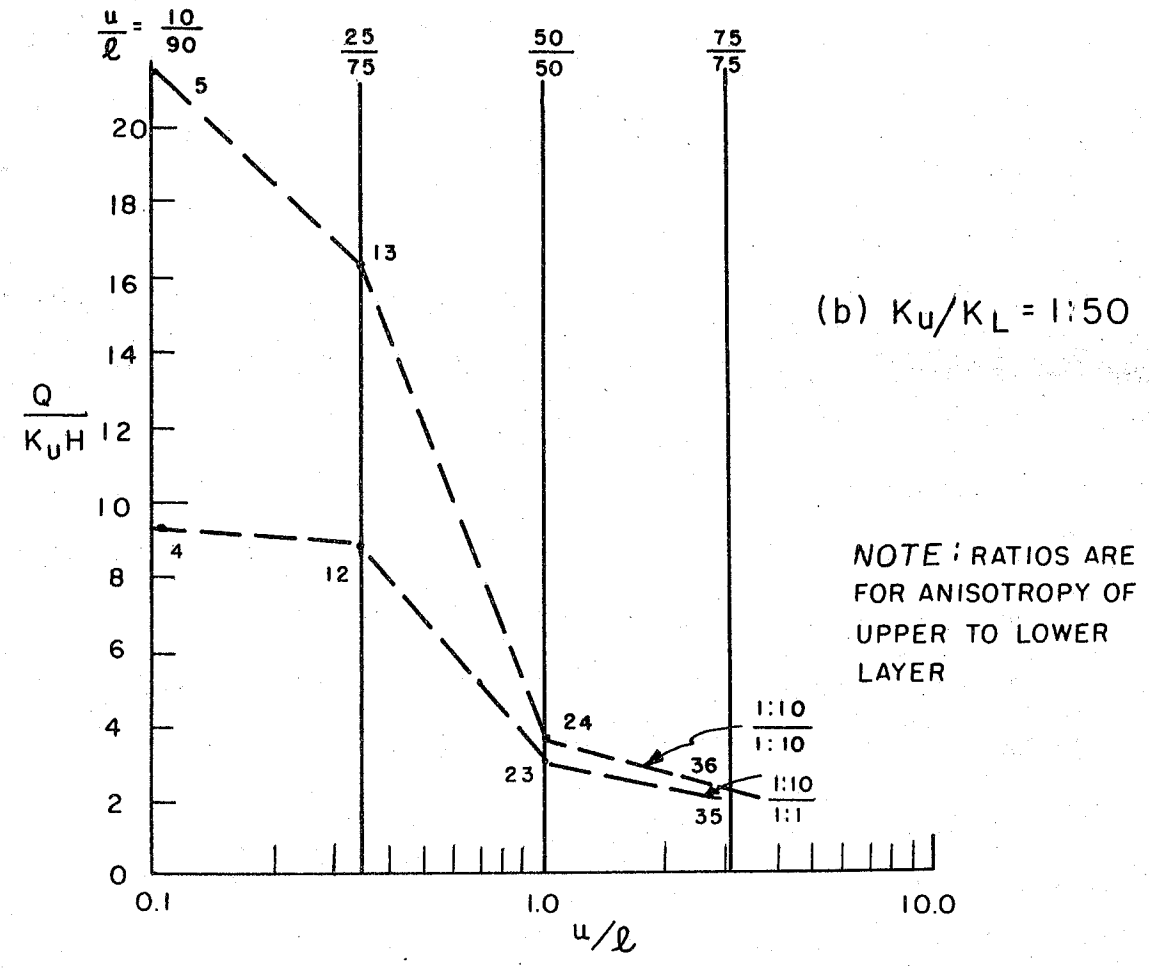

FIG. 23 EFFECT OF THICKNESS OF LAYERS

(6) Effect of Water Table Slope

This effect was studied by Tests 43 and 44. In both cases the water table slope was 1:500, but the total drop (in feet) represented a different percentage of the total head H. In Test 43 the difference of elevation along the slope amounted to 0.3 H, while in Test 44 it was 0.6 H. A direct comparison between Tests 43 and 44 cannot be made; however, individual comparisons are possible between these tests and Test 2, which represents a similar cross-section having a horizontal water table.

The head H in Tests 43 and 44, represented by a 100 per cent electric potential drop in the model, is measured from the lowest point of the slope, whereas in Test 2 it is measured from the toe of the levee. When the head H in Tests 43 and 44 is also measured from the toe of the levee, so as to enable a comparison with Test 2, the total heads represented by the 100 per cent electric potential drop in Tests 43 and 44 become H/0.7 and H/0.4. The resulting discharges are 1.3 KH and 3.88 KH, respectively, as compared to a flow of only 1.08 KH for Test 2.

The slope of the water table also affects the seepage distribution landward from the levee. The seepage is more concentrated near the levee for the horizontal water table with a reduction in concentration as the slope covers a larger portion of the total available head above the lowest point of the slope. Thus, 85 per cent of the seepage appears within 250 feet of the levee in Test 2, while 62 per cent and 45 per cent are the corresponding amounts in Tests 43 and 44, respectively.

C. Example of Seepage Determination for Any Cross-Section

To illustrate the application of the test results to any cross-section, which may only approximate one of the investigated cross-sections, the following example is carried out in detail.

Given: A channel 20 ft. deep and 500 ft. wide intersects permeable strata. The upper layer has a thickness of 15 ft; the lower, a thickness of 50 ft. The upper and lower equivalent permeabilities are 0.04 ft/day and 2.00 ft/day, respectively. The anisotropy of the upper layer, $K_{yU}:K_{xU} = 1:4$; that of the lower layer, $K_{yL}K_{xL} = 1:25$.

Required: To determine the rate and distribution of seepage when the water level in the channel is 10 ft. above the water table. Assume only the first 1000 ft. from the channel center to be important.

From the given data

$$K_U = 0.04 \text{ ft/day} = (K_{xU}K_{yU})^{\frac{1}{2}} = (K_{xU} \cdot \frac{K_{xU}}{4})^{\frac{1}{2}} = \frac{K_{xU}}{2}$$

so that $K_{xU} = 0.08$ ft/day. Similarly,

$$K_L = 2.00 \text{ ft/day} = (K_{xL}K_{yL})^{\frac{1}{2}} = (K_{xL} \cdot \frac{K_{xL}}{25})^{\frac{1}{2}} = \frac{K_{xL}}{5}$$

hence, $K_{xL} = 10$ ft/day.

Prototype data from test cross-sections in Table II are examined to find sections comparable with the above given section. Although none agree exactly (the usual situation), sections for Tests 5, 11, 22, and 25 may be regarded as rough approximations. To determine which cross-section by modification best represents the given one, a computation table, shown below, is prepared. Computations are based on the assumption that the more permeable layer (in this example the lower) governs the seepage. Explanation of each column item follows the table.

1	2	3	4	5	6	7	8	9
Test	U_d, in.	Y'_{rU}	α	X'_r	L_p, ft.	Y'_{rL}	l_d, in.	l_p, ft.
5	0.55	1:328	1.58	1:1040	865	1:132	4.45	48.8
11	0.55	1:328	1.89	1:1240	1032	1:132	4.45	48.8
22	0.45	1:400	1.36	1:1090	908	1:160	4.55	60.6
25	1.20	1:150	1.52	1:456	380	1:60	3.80	19.0

Col. 1: Selected test numbers (plate and test number correspond)

Col. 2: Measure U_d (in inches) from appropriate plate (U is defined in Fig. 3, and the subscript d refers to an actual plate dimension).

Col. 3: Compute Y'_{rU} from $Y'_{rU} = \frac{U_d}{12} \cdot \frac{1}{U_p} = \frac{U_d}{12} \cdot \frac{1}{15}$

Col. 4: Values of α are read from Table VI.

Col. 5: Compute X'_r from $X'_r = Y'_{rU} \frac{1}{\alpha} \sqrt{\frac{K_{yUp}}{K_{xUp}}}$

Col. 6: Compute L_p (in ft.) from $L_p = L_d/X'_r = \frac{10}{12} \cdot \frac{1}{X'_r}$

Col. 7: Compute Y'_{rL} from $Y'_{rL} = \alpha X'_r \sqrt{\frac{K_{xLp}}{K_{yLp}}}$

Col. 8: Measure l_d (in inches) from appropriate plate (see Fig. 3 for definition of l)

Col. 9: Compute l_p (in ft.) from $l_p = \frac{l_d}{12} \cdot \frac{1}{Y'_{rL}}$

Comparing Cols. (6) and (9) with the given data, it is found that Tests 5 and 11 closely fit the given data. The closer correspondence of L_p to 1000 ft. in Test 11 made this the first choice; therefore, Plate 11 with the scales of Cols. (3), (5), and (7) provides a means for mapping the flow net for the given cross-section.

Checking for the width of the channel and the base of the levee:

$$\text{Width of channel} = \frac{2 \times 3 \times 1240}{12} = 620 \text{ ft.}$$

$$\text{Base of levee} = \frac{1 \times 1240}{12} = 103 \text{ ft.}$$

Both results are acceptable. The effect of a small difference in the width of the channel is negligible.

From Test 11, $Q = 17.90\ K_U H$. With $K_U = 0.04$ ft./day and $H = 10$ ft., $Q = 7.16$ ft.^{3}/day/ft. on each side of the channel, or the total discharge per mile of channel is given by

$$Q_T = \frac{7.16 \times 2 \times 5280}{86,400} = 0.87 \text{ cfs.}$$

This example has shown how a test cross-section can be modified to furnish an estimate of the seepage through a given cross-section. The variety of cross-sections tested enables almost any given cross-section which can be treated as a two-layer system to be analyzed. Generally, the procedure requires some judgment and trial-and-error computations to select the most representative cross-section. Small differences of anisotropy, layer thickness, and channel width and depth have minor effects on the seepage, as shown previously by the analysis of results; hence, considering the accuracy of the field data, reasonable estimates of seepage can be obtained.

V. CONCLUSIONS

The model tests demonstrated that steady seepage from a leveed river into adjoining low-lying lands is a function of the permeabilities of the subsurface strata and of the river stage. Effects of channel depth and width on seepage are minor. The greater the base width of an impermeable levee, the less the seepage. It was found that with a smaller anistropy ratio (greater horizontal permeability) the seepage was greater and extended farther inland. Only rough estimates of anisotropy are necessary to define a seepage flow pattern. In two-layered strata, seepage is greater if the more permeable stratum is the upper one and increases with the thickness of the more permeable stratum. With a water table sloping away from the river, the seepage quantity and inland movement increases with slope.

The electric analogy model was found to provide a rapid and versatile means of evaluating seepage under a variety of boundary conditions. The model is general in application, being capable of representing an infinite number of geologic conditions. Only lack of subsurface data precludes analysis of seepage from given cross-sections.

Results of the model tests define seepage for a variety of geologic conditions, particularly those where two strata govern the flow. By means of the dimensionless scaling factor, these results can be modified to furnish good estimates of seepage quantity and distribution for many other cross-sections which only approximate the test conditions. These results should be helpful in solving seepage problems in Sacramento Valley and in other similar areas.

VI. REFERENCES

1. Barron, R. A., The effect of a slightly pervious top blanket on the performance of relief wells, Proc. Second Intl. Conf. on Soil Mech., vol. 4, pp. 324-328, 1948.
2. Bennett, P. T., The effect of blankets on seepage through pervious foundations, Trans. Amer. Soc. Civil Engrs., vol. 111, pp. 215-252, 1946.
3. Casagrande, A., Seepage through dams, Journ. New England Water Works Assoc., vol. 51, pp. 131-172, 1937.
4. Esmiol, E. E., Seepage through foundations containing discontinuities, Proc. Amer. Soc. Civil Engrs., vol. 83, SM1, 19 pp., 1957.
5. Hammad, H. Y., Seepage losses from irrigation canals, Proc. Amer. Soc. Civil Engrs., vol. 85, no. EM2, pp. 31-36, 1959.
6. Harza, L. F., Uplift and seepage under dams on sand, Trans. Amer. Soc. Civil Engrs., vol. 100, pp. 1352-1406, 1935.
7. Jahnke, E., and F. Emde, Tables of functions with formulae and curves, 4th ed., Dover Publ., New York, 382 pp., 1945.
8. Johnson, H. A., Seepage forces in a gravity dam by electrical analogy, Proc. Amer. Soc. Civil Engrs., vol. 81, Sep. 757, 16 pp., 1955.
9. Joint Committee on Water Problems of the California Legislature, Sacramento River seepage and erosion problems, Sixth Partial Report, San Francisco, pp. 22-29, 40-45, 1953.
10. Kabakov, S., Investigation of the Sacramento-San Joaquin Delta--Water supply and water utilization on Medford Island, Rep. 2, California Water Project Authority, Sacramento, 62 pp., 1956.
11. Lane, E. W., Security from under-seepage, masonry dams on earth foundations, Trans. Amer. Soc. Civil Engrs., vol. 100, pp. 1235-1351, 1935.

12. Lane, E. W., F. B. Campbell, and W. H. Price, The flow net and the electric analogy, Civil Engineering, vol. 4, pp. 510-514, 1934.

13. Luthra, S. D. L., and G. Ram, Electrical analogy applied to study seepage into drain tubes in stratified soil, Jour. Central Board Irrig. and Power (India), vol. 11, pp. 398-405, 1954.

14. Maasland, M., Soil anisotropy and land drainage, in Drainage of agricultural lands (J. N. Luthin, editor), Amer. Soc. of Agronomy, Madison, Wis., pp. 216-285, 1957.

15. Malavard, L. C., The use of rheoelectrical analogies in aerodynamics, AGARDograph 18, NATO Advisory Group for Aeronautical Research and Development, Paris, 175 pp., 1956.

16. Mansur, C. I., and R. I. Kaufman, Control of under seepage, Mississippi River levees, St. Louis District, Proc. Amer. Soc. Civil Engrs., vol. 82, Sep. 864, 31 pp., 1956.

17. McClure, C. R., and others, Investigation of the Sacramento-San Joaquin Delta-Ground water geology, Rep. 1, California Water Project Authority, Sacramento, 21 pp., 1956.

18. Middlebrooks, T. A., and W. H. Jervis, Relief wells for dams and levees, Trans. Amer. Soc. Civil Engrs., vol. 112, pp. 1321-1402, 1947.

19. Muskat, M., The flow of homogeneous fluids through porous media, McGraw-Hill, New York, 763 pp., 1937.

20. Pavlovsky, N. N., Motion of water under dams, 1st Congress on Large Dams, Stockholm, vol. 4, pp. 179-192, 1933.

21. Plumb, C. E., and others, Seepage conditions in Sacramento Valley, California Div. of Water Resources, Sacramento, 156 pp., 1955.

22. Reltov, B. F., Electrical analogy applied to three dimensional study of percolation under dams built on pervious heterogeneous foundations, 2nd Congress on Large Dams, Washington, D. C., vol. 5, pp. 73-85, 1936.

23. Scott, V. H., and J. N. Luthin, Investigation of an artesian well adjacent to a river, Proc. Amer. Soc. Civil Engrs., vol. 85, no. IR1, pp. 45-62, 1959.

24. Selim, M. A., Dams on porous media, Trans. Amer. Soc. Civil Engrs., vol. 112, pp. 488-505, 1947.

25. Shea, P. F., and H. E. Whitsett, Predicting seepage under dams on multi-layered foundations, Proc. Amer. Soc. Civil Engrs., vol. 84, no. SM3, 41 pp., 1958; Discussion by H. F. Cedergren, vol. 85, no. SM1, pp. 55-67, 1959.

26. Stevens, O., Discussion of paper by Vreedenburgh, Proc. Intl. Conf. Soil Mech. and Foundation Eng., vol. 3, pp. 165-166, 1936.

27. Stevens, O., Electrical determination of the line of seepage and flow net of a groundwater flow through joint regions with different anisotropy, De Ingenieur in Ned. Indie, vol. 9, pp. 205-212, 1938.

28. Todd, D. K., Ground-water flow in relation to a flooding stream, Proc. Amer. Soc. Civil Engrs., vol. 81, Sep. 628, 20 pp., 1955.

29. Todd, D. K., Ground water hydrology, John Wiley & Sons, New York, 336 pp., 1959.

30. Turnbull, W. J., and C. I. Mansur, Relief well systems for dams and levees, Trans. Amer. Soc. Civil Engrs., vol. 119, pp. 842-878, 1954.

31. Vreedenburgh, C. G. J., On the steady flow of water percolating through soils with homogeneous-anisotropic permeability, Prcc. Intl. Conf. Soil Mech. and Foundation Eng., vol. 1, Harvard Univ., Cambridge, Mass., pp. 222-225, 1936.

32. Vreedenburgh, C. G. J., and O. Stevens, Electric investigation of underground water flow nets, Proc. Intl. Conf. Soil Mech. and Foundation Eng., vol. 1, Harvard Univ., Cambridge, Mass., pp. 219-222, 1936.

PLATE 1

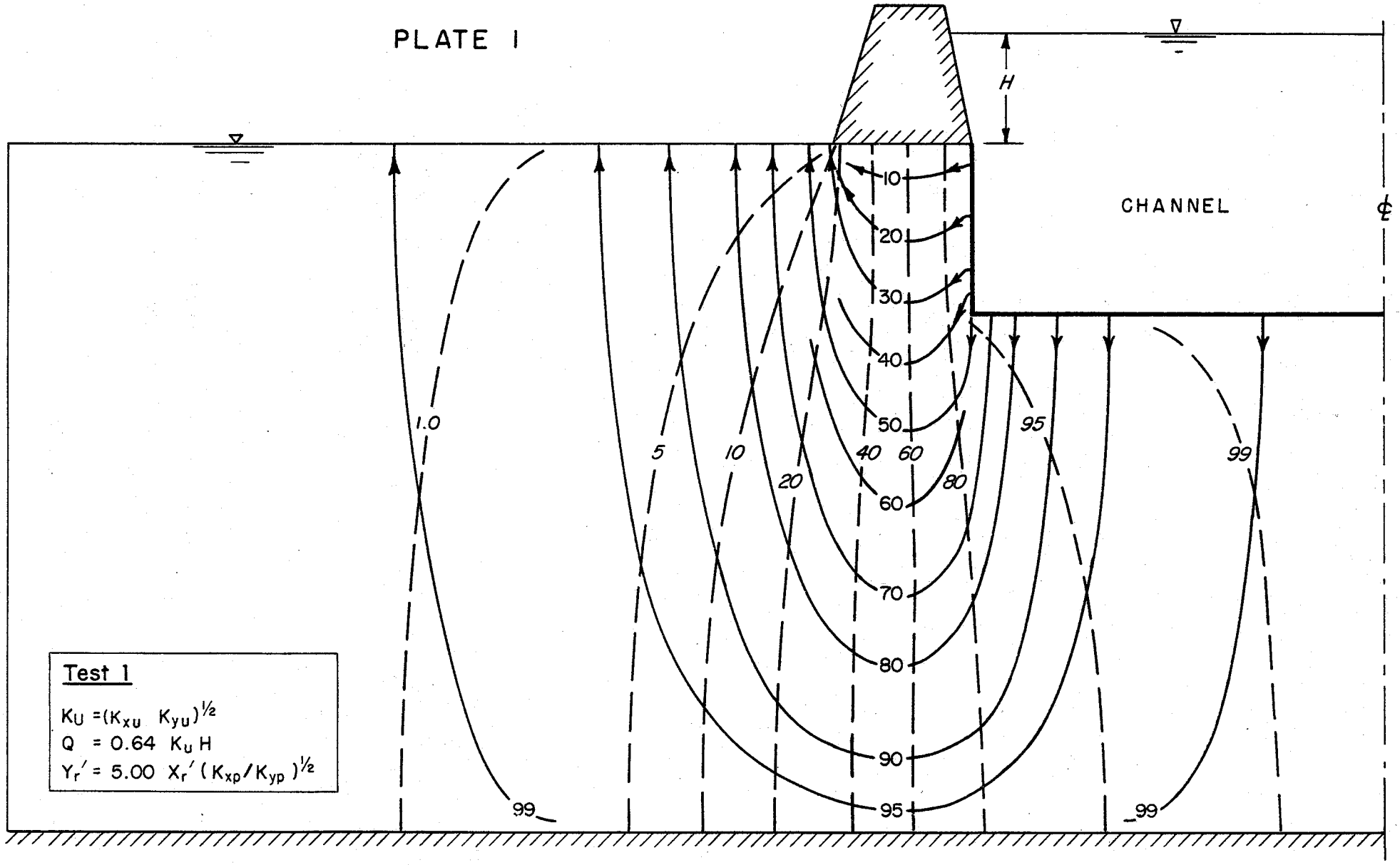
H
CHANNEL
℄
10
20
30
40
50
60
70
80
90
95
99
1.0
5
10
20
40
60
80
95
99
99
Test 1
$K_U = (K_{xu}\ K_{yu})^{1/2}$
$Q = 0.64\ K_u\ H$
$Y_r' = 5.00\ X_r'\ (K_{xp}/K_{yp})^{1/2}$

PLATE 2

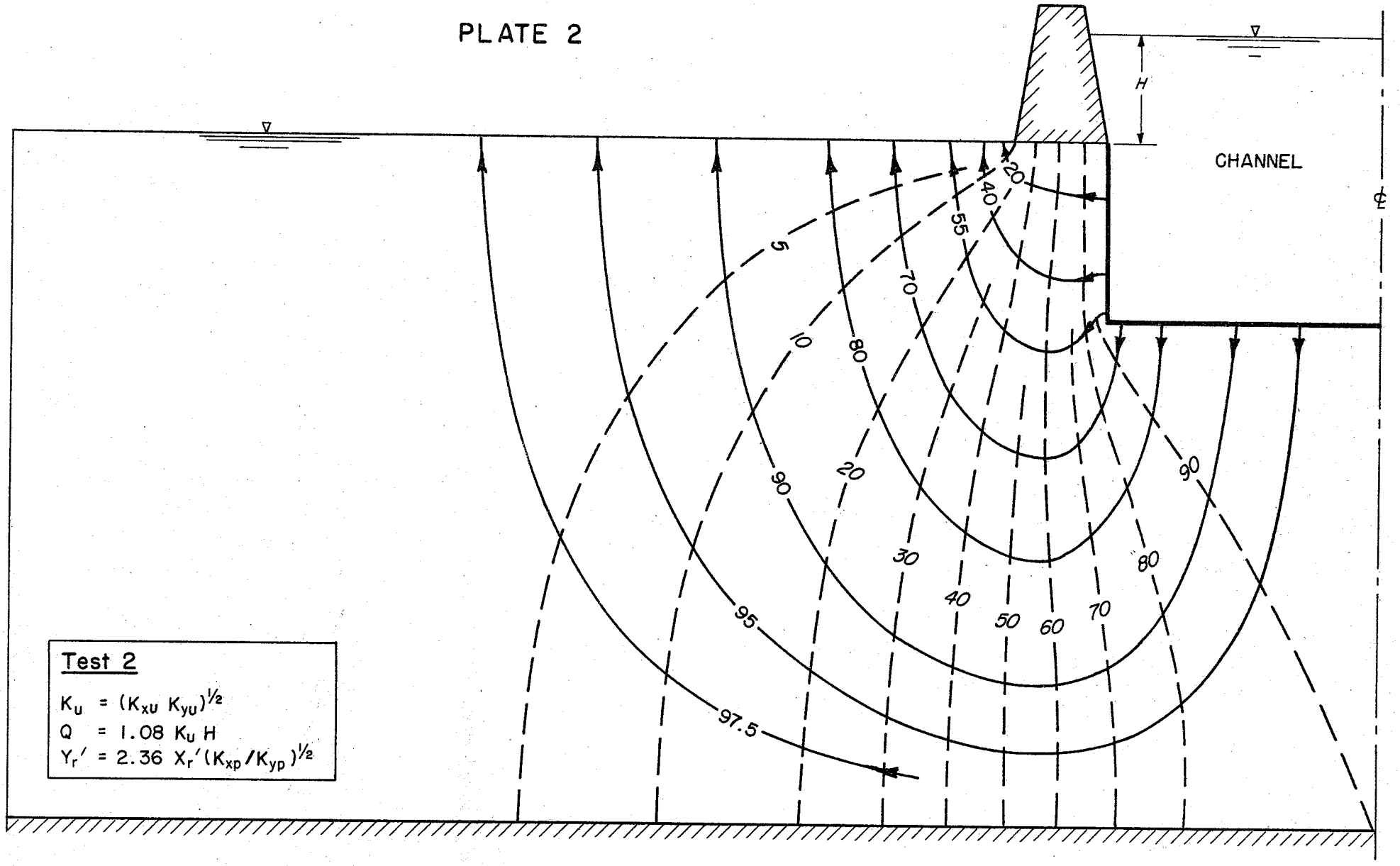
H
CHANNEL
℄
5
10
20
30
40
50
60
70
80
90
95
97.5
20
40
55
70
80
90
20
30
40
50
60
70
80
90
Test 2
$K_u = (K_{xu} K_{yu})^{1/2}$
$Q = 1.08 K_u H$
$Y_r' = 2.36 X_r' (K_{xp}/K_{yp})^{1/2}$

PLATE 3

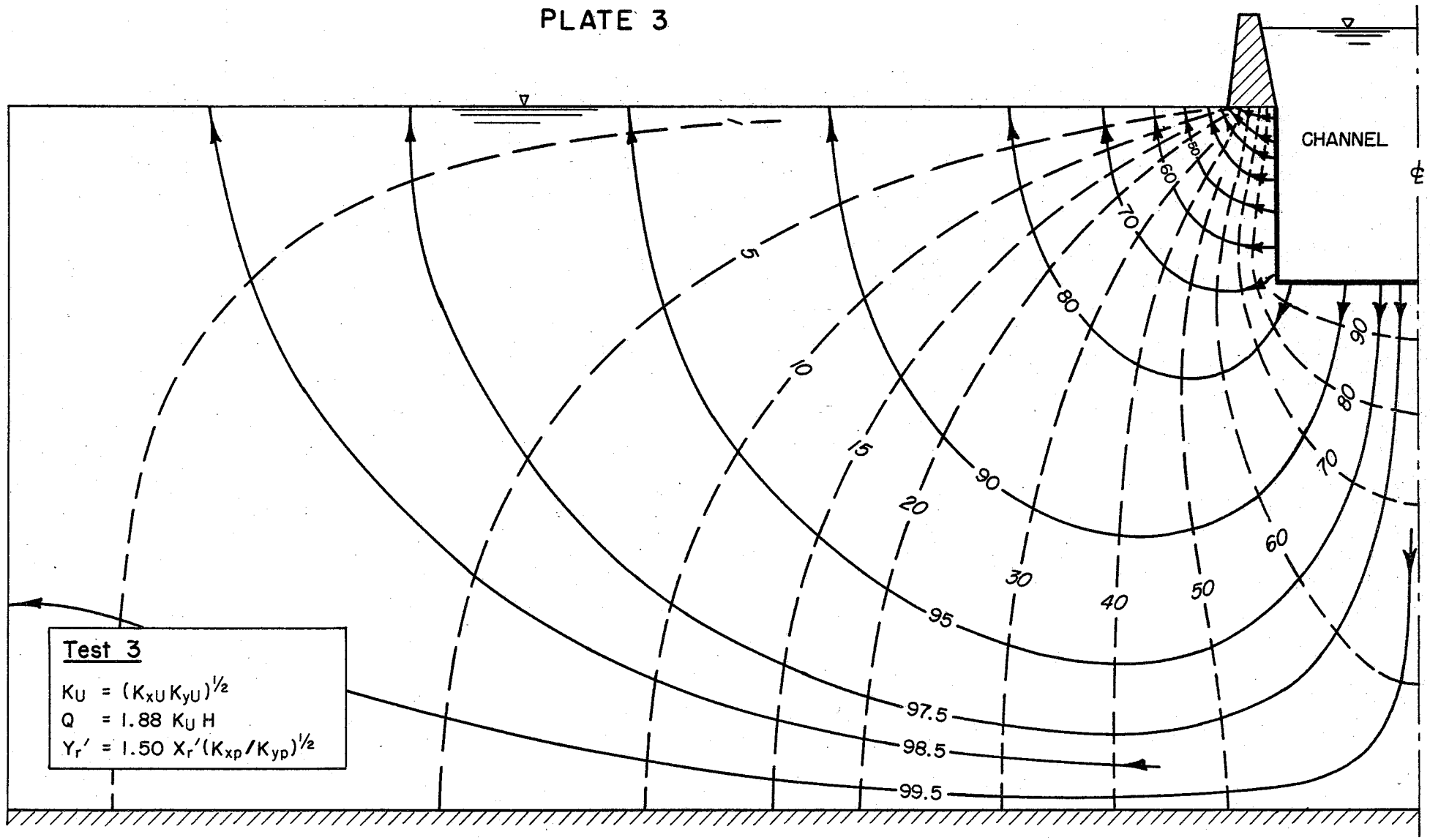
CHANNEL
5
10
15
20
30
40
50
60
70
80
90
95
97.5
98.5
99.5
Test 3
$K_U = (K_{xU} K_{yU})^{1/2}$
$Q = 1.88\ K_U\ H$
$Y_r' = 1.50\ X_r'(K_{xp}/K_{yp})^{1/2}$

PLATE 4

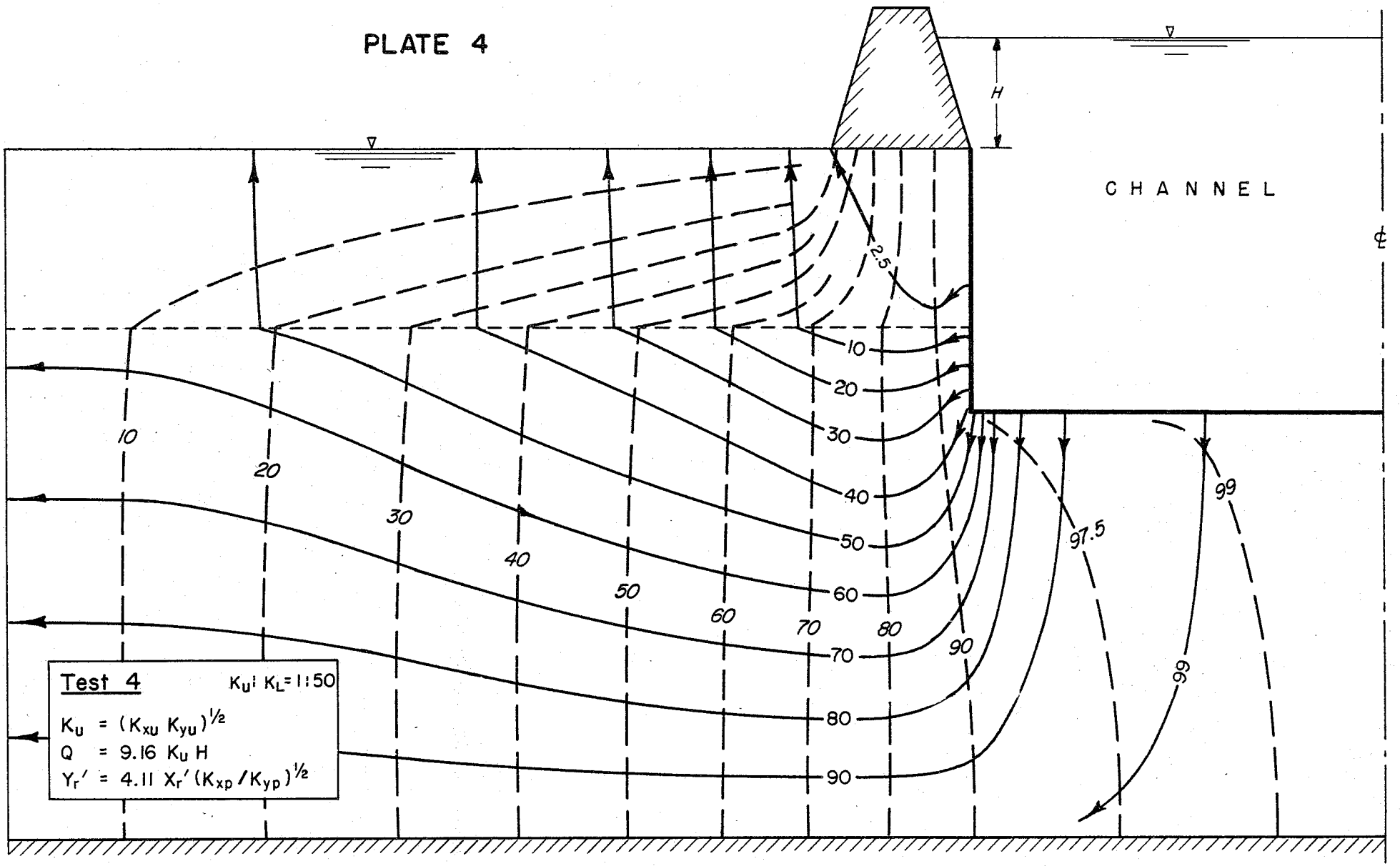
H
CHANNEL
℄
2.5
10
20
30
40
50
60
70
80
90
99
97.5
99
10
20
30
40
50
60
70
80
90
Test 4
K_u : K_L = 1:50
$K_u = (K_{xu} K_{yu})^{1/2}$
$Q = 9.16 K_u H$
$Y_r' = 4.11 X_r' (K_{xp}/K_{yp})^{1/2}$

PLATE 5

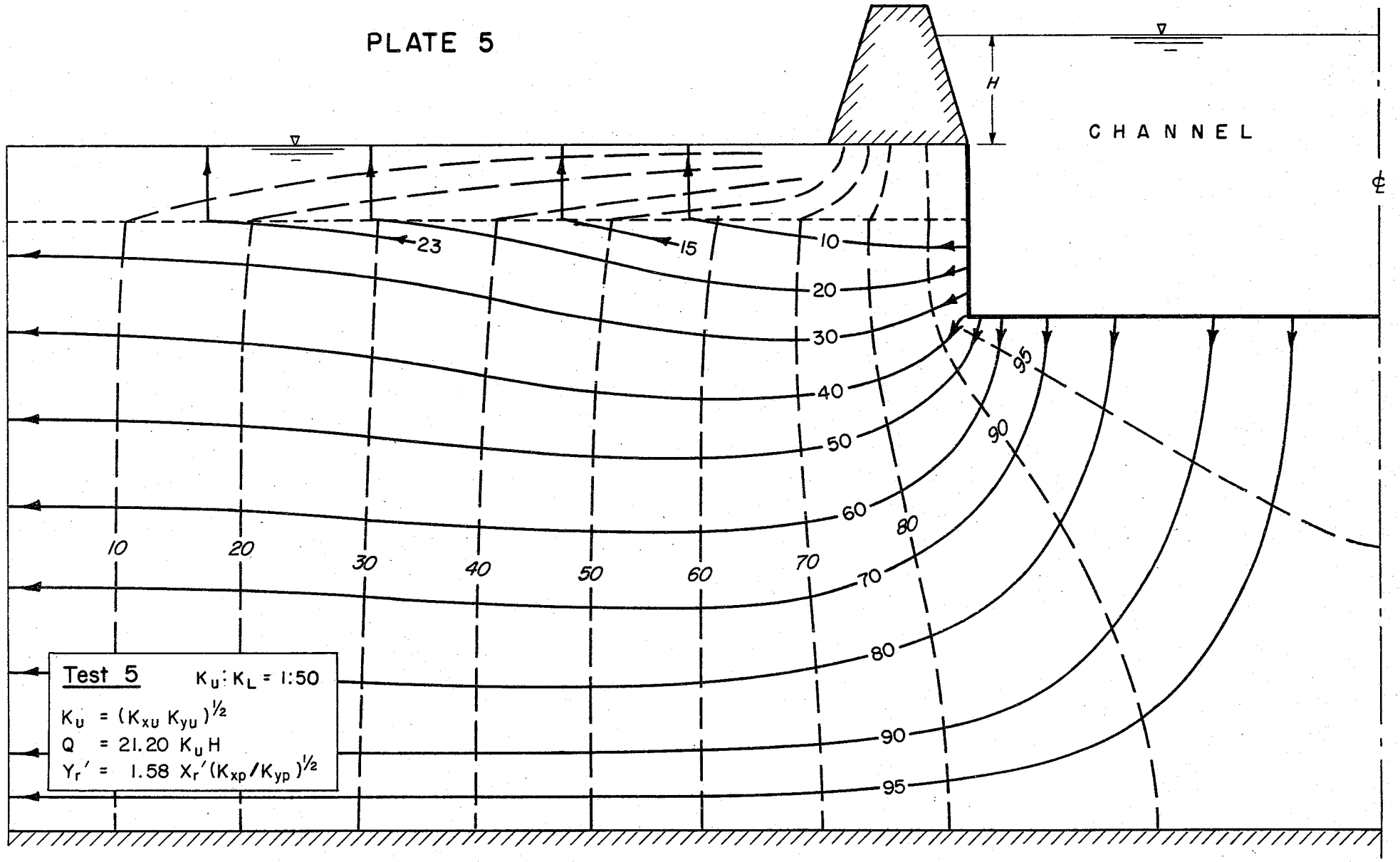
H
CHANNEL
℄
23
15
10
20
30
40
50
60
70
80
90
95
10
20
30
40
50
60
70
80
90
95
Test 5
$K_u : K_L = 1:50$
$K_u = (K_{xu} K_{yu})^{1/2}$
$Q = 21.20 K_u H$
$Y_r' = 1.58 X_r' (K_{xp}/K_{yp})^{1/2}$

PLATE 6

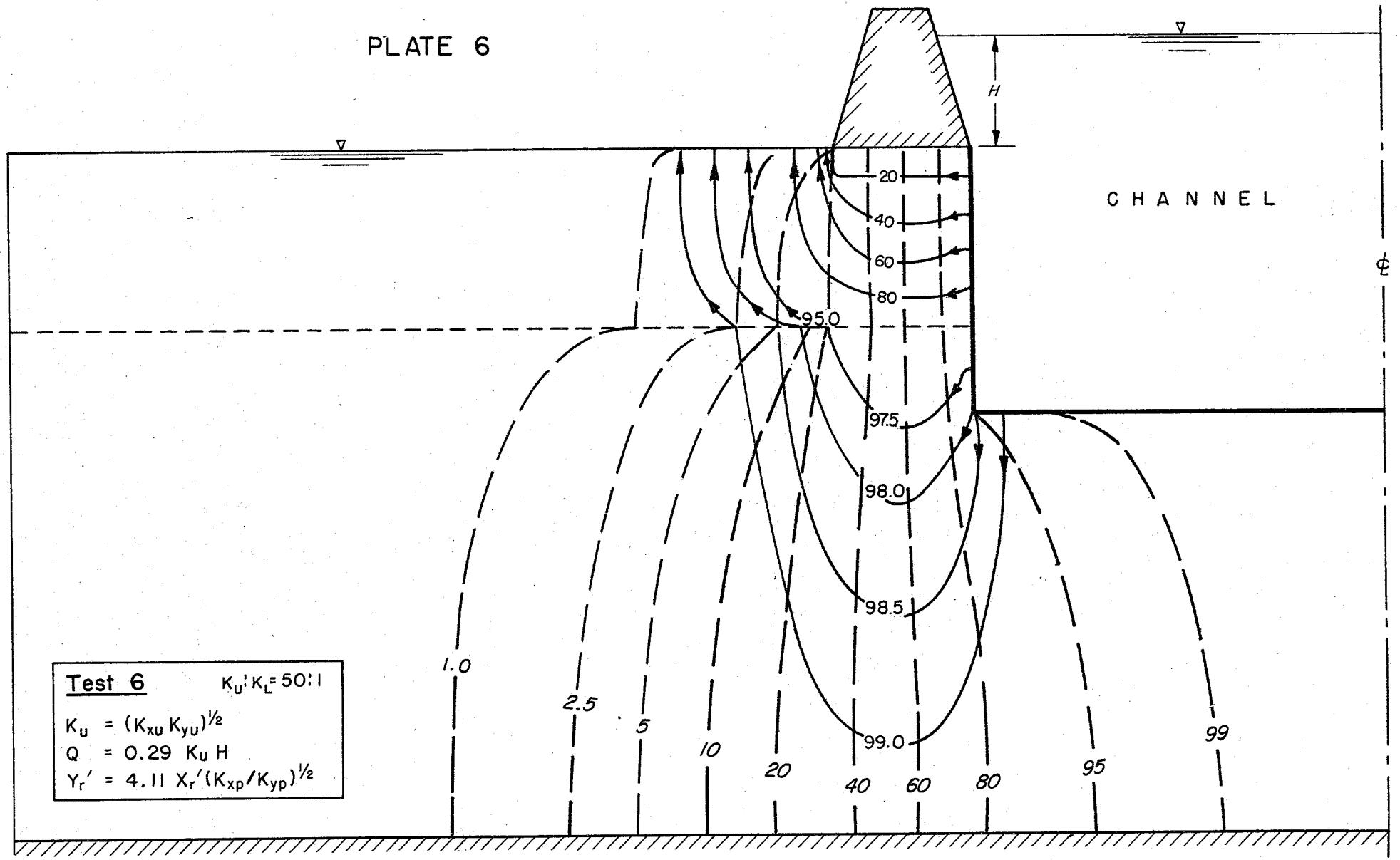
H
CHANNEL
20
40
60
80
95.0
97.5
98.0
98.5
99.0
1.0
2.5
5
10
20
40
60
80
95
99
Test 6
$K_u : K_L = 50:1$
$K_u = (K_{xu} K_{yu})^{1/2}$
$Q = 0.29\ K_u\ H$
$Y_r' = 4.11\ X_r'(K_{xp}/K_{yp})^{1/2}$

PLATE 7

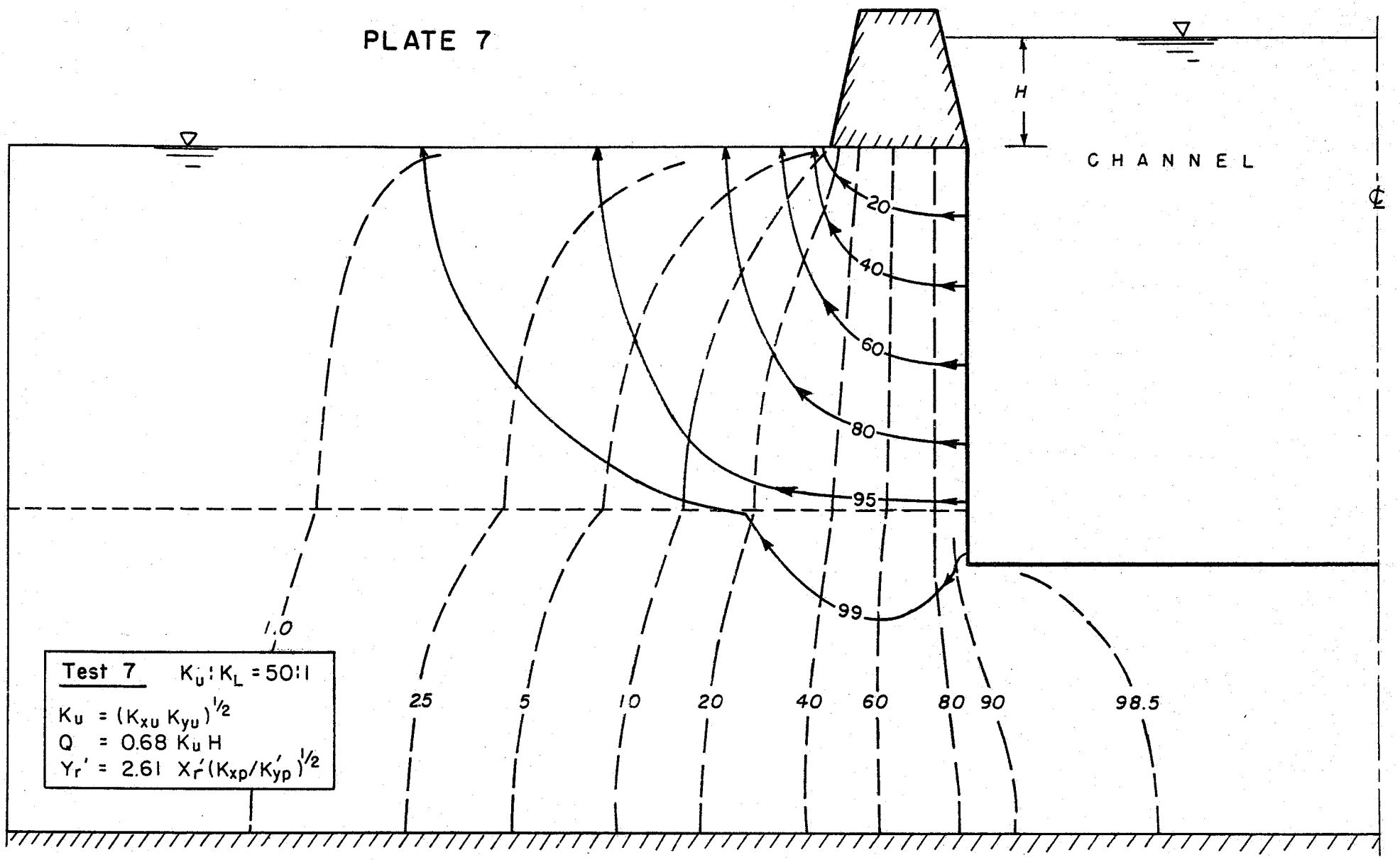
H
CHANNEL
℄
20
40
60
80
95
99
1.0
25
5
10
20
40
60
80
90
98.5
Test 7 $K_u : K_L = 50:1$
$K_u = (K_{xu} K_{yu})^{1/2}$
$Q = 0.68 K_u H$
$Y_r' = 2.61 X_r' (K_{xp}/K_{yp}')^{1/2}$

PLATE 8

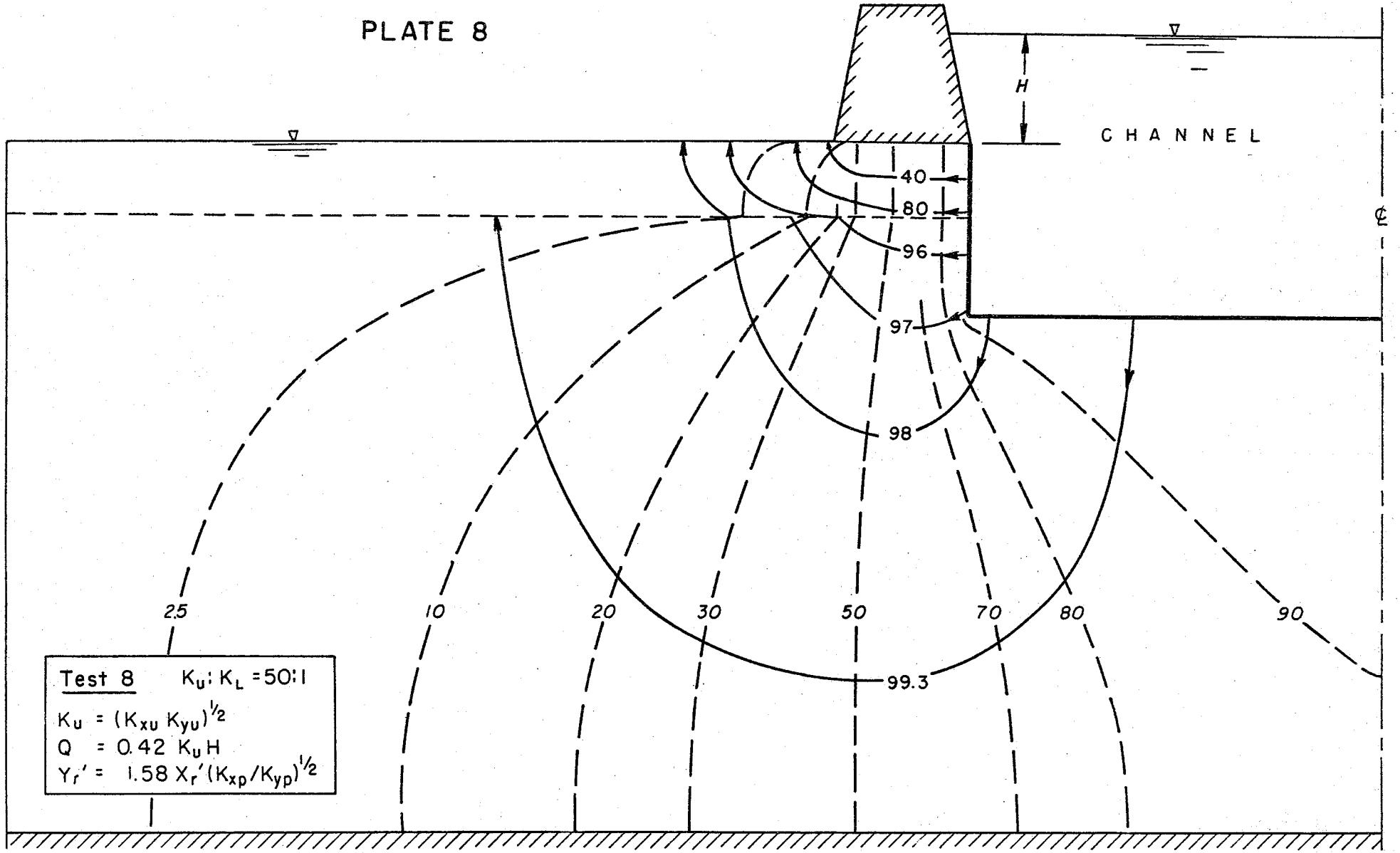
H
CHANNEL
40
80
96
97
98
99.3
2.5
10
20
30
50
70
80
90
Test 8 $K_u : K_L = 50:1$
$K_u = (K_{xu} K_{yu})^{1/2}$
$Q = 0.42 K_u H$
$Y_r' = 1.58 X_r' (K_{xp}/K_{yp})^{1/2}$

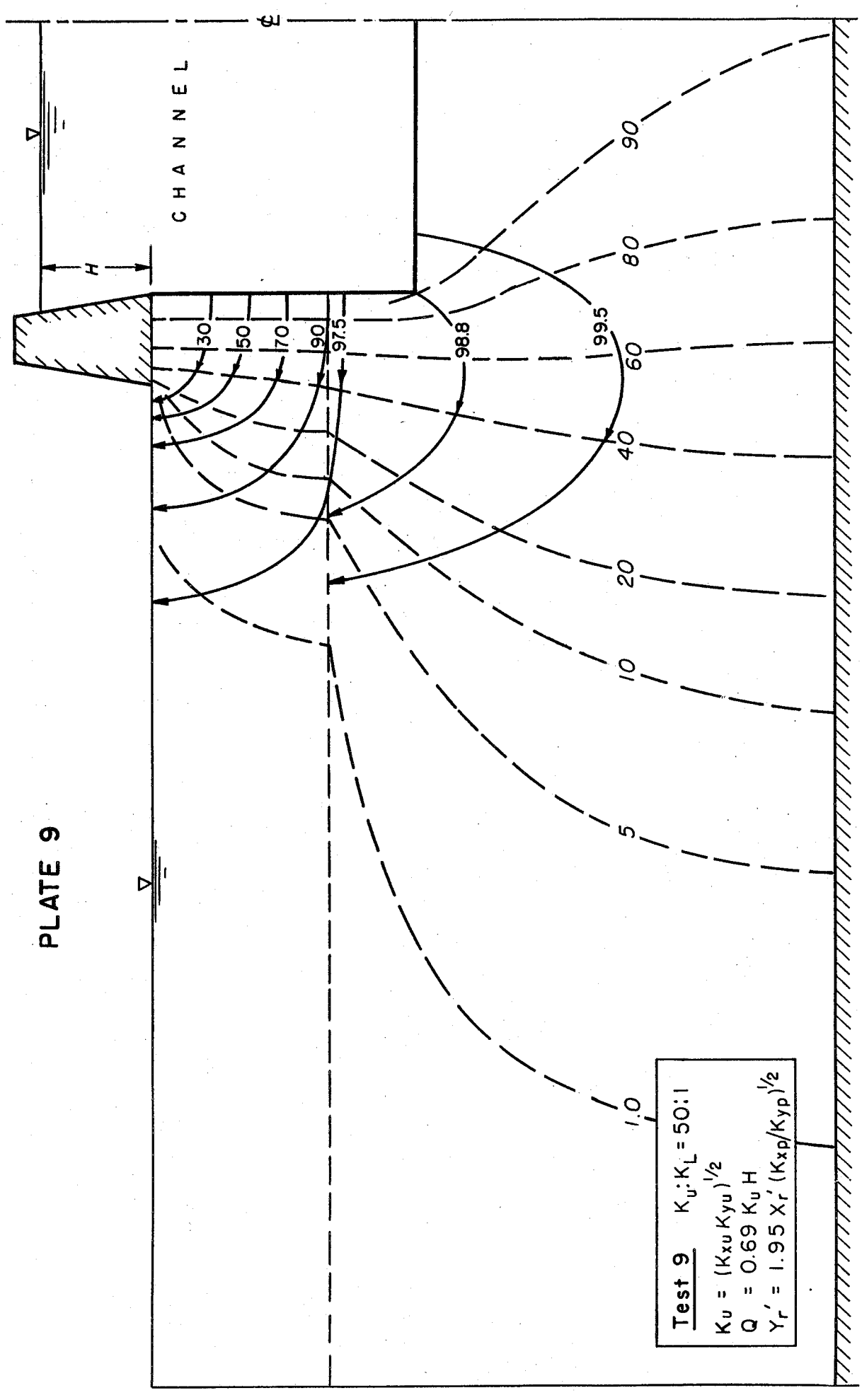
℄
CHANNEL
H
30
50
70
90
97.5
98.8
99.5
90
80
60
40
20
10
5
1.0
Test 9 $K_u : K_L = 50:1$
$K_u = (K_{xu} K_{yu})^{1/2}$
$Q = 0.69 K_u H$
$Y_r' = 1.95 X_r' (K_{xp}/K_{yp})^{1/2}$

PLATE 9

PLATE 10

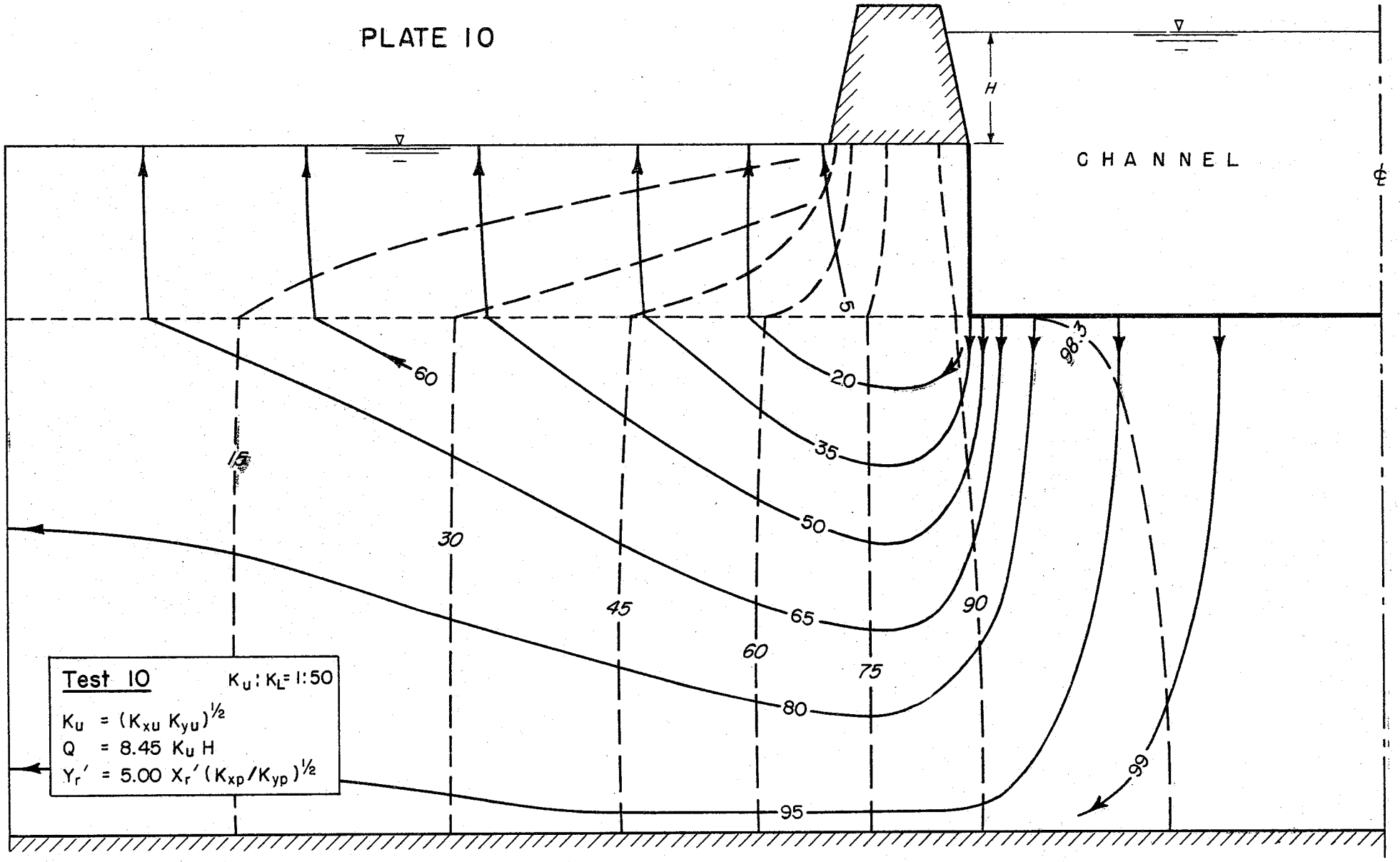
H
CHANNEL
℄
5
20
35
50
65
80
95
99
98.3
90
75
60
45
30
15
Test 10
$K_u : K_L = 1:50$
$K_u = (K_{xu} K_{yu})^{1/2}$
$Q = 8.45 K_u H$
$Y_r' = 5.00 X_r' (K_{xp}/K_{yp})^{1/2}$

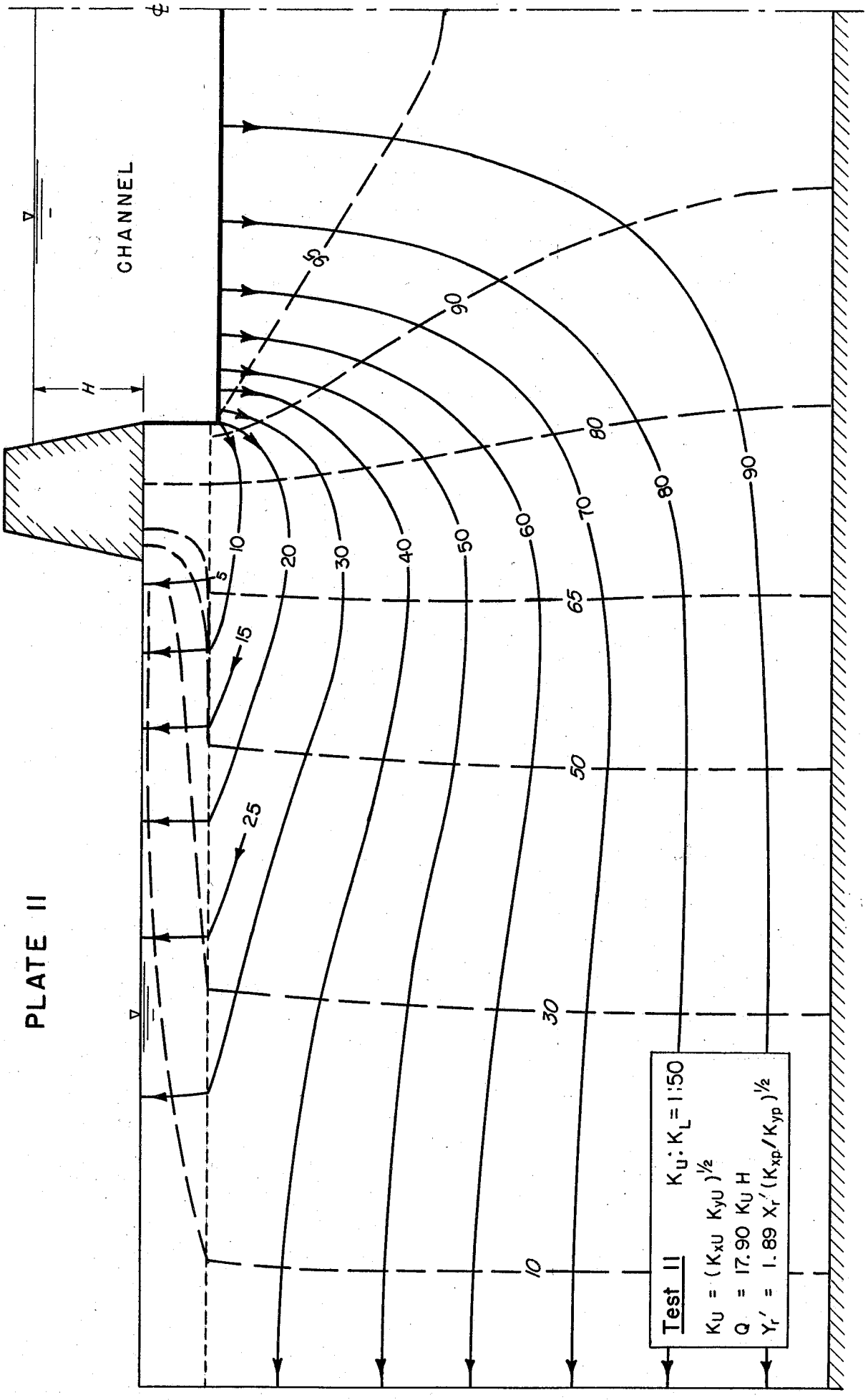
CHANNEL
H
10
20
30
40
50
60
70
80
90
65
50
30
10
5
15
25
Test 11
$K_U : K_L = 1:50$
$K_U = (K_{xU}\ K_{yU})^{1/2}$
$Q = 17.90\ K_U\ H$
$Y_r' = 1.89\ X_r' (K_{xp}/K_{yp})^{1/2}$

PLATE II

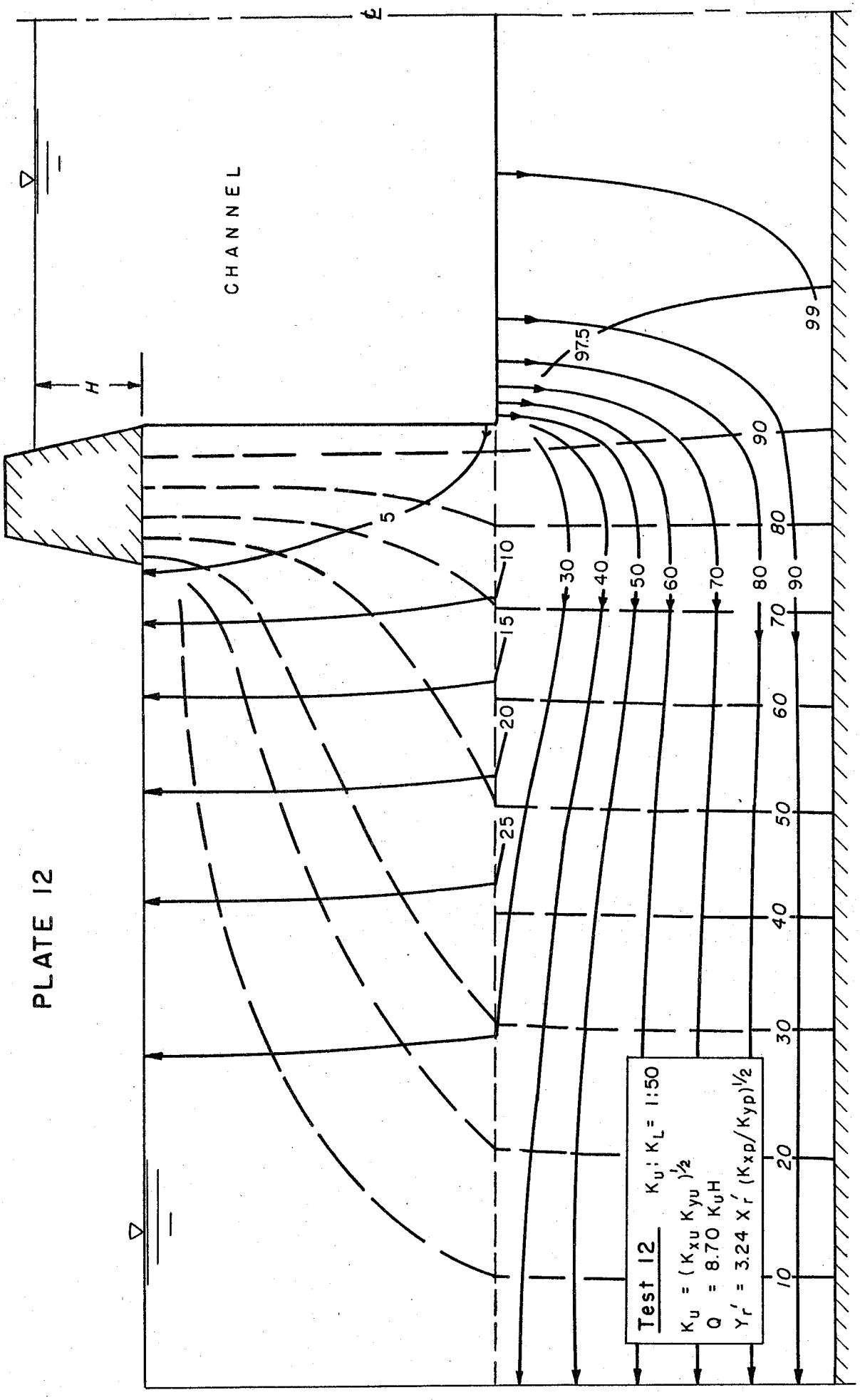
CHANNEL
H
5
10
15
20
25
30
40
50
60
70
80
90
97.5
99
Test 12 $K_u : K_L = 1:50$
$K_u = (K_{xu} K_{yu})^{1/2}$
$Q = 8.70 K_u H$
$Y_r' = 3.24 X_r' (K_{xp}/K_{yp})^{1/2}$

PLATE 12

PLATE 13

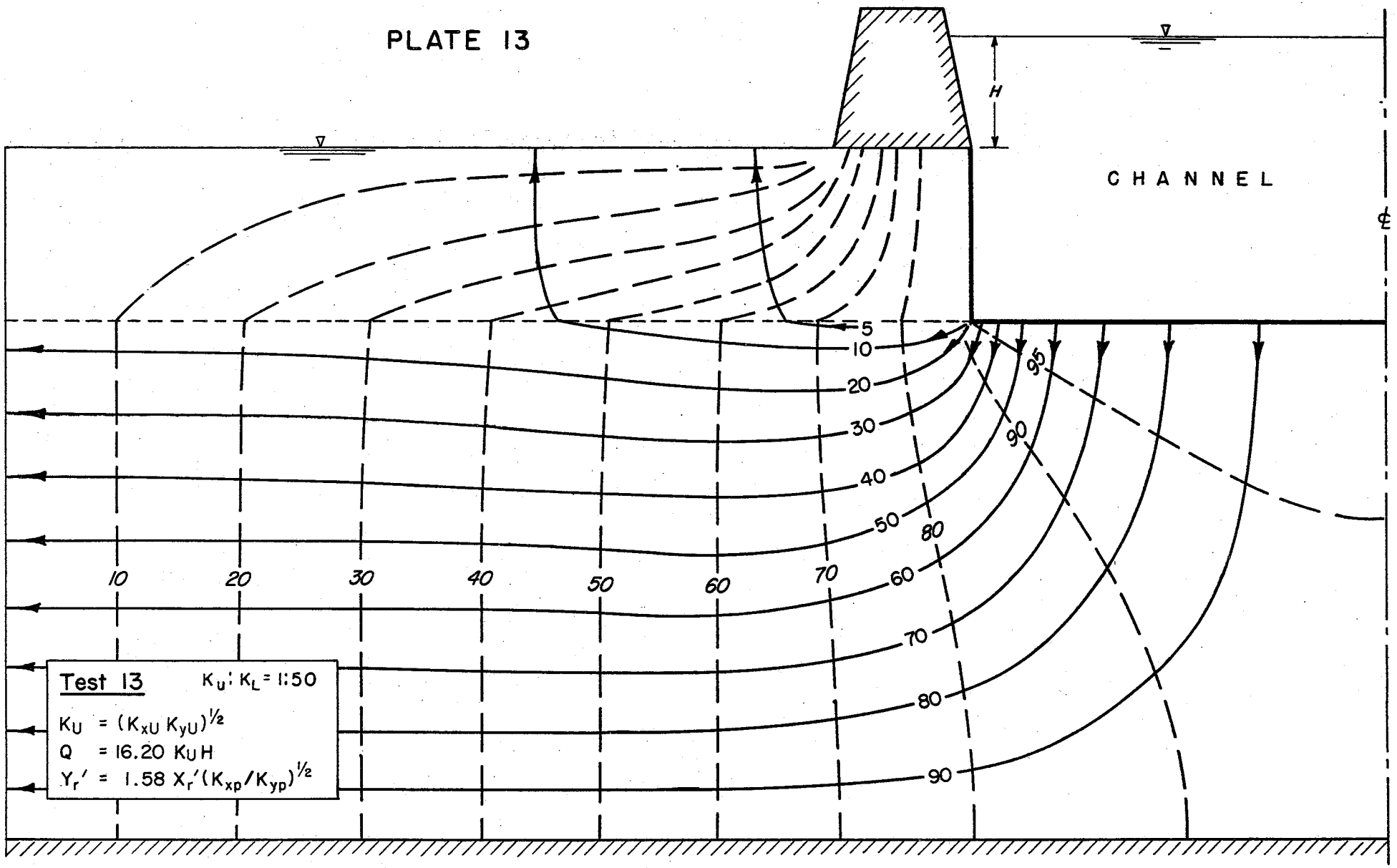
H
CHANNEL
5
10
20
30
40
50
60
70
80
90
95
10
20
30
40
50
60
70
80
90
Test 13
$K_U : K_L = 1:50$
$K_U = (K_{xU} K_{yU})^{1/2}$
$Q = 16.20 K_U H$
$Y_r' = 1.58 X_r' (K_{xp}/K_{yp})^{1/2}$

PLATE 14

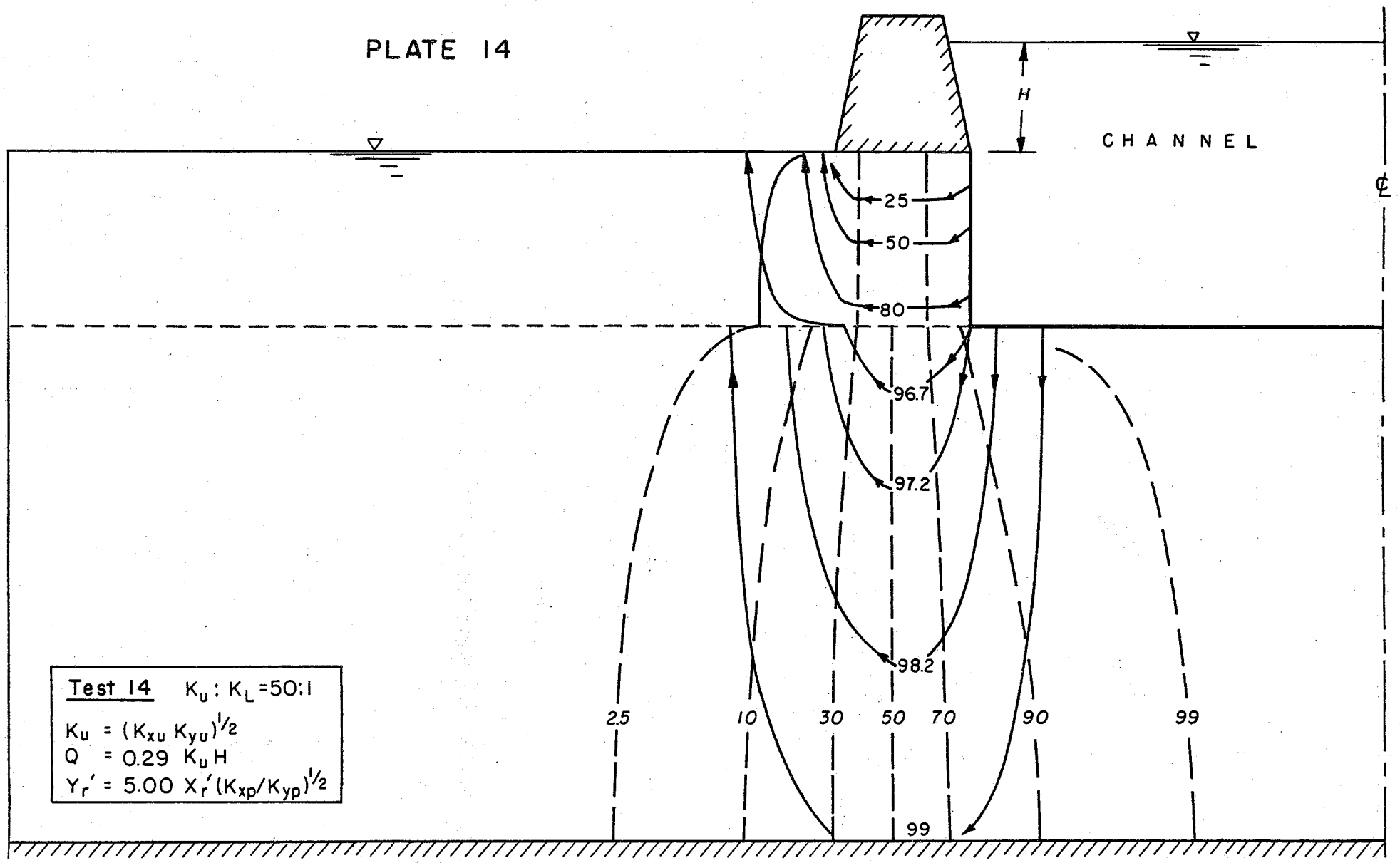
H
CHANNEL
℄
25
50
80
96.7
97.2
98.2
99
2.5
10
30
50
70
90
99
Test 14 $K_u : K_L = 50:1$
$K_u = (K_{xu} K_{yu})^{1/2}$
$Q = 0.29 K_u H$
$Y_r' = 5.00 X_r' (K_{xp}/K_{yp})^{1/2}$

PLATE 15

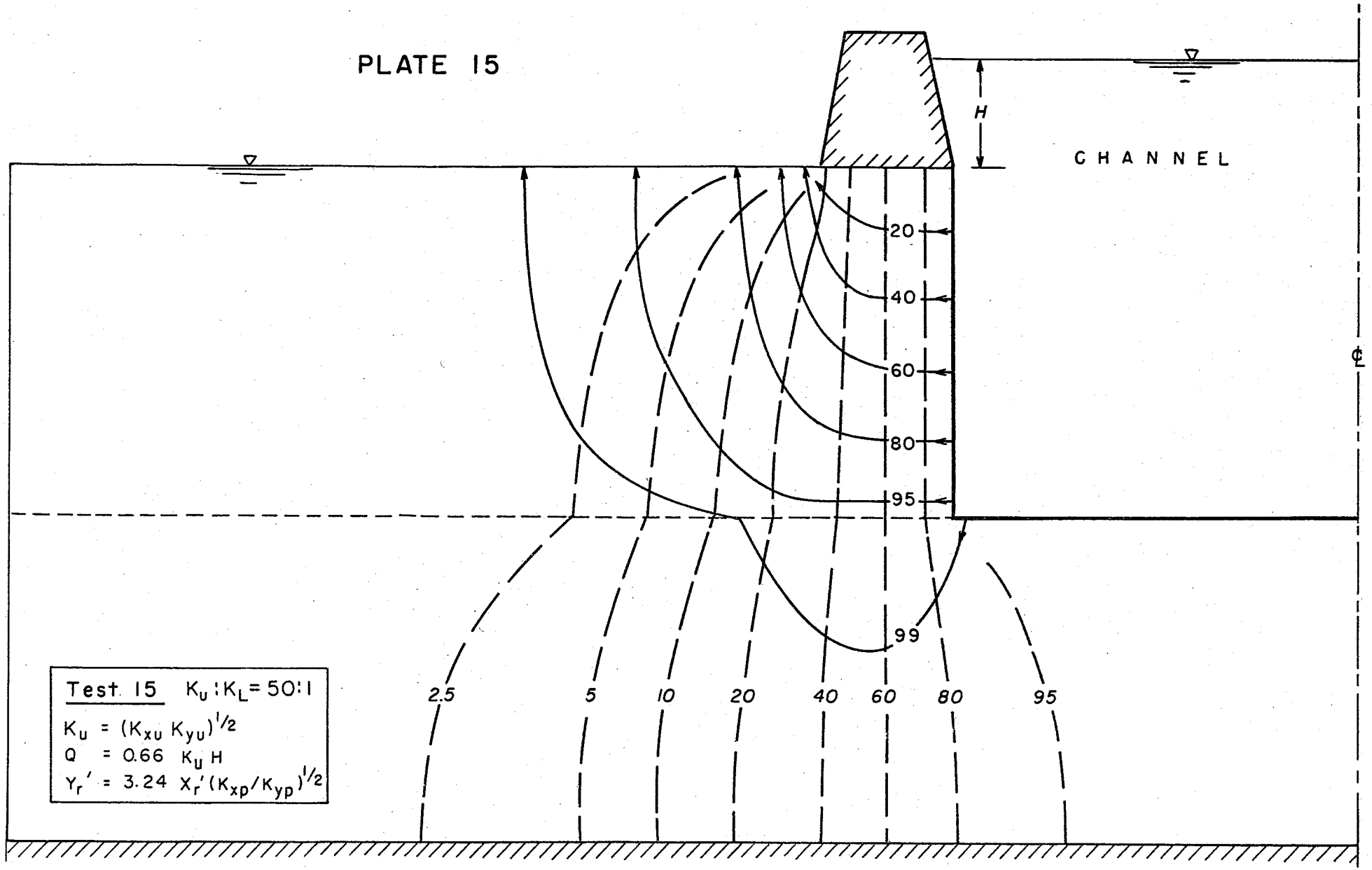
H
CHANNEL
20
40
60
80
95
99
2.5
5
10
20
40
60
80
95
℄
Test 15 $K_u : K_L = 50:1$
$K_u = (K_{xu} K_{yu})^{1/2}$
$Q = 0.66 K_u H$
$Y_r' = 3.24 X_r' (K_{xp}/K_{yp})^{1/2}$

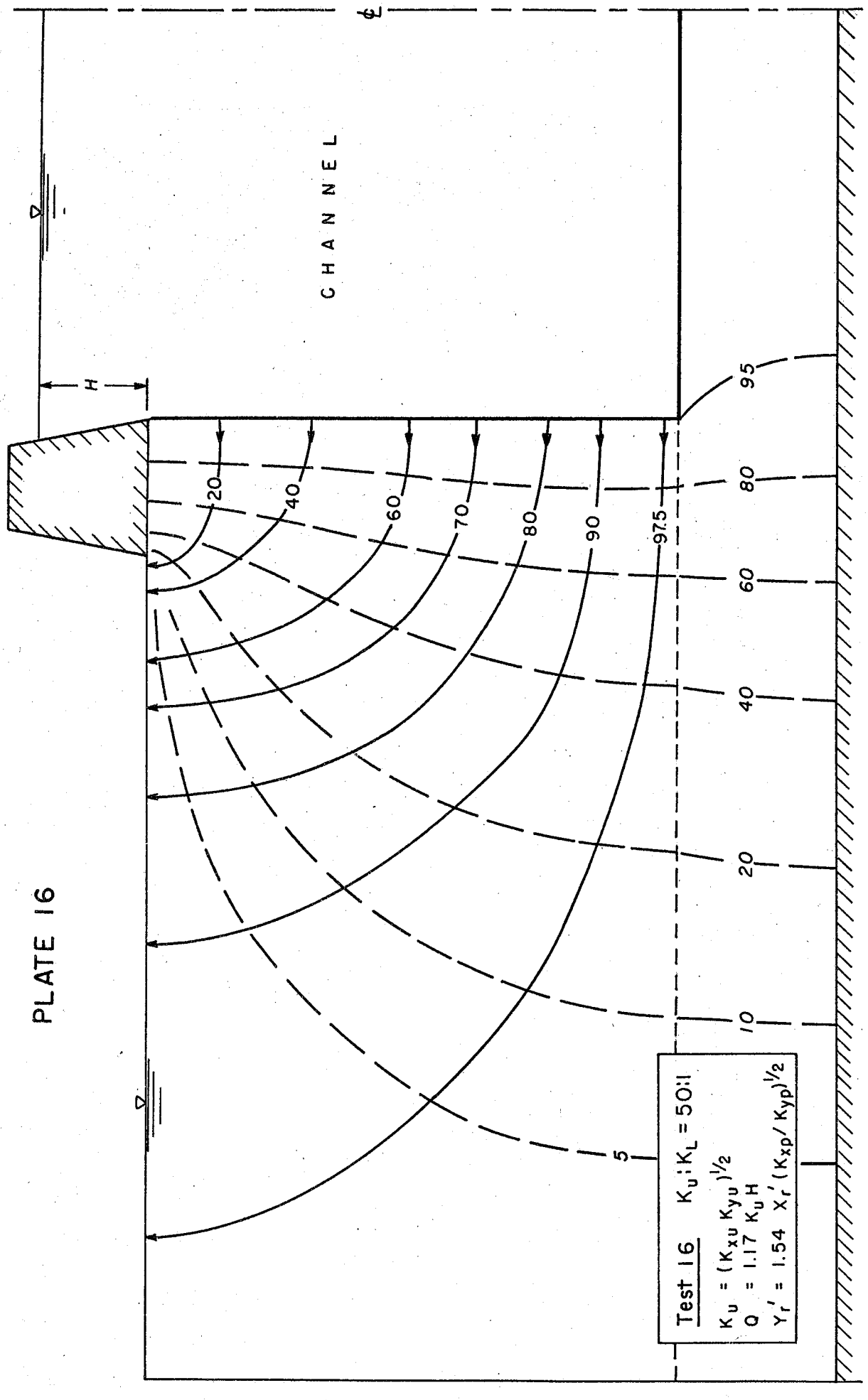
CHANNEL
H
20
40
60
70
80
90
97.5
95
80
60
40
20
10
5
Test 16 $K_u : K_L = 50:1$
$K_u = (K_{xu} K_{yu})^{1/2}$
$Q = 1.17 K_u H$
$Y_r' = 1.54 X_r' (K_{xp}/K_{yp})^{1/2}$

PLATE 16

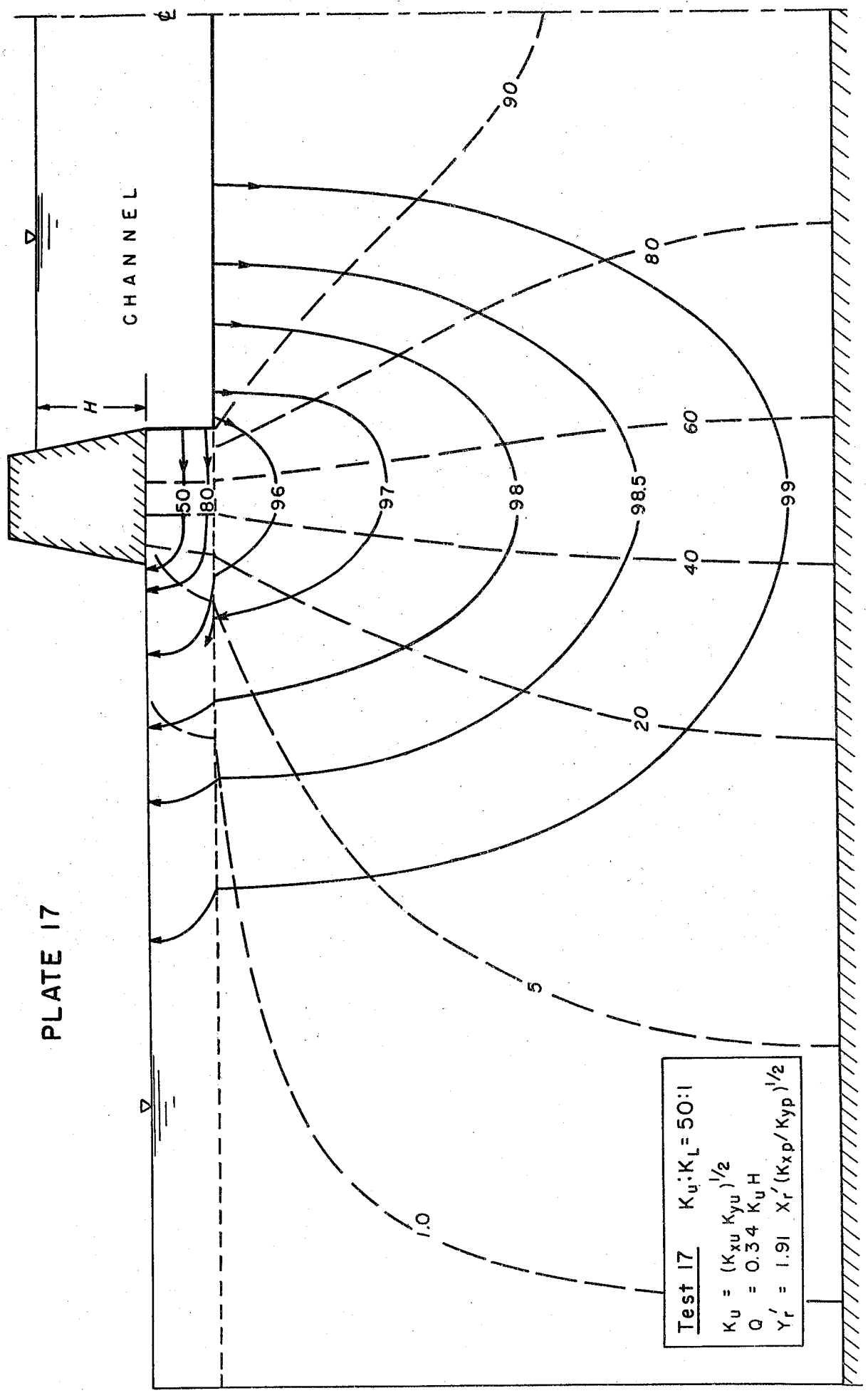
℄
CHANNEL
H
50
80
90
80
60
40
20
5
1.0
96
97
98
98.5
99
Test 17 $K_u : K_L = 50:1$
$K_u = (K_{xu} K_{yu})^{1/2}$
$Q = 0.34\ K_u H$
$Y_r' = 1.91\ X_r' (K_{xp}/K_{yp})^{1/2}$

PLATE 17

PLATE 18

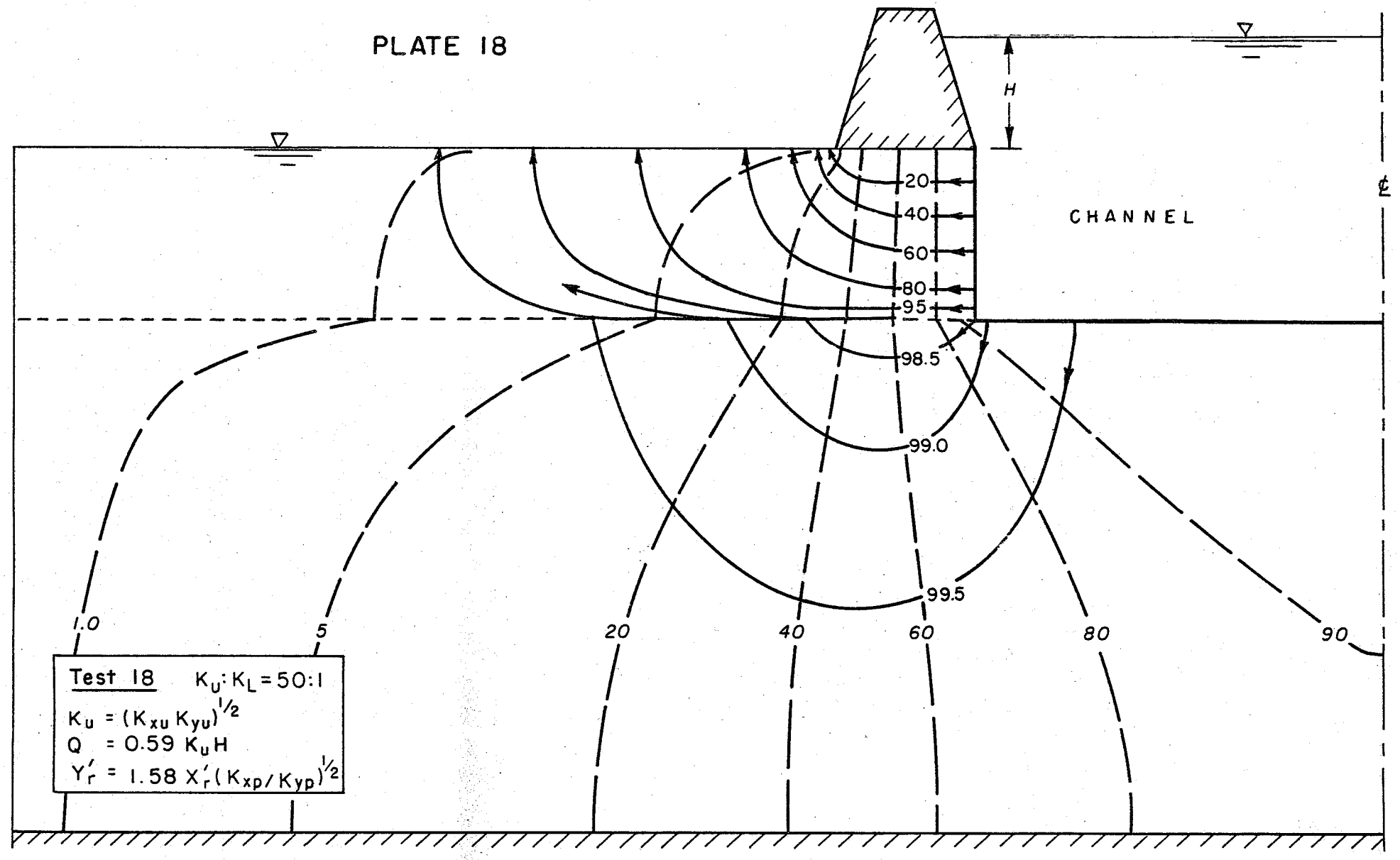
H
CHANNEL
℄
20
40
60
80
95
98.5
99.0
99.5
1.0
5
20
40
60
80
90
Test 18 $K_U : K_L = 50:1$
$K_u = (K_{xu} K_{yu})^{1/2}$
$Q = 0.59 K_u H$
$Y'_r = 1.58 X'_r (K_{xp}/K_{yp})^{1/2}$

PLATE 19

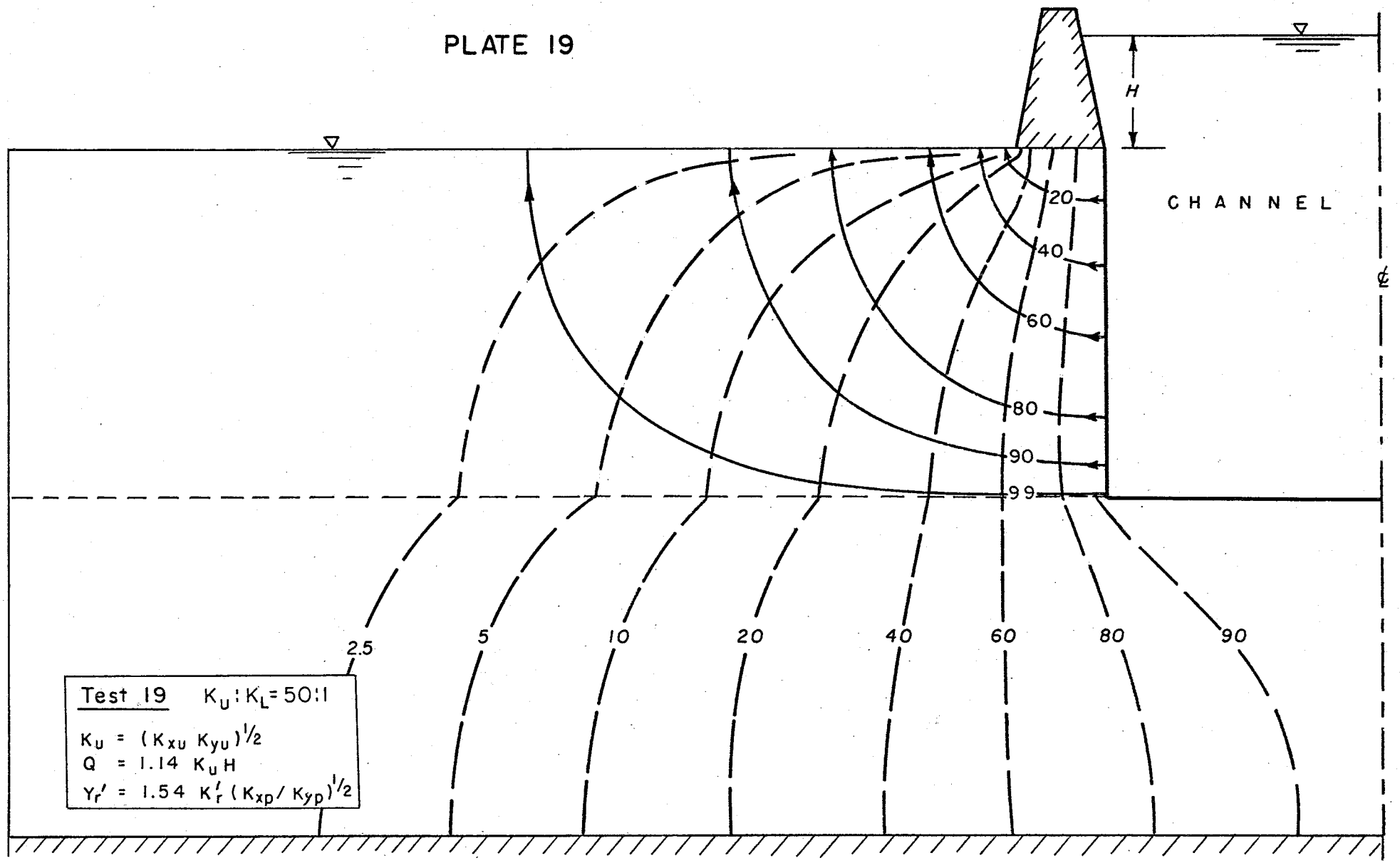
H
CHANNEL
20
40
60
80
90
99
2.5
5
10
20
40
60
80
90
Test 19 $K_U : K_L = 50:1$
$K_u = (K_{xu} K_{yu})^{1/2}$
$Q = 1.14 K_u H$
$Y_r' = 1.54 K_r' (K_{xp}/K_{yp})^{1/2}$

PLATE 20

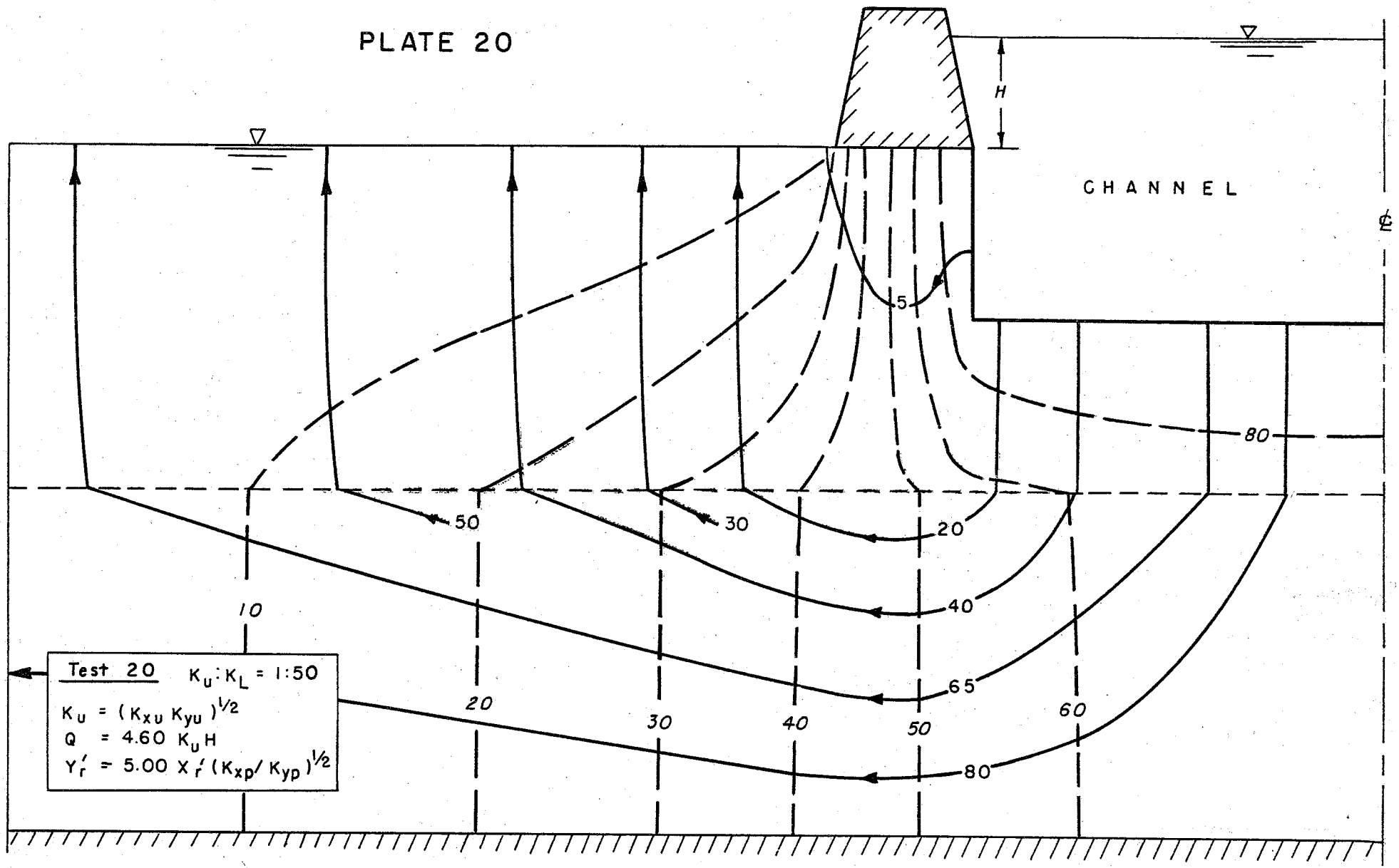
H
CHANNEL
5
80
50
30
20
40
65
60
10
20
30
40
50
80
Test 20 $K_u : K_L$ = 1:50
$K_u = (K_{xu} K_{yu})^{1/2}$
$Q = 4.60 K_u H$
$Y_r' = 5.00 X_r' (K_{xp}/K_{yp})^{1/2}$

PLATE 21

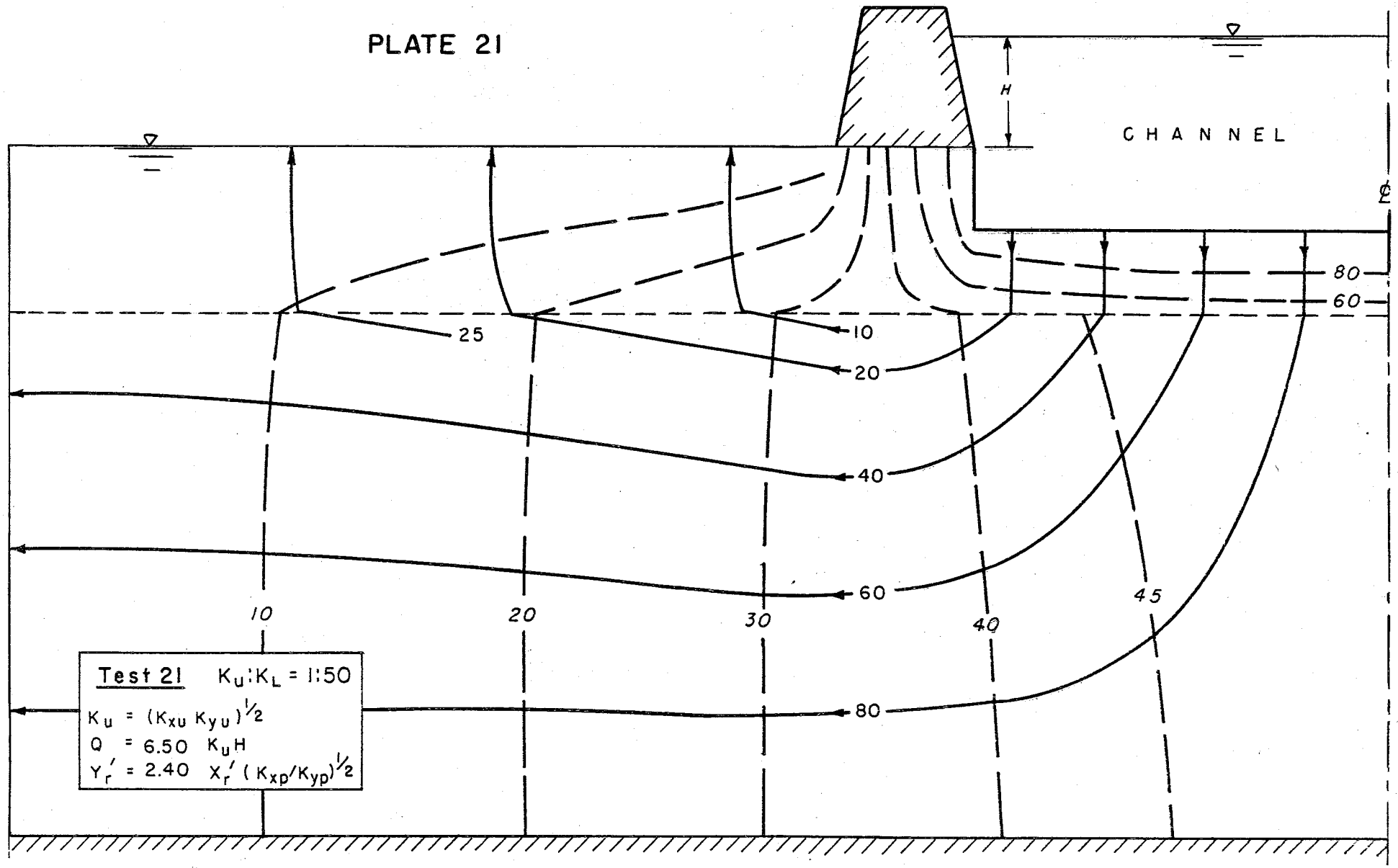
H
CHANNEL
℄
80
60
25
10
20
40
60
80
10
20
30
40
45
Test 21 $K_u : K_L$ = 1:50
$K_u = (K_{xu} K_{yu})^{1/2}$
$Q = 6.50\ K_u H$
$Y_r' = 2.40\ X_r' (K_{xp}/K_{yp})^{1/2}$

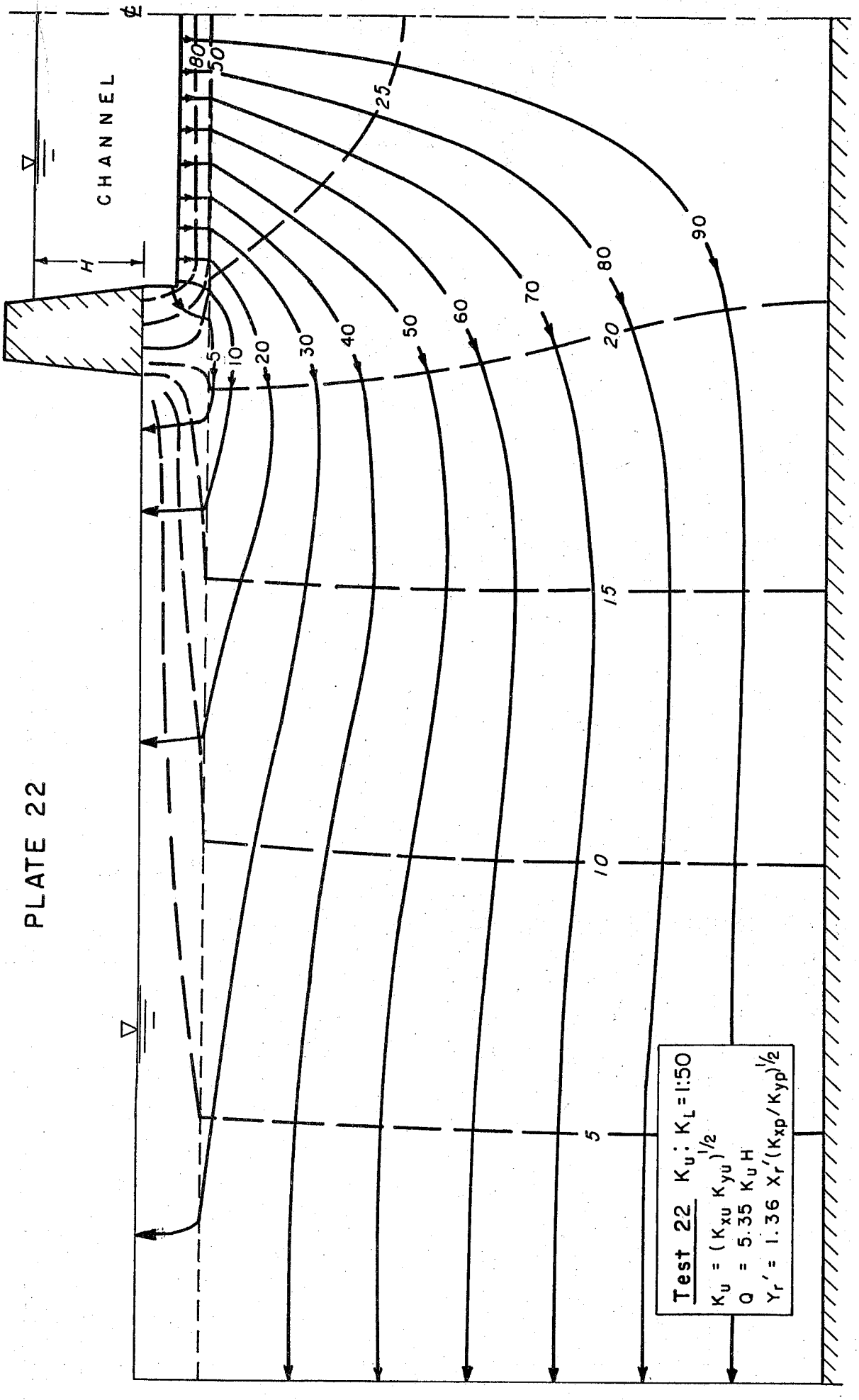
℄
CHANNEL
H
180
50
25
90
80
70
60
50
40
30
20
10
5
20
15
10
5
Test 22 K_u; K_L = 1:50
$K_u = (K_{xu} K_{yu})^{1/2}$
Q = 5.35 $K_u H'$
$Y_r' = 1.36\ X_r'(K_{xp}/K_{yp})^{1/2}$

PLATE 22

PLATE 23

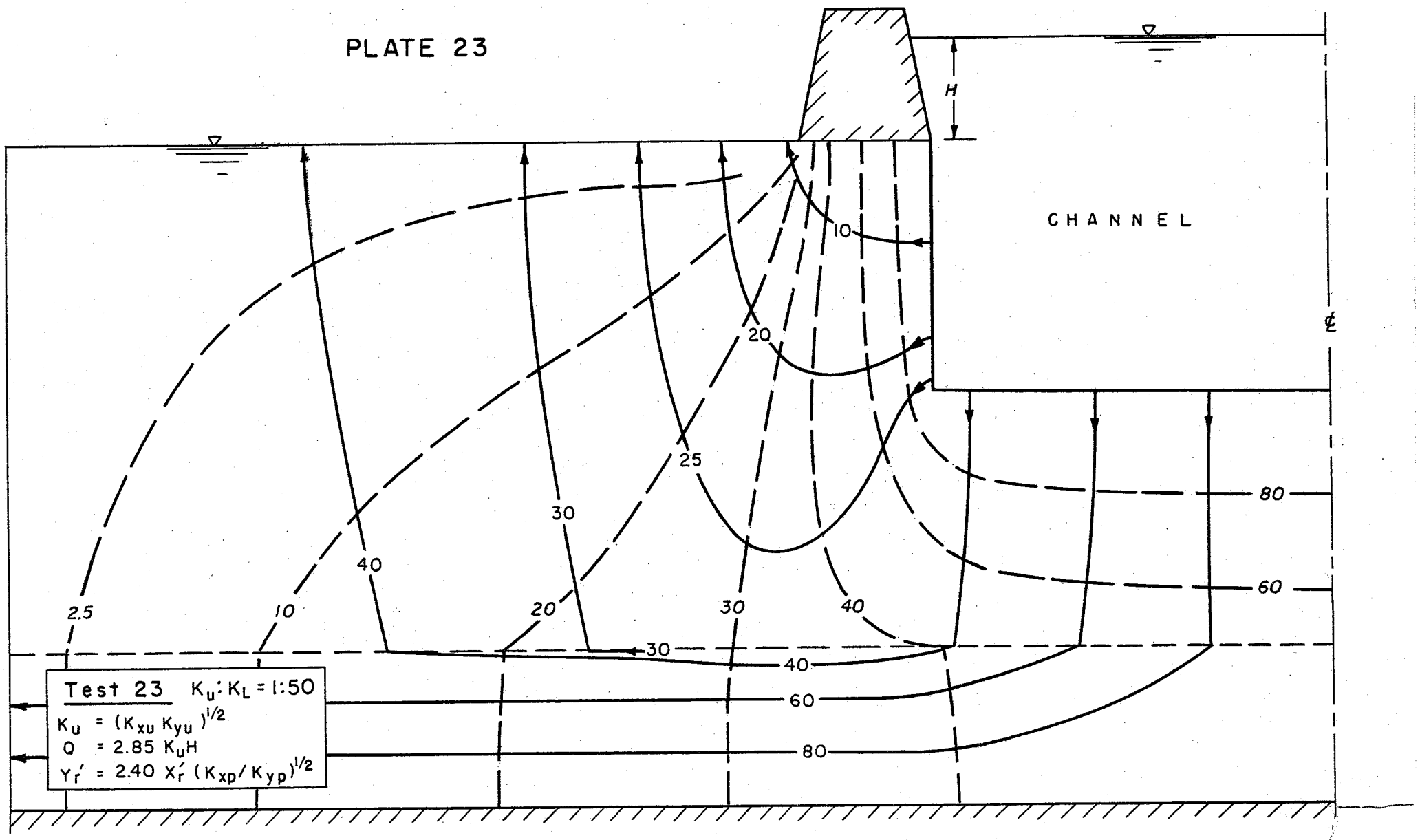
H
CHANNEL
℄
10
20
25
30
40
80
60
2.5
10
20
30
40
30
40
60
80
Test 23 $K_u : K_L = 1:50$
$K_u = (K_{xu} K_{yu})^{1/2}$
$Q = 2.85 K_u H$
$Y_r' = 2.40 X_r' (K_{xp}/K_{yp})^{1/2}$

PLATE 24

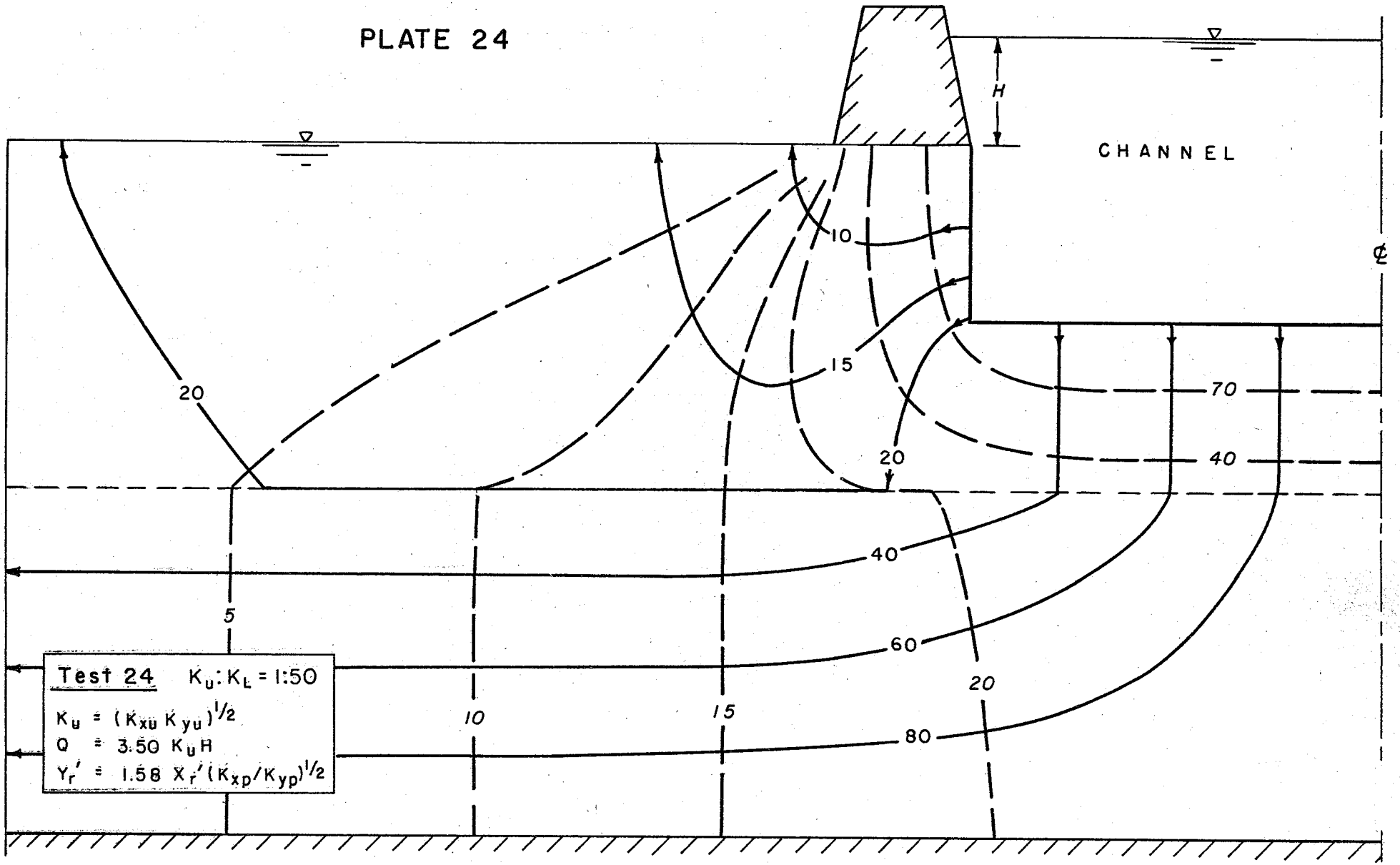
H
CHANNEL
10
15
20
70
40
20
40
5
60
10
15
20
80
Test 24 $K_u : K_L$ = 1:50
$K_u = (K_{xu} K_{yu})^{1/2}$
$Q = 3.50 K_u H$
$Y_r' = 1.58 X_r' (K_{xp}/K_{yp})^{1/2}$

PLATE 25

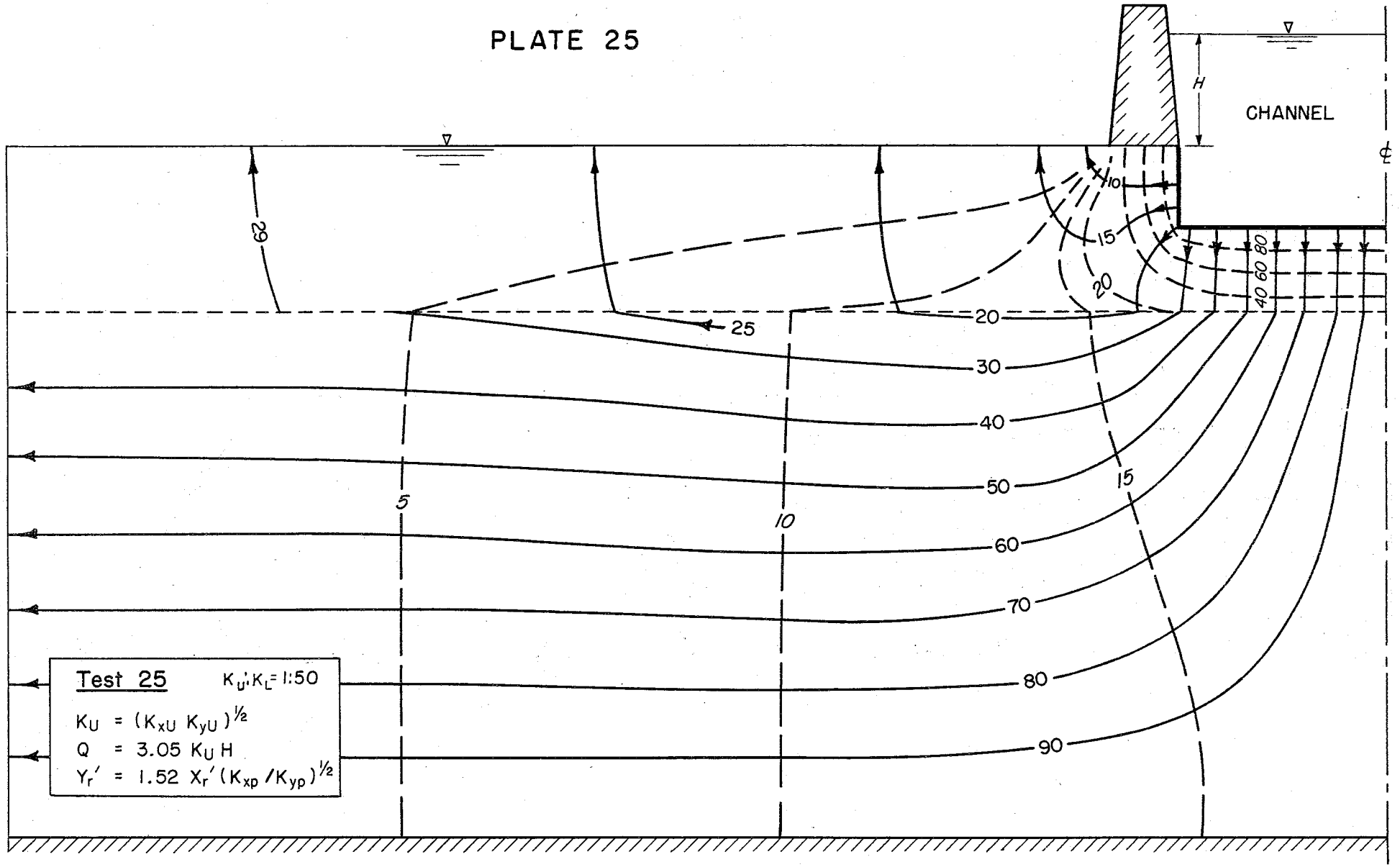
H
CHANNEL
℄
25
20
30
40
50
60
70
80
90
5
10
15
20
15
10
40 60 80
Test 25
$K_U : K_L = 1:50$
$K_U = (K_{xU}\ K_{yU})^{1/2}$
$Q = 3.05\ K_U\ H$
$Y_r' = 1.52\ X_r'\ (K_{xp}/K_{yp})^{1/2}$

PLATE 26

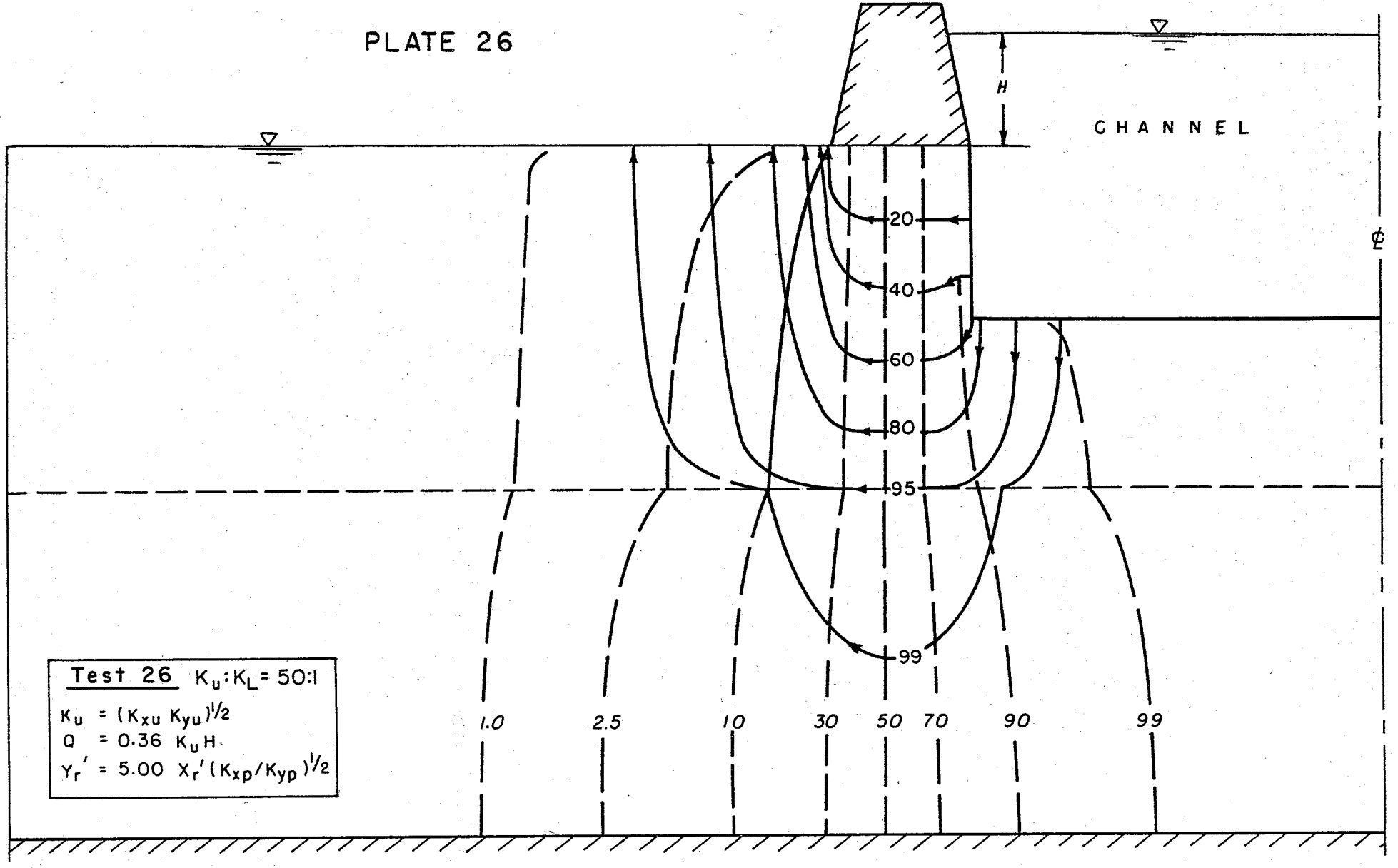
H
CHANNEL
℄
20
40
60
80
95
99
1.0
2.5
10
30
50
70
90
99
Test 26 $K_u : K_L = 50:1$
$K_u = (K_{xu} K_{yu})^{1/2}$
$Q = 0.36 K_u H$
$Y_r' = 5.00 X_r' (K_{xp}/K_{yp})^{1/2}$

PLATE 27

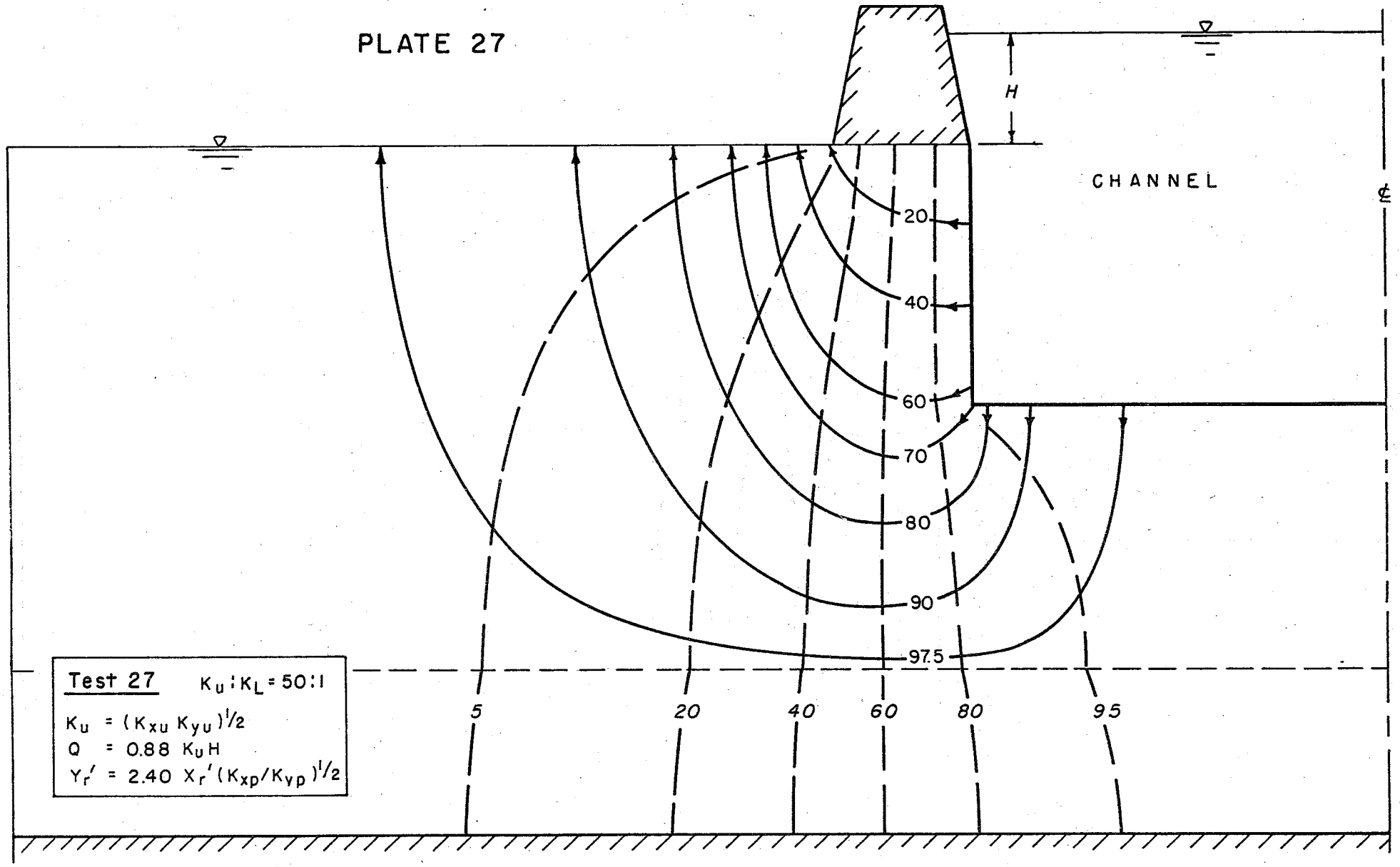
H
CHANNEL
20
40
60
70
80
90
97.5
5
20
40
60
80
95
Test 27 $K_u : K_L = 50:1$
$K_u = (K_{xu} K_{yu})^{1/2}$
$Q = 0.88 K_u H$
$Y_r' = 2.40 X_r' (K_{xp}/K_{yp})^{1/2}$

PLATE 28

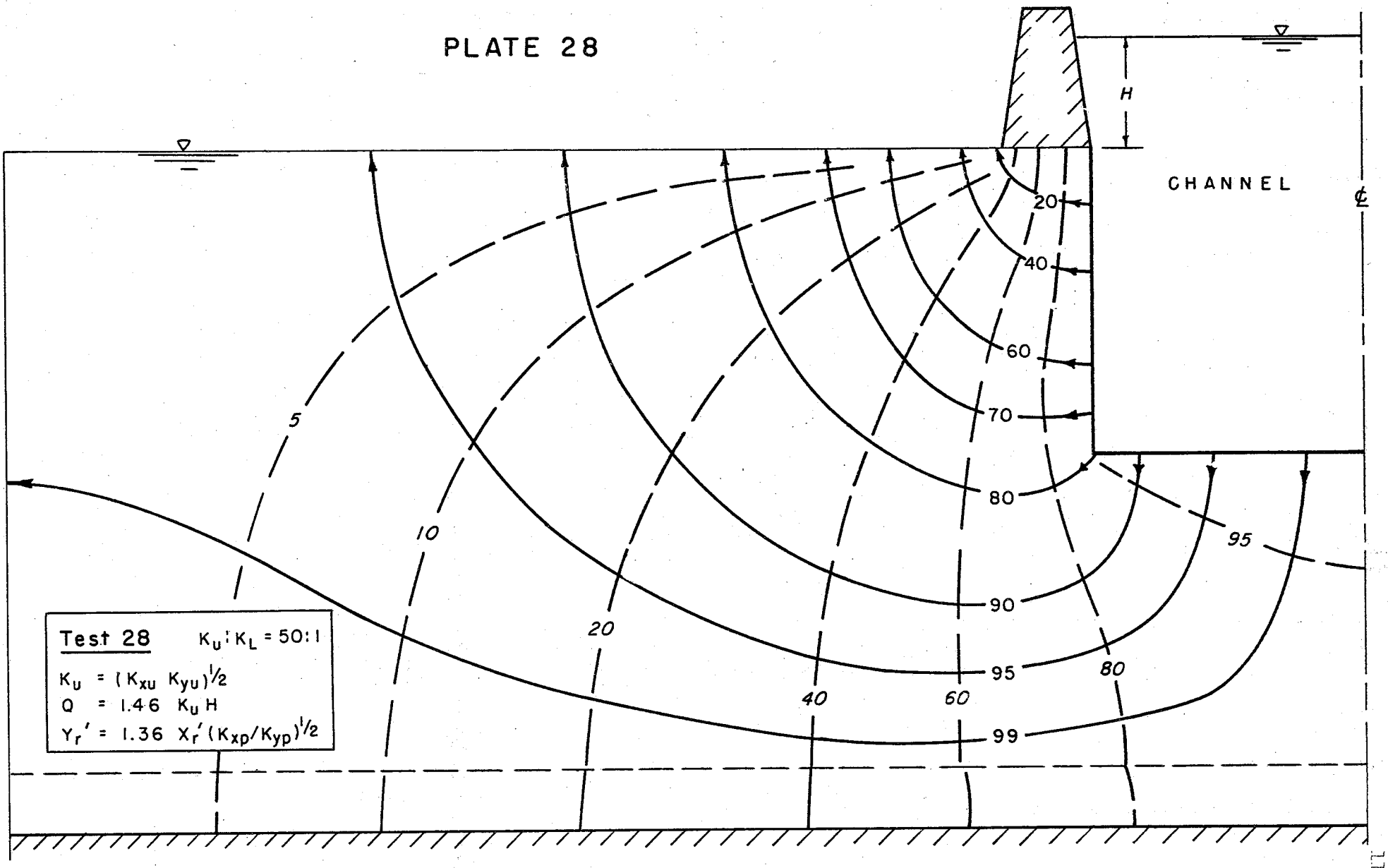
H
CHANNEL
℄
20
40
60
70
80
90
95
99
5
10
20
40
60
80
95
Test 28 $K_u : K_L = 50:1$
$K_u = (K_{xu}\ K_{yu})^{1/2}$
$Q = 1.46\ K_u\ H$
$Y_r' = 1.36\ X_r' (K_{xp}/K_{yp})^{1/2}$

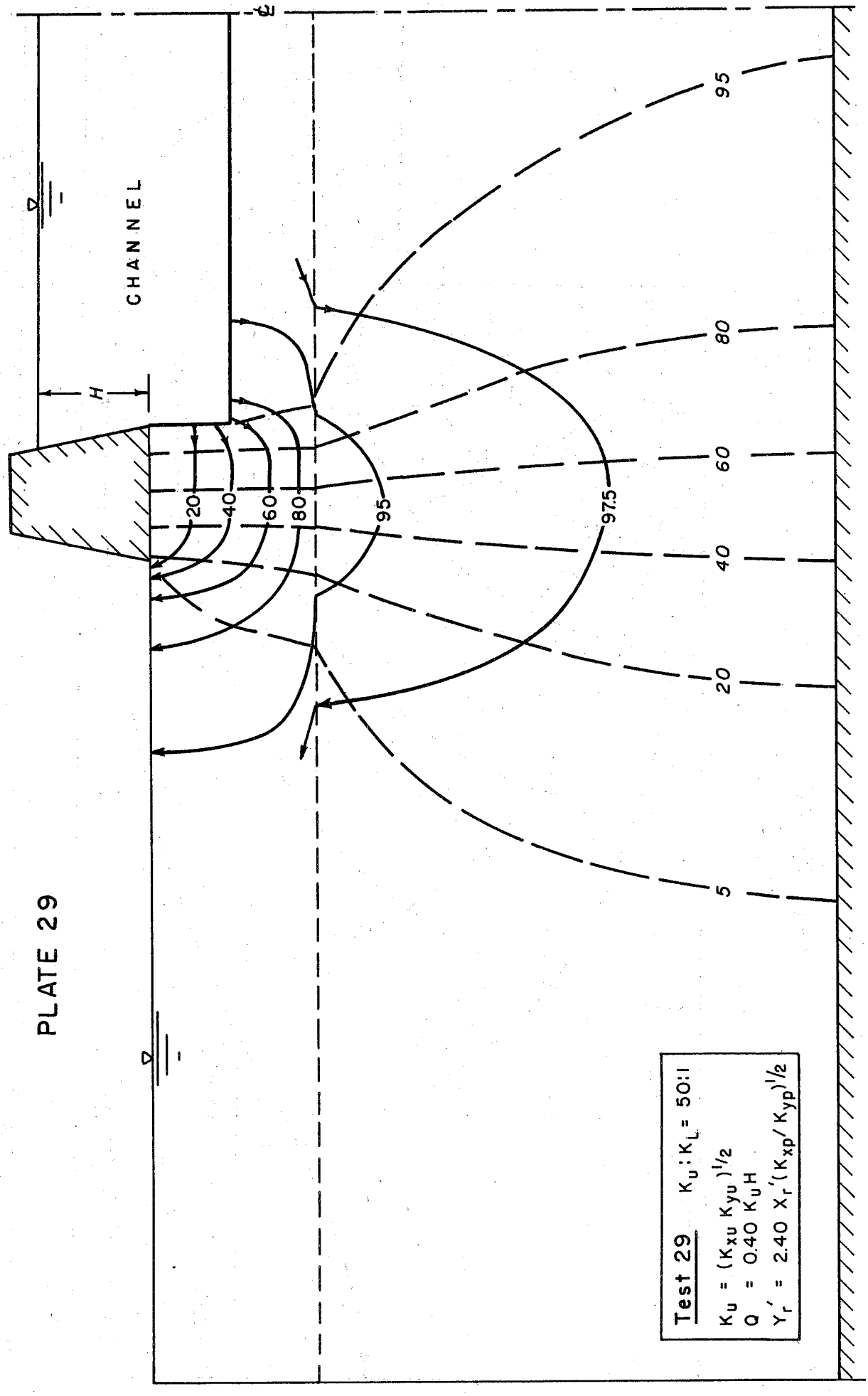
CHANNEL
H
20
40
60
80
95
97.5
95
80
60
40
20
5
Test 29 $K_u : K_L = 50:1$
$K_u = (K_{xu} K_{yu})^{1/2}$
$Q = 0.40 K_u H$
$Y_r' = 2.40 X_r' (K_{xp}/K_{yp})^{1/2}$

PLATE 29

PLATE 30

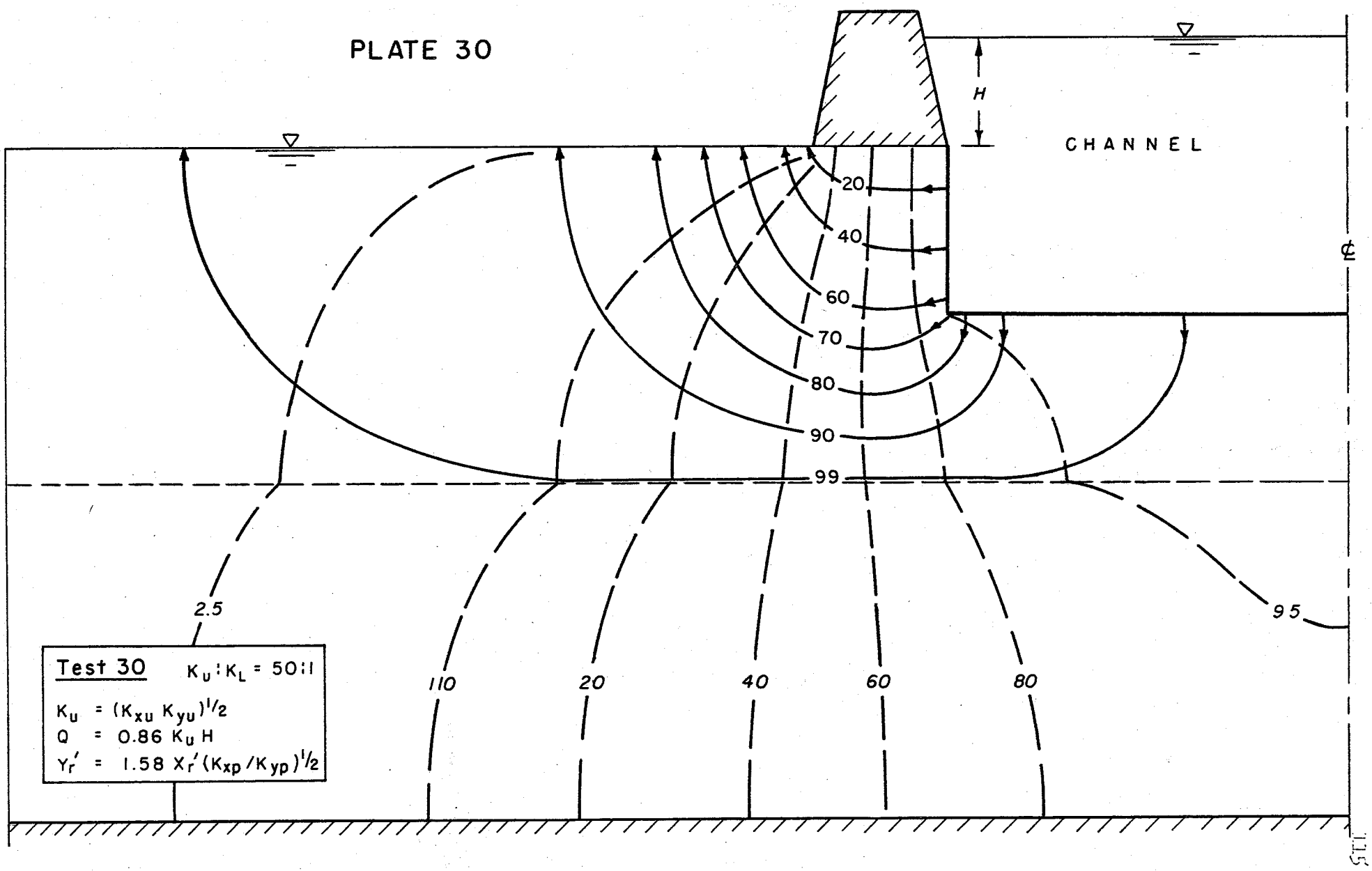
H
CHANNEL
20
40
60
70
80
90
99
2.5
110
20
40
60
80
95
Test 30 $K_u : K_L = 50:1$
$K_u = (K_{xu} K_{yu})^{1/2}$
$Q = 0.86 K_u H$
$Y_r' = 1.58 X_r' (K_{xp}/K_{yp})^{1/2}$

PLATE 31

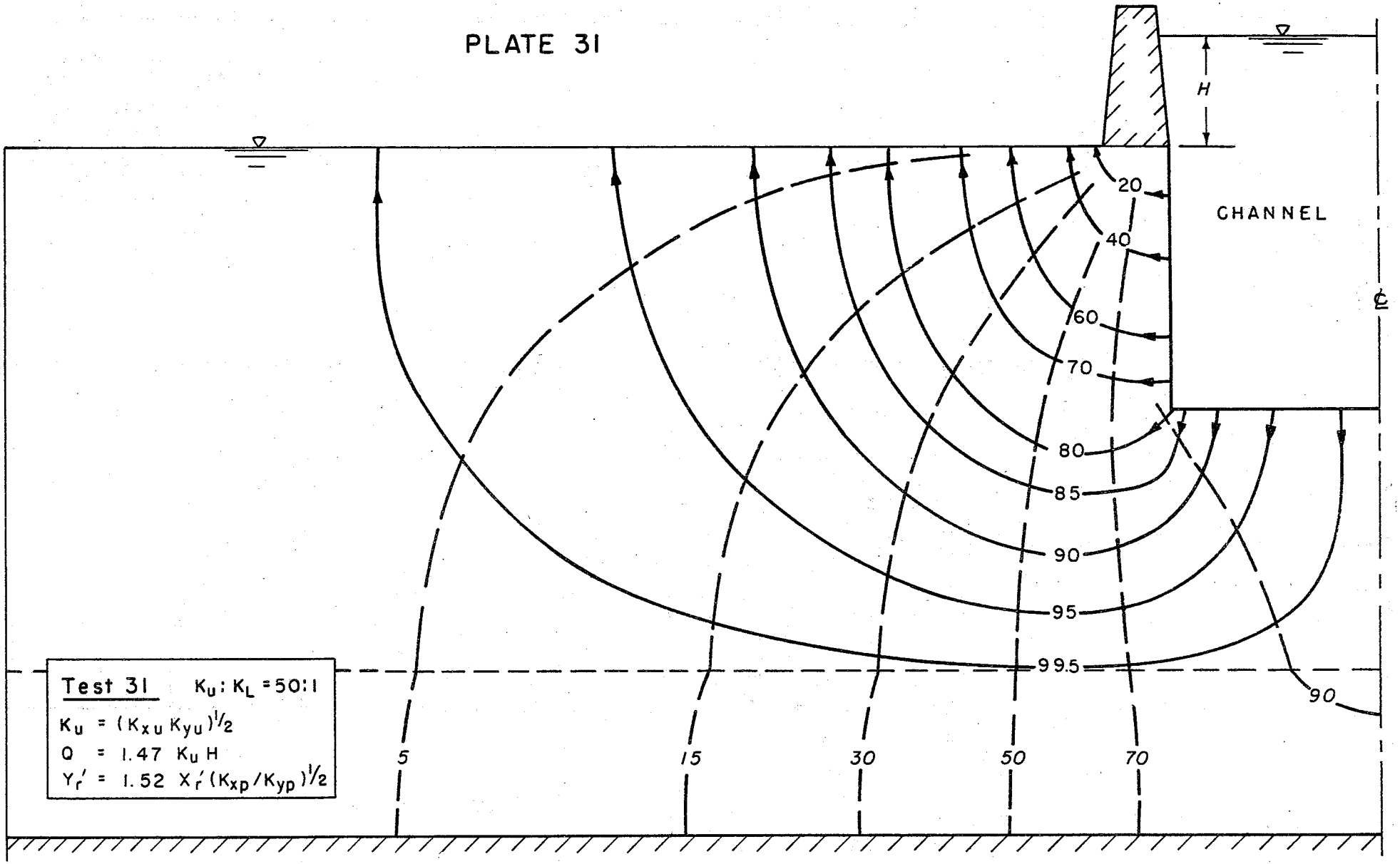
H
CHANNEL
20
40
60
70
80
85
90
95
99.5
90
5
15
30
50
70
Test 31 $K_u : K_L = 50:1$
$K_u = (K_{xu} K_{yu})^{1/2}$
$Q = 1.47\ K_u H$
$Y_r' = 1.52\ X_r' (K_{xp}/K_{yp})^{1/2}$

PLATE 32

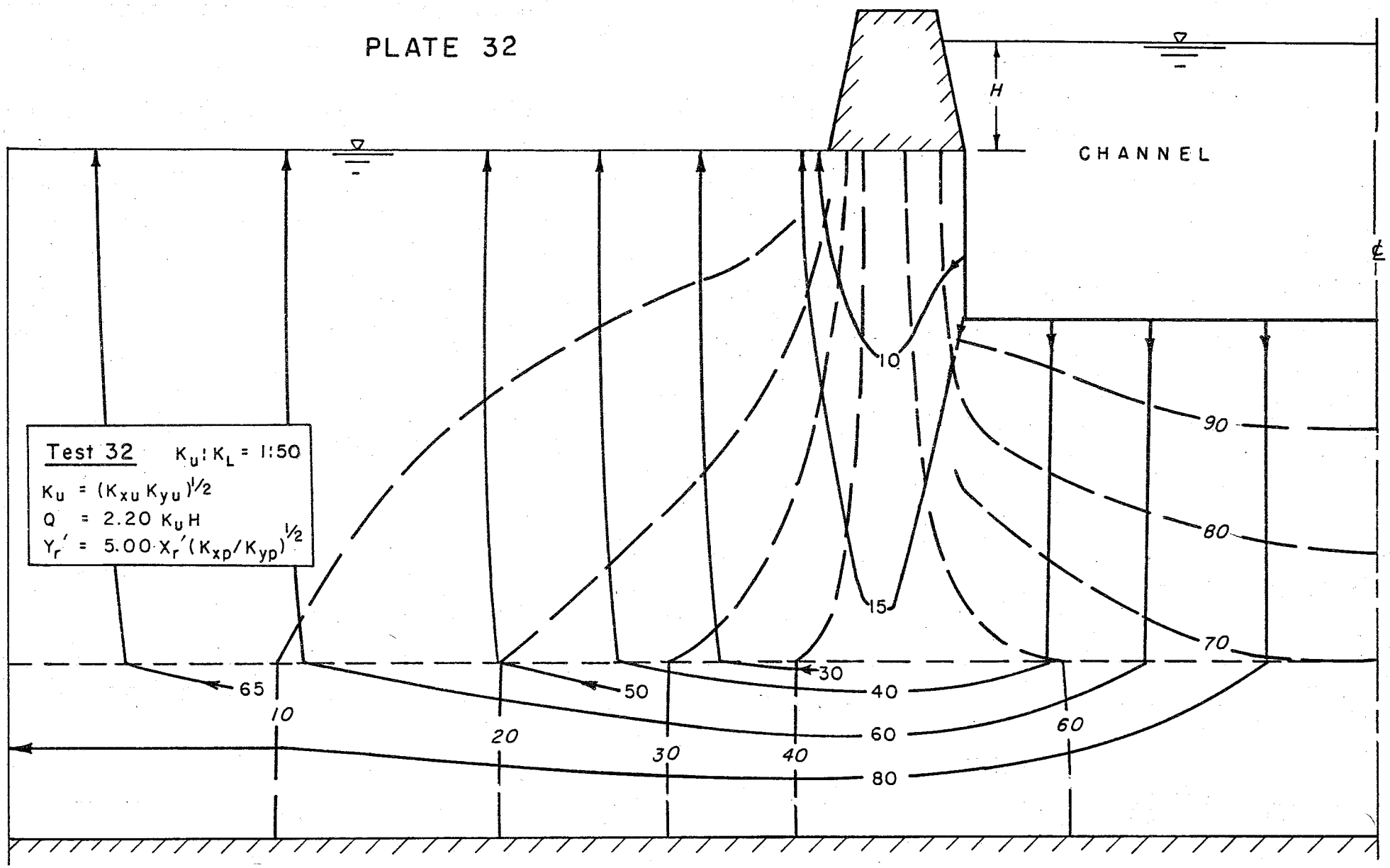
H
CHANNEL
℄
Test 32 $K_u : K_L$ = 1:50
$K_u = (K_{xu} K_{yu})^{1/2}$
$Q = 2.20 K_u H$
$Y_r' = 5.00 X_r' (K_{xp}/K_{yp})^{1/2}$
10
15
30
40
50
60
65
70
80
90
10
20
30
40
60
80

PLATE 33

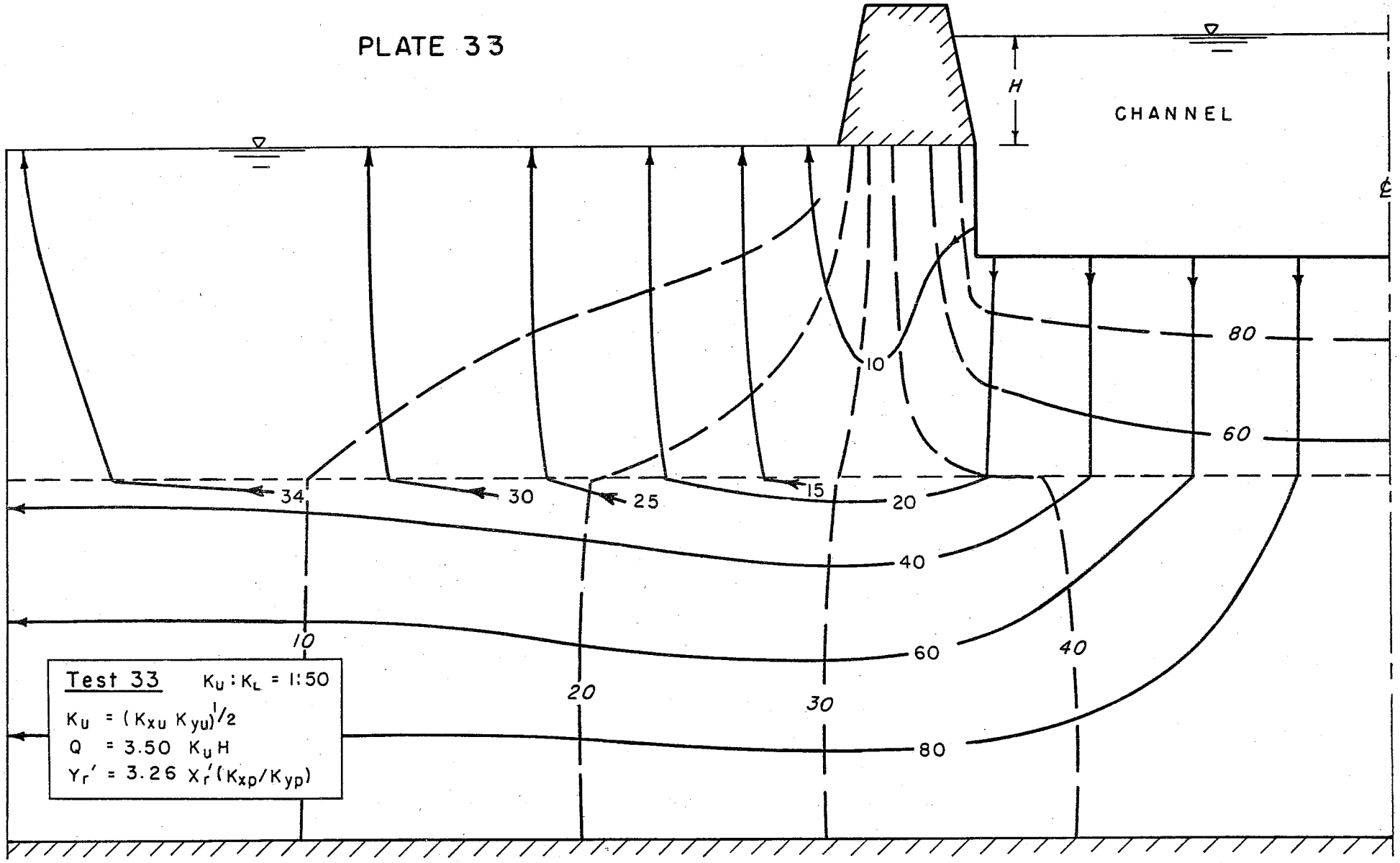
H
CHANNEL
℄
80
10
60
34
30
25
15
20
40
10
60
40
20
30
80
Test 33 $K_u : K_L$ = 1:50
$K_u = (K_{xu} K_{yu})^{1/2}$
$Q = 3.50 K_u H$
$Y_r' = 3.26 X_r' (K_{xp}/K_{yp})$

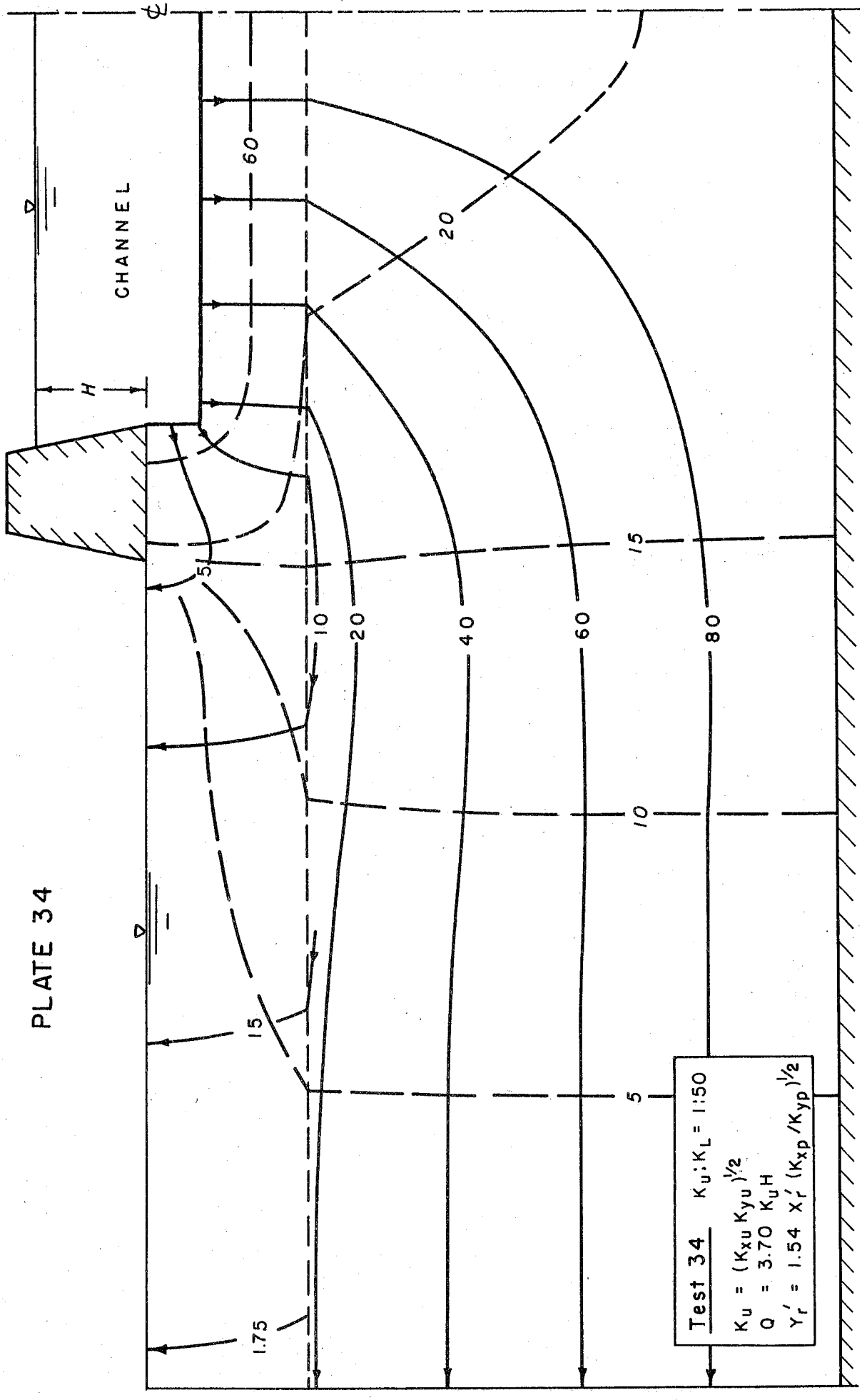
CHANNEL
H
60
20
15
10
5
1.75
5
10
20
40
60
80
Test 34 $K_u : K_L = 1:50$
$K_u = (K_{xu} K_{yu})^{1/2}$
$Q = 3.70\ K_u H$
$Y_r' = 1.54\ X_r' (K_{xp}/K_{yp})^{1/2}$

PLATE 34

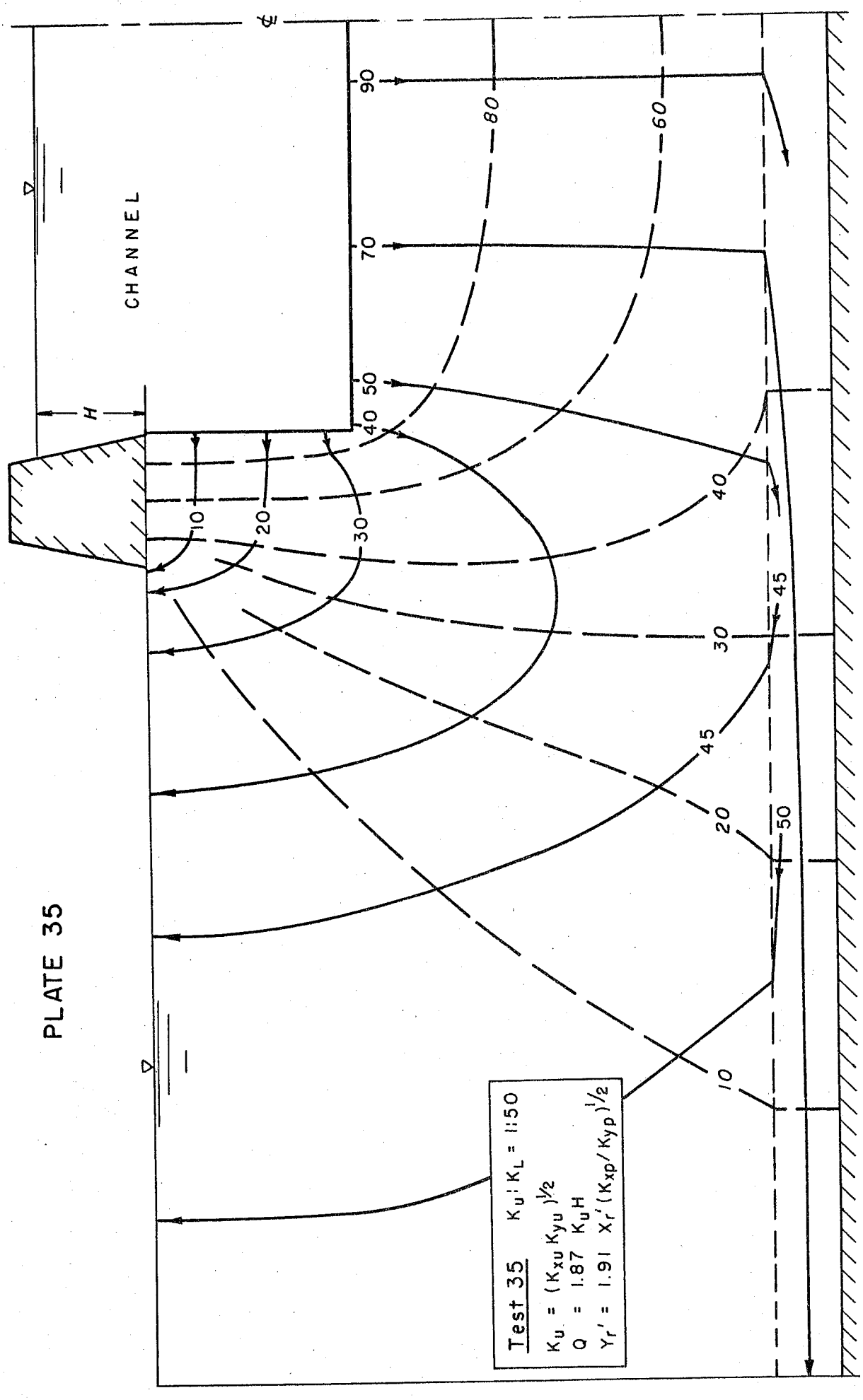
℄
CHANNEL
H
90
80
70
60
50
40
10
20
30
40
45
30
45
20
50
10
Test 35 Ku : KL = 1:50
Ku = (Kxu Kyu)1/2
Q = 1.87 KuH
Yr' = 1.91 Xr' (Kxp/Kyp)1/2

PLATE 35

PLATE 36

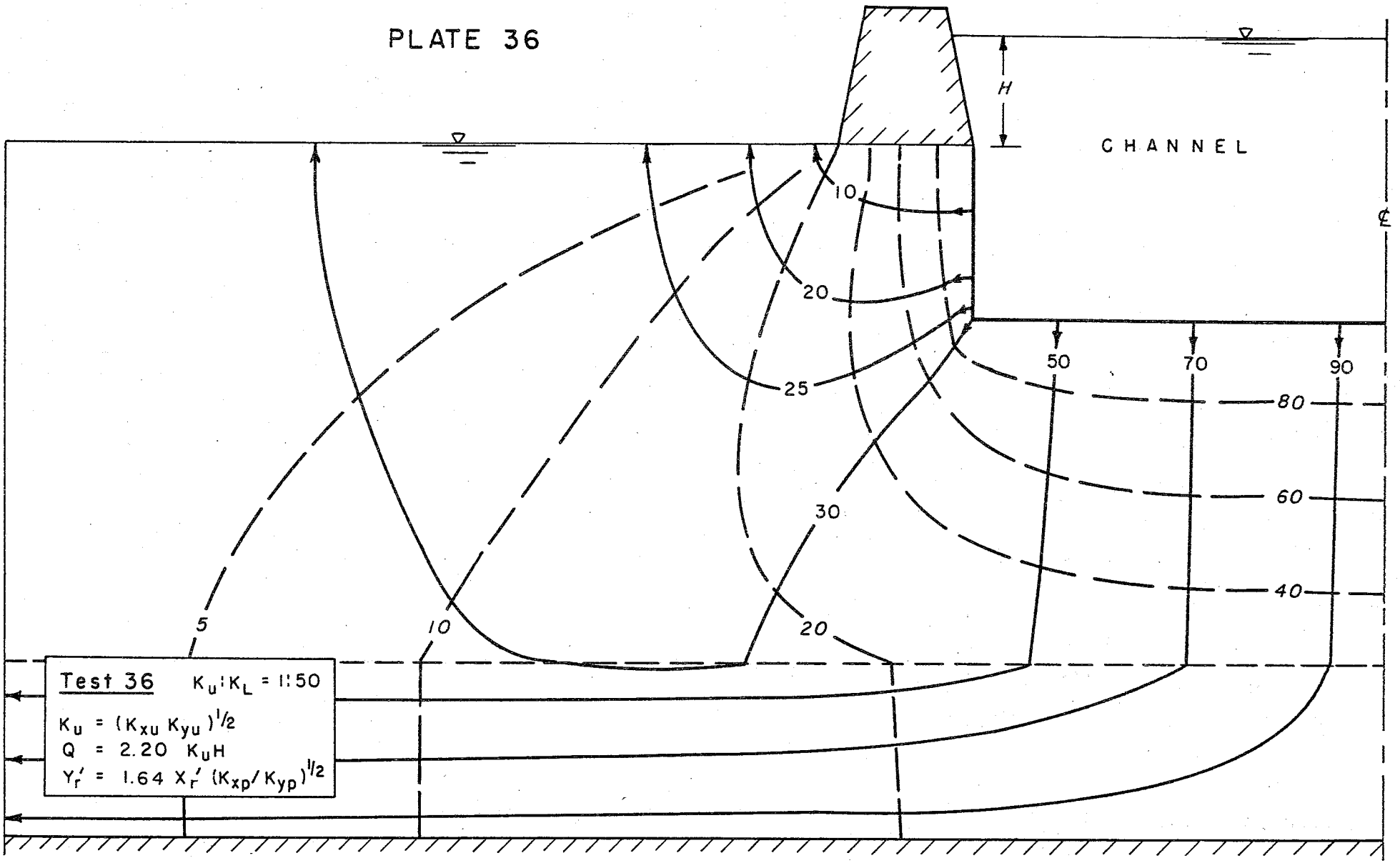
H
CHANNEL
℄
10
20
25
30
50
70
90
80
60
40
5
10
20
Test 36 $K_u : K_L$ = 1:50
$K_u = (K_{xu} K_{yu})^{1/2}$
$Q = 2.20\ K_u H$
$Y_r' = 1.64\ X_r' (K_{xp}/K_{yp})^{1/2}$

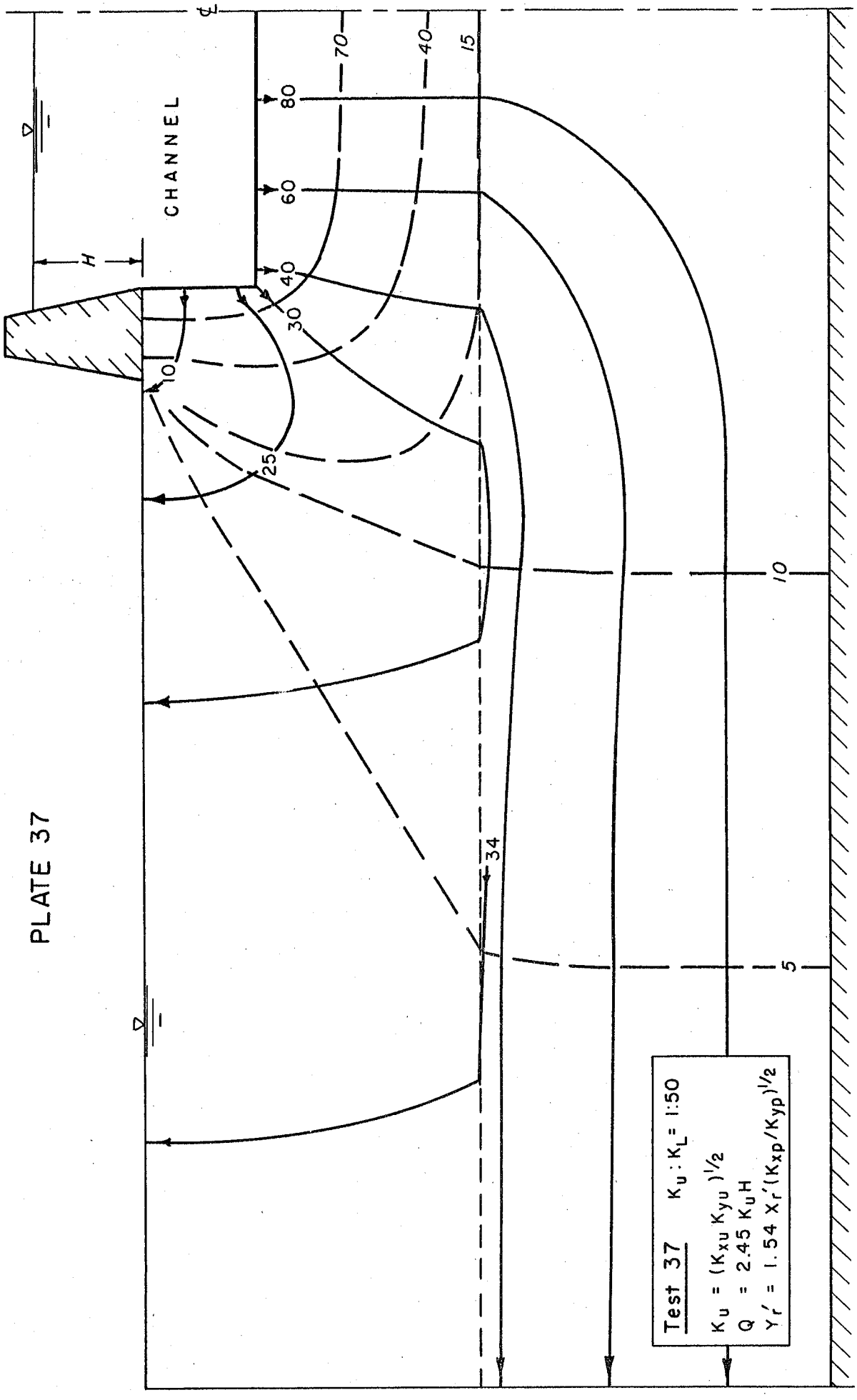
CHANNEL
H
80
70
60
40
30
25
15
10
34
5
Test 37 $K_u : K_L = 1:50$
$K_u = (K_{xu} K_{yu})^{1/2}$
$Q = 2.45 K_u H$
$Y_r' = 1.54 X_r' (K_{xp}/K_{yp})^{1/2}$

PLATE 37

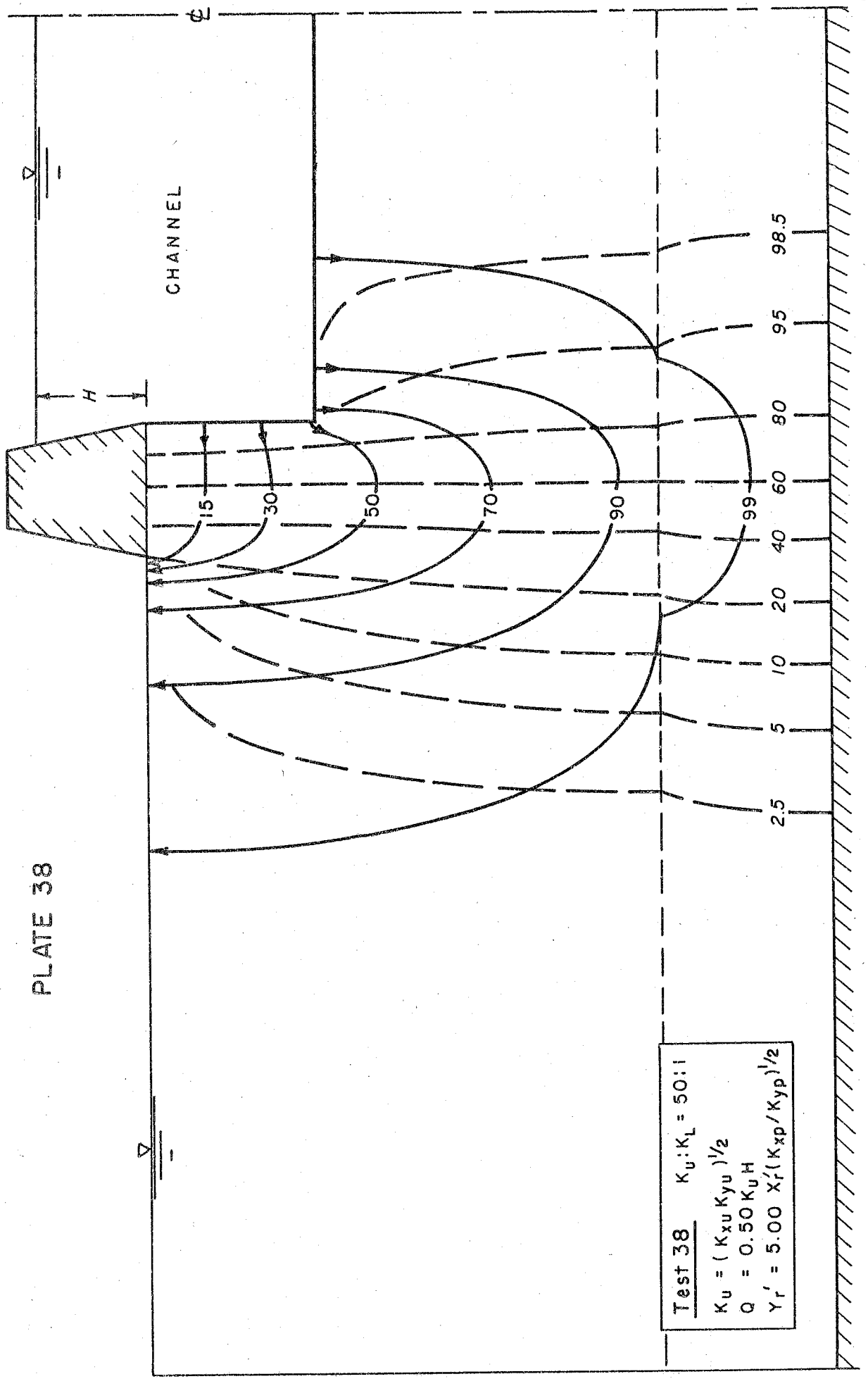
CHANNEL
H
15
30
50
70
90
99
98.5
95
80
60
40
20
10
5
2.5
Test 38 $K_u : K_L = 50:1$
$K_u = (K_{xu} K_{yu})^{1/2}$
$Q = 0.50 K_u H$
$Y_r' = 5.00 X_r' (K_{xp}/K_{yp})^{1/2}$

PLATE 38

PLATE 39

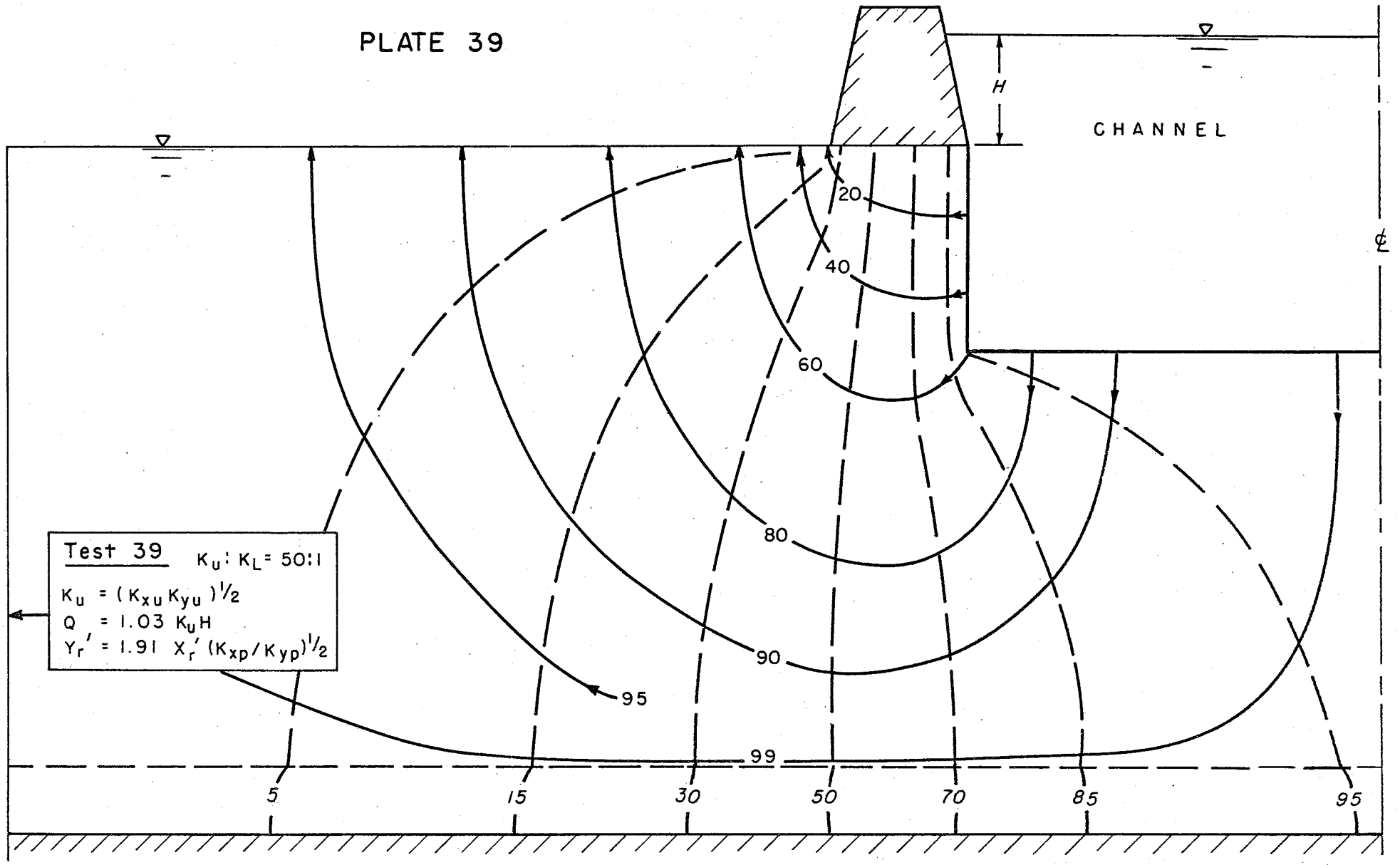
H
CHANNEL
℄
20
40
60
80
90
95
99
5
15
30
50
70
85
95
Test 39
$K_u : K_L = 50:1$
$K_u = (K_{xu} K_{yu})^{1/2}$
$Q = 1.03\ K_u H$
$Y_r' = 1.91\ X_r' (K_{xp}/K_{yp})^{1/2}$

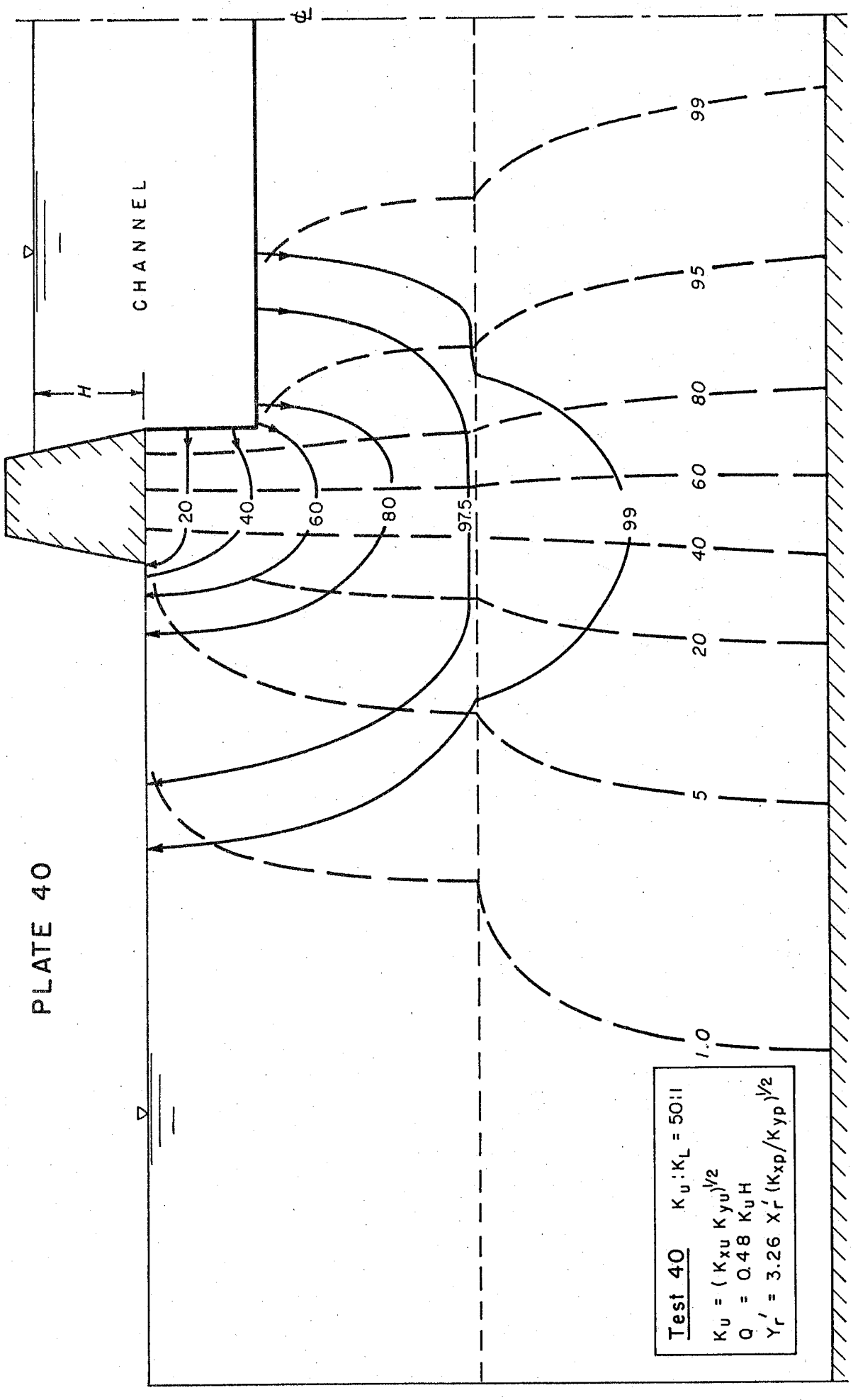
CHANNEL
H
20
40
60
80
97.5
99
99
95
80
60
40
20
5
1.0
Test 40 $K_u : K_L = 50:1$
$K_u = (K_{xu} K_{yu})^{1/2}$
$Q = 0.48 K_u H$
$Y_r' = 3.26 X_r' (K_{xp}/K_{yp})^{1/2}$

PLATE 40

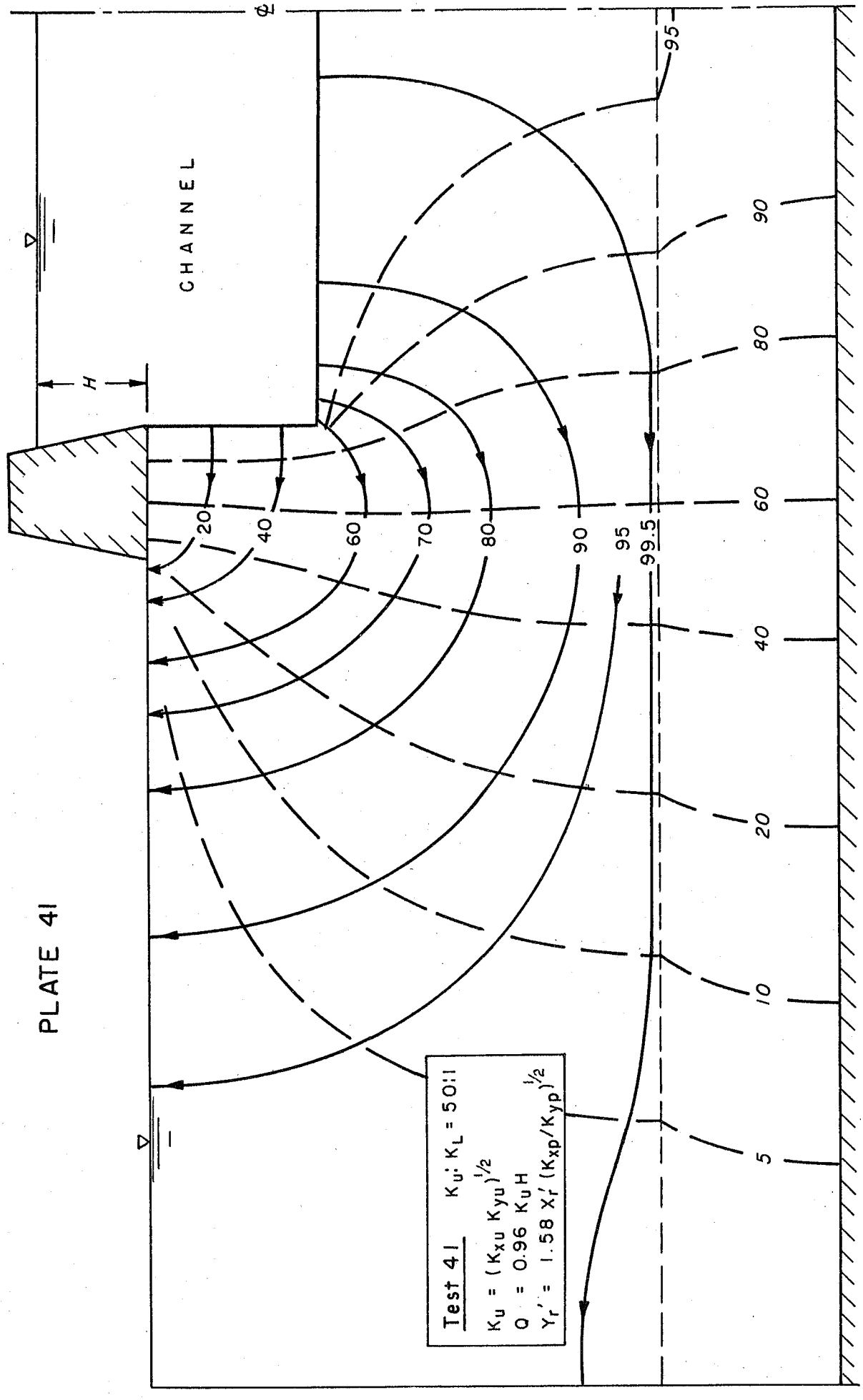
CHANNEL
H
20
40
60
70
80
90
95
99.5
95
90
80
60
40
20
10
5
Test 41 $K_u : K_L = 50:1$
$K_u = (K_{xu} K_{yu})^{1/2}$
$Q = 0.96 K_u H$
$Y_r' = 1.58 X_r' (K_{xp}/K_{yp})^{1/2}$

PLATE 41

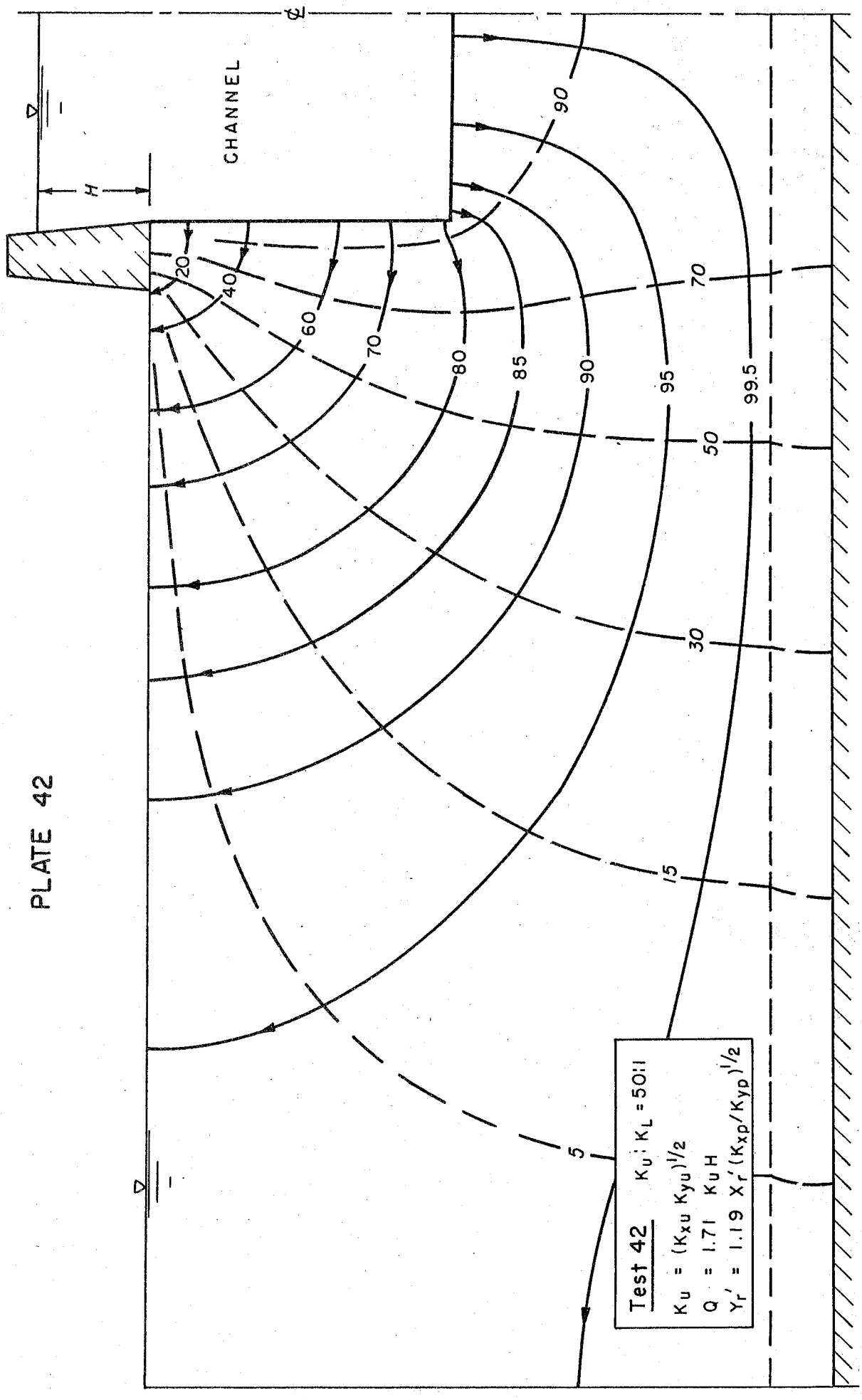
CHANNEL
H
20
40
60
70
80
85
90
95
99.5
90
70
50
30
15
5
Test 42 Ku : KL = 50:1
Ku = (Kxu Kyu)1/2
Q = 1.71 Ku H
Yr' = 1.19 Xr' (Kxp/Kyp)1/2

PLATE 42

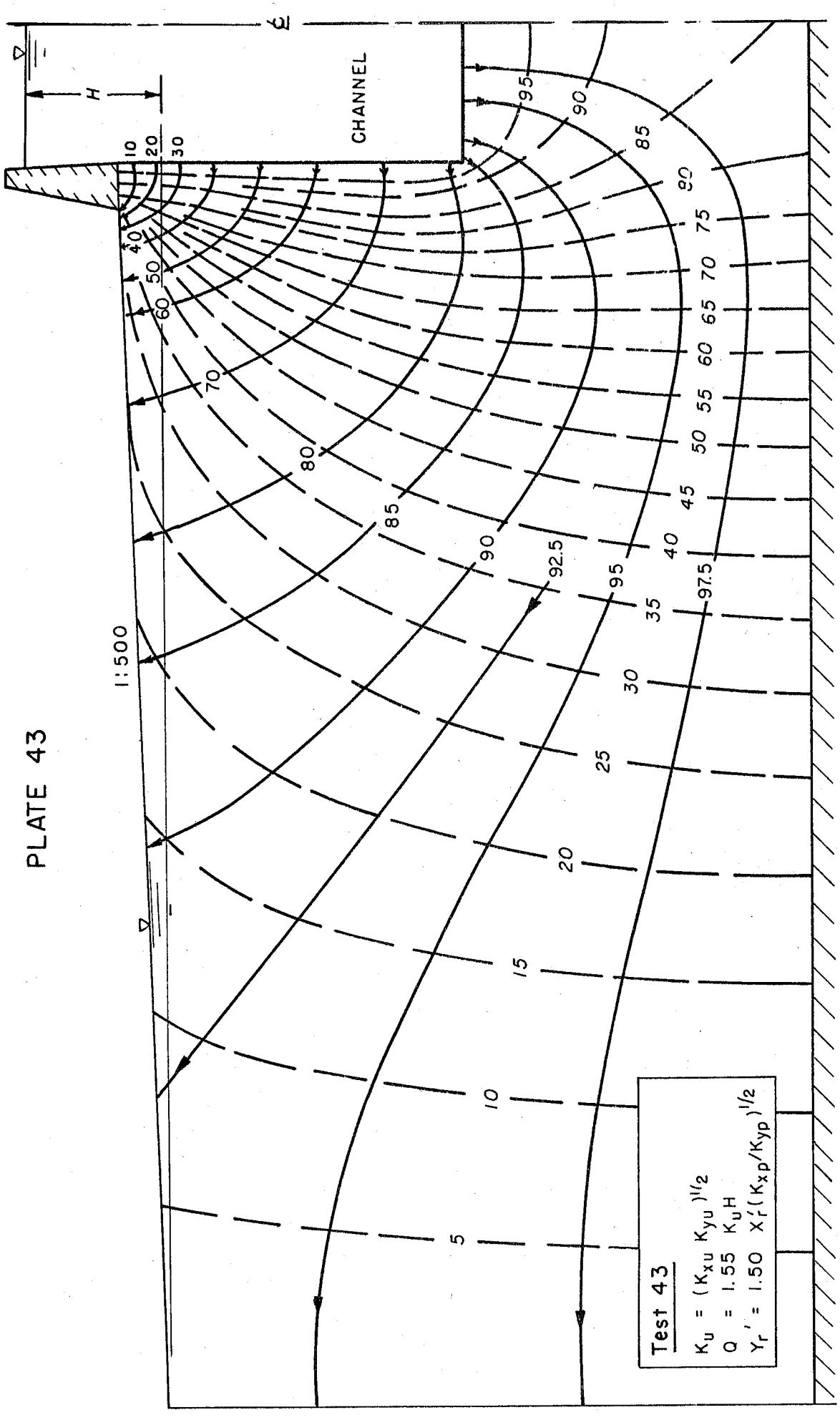
CHANNEL
H
1:500
Test 43
$K_u = (K_{xu} K_{yu})^{1/2}$
$Q = 1.55 K_u H$
$Y_r' = 1.50 X_r' (K_{xp}/K_{yp})^{1/2}$

PLATE 43

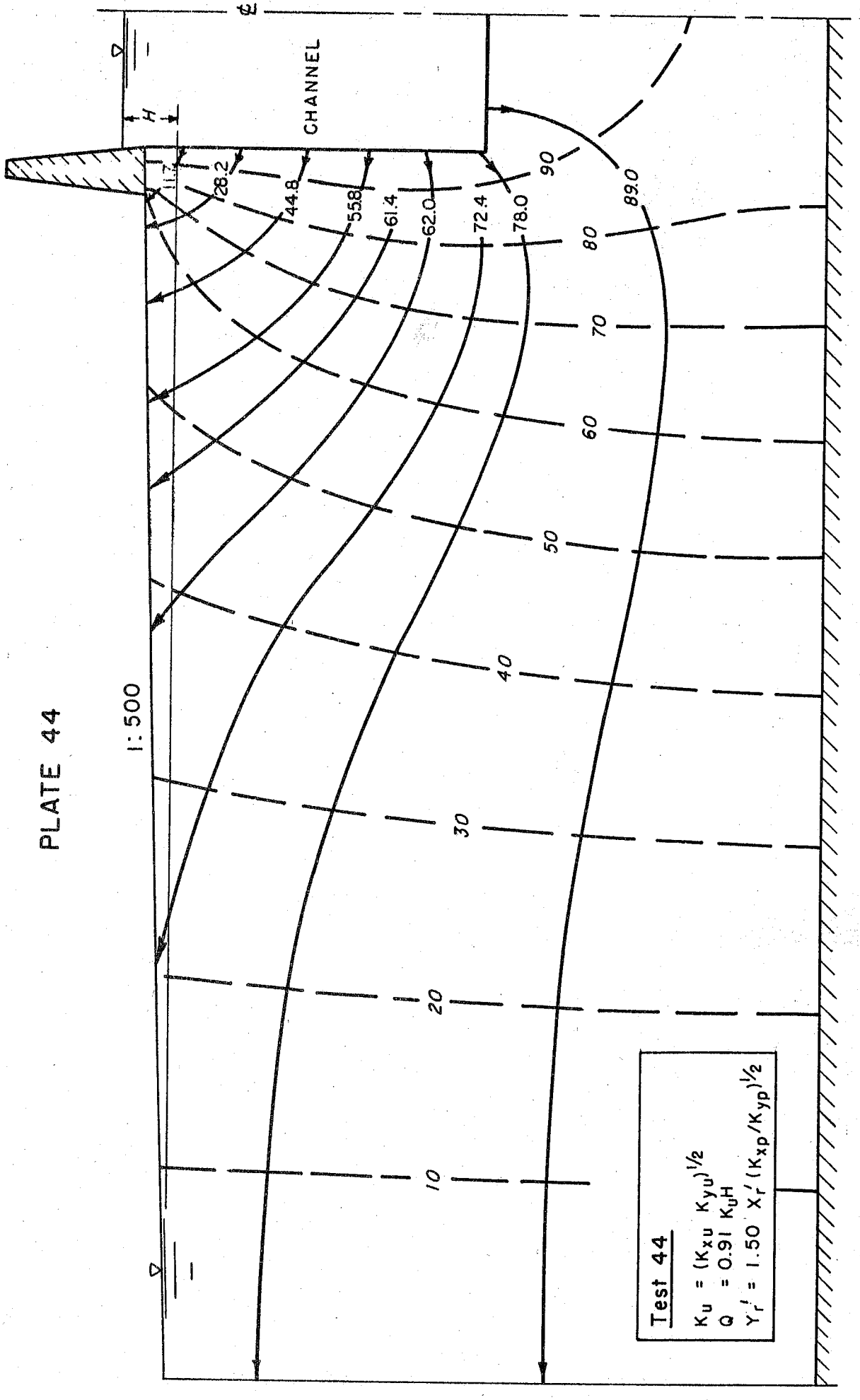
℄
CHANNEL
H
11.7
28.2
44.8
55.8
61.4
62.0
72.4
78.0
89.0
90
80
70
60
50
40
30
20
10
1:500
Test 44
Ku = (Kxu Kyu)1/2
Q = 0.91 KuH
Yr' = 1.50 Xr' (Kxp/Kyp)1/2

PLATE 44

PLATE 45

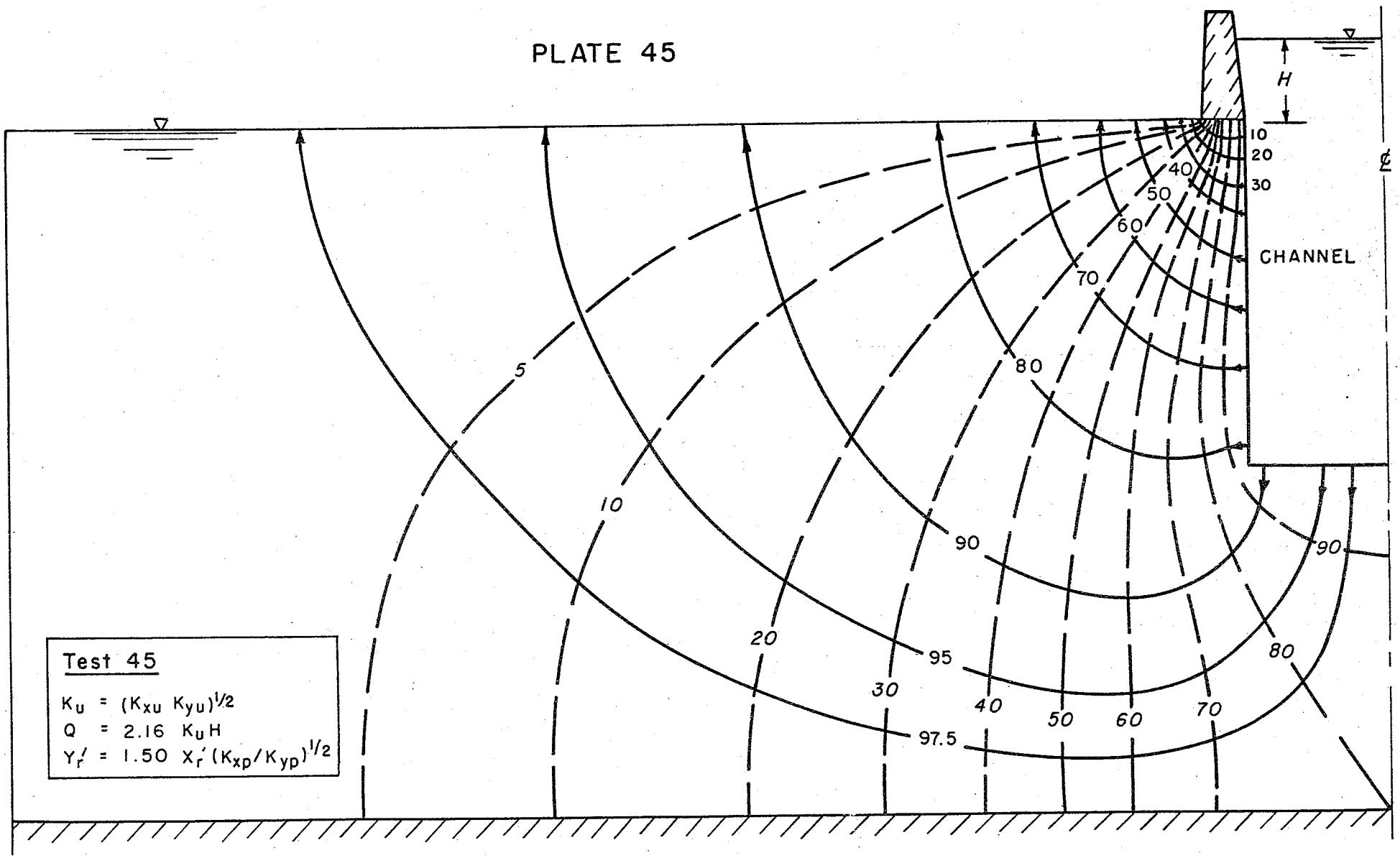
H
10
20
40
30
50
60
CHANNEL
70
80
5
10
90
90
20
95
80
30
40
50
60
70
97.5
Test 45
$K_u = (K_{xu} K_{yu})^{1/2}$
$Q = 2.16 K_u H$
$Y_r' = 1.50 X_r' (K_{xp}/K_{yp})^{1/2}$

PLATE 46

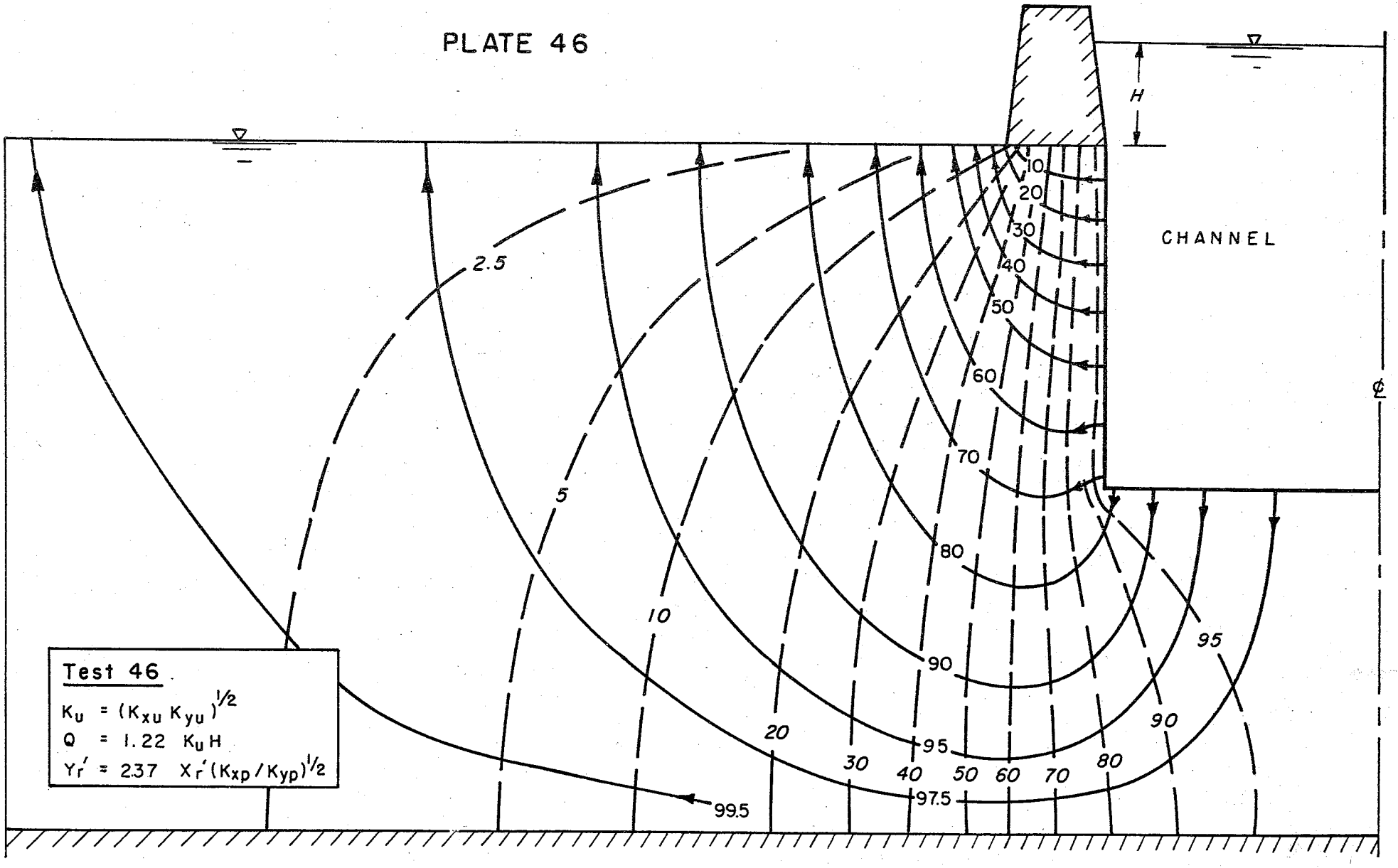
H
CHANNEL
℄
2.5
5
10
20
30
40
50
60
70
80
90
95
97.5
99.5
10
20
30
40
50
60
70
80
90
95
Test 46
$K_u = (K_{xu} K_{yu})^{1/2}$
$Q = 1.22 K_u H$
$Y_r' = 2.37 X_r' (K_{xp}/K_{yp})^{1/2}$

PLATE 47

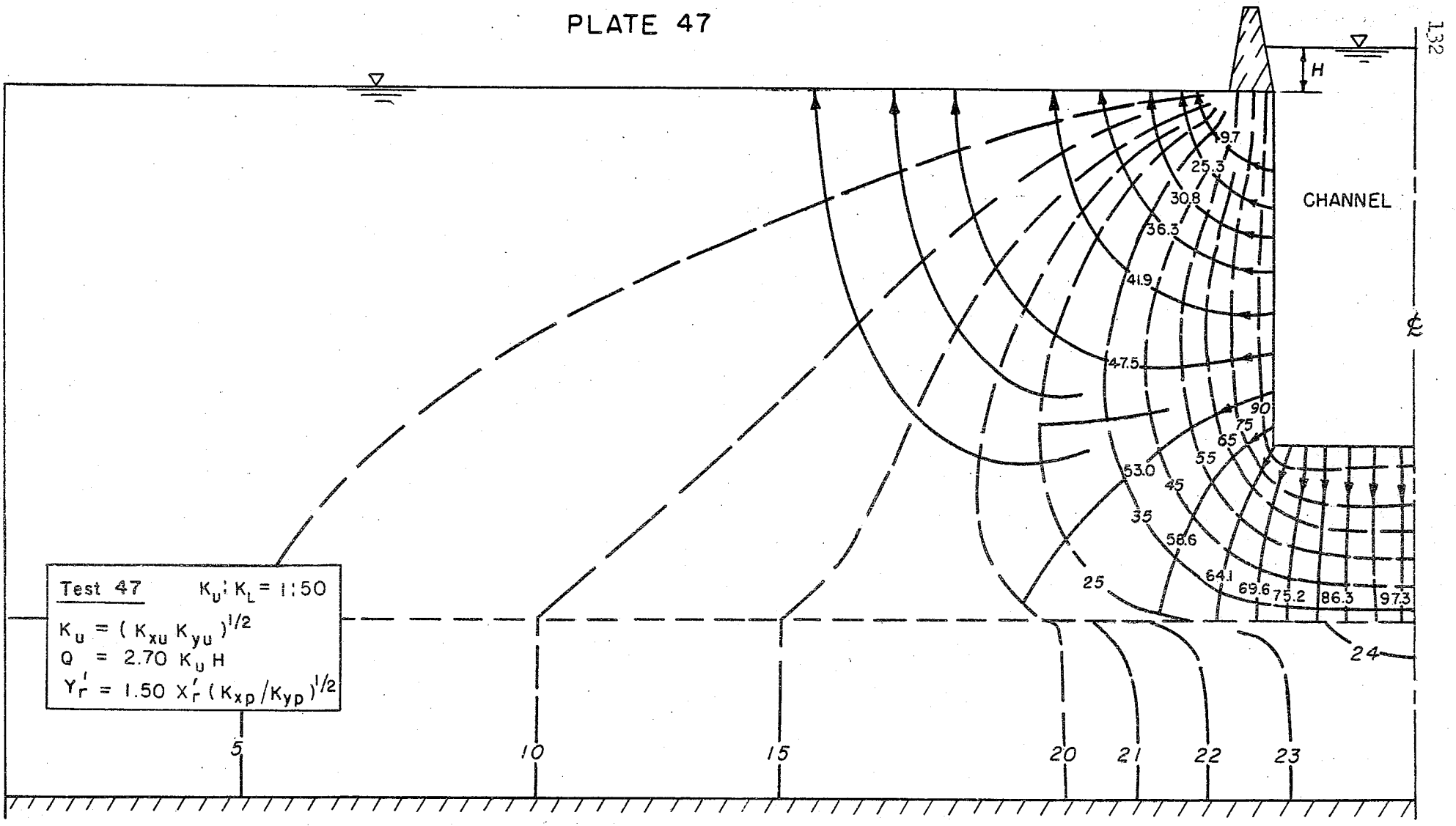
H
CHANNEL
℄
19.7
25.3
30.8
36.3
41.9
47.5
90
75
65
55
53.0
45
35
58.6
64.1
69.6
75.2
86.3
97.3
25
24
Test 47 K_u : K_L = 1:50
K_u = (K_xu K_yu)^1/2
Q = 2.70 K_u H
Y'_r = 1.50 X'_r (K_xp / K_yp)^1/2
5
10
15
20
21
22
23

PLATE 48

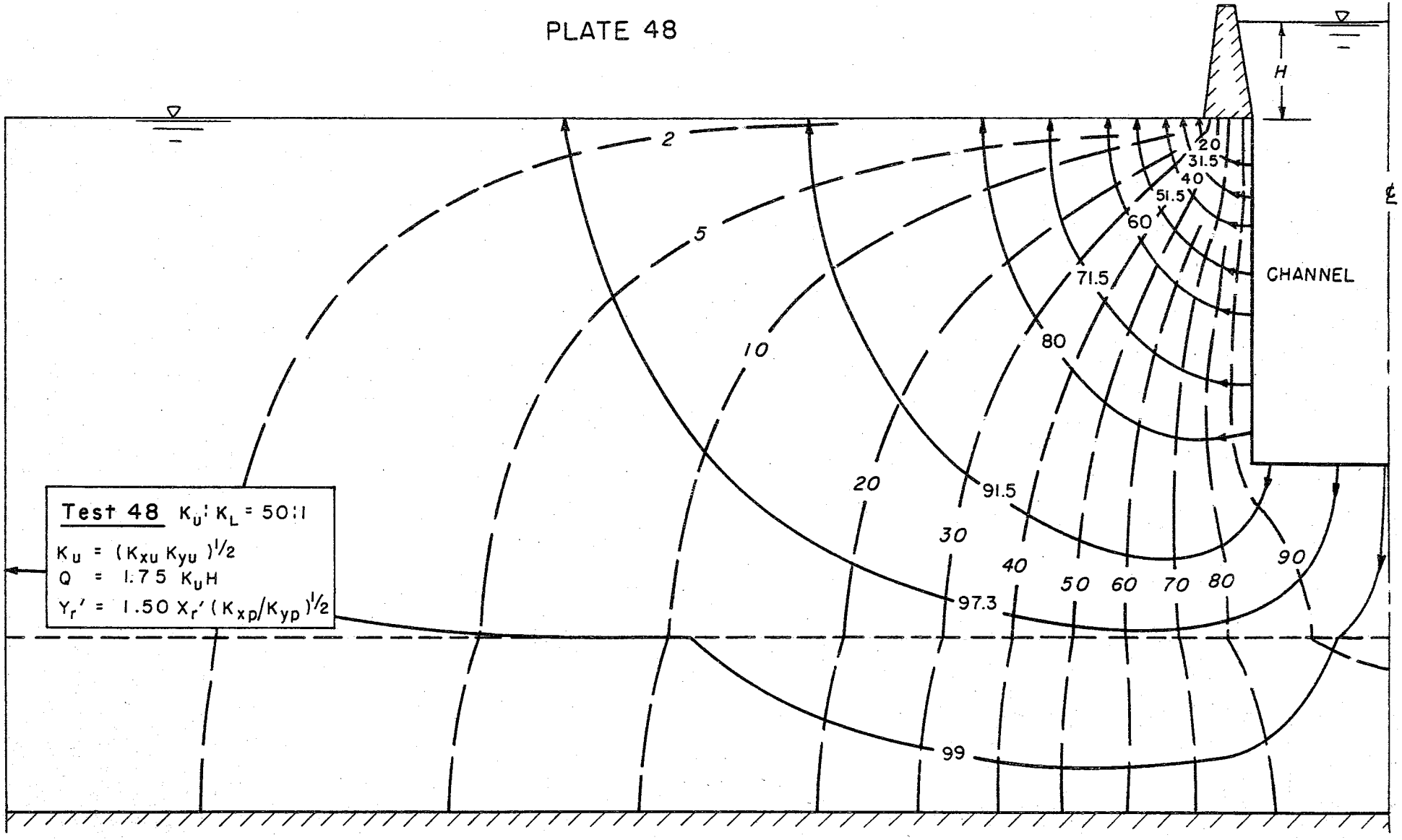
H
2
5
10
20
30
40
50
60
70
80
90
91.5
97.3
99
20
31.5
40
51.5
60
71.5
80
CHANNEL
Test 48 $K_u : K_L = 50:1$
$K_u = (K_{xu} K_{yu})^{1/2}$
$Q = 1.75 K_u H$
$Y_r' = 1.50 X_r' (K_{xp}/K_{yp})^{1/2}$

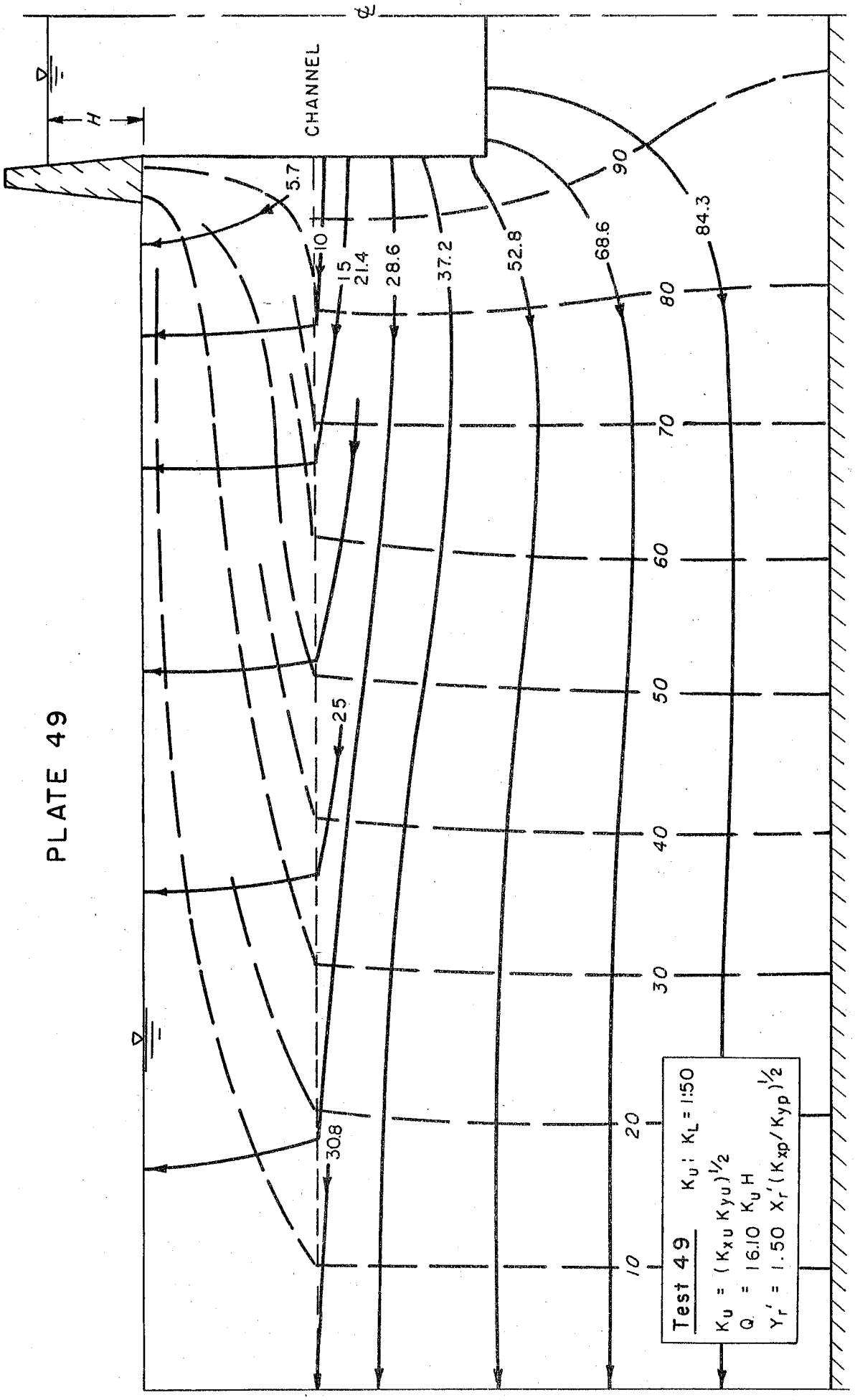
CHANNEL
H
5.7
10
15
21.4
28.6
37.2
52.8
68.6
84.3
90
80
70
60
50
40
30
20
10
25
30.8
Test 49 K_u : K_L = 1:50
$K_u = (K_{xu} K_{yu})^{1/2}$
$Q = 16.10\ K_u H$
$Y_r' = 1.50\ X_r' (K_{xp}/K_{yp})^{1/2}$

PLATE 49

PLATE 50

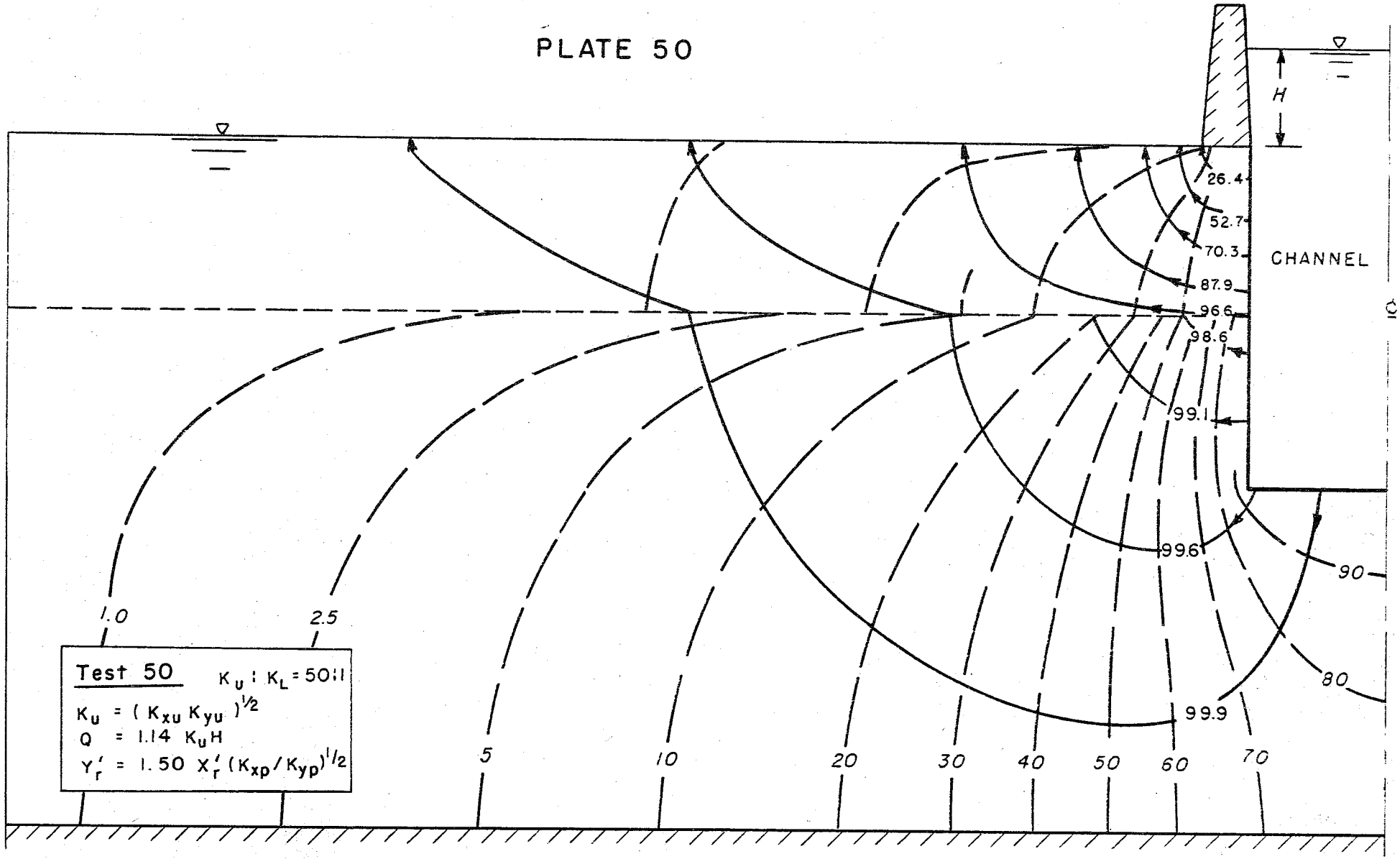
H
CHANNEL
26.4
52.7
70.3
87.9
96.6
98.6
99.1
99.6
99.9
90
80
1.0
2.5
5
10
20
30
40
50
60
70
Test 50
$K_u : K_L = 50:1$
$K_u = (K_{xu} K_{yu})^{1/2}$
$Q = 1.14 K_u H$
$Y_r' = 1.50 X_r' (K_{xp}/K_{yp})^{1/2}$

PLATE 51

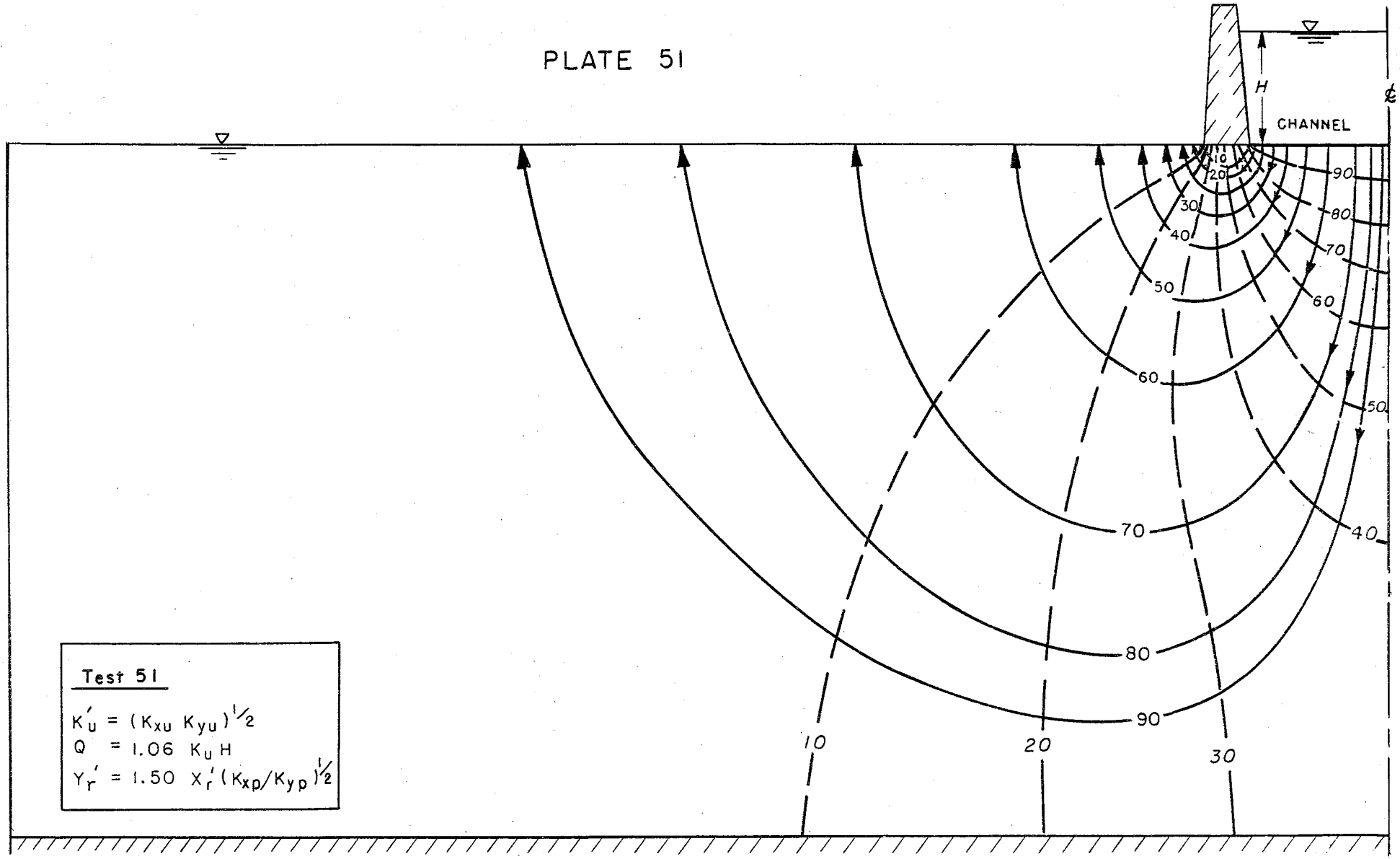
H
CHANNEL
10
20
30
40
50
60
70
80
90
Test 51
$K'_u = (K_{xu}\ K_{yu})^{1/2}$
$Q = 1.06\ K_u\ H$
$Y'_r = 1.50\ X'_r\ (K_{xp}/K_{yp})^{1/2}$

PLATE 52

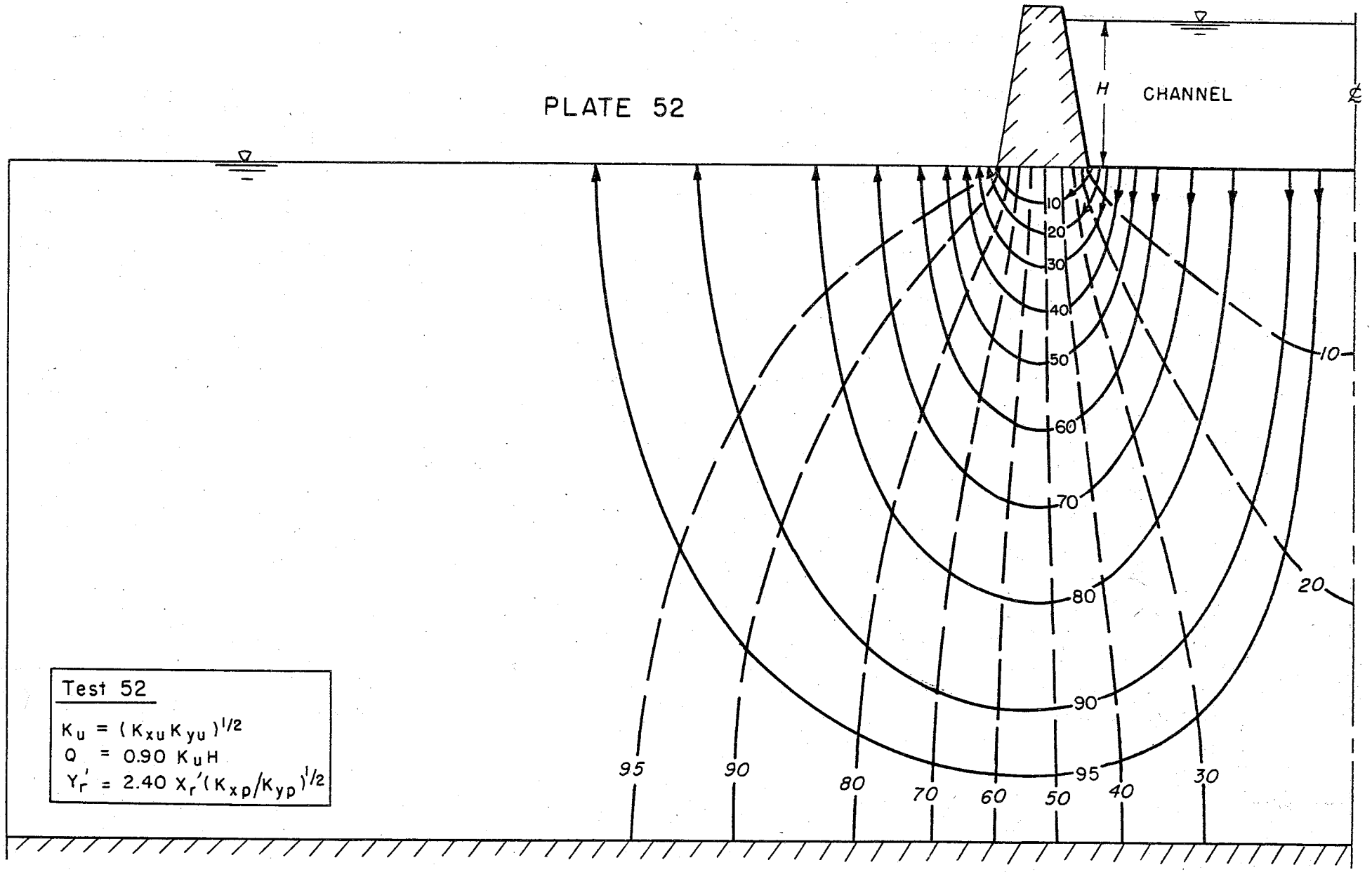
H
CHANNEL
℄
10
20
30
40
50
60
70
80
90
95
10
20
30
40
50
60
70
80
90
95
Test 52
$K_u = (K_{xu} K_{yu})^{1/2}$
$Q = 0.90\ K_u H$
$Y_r' = 2.40\ X_r' (K_{xp}/K_{yp})^{1/2}$

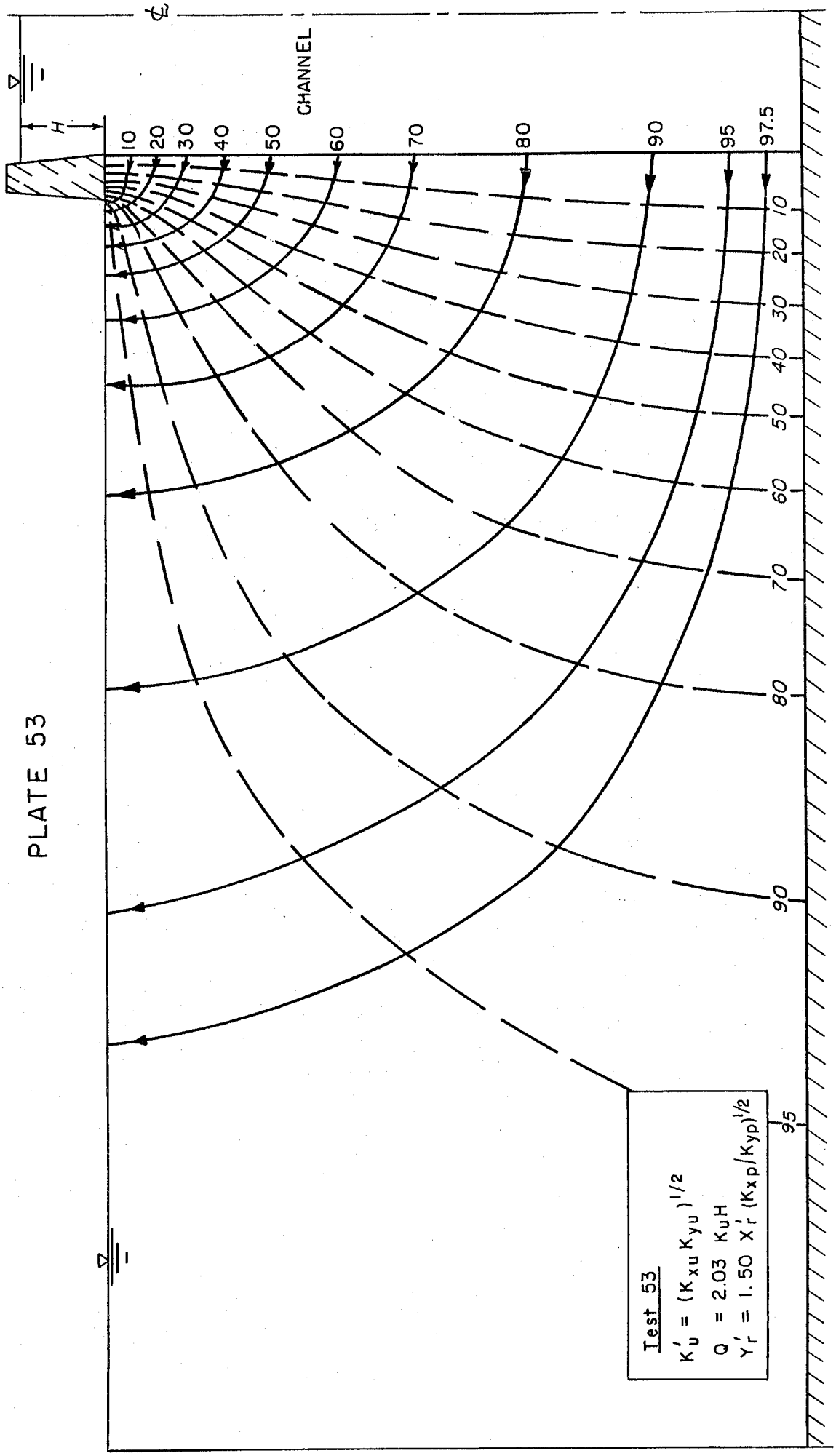
℄
CHANNEL
H
10
20
30
40
50
60
70
80
90
95
97.5
Test 53
$K'_u = (K_{xu} K_{yu})^{1/2}$
Q = 2.03 $K_u H$
$Y'_r = 1.50\ X'_r\ (K_{xp}/K_{yp})^{1/2}$

PLATE 53

PLATE 54

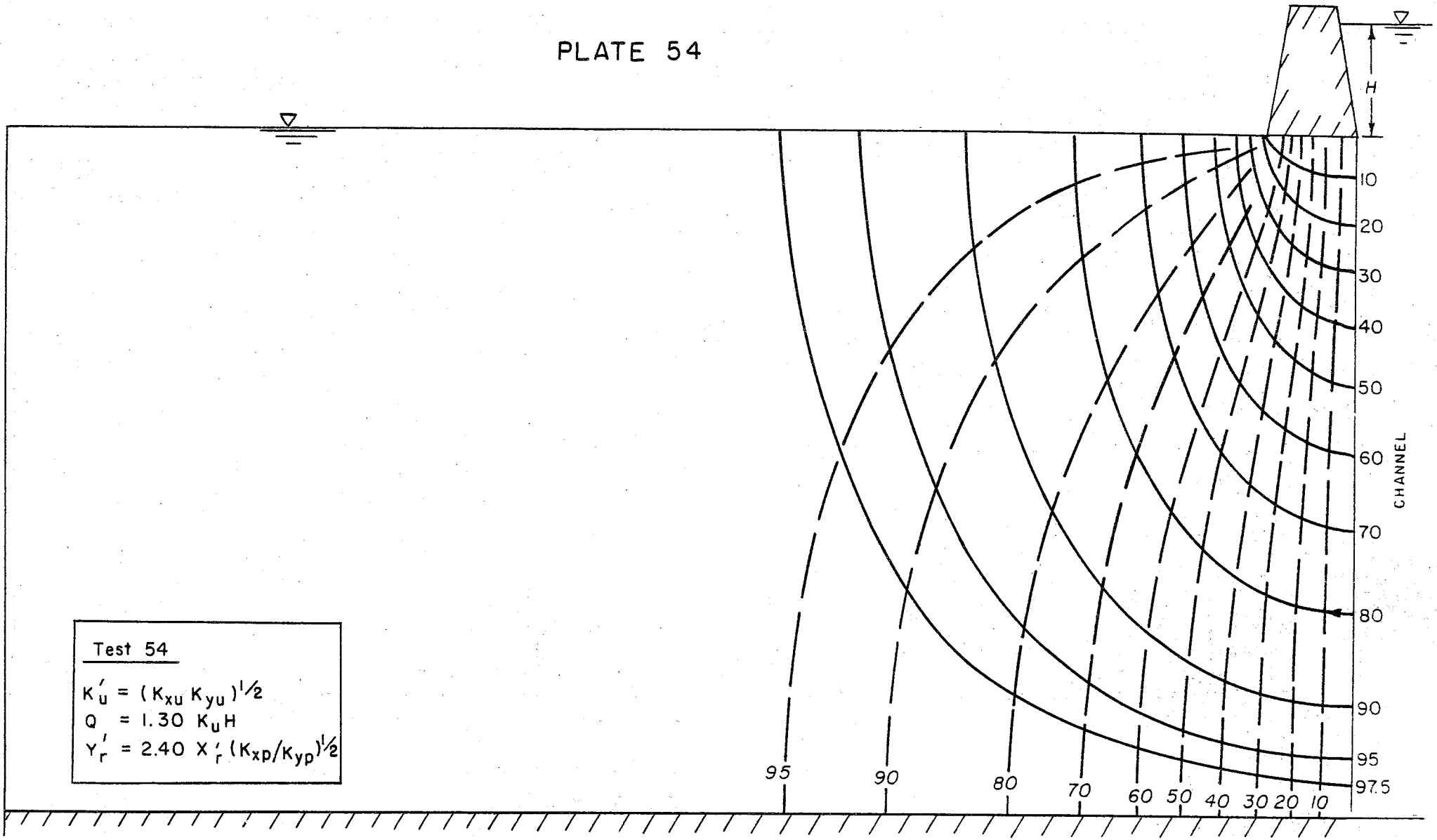
H
10
20
30
40
50
60
70
80
90
95
97.5
CHANNEL
95
90
80
70
60
50
40
30
20
10
Test 54
$K'_u = (K_{xu} K_{yu})^{1/2}$
$Q = 1.30 K_u H$
$Y'_r = 2.40 X'_r (K_{xp}/K_{yp})^{1/2}$

PLATE 55

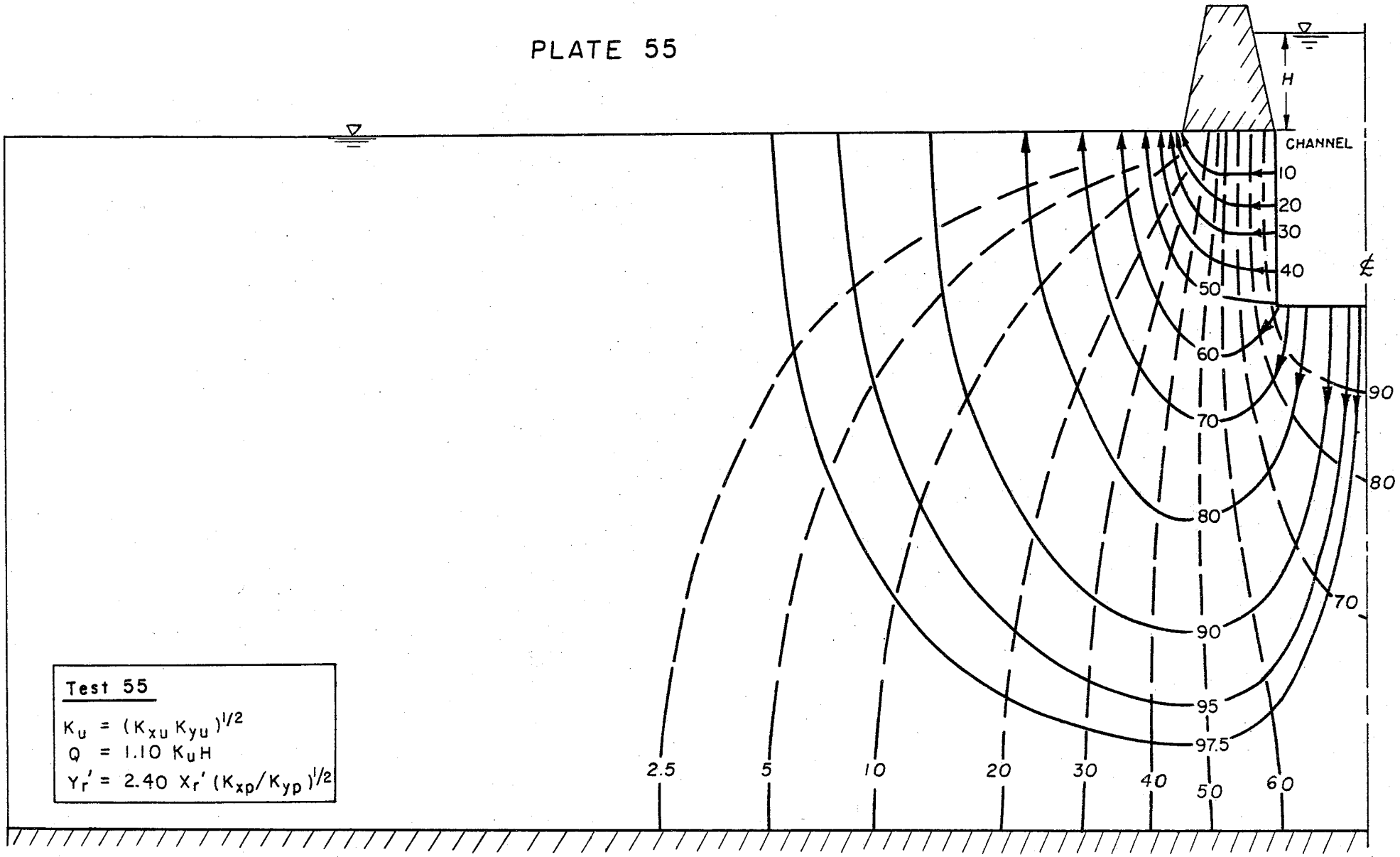
H
CHANNEL
10
20
30
40
50
60
70
80
90
95
97.5
2.5
5
10
20
30
40
50
60
70
80
90
Test 55
$K_u = (K_{xu} K_{yu})^{1/2}$
$Q = 1.10 K_u H$
$Y_r' = 2.40 X_r' (K_{xp}/K_{yp})^{1/2}$

PLATE 56

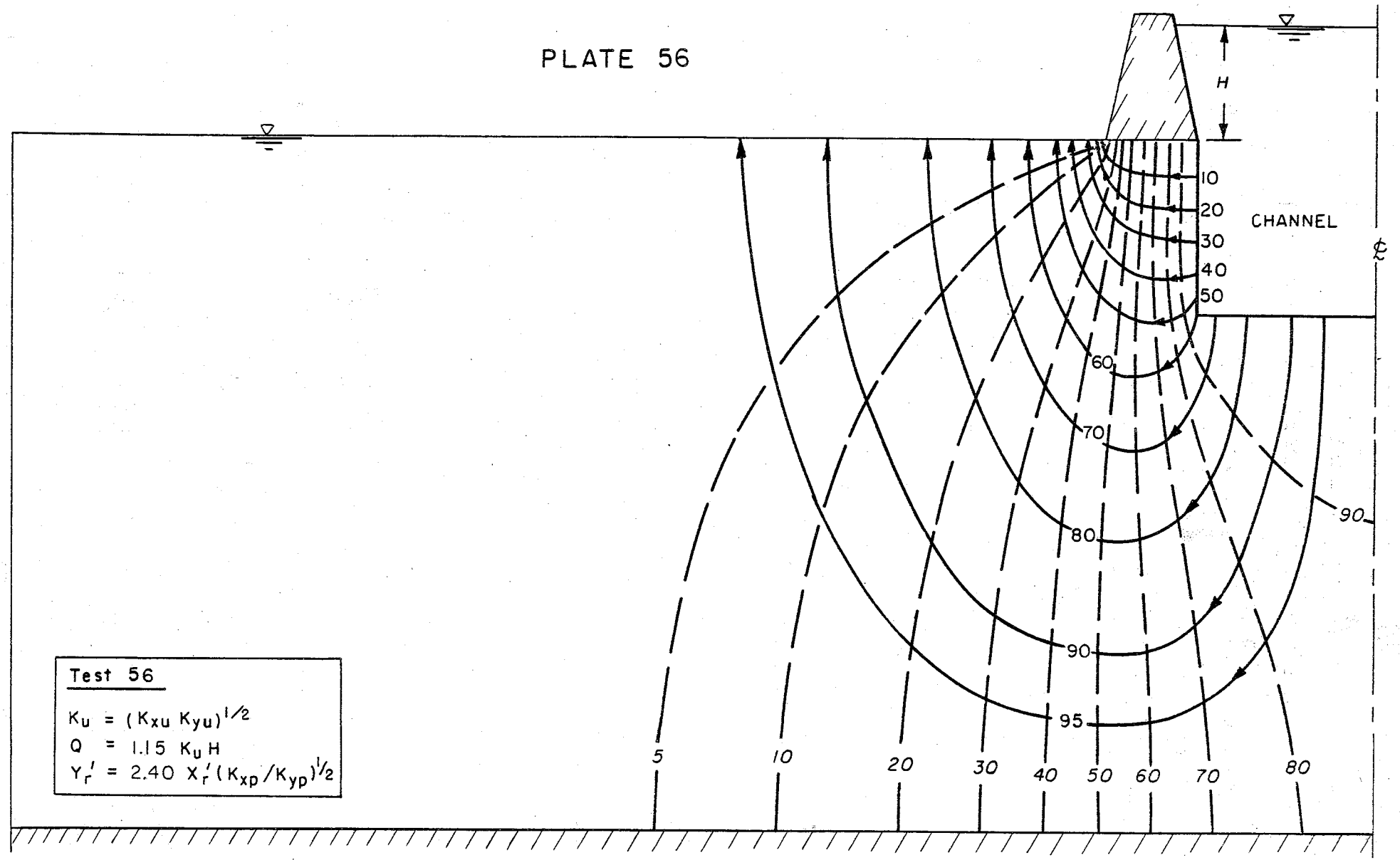
H
CHANNEL
10
20
30
40
50
60
70
80
90
95
5
10
20
30
40
50
60
70
80
90
Test 56
$K_u = (K_{xu} K_{yu})^{1/2}$
$Q = 1.15 K_u H$
$Y_r' = 2.40 X_r' (K_{xp}/K_{yp})^{1/2}$

T-11

Appendix I

Discharge Scale for Electric Analogy Model

The discharge scale is obtained by comparing Ohm's law with Darcy's law. If the flow per unit width (Q for the prototype and I in the model) is considered, then for an isotropic prototype (see Fig. I-1)

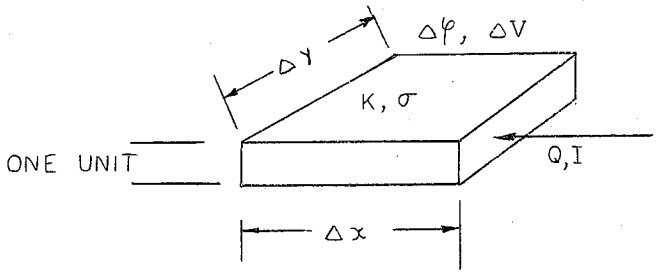

FIG. I-1

$$Q = K \quad \Delta Y_p \frac{\Delta \varphi}{\Delta X_p}$$

and

$$I = \sigma \Delta Y_m \frac{\Delta V}{\Delta X_m}$$

hence

$$Q = I \cdot \frac{K}{\sigma} \frac{\Delta Y_p}{\Delta Y_m} \frac{\Delta X_m}{\Delta X_p} \frac{\Delta \varphi}{\Delta V}$$

For the isotropic case there is no distortion of scales; therefore,

$$\frac{\Delta Y_m}{\Delta Y_p} = \frac{\Delta X_m}{\Delta X_p}$$

and

$$Q = I \frac{K}{\sigma} \quad \frac{\Delta \varphi}{\Delta V} = I \frac{K}{\sigma} m$$

where m is defined by Eqn. (22).

For a nonisotropic case,

$$Q_x = K_{xp} \Delta Y_p \frac{\Delta \varphi}{\Delta X_p}$$

$$I_x = \sigma \Delta Y_m \frac{\Delta V}{\Delta X_m}$$

or

$$\frac{Q_x}{I_x} = \frac{K_{xp}}{\sigma} \frac{X_r}{Y_r} \frac{\Delta \varphi}{\Delta V}$$

and

$$Q_y = K_{yp} \Delta X_p \frac{\Delta \varphi}{\Delta Y_p}$$

$$I_y = \sigma \Delta X_m \frac{\Delta V}{\Delta X_m}$$

or

$$\frac{Q_y}{I_y} = \frac{K_{yp}}{\sigma} \frac{Y_r}{X_r} \frac{\Delta \varphi}{\Delta V}$$

But

$$\frac{Q_x}{I_x} = \frac{Q_y}{I_y} = \frac{Q}{I}$$

hence,

$$\frac{Q}{I} = \frac{K_{xp}}{\sigma} \frac{X_r}{Y_r} \frac{\Delta \varphi}{\Delta V}$$

Multiplying both numerator and denominator by $K_{yp}^{\frac{1}{2}}$, then

$$\frac{Q}{I} = \frac{K_e}{\sigma} \frac{\Delta \varphi}{\Delta V} = m \frac{K_e}{\sigma}$$

In the model for $\Delta\varphi = H$, $\Delta V = 12.6$ volts, and K in cm/sec. is represented by σ mhos/cm. If I is measured in amperes, then

$$Q = I\ (\text{amp})\ \frac{K\ (\text{cm/sec})}{\sigma\ (\text{mhos/cm})} \cdot \frac{H\ (\text{cm})}{12.6\ (\text{volts})} = I\ \frac{KH}{\sigma}\ \text{cm}^3/\text{sec}.$$

Appendix II

Determination of Streamlines for Variable Potential Boundaries

The equipotentials shown in Fig. II-1 are first obtained directly by the model. The line AB is the given sloping water table. The problem is to determine the distribution of streamlines ψ_k reaching this line from a given potential distribution along this line. If the number of equipotential drops m equals the number of flow channels, then for any rectangle DEFG of the flow net in the interior of the field of flow

$$\tan \beta = \frac{c}{d}$$

On the boundary AB

$$\psi_{k+1} - \psi_k = \Delta\psi$$

$$\psi'_{k+1} - \psi_k = \Delta\psi'$$

As

$$\frac{a}{b} = \tan \beta \quad ; \quad b = \frac{a}{\tan \beta}$$

$$\frac{a}{b'} = \tan \alpha \quad ; \quad b' = \frac{a}{\tan \alpha}$$

$$\frac{b}{b'} = \frac{\tan \alpha}{\tan \beta} \cong \frac{\Delta\psi}{\Delta\psi'}$$

hence

$$\Delta\psi' \cong \Delta\psi \frac{\tan \beta}{\tan \alpha} = \Delta\psi \frac{c}{d} \frac{b'}{a}$$

For a given m (in the present investigation m = 20), $\Delta\psi$ is known (5%), and the ratio $\frac{c}{d}$ is determined by constructing the rectangles between two equipotential lines in any part of the region not bounded by the sloping

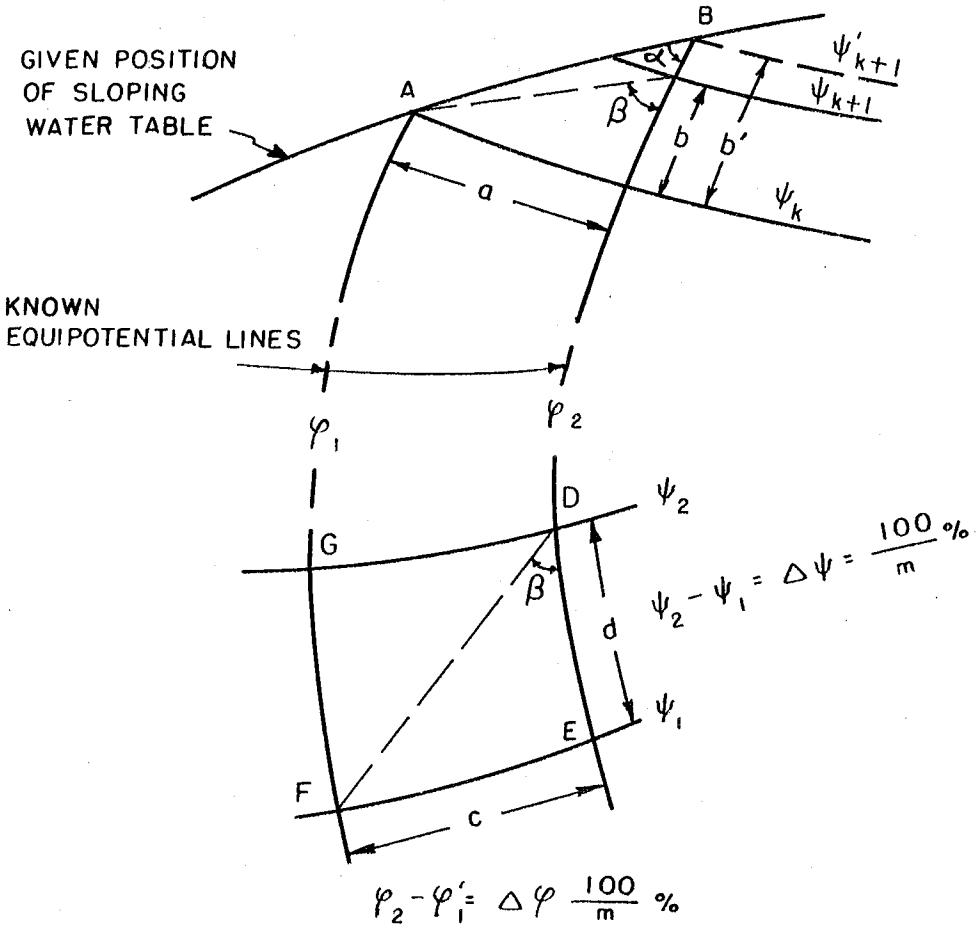

FIG. II-1 FLOW NET WITH A SLOPING WATER TABLE

water table (Fig. II-2a) and the ratio $\frac{b'}{a}$ is determined by perpendiculars drawn from the points A, B, C, etc., where the equipotentials meet the sloping water table (see Fig. II-2b). When all the values of $\Delta\psi'$ have been determined, the values of ψ can be determined by starting from any known value of ψ . The distribution of ψ thus obtained is then used as the potential distribution when the boundaries are interchanged.

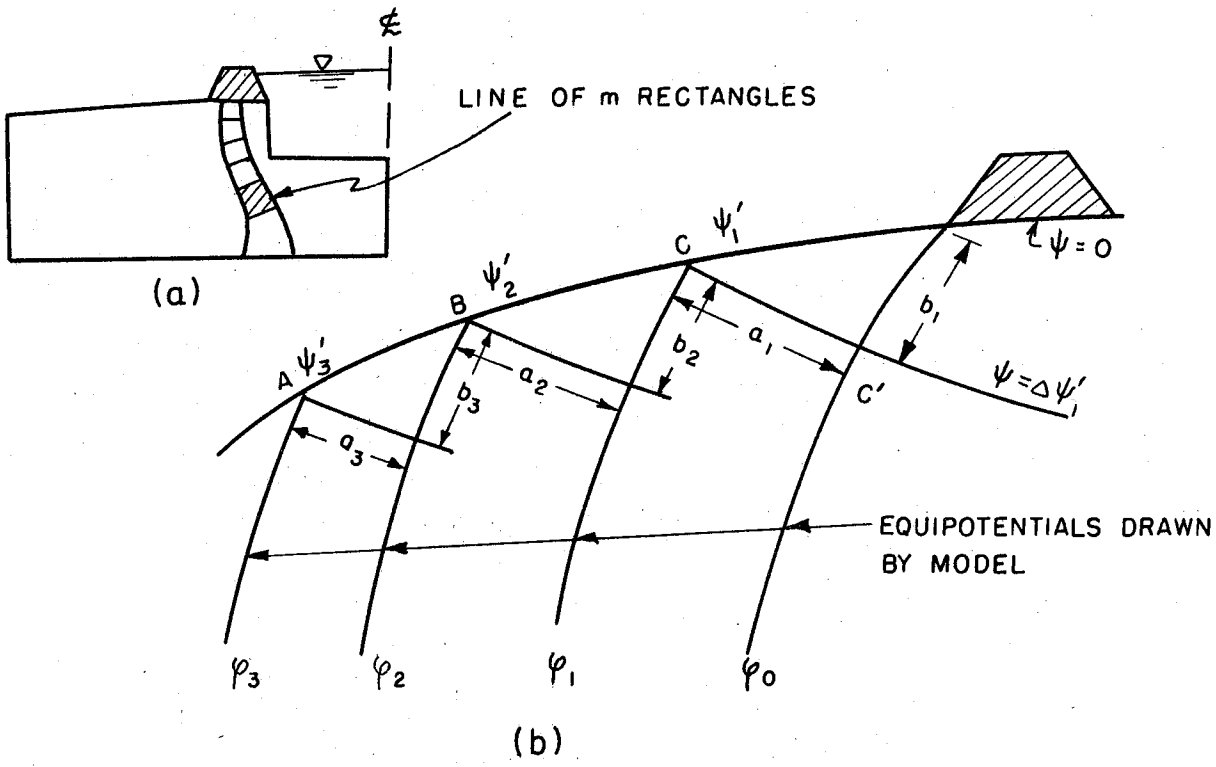

FIG. II - 2 DETERMINATION OF BOUNDARY CONDITIONS FOR A SLOPING WATER TABLE

Appendix III

Analytic Evaluation of Effect of Channel Depth on Seepage for d = 0 and d = D

Analytic determination of seepage is practicable only for a very few simplified cross-sections. Solutions are presented here for two cases: a channel depth equal to zero (d = 0) and a fully penetrating channel (d = D). These supplement the model results and their interpretation.

Case 1 - Channel with Zero Depth (d = 0)

Fig. III-a shows the cross-section of this case. With regard to the resulting flow net, Figs. III-b and III-c are equivalent to Fig. III-a. Fig. III-c is then used as a starting point for a set of Schwartz-Christofel transformations. The Z-plane shown in Fig. III-d is transformed into the ζ_1-plane of Fig. III-e by means of the transformation

$$\zeta_1 = \sin \frac{\pi Z}{2D}$$

and m and n in Fig. III-e are defined by

$$m = \frac{e^{\frac{\pi B}{2D}} - e^{-\frac{\pi B}{2D}}}{2} \qquad n = \frac{e^{\frac{\pi (b\ B)}{2D}} - e^{-\frac{\pi (b\ B)}{2D}}}{2}$$

The ζ_2-plane shown in Fig. III-f is equivalent to the ζ_1-plane shown in Fig. III-e. By this transformation the entire width (2B) of the channel is considered and, accordingly, the resulting discharge will correspond to the whole channel. The ζ_3-plane is obtained from the ζ_2-plane by rotating

$$\zeta_3 = -i\ \zeta_2$$

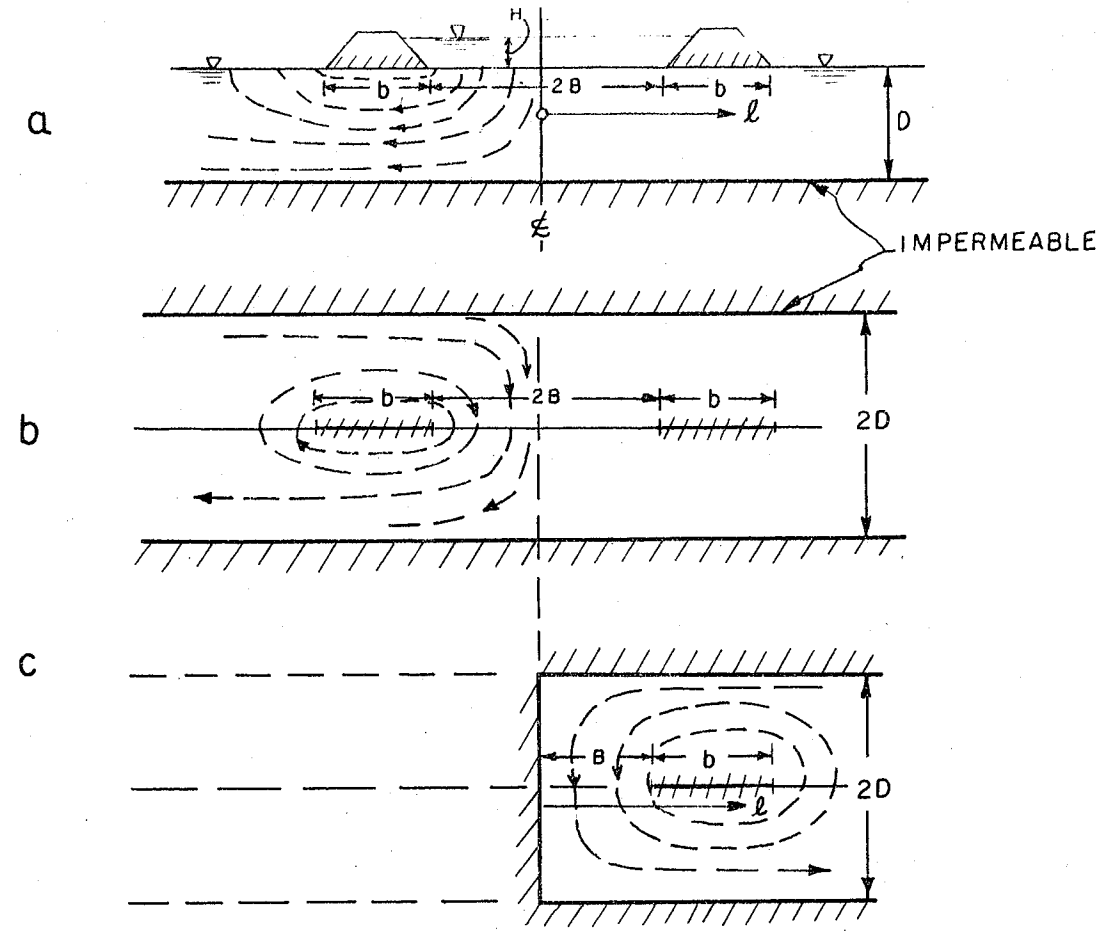

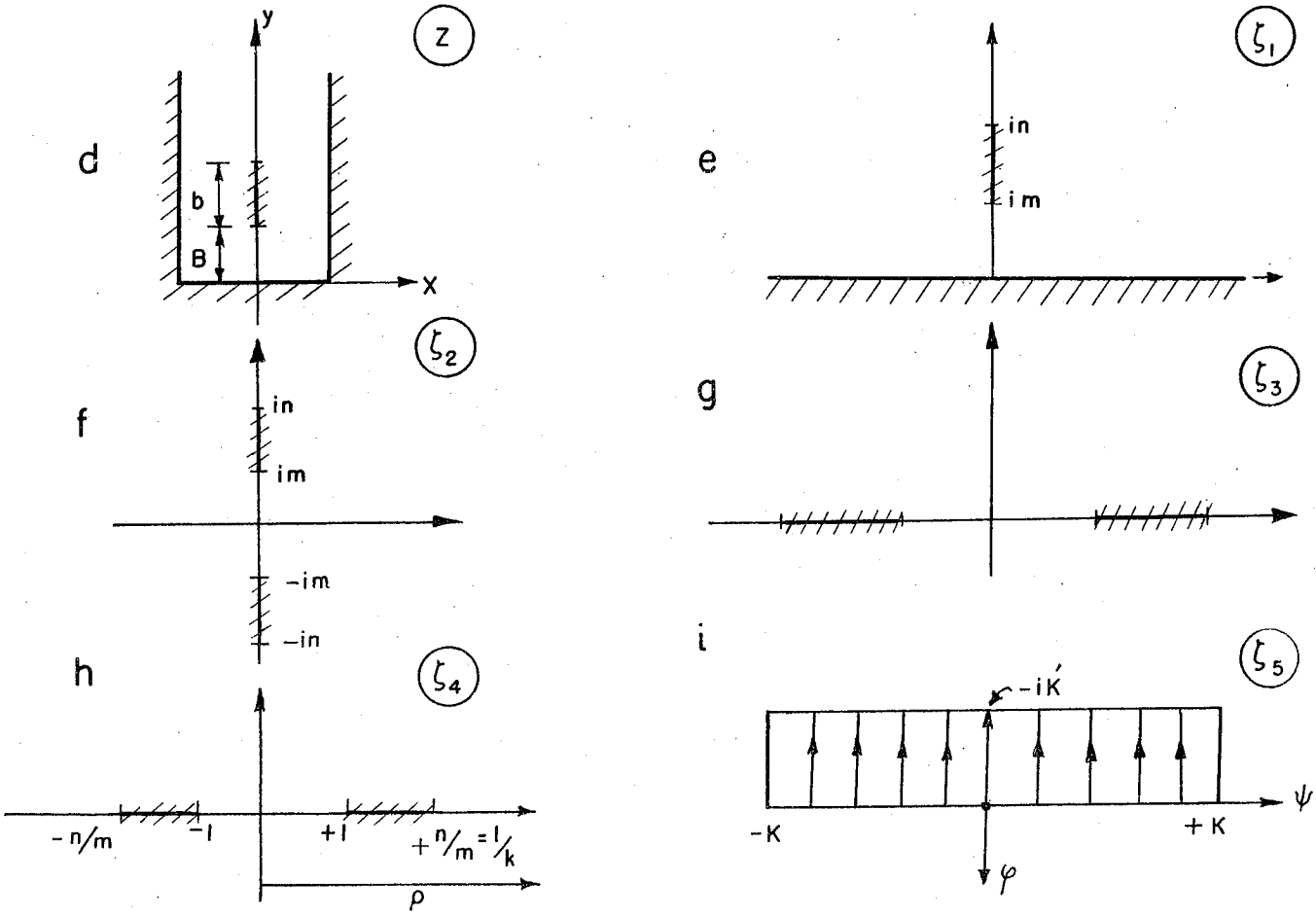

FIGS. III - a TO III - i

The ζ_4-plane is obtained from the ζ_3-plane by reducing the scale by a factor m. Finally, the upper half of the ζ_4-plane is transformed into the inside of the rectangle in the ζ_5-plane by the transformation

$$\zeta_5 = \int_0^{\zeta_4} \frac{dt}{\sqrt{(1-t^2)\,(1-k^2t^2)}}$$

In Fig. III-i

$$K = \int_0^{\zeta_1} \frac{dt}{\sqrt{(1-t^2)\,(1-k^2t^2)}}$$

and

$$iK' = \int_1^{1/k} \frac{ds}{\sqrt{(1-s^2)\,(1-k^2s^2)}}$$

where $k = \frac{m}{n}$.

The total flow from the channel (2Q) is equal to the flow through the rectangle of Fig. III-i which is

$$2Q = K_e \times 2K \times \frac{H}{K'} = K_e H \ \frac{2K}{K'}$$

where K_e is the hydraulic conductivity of the porous media and H is the head difference between the water in the channel and the water table. The quantities K and K' are shown in Fig. III-i.

Test 51 will serve as an example. The above considerations apply to isotropic media; hence the given cross-section has first to be transformed into an isotropic one. The discharge is determined by the ratio $\frac{K}{K'}$. It follows that the scale can be reduced arbitrarily; consequently, the model dimensions (distorted) given in Table III are used in examples throughout this appendix.

$B = 6$ in. $\qquad \frac{B}{D} = 0.3 \qquad ; \qquad \frac{\pi B}{2D} = 0.471$

$b = 2$ in. $\qquad \frac{B + b}{D} = 0.4 \qquad ; \qquad \frac{\pi (B + b)}{2D} = 0.628$

$D = 20$ in.

$$k = \frac{m}{n} = \frac{e^{0.471} - e^{-0.471}}{e^{0.628} - e^{-0.628}} = \frac{1.602 - 0.624}{1.875 - 0.534} = \frac{0.978}{1.341} = 0.727$$

From (7),

$$\sin \alpha = k = 0.727 \; ; \qquad \alpha = 46^{\circ}40' \; ; \qquad \varphi = \frac{\pi}{2}$$

$$k' = 0.686 \; ; \qquad K = 1.880 \qquad K' = 1.830$$

$$2Q = \frac{2 \times 1.880}{1.830} K_e H = 2.06 K_e H \; ; \quad Q = 1.03 K_e H$$

The result of Test 51 was $Q = 1.06 K_e H$. Similarly for test 52: from the test

$$Q = 0.9 K_e H$$

while by computation

$$Q = 0.935 K_e H$$

Fig. III-j gives the discharge for various ratios of $\frac{b}{D}$ and $\frac{B}{D}$.

The distribution of seepage with distance from the levee can now be computed. The complex potential $w = \varphi + i \psi$ for the rectangle is

$$w = i \quad \zeta_5 = i \int_0^{\zeta_4} \frac{dt}{\sqrt{(1-t^2)(1-k^2t^2)}} = \varphi + i \psi$$

or

$$w = i \int_0^{-\frac{i}{m} \sin \frac{\pi Z}{2D}} \frac{dt}{\sqrt{(1-t^2)(1-k^2t^2)}}$$

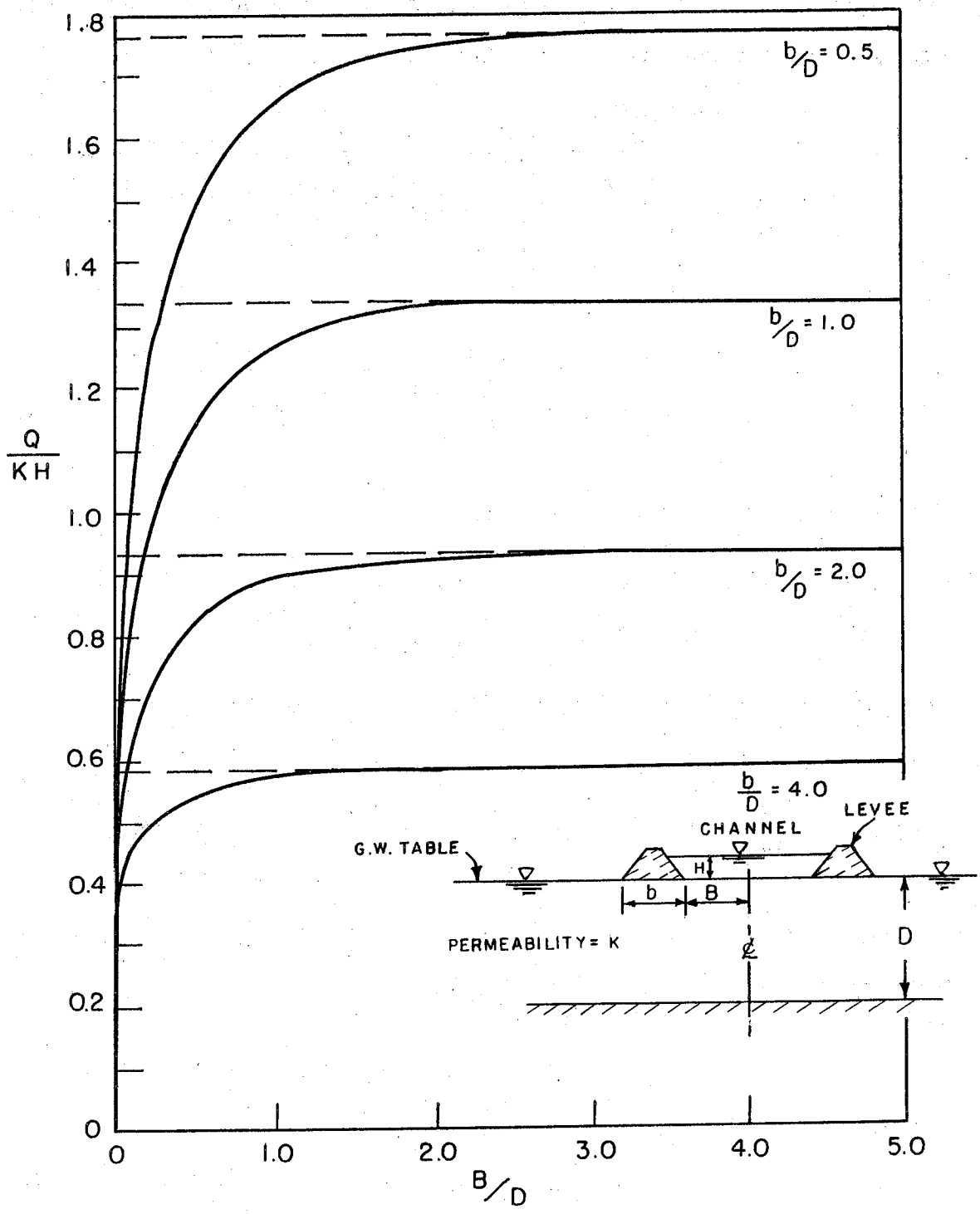

FIG. III-j SEEPAGE FROM CHANNEL OF ZERO DEPTH AS A FUNCTION OF b/D AND B/D

Let l denote the distance from the origin in the horizontal direction (Fig. III-a). In the transformed z-plane this distance is represented by y along the imaginary axis. Along this axis

$$w = i \int_0 \frac{-\frac{i}{m}\sin\frac{\pi i y}{2D}\, dt}{\sqrt{(1-t^2)\,(1-k^2t^2)}} = i \int_0 \frac{\frac{e^{\frac{\pi y}{2D}} - e^{-\frac{\pi y}{2D}}}{2m}\, dt}{\sqrt{(1-t^2)\,(1-k^2t^2)}}$$

or

$$w = i \int_0^{\rho} \frac{dt}{\sqrt{(1-t^2)\,(1-k^2t^2)}}$$

where

$$\rho = \frac{e^{\frac{\pi y}{2D}} - e^{-\frac{\pi y}{2D}}}{2m}$$

The integral must be evaluated in three separate parts:

(1) $o \leqslant y \leqslant B$ or $o \leqslant \rho \leqslant 1$

for this case

$$\psi = \int_0^{\rho} \frac{dt}{\sqrt{(1-t^2)\,(1-k^2t^2)}}$$

for

$$y = 0, \quad \rho = 0, \quad \psi = 0$$

and for

$$y = B, \quad \rho = 1, \quad \psi = K.$$ (The total flow from half a channel.)

(2) $B < y < B + b$, or $1 < \rho < \frac{1}{k}$, or ζ_5 from K to K + iK'.

Along this line ψ remains constant and only the value of φ changes. This follows from the fact that the integral has a real part, which is the same as that of part (1), and an imaginary part which gives the change of potential along the base of the levee.

In general, values for φ and ψ can be obtained from w; however, only the values of ψ are considered here.

(3) $B + b < y < \infty$ or $\frac{1}{k} < \rho < \infty$ or ζ_5 from $K + iK'$ to iK'.

For this case

$$\psi = \mathrm{Re} \int_0^{\rho} \frac{dt}{\sqrt{(1-t^2)\,(1-k^2t^2)}}$$

$$= \mathrm{Re} \left[\int_0^{1} \frac{dt}{\sqrt{(1-t^2)\,(1-k^2t^2)}} - i \int_1^{1/k} \frac{dt}{\sqrt{(t^2-1)(1-k^2t^2)}} + \int_{1/k}^{\rho} \frac{dt}{\sqrt{(1-t^2)(1-k^2t^2)}} \right]$$

$$= \int_0^{1} \frac{dt}{\sqrt{(1-t^2)(1-k^2t^2)}} - \frac{1}{k} \int_{\frac{1}{k}}^{\rho} \frac{dt}{\sqrt{(t^2-1)(t^2-\frac{1}{k^2})}}$$

where both integrands (and also the integrals) are real in their intervals. Evaluation by tables yields

$$\psi = K - F(\alpha, \varphi)$$

where

$$\sin \varphi = \frac{1}{k} \sqrt{\frac{1-\rho^2 k^2}{1-\rho^2}}$$

$$\sin \alpha = k$$

Thus the value of ψ is

$$\text{for } y = 0, \quad \psi = 0$$

$$y = B, \quad \psi = B + b; \quad \psi = K = 0$$

$$y = \infty, \quad \psi = 0$$

The following example shows how this last equation can aid in determining the distribution of seepage.

Example: At 100 ft. from the levee in Test 51, where

$B = 6$ in., $b = 2$ in., $y = 6 + 2 + 2 = 10$ in., $D = 20$ in., $2m = 0.978$

$$= \frac{e^{\frac{\pi}{2}} - e^{-\frac{\pi}{2}}}{0.978} = \frac{e^{0.785} - e^{-0.785}}{0.978} = 1.775$$

$$k = 0.727; \quad \frac{1}{k} = 1.372; \quad K = 1.880$$

$$\sin \varphi = 1.375 \sqrt{\frac{1 - 1.775^2 \times 0.727^2}{1 - 1.775^2}} = 0.762$$

$$\varphi = 49.6^\circ$$

$$\sin \alpha = k = 0.727 \qquad \alpha = 46.7^\circ$$

$$F(0.727; 49.5^\circ) = 0.92$$

$$\psi = 1.88 - 0.92 = 0.96$$

As a percentage the value of ψ equals $\frac{0.96}{1.88} \times 100 = 51.2$ % as compared to approximately 53 % obtained by the model.

Case 2 - Fully Penetrating Channel ($d = D$)

Fig. III-k shows the cross-section for this case. Following a series of transformations similar to those described for Case 1 (Figs. III-l to III-p), the following results can be written:

k

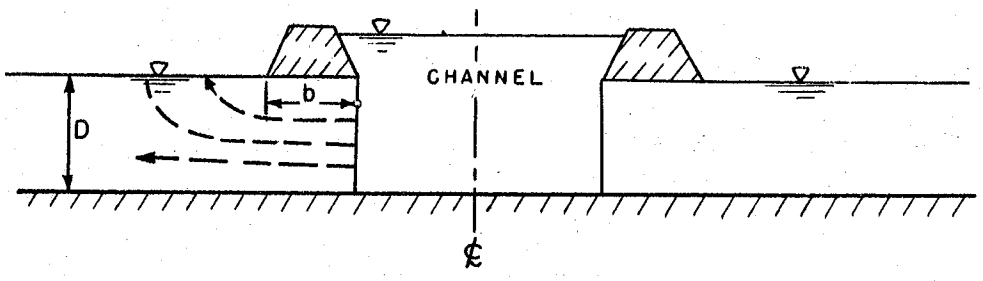

l

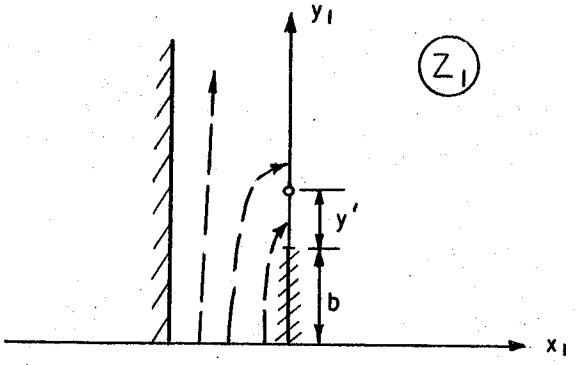

m

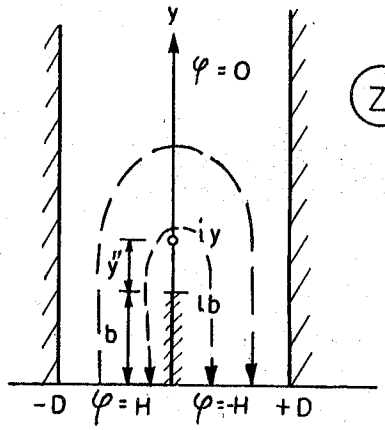

n

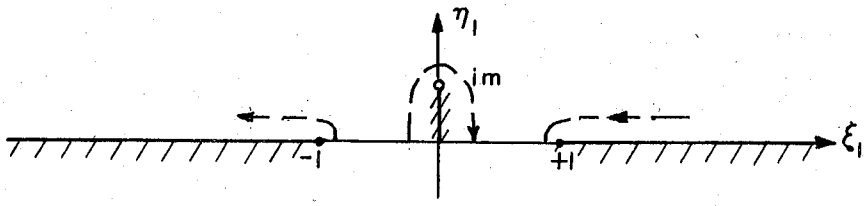

o

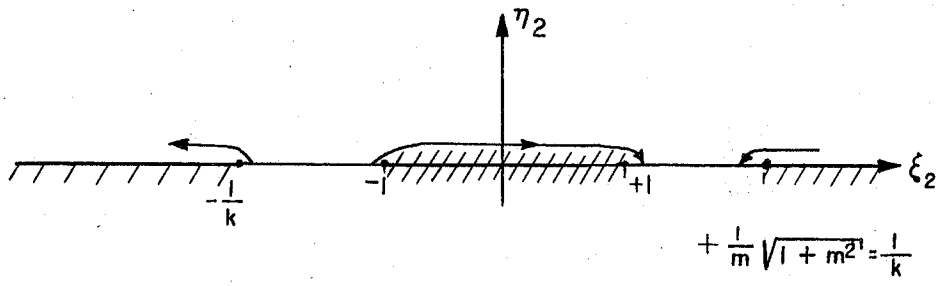

p

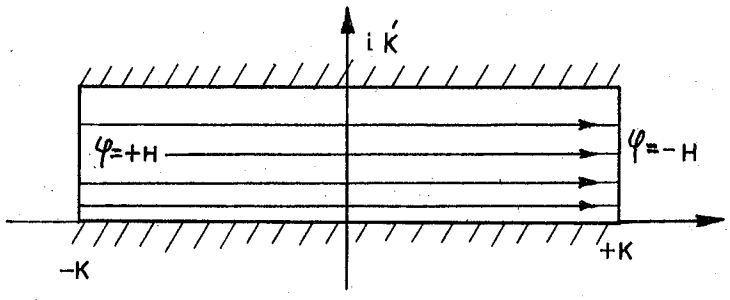

FIGS. III - k TO III - p

$$\zeta_1 = \sin \frac{\pi Z}{2D}$$

which for Z = ib yields

$$\zeta_1 = i \frac{e^{\frac{\pi b}{2D}} - e^{-\frac{\pi b}{2D}}}{2} = im; \quad m = \frac{e^{\frac{\pi b}{2D}} - e^{-\frac{\pi b}{2D}}}{2}$$

Also,

$$\zeta_2 = \frac{1}{m} \sqrt{\zeta_1^2 + m^2}$$

from which it follows that

$$\frac{1}{k} = \frac{1}{m} \sqrt{1 + m^2} \quad \text{or:} \quad k = \frac{m}{\sqrt{1 + m^2}}$$

and finally,

$$\zeta_3 = F(\zeta_2) = \int_0^{\zeta_2} \frac{dt}{\sqrt{(1-t^2)(1-k^2t^2)}}$$

for which

$$K = \int_0^1 \frac{dt}{\sqrt{(1-t^2)(1-k^2t^2)}}$$

$$iK' = \int_1^{\frac{1}{k}} \frac{ds}{\sqrt{(1-s^2)(1-k^2s^2)}}$$

The total discharge (for one side) is

$$Q = K_e \frac{2H}{2K} K' = K_e H \cdot \frac{K'}{K}$$

Example (Test 53):

$b = 2$ in. (corresponding to 100 ft.)

$D = 20$ in. (corresponding to 100 ft. The region is non-isotropic).

$$m = \frac{e^{0.157} - e^{-0.157}}{2} = \frac{1.170 - 0.855}{2} = 0.158$$

$$k = \frac{0.158}{\sqrt{1 + 0.158^2}} = 0.156$$

From tables in (7),

$$\varphi = \frac{\pi}{2}\ ;\ \sin \alpha = k;\quad \alpha = 8^{\circ}55'$$

$$K = 1.58 \qquad K' = 3.265$$

$$Q = K_e H \frac{3.26}{1.58} = 2.06\ K_e H$$

This compares with approximately $2.03\ K_e H$ obtained by the model.

The seepage distribution can be obtained in a similar way to that described for Case 1. The complex potential for this case is

$$w = \zeta_3 = \int_0^{\zeta_2} \frac{dt}{\sqrt{(1-t^2)\ (1-k^2t^2)}}$$

The distance from the levee is represented by the η_2 axis in Fig. III-o (ζ_2-plane). Along this axis

$$w = \int_0^{i\eta_2} \frac{dt}{\sqrt{(1-t^2)(1-k^2t^2)}}$$

Substituting $t = it'$ yields

$$w = i \int_0^{\eta_2} \frac{dt'}{\sqrt{(1+t'^2)(1+k^2t'^2)}} = \frac{i}{k} \int_0^{\eta_2} \frac{dt'}{\sqrt{(1+t'^2)(\frac{1}{k^2}+t'^2)}}$$

From (7),

$$w = iF(\alpha, \varphi) \quad \text{where} \quad k = \cos\alpha \; ; \; \tan\varphi = \eta_2$$

Hence

$$\psi = Im(w) = F(\alpha, \varphi)$$

represents the flow. For data of Test 53, the total flow is found from $\eta_2 = \infty$, $\varphi = \frac{\pi}{2}$, $k = 0.156$, and $\alpha = 81^{\circ}05'$; therefore, the total flow is given by $F = 3.27$. In order to compute the flow in the distance y' from the toe of the levee, the distance in the original z-plane (Fig. III-m) is converted into η_2 in the transformed ζ_2-plane (Fig. III-o) by $y = y' + b$.

For $Z = iy$, $\zeta_1 = \sin\frac{\pi Z}{2D} = \sin\frac{\pi iy}{2D} = i\left(\frac{e^{\frac{\pi y}{2D}} - e^{-\frac{\pi y}{2D}}}{2}\right) = i\,\eta_1$

Hence,

$$\zeta_2 = \frac{1}{m}\sqrt{\zeta_1^2 + m^2} = \sqrt{1 - \frac{e^{\frac{\pi y}{2D}} - e^{-\frac{\pi y}{2D}}}{2m}}$$

$$= i\sqrt{\left(\frac{e^{\frac{\pi y}{2D}} - e^{-\frac{\pi y}{2D}}}{2m}\right)^2 - 1}$$

and

$$\eta_2 = \sqrt{\left(\frac{e^{\frac{\pi y}{2D}} - e^{-\frac{\pi y}{2D}}}{2m}\right)^2 - 1}$$

As an example, for $y' = 1$ inch (equal to 50 ft. in prototype), $y = 3$ inches,

$$\eta_2 = \sqrt{\left(\frac{e^{0.236} - e^{-0.236}}{2 \times 0.158}\right)^2 - 1} = \sqrt{\left(\frac{1.266 - 0.790}{0.316}\right)^2 - 1} = 1.12$$

hence $\varphi = 48.2^\circ$ and $F = 0.957$. It follows that the percentage of flow in y' of the total flow is $\frac{0.957}{3.27} \times 100 = 29.3\%$. For y' = 3 in., y = 5 in.,

$$\eta_2 = \sqrt{\left(\frac{e^{0.392} - e^{-0.392}}{2 \times 0.158}\right)^2 - 1} = \sqrt{\frac{1.480 - 0.676}{0.316} - 1} = 2.342$$

hence $\varphi = 65.9$ and $F = 1.52$. The flow percentage in y' amounts to $\frac{1.52}{3.27} \times 100 = 46.5\%$. These results compare with 28% and 48%, respectively, from data of Test 53.

Fig. III-q shows the relationship between the discharge (expressed as $\frac{Q}{K_e H}$) and the width of the levee (expressed as $\frac{b}{D}$).

Discussion

Cases 1 and 2 lead to the following conclusions:

(a) Increasing the width of the channel increases the discharge very rapidly at first, but has almost no effect for $\frac{B}{D} > 2$.

(b) For a fixed ratio of $\frac{B}{D}$, the discharge increases as the ratio $\frac{b}{D}$ decreases.

(c) For a fully penetrating channel, its width has no effect on the discharge. The discharge from the channel increases as the length of the base of the levee decreases.

Although these conclusions were obtained from the theoretical cases of a channel with no depth and a fully penetrating channel, it is believed that these trends remain true also for the cross-sections investigated in the model.

The analytic study was based on an aquifer of infinite extent, whereas the model tests of necessity presupposed an aquifer of limited

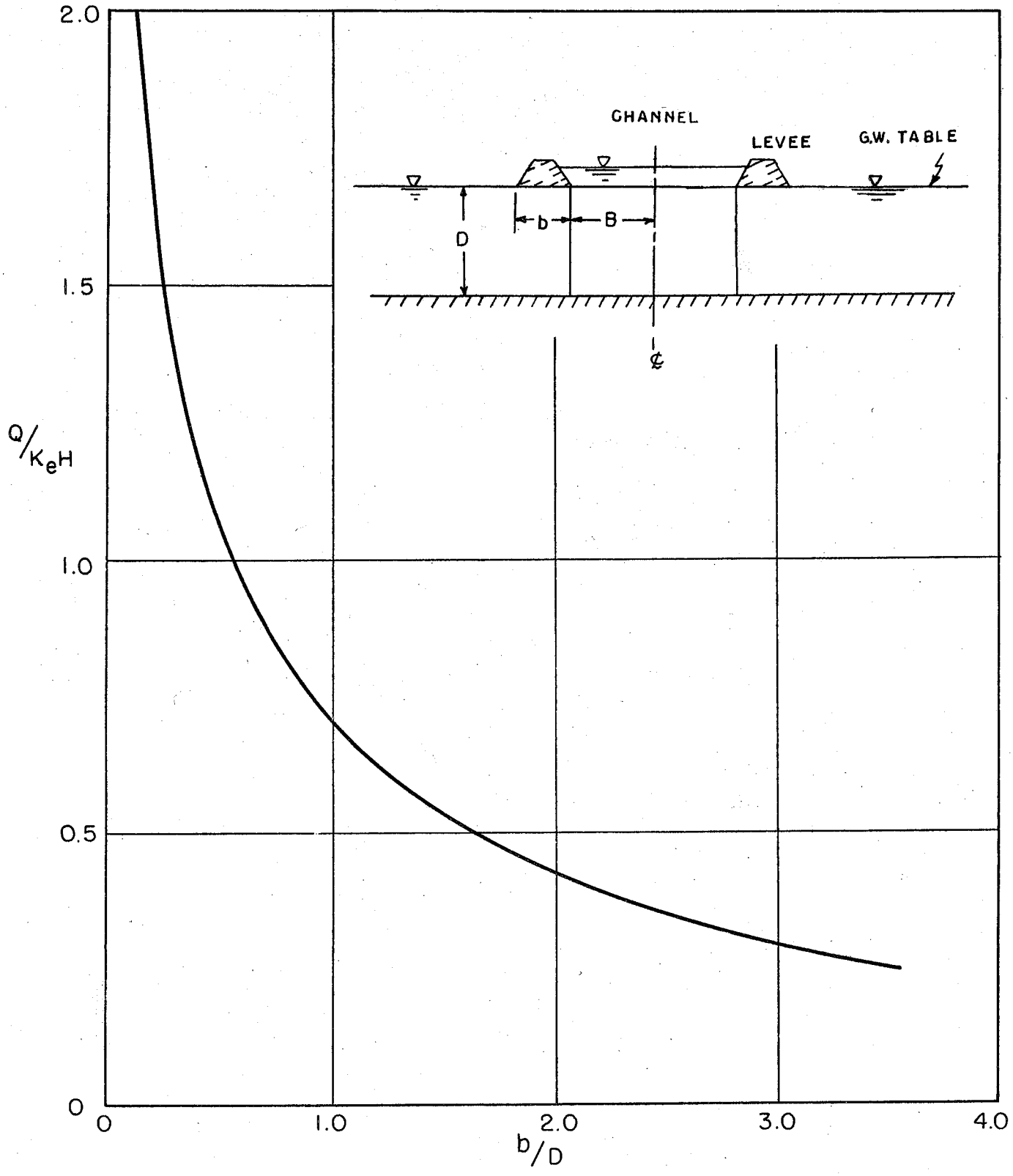

FIG III - q SEEPAGE FROM A FULLY PENETRATING CHANNEL

extent. Comparison of results by the two methods reveal that differences were negligible, thus justifying the model work.

In general, the theoretical approach described above is applicable only to a limited number of simplified cross-sections in a homogeneous aquifer. Even for these cases, the determination of the complete flow net requires many hours of calculation for each case. From a practical point of view, therefore, the electric analogy model was essential to investigate the seepage through cross-sections approximating field conditions.